Exceptional Event Demonstration for Ozone Exceedances in Clark County, Nevada – May 6, 2020

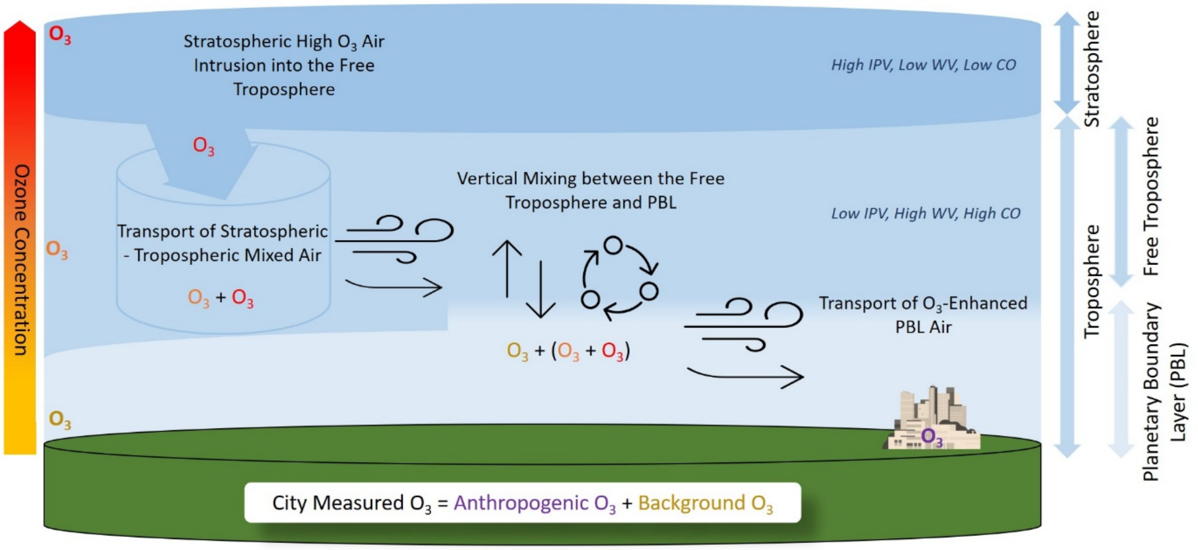

Final Report Prepared for

U.S. EPA Region 9
San Francisco, CA

July 2021

STi Sonoma Technology

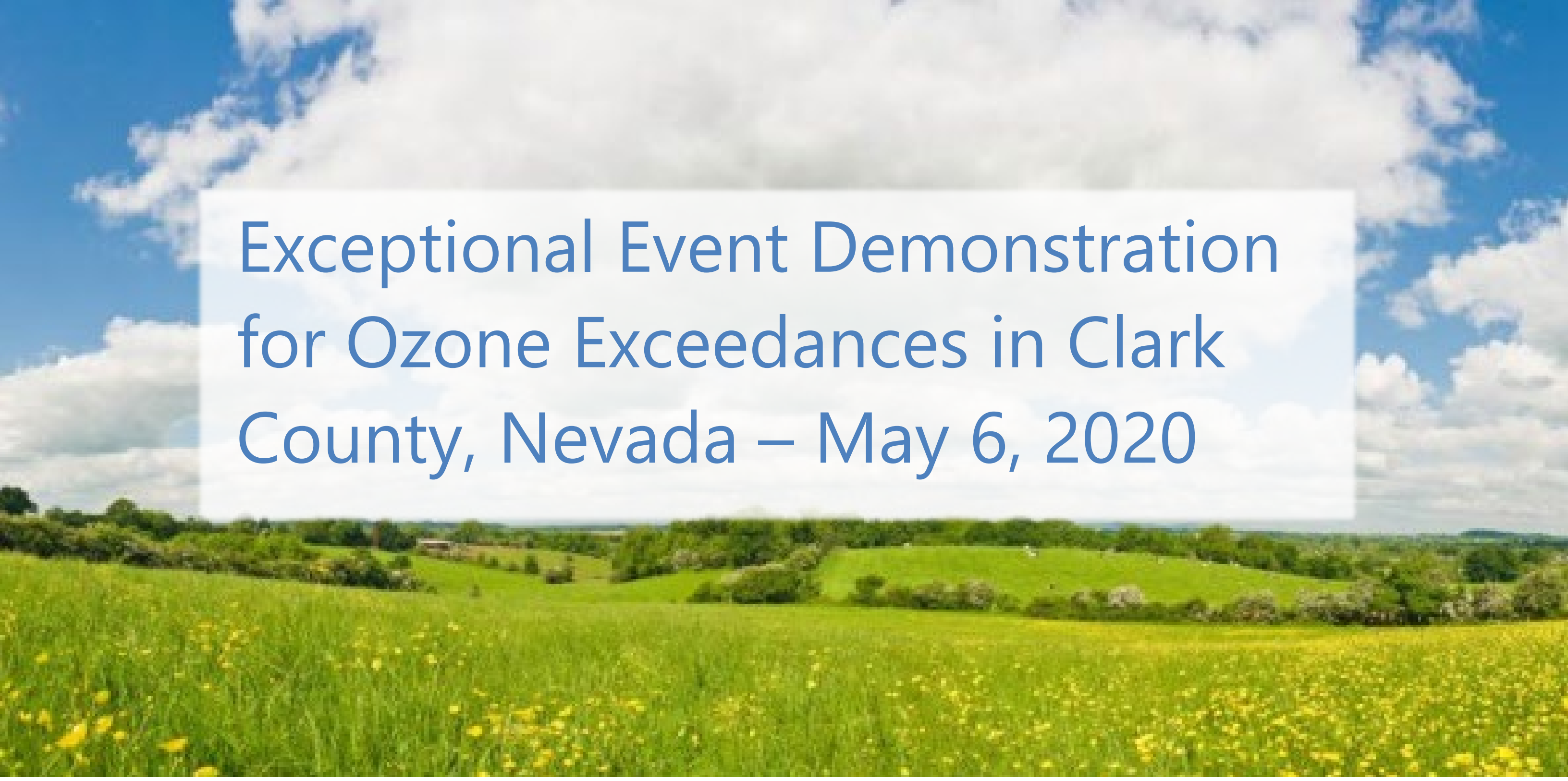

Exceptional Event Demonstration for Ozone Exceedances in Clark County, Nevada – May 6, 2020

Prepared by

Steve Brown, PhD
Crystal McClure, PhD
Cari Gostic
Samantha Kramer, PhD
David Miller, PhD
Charles Scarborough
Ningxin Wang, PhD

Sonoma Technology
1450 N. McDowell Blvd., Suite 200
Petaluma, CA 94954
Ph 707.665.9900 | F 707.665.9800
sonomatech.com

Prepared for

Clark County Department of Environment & Sustainability
Division of Air Quality
4701 W. Russell Road, Suite 200
Las Vegas, NV 89118
Ph 702.455.3206
www.clarkcountynv.gov

Final Report

STI-920053-7477

July 1, 2021

Cover graphic illustrates stratospheric intrusion and transport. See section 2.4 for more details.

Contents

Figures

Tables

Executive Summary

On May 6, 2020, Clark County experienced an atypical, area-wide episode of elevated ambient ozone; during this episode, the 2015 8-hr ozone National Ambient Air Quality Standards (NAAQS) threshold (0.070 ppm) was exceeded at the Walter Johnson, Paul Meyer, Joe Neal, Jerome Mack, Green Valley, Jean, and Apex sites. The exceedances at Walter Johnson, Paul Meyer, Joe Neal, and Green Valley could lead to an ozone nonattainment designation for the Clark County area. Air trajectory analysis and air quality modeling suggest that this ozone exceedance was influenced by a Stratospheric Ozone Intrusion (SOI) over the northwestern United States (U.S.) and eastern Pacific Ocean that transported ozone-rich air to Clark County. The EPA Exceptional Event Rule (U.S. Environmental Protection Agency, 2018) allows air agencies to omit air quality data from the design value calculation if it can be demonstrated that the measurement in question was caused by an exceptional event. This report describes analyses that help to establish a clear causal relationship between the SOI and the May 6, 2020, ozone exceedance at all seven sites.

The analyses provide evidence supportive of SOI impacts on ozone concentrations in Clark County. Analyses show that (1) prior to May 6, multiple atmospheric models provide evidence that there was an SOI event upwind of Clark County signified by an area of stratosphere-troposphere exchange over the northwestern U.S. and eastern Pacific Ocean, (2) ozone-rich stratospheric air was transported from the SOI to the lower troposphere and surface of the Clark County area, (3) the SOI and subsequent transport of dry stratospheric air impacted the typical diurnal profiles of ground-level meteorological measurements, including relative and absolute humidity, in the Clark County area on May 6, and (4) meteorological regression modeling and similar meteorological day analysis show that ozone observations on May 6 were unusual in the historical record given the meteorological conditions. Sources of evidence used in these analyses include air quality monitor data to show that supporting pollutant trends at the surface were influenced by upwind effects from the SOI, air trajectory analysis to show transport from the SOI to the Clark County area, satellite imagery and meteorological model results, meteorological regression modeling, and meteorologically similar day analysis.

The EPA "Guidance on the Preparation of Exceptional Events Demonstration for Stratospheric Ozone Intrusions" (U.S. Environmental Protection Agency, 2018) describes a two-tier approach to evaluating an SOI event and then developing evidence for the EE demonstration; depending on the complexity of the event, increasingly involved information may be required to demonstrate a causal relationship between an SOI event and an exceedance. This report documents the results of analyses conducted to address Tier 1 and Tier 2 exceptional event demonstration requirements.

These analyses show that ozone-laden air was transported from the northwestern U.S. and eastern Pacific Ocean to the Clark County area on the days leading up to May 6. Combined with additional evidence, such as meteorologically similar day analysis, our results provide key evidence to support SOI impacts on ozone concentrations in Clark County on May 6, 2020.

1. Overview

1.1 Introduction

Stratospheric Ozone Intrusions (SOIs) occur when ozone-enriched, stratospheric air descends into the troposphere and injects ozone (O_3) at elevations where ozone concentrations are usually lower. SOIs can directly affect surface-level ozone when a tropopause fold (carrying ozone-enriched stratospheric air) extends down to the surface. However, because tropopause folds do not typically extend below around 600 hPa (4.5 km above ground level [agl]) in the mid-latitudes, this effect typically only occurs at high altitude sites. Alternatively, a tropopause fold (or other stratospheric-tropospheric mixing) can occur at high altitudes, and then ozone can be directly transported to the surface downwind of the event. The mixing of ozone-enriched air can be enhanced where the boundary layer (i.e., the lowest well-mixed atmospheric layer that reaches the surface) is very deep (4-5 km) on hot, dry days. In desert regions such as Clark County, Nevada, an upwind SOI can efficiently be mixed down to the surface during hot spring and summer days, which can enhance ozone concentrations. An SOI event occurred upwind of Clark County on May 4-5, 2020, and then affected ozone concentrations on May 6. On May 6, 7 of the 14 ozone monitoring locations around Clark County recorded an exceedance of the 2015 National Ambient Air Quality Standard (NAAQS) for 8-hour ozone (0.070 ppm).

Typically, ozone concentrations in the stratosphere are around 5-10 parts per million (ppm). Depending on the amount of dilution after the SOI event, ozone concentrations can be significantly enhanced above background tropospheric levels (~0.040-0.050 ppm). Even in areas with urban emissions, such as Las Vegas, the addition of ozone from an upwind SOI event can enhance ozone concentrations above usual levels, potentially driving concentrations above the ozone standard. SOIs in the western U.S. typically occur in spring and are well documented to affect ozone concentrations in Clark County (Langford, 2014; Langford and Senff, 2019). We can identify and track the movement of air from an SOI event because stratospheric air (1) is typically depleted in both anthropogenic compounds (i.e., particulate matter [PM], carbon monoxide [CO], and nitrogen oxides [NO_x]) and water vapor compared with tropospheric air, and (2) shows enhanced isentropic potential vorticity (IPV). According to guidance from the U.S. Environmental Protection Agency (EPA), exceptional events (EE) such as SOIs that affect ozone concentrations can be subject to exclusion from calculations of NAAQS attainment if a clear causal relationship can be established between a specific event and the monitoring exceedance (U.S. Environmental Protection Agency, 2018).

For the May 6, 2020, case in Clark County, we describe the clear causal relationship between the event causing the exceedance (the SOI over the northwest U.S. and westward into the Pacific) and the downwind effects on the monitoring sites in Clark County that recorded an exceedance of the maximum daily 8-hour ozone average (MDA8). The evidence in this report provides a Tier 2 analysis required by EPA's Exceptional Event Guidance for more complex SOI events: comparison with non-event ozone concentrations, analysis of meteorological transport, satellite and model analysis of stratospheric tracers, transport analysis from the SOI to the surface, measurements of column ozone at a high-altitude site, meteorologically similar day analyses, and the effect of the SOI on surface ozone (and other tracer) concentrations. Additionally, we provide Generalized Additive Model (GAM) statistical results to help quantify the effect of the SOI on this EE. The SOI that affected ozone concentrations in Clark County could not be reasonably controlled or prevented because SOIs are considered natural events. Table 1-1 lists the sites affected during the May 6 event, as well as their locations and MDA8 ozone concentrations.

Table 1-1. May 6, 2020, EE information. All monitoring sites in Clark County that exceeded the 2015 NAAQS standard during May 6, 2020, are listed along with EPA Air Quality System (AQS) site codes, location information, and MDA8 ozone concentrations.

AQS Site Code	Site Name	Latitude (degrees N)	Longitude (degrees W)	MDA8 O_3 Concentration (ppb)
320030071	Walter Johnson	36.170	-115.263	78
320030043	Paul Meyer	36.106	-115.253	77
320030075	Joe Neal	36.271	-115.238	76
320030540	Jerome Mack	36.142	-115.079	73
320030298	Green Valley	36.049	-115.053	72
320031019	Jean	35.786	-115.357	75
320030022	Apex	36.391	-114.907	76

Concurrent with this document, Clark County is submitting documentation for other ozone EEs in 2018 and 2020 due to wildfires and stratospheric intrusions. These events are mentioned throughout this report and are referred to as “proposed 2018 and 2020 EEs,” recognizing that discussion with EPA is still pending. All proposed EEs for Clark County in 2018 and 2020 are listed in Tables 1-2 and 1-3. Wherever possible, we calculated statistics to provide context both including and excluding the proposed EEs from 2018 and 2020.

Table 1-2. Proposed Clark County 2018 EEs. For each site and date combination where the 2015 NAAQS standard was exceeded, the MDA8 ozone concentration is shown in parts per billion (ppb). Blank cells indicate that there was no exceedance on that site/date combination.

Date	Paul Meyer	Walter Johnson	Green Valley	Jerome Mack	Joe Neal	Palo Verde	Jean	Indian Springs	Apex	Boulder City
6/19/2018	72	72	77	75						
6/20/2018	71	74			72					
6/23/2018	72	76	75	72	72	71	77	73		
6/27/2018	75	76	78	76	72	72	81	78	74	72
7/14/2018	72		78	78						
7/15/2018		71	73	73	78					
7/16/2018	75	79	71	73	80	75				
7/17/2018	74	77				74				
7/25/2018	71	72	72							
7/26/2018	72	75	77	77					71	
7/27/2018	72	74			76					
7/30/2018			73	72						
7/31/2018		73			73					
8/6/2018	79	77	74	71	76	72			74	
8/7/2018	73	74	72	71	74				71	

Table 1-3. Proposed Clark County 2020 EEs. For each site and date combination where the 2015 NAAQS standard was exceeded, the MDA8 ozone concentration is shown in ppb. Blank cells indicate that there was no exceedance on that site/date combination.

Date	Walter Johnson	Paul Meyer	Joe Neal	Jerome Mack	Green Valley	Boulder City	Jean	Indian Springs	Apex
5/6/2020	78	77	76	73	72		75		76
5/9/2020	71	74							
5/28/2020	71	76							
6/22/2020	73	74	78						
6/26/2020		73							
8/3/2020	82	78	81		72	72	73	71	
8/7/2020	71		72					72	
8/18/2020	82	79	78						
8/19/2020	74	74	73		71				
8/20/2020			71						
8/21/2020		71							
9/2/2020	75	73							
9/26/2020	71		75						

1.2 Exceptional Event Rule Summary

The EPA "Guidance on the Preparation of Exceptional Events Demonstration for Stratospheric Ozone Intrusions" (U.S. Environmental Protection Agency, 2018) describes a two-tier approach to evaluating an SOI event and then developing evidence for the EE demonstration. A summary of event requirements for both tiers is listed in **Table 1-4**. From the EPA 2018 SOI Guidance:

- Tier 1 analyses can be used for events when ground ozone concentrations are much higher than typical observations, with conditions unfavorable to photochemical ozone production, and with synoptic meteorological conditions conducive to stratospheric intrusion being the cause.
- Tier 2 analyses are appropriate for cases when both local photochemical ozone production and stratospheric ozone contributions are present, or for events where the observed ozone is within range of typical seasonal values of that location. Tier 2 demonstrations involve more supporting analytical documentation than Tier 1 demonstrations.

In this demonstration, we conduct the Tier 2 analysis (which is cumulative with Tier 1) because local photochemical ozone production existed simultaneously with the SOI contribution.

Table 1-4. Tier 1 and 2 requirements for evaluating stratospheric intrusion impacts on ozone exceedances.

Tier	Elements of SOI Event
1	• Stratospheric intrusion events that cause obvious ozone impacts during periods when: – ozone concentrations are typically low, and – meteorological patterns are suggestive of potential transport from the stratosphere. • Meteorological analyses suggest intrusion was recent, nearby, and expansive: – associated with a frontal passage, and – with elevated ozone observed across a large region. • Ozone concentrations are clearly distinguishable from usual conditions. • Occurred outside the period in which high ozone from local and/or regional production is typically observed. • Occurred when and where local photochemical production was minimal: – at night, – associated with cold air advection, high wind speeds, and/or – strong dispersion conditions.
2	• The relationship between the stratospheric intrusion and influenced ozone concentrations is complex and not fully elucidated with Tier 1 elements. • Resulted from long-distance, multi-day transport requiring detailed analyses. • The event-influenced concentrations were in the range of typical exceedances (i.e., close to the area's design value). • Occurred in season when ozone exceedances are historically common. • Occurred in association with other processes and sources of ozone, or on days where meteorological conditions were conducive to local ozone formation.

1.3 Demonstration Outline

Although each stratospheric intrusion event is likely to have unique characteristics, this demonstration shows that stratospheric air entered the free troposphere (FT), was mixed down to the surface, and subsequently caused an ozone exceedance at the surface. We use the recommended analyses listed throughout the EPA 2018 SOI guidance. Table 1-5 summarizes the required and recommended analyses for both Tier 1 and Tier 2 SOI analyses and shows the corresponding sections for each analysis in this report.

Table 1-5. Locations of Tier 1 and 2 analyses within this report.

Type of Analysis	Tier 1 + Tier 2	Section of This Report (Analysis Type)
Conceptual model	What conditions generally lead to high ozone in the area?	Section 2.3 (Characteristics of non-event historical O_3 formation)
Historical comparison	• ≥ 5 years of peak daily ozone data with other high event days flagged. • Table with percentile ranks of days. • Historical diurnal profile comparison (Tier 2).	Section 3.1 (Comparison of event with historical data)
Event overview	• Spatial and temporal depictions of ozone during the event. • Description of surface and upper air meteorological conditions during the event. • Begin to establish the complex relationship between the intrusion and eventual impact at surface (Tier 2).	Section 2.4 (Stratospheric intrusion event description)
Establish stratospheric intrusion	Several of following are likely needed: • Water vapor imagery • Total column ozone • Meteorological evidence	Sections 3.2.1 (Total column ozone and water vapor); Section 3.2.2 (Model results of ozone, CO, water vapor, & meteorological conditions)
Establish stratospheric air reached surface	Several of following are likely needed: • LIDAR, rawinsonde data • Meteorological evidence • Modeled parameter cross sections • Trajectory models	Section 3.2.2 (Model parameter cross sections); Section 3.3.1 (HYSPLIT trajectories); Sections 3.3.2 (LIDAR measurements of the ozone vertical profile); Section 3.3.3 (Meteorological analysis)
Impacts at the surface	Several of following are likely needed: • Coincidence between high ozone and meteorological/parameter conditions characteristic of stratospheric intrusions • Statistical model evidence of impacts • Summary narrative	Section 3.4 (Ozone & RH, ozone & NO_x diurnal patterns, surface ozone concentration time series); Section 3.5.1 (Meteorologically similar matching day analysis); Section 3.5.2 (GAM statistical analysis); Section 3.6 (Summary narrative)

In Chapter 2 of this report, we establish a narrative conceptual model of the EE with a description of the monitoring network, the event causing the exceedance, and transport from the event that led to the exceedance at the affected monitors. Section 2.1 and 2.2 provides detailed information of the region and the existing ozone monitors. Section 2.3 summarizes the processes that led to high ozone concentrations at the monitor on non-event days and the ozone seasonality. In Section 2.4, we introduce the meteorology that caused the stratospheric ozone intrusion and provide a brief narrative for how stratospheric air was transported into the free troposphere and ultimately mixed down through the planet boundary layer (PBL) to the surface monitors.

In Section 3 of this report, we establish the clear causal relationship between the event and the monitored ozone exceedance. As a first step, we provide a comparison of the exceedance concentrations with historical data in Section 3.1. In Section 3.2, we provide evidence of Stratospheric-Tropospheric exchange using satellite imagery and meteorological model results. Section 3.3 shows evidence of stratospheric air reaching the surface using trajectory analysis, lidar ozone measurements, and meteorological observations. We then demonstrate the event impact at the surface in Section 3.4. Additionally, we developed a statistical GAM to estimate the contribution of stratospheric ozone to the monitored ozone concentrations in Section 3.5.

Following the EPA's SOI event guidance, we performed both Tier 1 and Tier 2 analyses to show the clear causal relationship between the stratospheric intrusion event that occurred over the northwest U.S. and the exceedance event in Clark County, Nevada, on May 6, 2020. Focusing on the characterization of the meteorology, transport, and air quality on the days leading up to the event, we conducted the following specific analyses (results from these analyses are presented in both Section 2 and 3):

- Developed time series plots that show the May 6 ozone concentrations in historical context at each affected monitoring site for both 2020 and the past five years.
- Compiled maps of ozone and water vapor in the area from satellite data.
- Retrieved total column ozone from Modern Era Retrospective Analysis for Research and Analysis, Version 2 (MERRA-2) and Ozone Mapping and Profile Suite (OMPS) instrument aboard the Suomi NPP satellite.
- Provided evidence of a stratospheric intrusion event over the northwest U.S. and eastern Pacific using model results of IPV, relative humidity (RH), and potential vorticity (PV) at 250 hPa using the Global Forecast System (GFS).
- Provided model results and cross sections of ozone and CO concentrations using the Realtime Air Quality Modelling System (RAQMS).
- Provided model results of ozone at 500 hPa height using the NCAR Whole Atmosphere Community Climate Model (WACCM).
- Provided surface and upper-level (500 hPa) meteorological maps using the North American Surface Analysis.

- Provided boundary layer depth analysis on the EE day using North American Mesoscale (NAM) data and the UCAR Integrated Data Viewer (IDV).
- Showed the transport patterns of stratospheric ozone from the intrusion location to the Clark County region via the Hybrid Single-Particle Lagrangian Integrated Trajectory (HYSPLIT) model.
- Performed statistical analysis to compare event ozone concentrations to non-event concentrations.
- Developed plots to show diurnal patterns of ozone and supporting pollutants such as RH and NO_x.
- Assessed vertical transport of stratospheric ozone using Tunable Optical Profiler for Aerosol and Ozone (TOPAZ) Light Detection and Ranging (LIDAR) measurements from the National Oceanic and Atmospheric Administration's (NOAA) Chemical Sciences Laboratory site in Boulder, CO.
- Created a GAM model of MDA8 ozone concentrations to assess the enhancement of ozone concentrations at the impacted monitors due to the transported stratospheric ozone.

1.4 Conceptual Model

The conceptual model for the exceptional event on May 6, 2020, leading to the ozone exceedances at the Walter Johnson, Paul Meyer, Joe Neal, Jerome Mack, Green Valley, Jean, and Apex monitoring sites is outlined in Table 1-5. We provide the analysis techniques performed and evidence for each Tier. This establishes a weight of evidence for the clear causal relationship between a stratospheric intrusion over the eastern Pacific Ocean and the northwestern U.S. and the May 6, 2020, exceptional ozone event. We assert that stratospheric ozone was transported into the upper troposphere over the eastern Pacific Ocean and northern California and Oregon, and subsequently reached Clark County, where it contributed to the ozone exceedances at seven monitoring sites on May 6. In support of this assertion, the key points of evidence for the conceptual model are summarized below.

1. The May 6, 2020, ozone exceedance occurred during a typical ozone season, but event concentrations at the seven exceedance sites were significantly higher than non-event concentrations. Ozone concentrations at all exceedance sites showed high percentile rank and regional enhancements when compared with the past six years and ozone seasons.
2. Multiple atmospheric models (GFS, WACCM, and RAQMS) provide consistent evidence from isentropic potential vorticity, water vapor, and carbon monoxide concentrations for a stratospheric intrusion event that injected ozone-rich stratospheric air into the upper troposphere over the northwestern U.S. and eastern Pacific Ocean on May 4, 2020, at 00:00 UTC. Time series of mid-tropospheric ozone profile simulations from May 4 through the event date indicate a continuous stratospheric-tropospheric ozone tongue that descended in altitude as it was transported from the northwestern U.S. southeastward toward Clark County.
3. Back and forward trajectories from the exceedance sites, at near-surface altitude and the time of maximum ozone concentration, show consistent transport patterns from the mid-troposphere (4-5 km altitude) coinciding with the SOI source and model ozone “tongue” to the boundary layer in Clark County on May 5 and 6, 2020. The lower tropopause heights and deep mixed layer observed upwind on the preceding days and in Clark County on the event day provide evidence for sufficient vertical mixing between the stratosphere, mid-troposphere and the surface.
4. Meteorological conditions on May 6, 2020, did not favor enhanced local ozone production when compared with meteorologically similar ozone season days. Average MDA8 ozone across similar days was well below the ozone NAAQS and >10 ppb lower than the May 6 exceedance.
5. GAM model predictions of MDA8 ozone on May 6 are all well below the 70-ppb ozone NAAQS for each EE-affected site. Using the GAM residuals (observed MDA8 ozone minus GAM-predicted MDA8 ozone) to estimate the effect of the SOI on Clark County, we find a contribution of 10-16 ppb ozone from an atypical source; in this case, likely the stratospheric intrusion in the northwestern U.S.

6. The arrival of dry, SOI influenced air to Clark County coincided with abnormally lower daytime surface absolute humidity on May 6, 2020, in Clark County. nitric oxide (NO) and nitrogen dioxide (NO_2) concentrations were within average levels on May 5 and 6 in Clark County, suggesting that photochemical ozone production was unlikely the only source of the high ozone exceedance event.

2. Historical and Non-Event Model

2.1 Regional Description

Clark County is located in the southern portion of Nevada and borders California and Arizona. Clark County includes the City of Las Vegas, which has a population of approximately 2 million and is one of the fastest growing metropolitan areas in the United States (U.S. Census Bureau, 2010). Las Vegas is located in a 1,600 km^2 desert valley basin at 500 to 900 m above sea level (Langford et al., 2015). It is surrounded by the Spring Mountains to the west (3,000 m elevation) and the Sheep Mountain Range to the north (2,500 m elevation), and three mountain ranges to the south. The valley floor slopes downward from west to east, which influences surface wind, temperature, precipitation, and runoff patterns. The Cajon Pass and I-15 corridor to the west is an important atmospheric transport pathway from the Los Angeles Basin into the Las Vegas Valley (Langford et al., 2015). **Figures 2-1 and 2-2** show the topography of the Clark County area and surrounding areas.

The Las Vegas Valley climatology features abundant sunshine and hot summertime temperatures, with average summer month high temperatures of 34-40°C. Because of the mountain barriers to moisture inflow, the region experiences dry conditions year-round (~107 mm annual precipitation, 22% of which occurs during the summer monsoon season in July through September). The urban heat island effect in Las Vegas during the summer leads to large temperature gradients within the valley, with generally cooler temperatures on the eastern side. During the summer season, monsoon moisture brings high humidity and thunderstorms to the region, typically in July and August (National Weather Service Forecast Office, 2020). Winds in the Las Vegas basin tend to be out of the southwest (from Los Angeles) during the spring and summer; winds in the fall and winter tend to be out of the northwest, with air transported between the neighboring mountain ranges and along the valley.

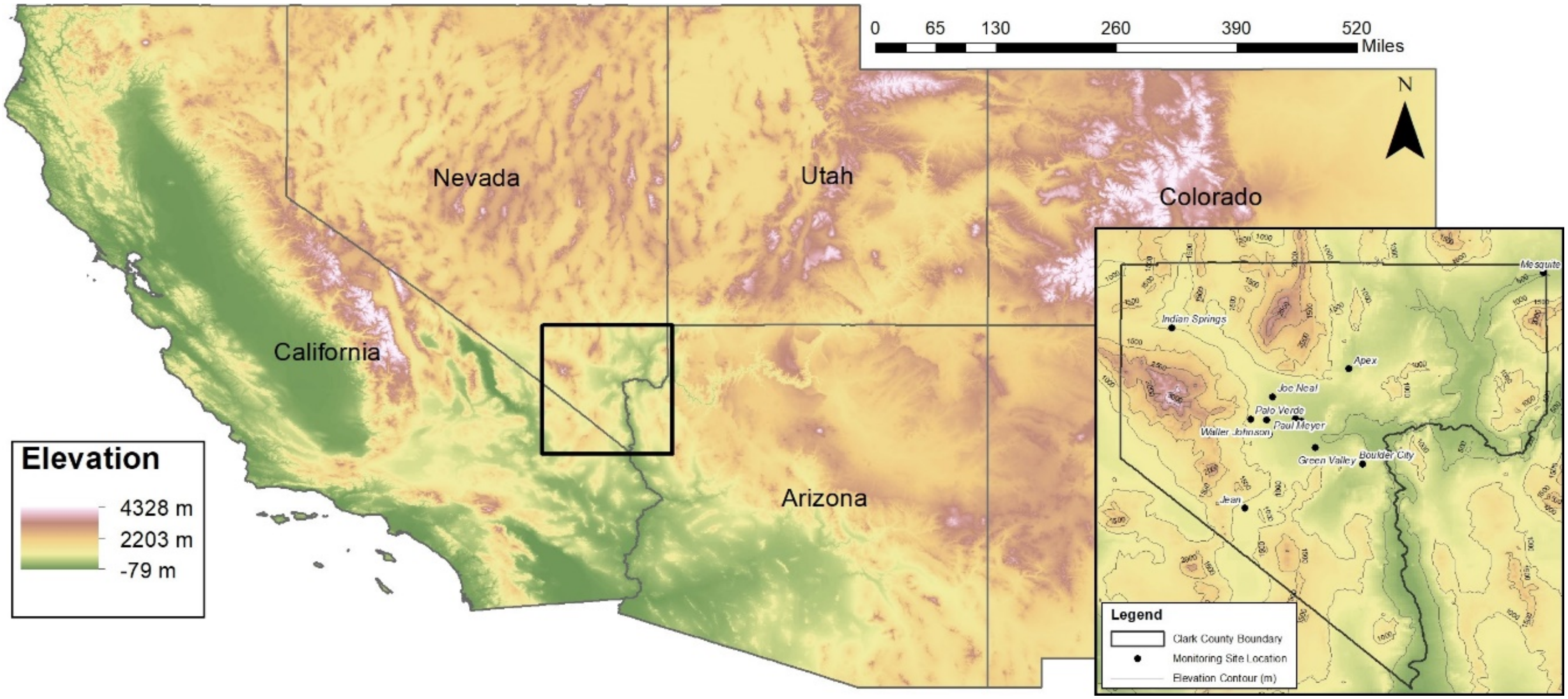

Figure 2-1. Regional topography around Clark County, with an inset showing the county boundaries and the air quality monitoring sites analyzed in this report.

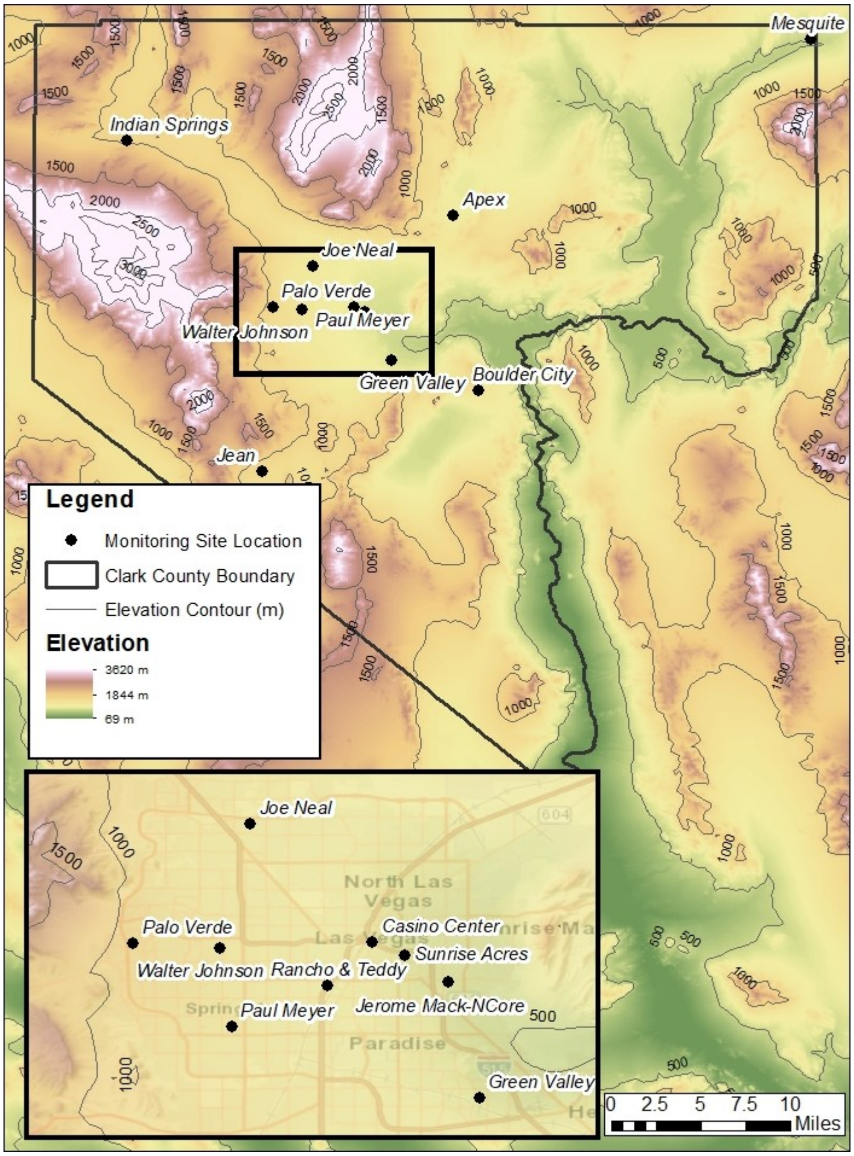

Figure 2-2. Clark County topography, with an inset showing air quality monitoring sites that measure ozone in the Clark County area.

2.2 Overview of Monitoring Network

The Clark County Department of Environment and Sustainability, Division of Air Quality (DAQ), operated 14 ambient air monitoring sites in the region during 2020 (shown in Figure 2-2). These sites measure hourly ozone, particulate matter with a diameter less than 2.5 micrometers ($PM_{2.5}$), particulate matter with a diameter less than 10 micrometers (PM_{10}), NO_x, total nonmethane organic compounds (TNMOC), and CO concentrations along with meteorological parameters. Table 2-1 presents the monitoring data coverage for all the monitoring sites used in this report across time and space for criteria pollutants, surface meteorological parameters (barometric pressure, temperature, wind speed, and direction), and mixing height. We examined ozone and other criteria pollutants at 11 sites around Clark County to investigate the high ozone event observed on May 6, and Table 1-1 shows the seven monitoring sites that are investigated for NAAQS ozone exceedances due to a stratospheric ozone intrusion. DAQ’s ambient air monitoring network meets the monitoring requirements for criteria pollutants pursuant to Title 40, Part 58, of the Code of Federal Regulations (CFR), Appendix D (Code of Federal Regulations, 1997). Data are quality-assured in accordance with 40 CFR 58 and submitted to the EPA’s AQS. The spatial distribution of the monitoring sites characterizes the regional air quality in Las Vegas, as well as air quality upwind and downwind of the urban valley region (Figure 2-2). The Jean monitoring site along the I-15 corridor is generally upwind such that it captures atmospheric transport into the region and is least impacted by local sources.

Table 2-1. Clark County monitoring site data. The available date ranges of all parameters and monitoring sites used in this report are shown for Clark County, Nevada.

Site	AQS Sitecode	O_3	$PM_{2.5}$	CO	NO	NO_2	TNMOC	Temp.	Wind Speed	Wind Direction	Barom. Pressure	Mixing Height
Apex	320030022	2014-2020						2014-2020	2014-2020	2014-2020		
Boulder City	320030601	2014-2020									2014-2016	
Casino Center	320031502							2014-2020	2016-2020	2016-2020		
Green Valley	320030298	2015-2020	2014-2020	2020				2016-2020	2014-2020	2014-2020	2014-2016	
Indian Springs	320037772	2014-2020										
Jean	320031019	2014-2020	2014-2020					2014-2020	2014-2020	2014-2020	2014-2016	
Jerome Mack	320030540	2014-2020	2014-2020	2015-2020[1,2]	2015-2020	2015-2020	2020	2014-2020	2014-2020	2014-2020	2014-2020	2020
Joe Neal	320030075	2020	2018-2020	2019-2020		2015-2020		2014-2020	2014-2020	2014-2020	2014-2016	
Mesquite	320030023	2014-2020						2014-2020	2014-2020	2014-2020		
Palo Verde	320030073	2014-2020	2020					2014-2020	2014-2020	2014-2020	2014-2016	
Paul Meyer	320030043	2014-2020	2017-2020					2014-2020	2014-2020	2014-2020	2014-2016	
RT	320031501							2015-2020	2015-2020	2015-2020	2014-2016	
Sunrise Acres	320030561			2020				2014-2020	2014-2020	2014-2020	2014-2016	
Walter Johnson	320030071	2014-2020	2020					2015-2020	2015-2020	2015-2020	2014-2016	

[1] CO data invalid at Jerome Mack on Sep. 2, 2020

[2] CO data invalid at Jerome Mack Apr. 28, 2020 – May 20, 2020

2.3 Characteristics of Non-Event Historical O_3 Formation

During the ozone season (April–September) in Clark County, ozone concentrations are typically influenced by local formation, transport into the region, and on occasion by EEs such as wildfires and stratospheric intrusions. Transport from upwind source regions (e.g., the Los Angeles Basin, Mojave Desert, Asia) occurs with southwesterly winds, and southerly transport dominates the later portion of the season due to the summer monsoon (Langford et al., 2015; Zhang et al., 2020). Local precursor emissions in Clark County include mobile NO_x and volatile organic compound (VOC) sources, natural-gas fueled power generation NO_x sources, and biogenic VOC emissions. Based on 2017 Las Vegas emission inventories, on a typical ozone season weekday there are 98 tons of NO_x emissions per day and 238 tons of VOC emissions per day (Clark County Department of Environment and Sustainability, 2020). On-road mobile sources comprise 40% of NO_x emissions and total mobile emissions comprise 88% of total NO_x emissions during the ozone season. In contrast, 52% of VOC emissions originate from biogenic sources within Clark County. Local emissions and/or precursors transported into the region contribute to ozone formation within Clark County (Langford et al., 2015; Clark County Department of Air Quality, 2019).

Stratospheric ozone intrusion events over the western U.S. have impacted Clark County when stratospheric ozone mixes with regional pollutants and local photochemical ozone leading to exceedance events (Zhang et al., 2020). The 2017 Fires, Asian, and Stratospheric Transport-Las Vegas Ozone Study (FAST-LVOS) provides evidence for April, May, and June stratospheric intrusion events impacting ozone in Clark County (Zhang et al., 2020). Figure 2-3 depicts contributions of stratospheric ozone (stratospheric O_3 tracer (O3Strat) and non-anthropogenic ozone to MDA8 surface O_3 concentrations across the western U.S. from the NOAA GFDL AM4 model on two exemplary SOI events in April and May 2017. AM4 model results generally agree well with observations, and show reduced ozone biases compared with AM3. O3Strat tracks ozone of stratospheric origin, and its anomaly can be used qualitatively because it is subject to tropospheric chemical and depositional losses. Based on the FAST-LVOS study, Clark County typically experiences episodes with elevated O3Strat of 20–40 ppbv above April-June mean O3Strat ozone and larger non-anthropogenic ozone contributions. The exceedance event examples in Figure 2-3 show 5 and 15 ppb O3Strat anomalies along with ~60 ppb ozone contributed from non-anthropogenic sources. Overall, stratospheric ozone intrusions can play a large role in ozone exceedances during April through June in the Clark County area.

Typical SOI events in Clark County occur under similar meteorological conditions as those on May 6, 2020. The LVOS study ozone exceedances occurred during periods with south-southwest winds and dry air (Langford, 2014), similar to the meteorological conditions on May 6 in Clark County. These meteorological conditions are typical for late spring ozone exceedances and well-documented in the LVOS and FAST-LVOS study periods.

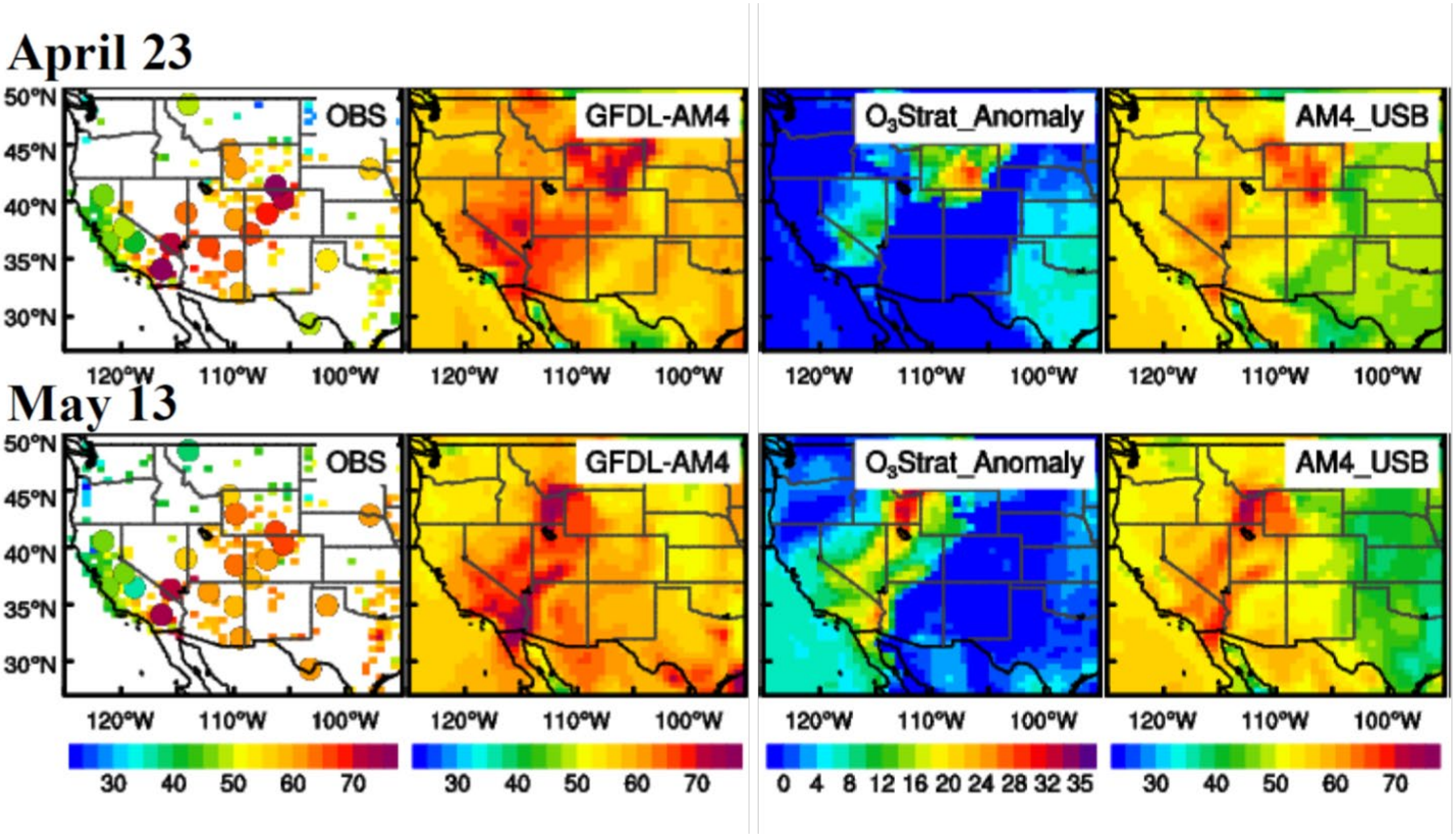

Figure 2-3. Observed (left) and NOAA GFDL AM4 modeled MDA8 ozone, along with stratospheric ozone tracer anomaly in AM4 relative to monthly means (O3Strat_Anomaly), and the non-anthropogenic emissions AM4 ozone simulation (AM4_USB). Two examples of stratospheric intrusion influenced days in Clark County are shown during the FASTLVOS study (April 23 and May 13, 2017) Adapted from Figure S6 in Zhang et al. (2020).

In this demonstration, we discuss the impacts of a stratospheric intrusion event on ozone concentrations in Clark County on May 6, 2020. In order to fully discern the effect of the stratospheric intrusion on ozone concentrations in Clark County on this date, we examine the historical ozone record for all affected sites (Table 1). *Non-event days* refer to all days other than the May 6 event. Because percentile rankings are sensitive to including the relatively large number of potential EE days during 2018 and 2020, we also provide statistics *excluding potential EE days* (i.e., without including the 2018 and 2020 potential EE days as defined in Tables 1-2 and 1-3 in Section 1). The 8-hour ozone design value (DV) is the three-year running average of the fourth-highest MDA8 ozone concentration (U.S. Environmental Protection Agency, 2015). Within Clark County, Las Vegas is classified as an EPA Region 9 marginal nonattainment region, with a 73 ppb ozone DV for 2017-2019 (U.S. Environmental Protection Agency, 2020). Ozone EE days are identified as days with significant wildfire or stratospheric intrusion influence in addition to an MDA8 concentration greater than 70 ppb. By this criterion, 15 possible EE days in 2018 and 13 possible EE days in 2020 were identified, with no EE days in 2019 identified.

The May 6, 2020, EE occurred early in the ozone season under hot, dry air conditions with a deep mixed layer and surface level trough of low pressure over Clark County. These meteorological conditions, which are often associated with a typical high ozone day (non-event conceptual model), favor enhanced vertical mixing of free tropospheric air into the boundary layer. Compared with a non-event conceptual model of local precursor emissions contributing to ozone formation at ground level under similar conditions, the May 6 conditions indicate additional transport of free tropospheric air via upper-level west and northwest winds.

Figures 2-4 through 2-17 depict the six-year historical record and seasonality of MDA8 ozone concentrations at each EE affected monitoring site, along with the 99th percentile and NAAQS standard ozone concentrations. May 6 ranks in the top 1% for daily maximum ozone concentration in the six-year historical record at all EE affected sites.

Figure 2-18 depicts a two-week ozone diurnal cycle of 1-hour ozone, beginning one week before the May 6 event and ending one week after. On May 6, daily maximum 1-hour ozone concentrations were the highest at all seven EE affected monitoring sites during this two-week period. The second highest concentrations during this two-week period were on May 9, which is another EE submitted concurrently with this report.

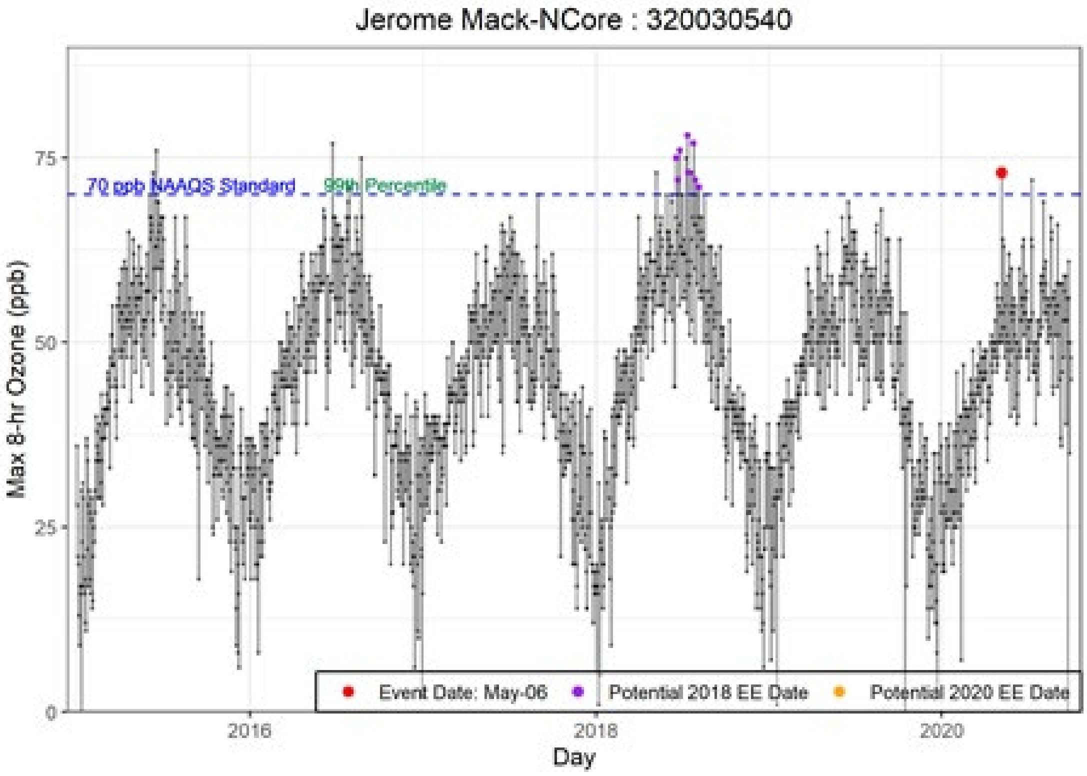

Figure 2-4. Time series of 2015-2020 ozone concentrations at the Jerome Mack-NCore site. May 6, 2020, is shown in red.

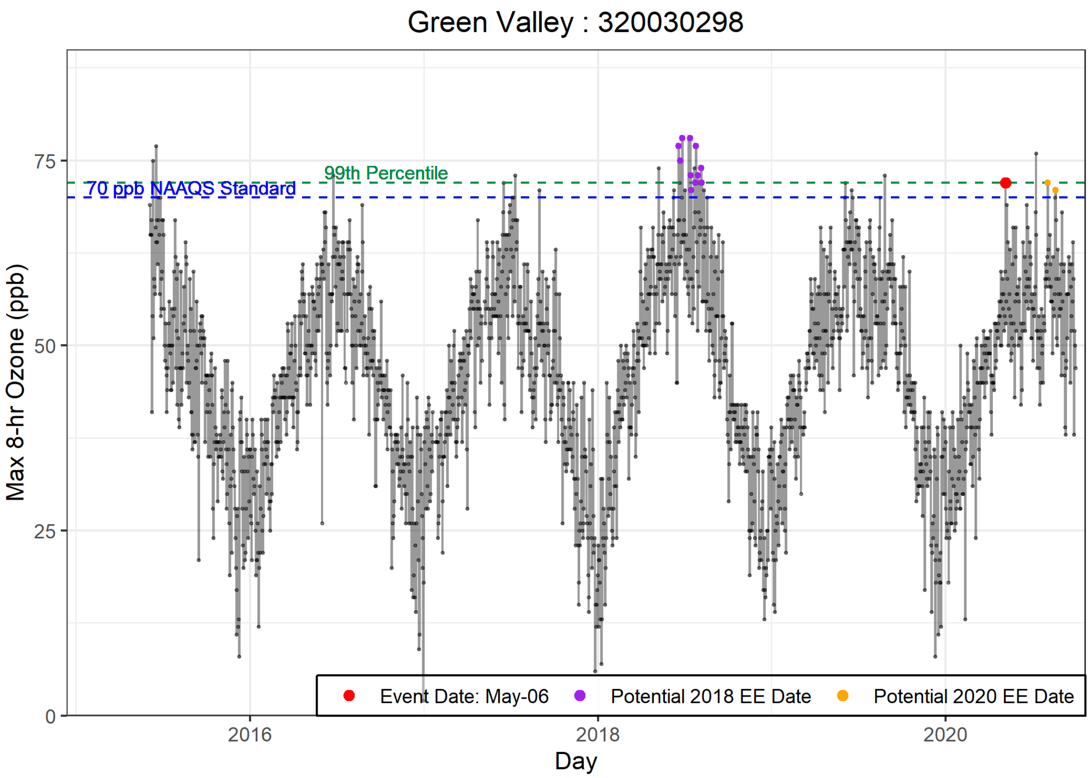

Figure 2-5 Time series of 2015-2020 ozone concentrations at the Green Valley site. May 6, 2020, is shown in red.

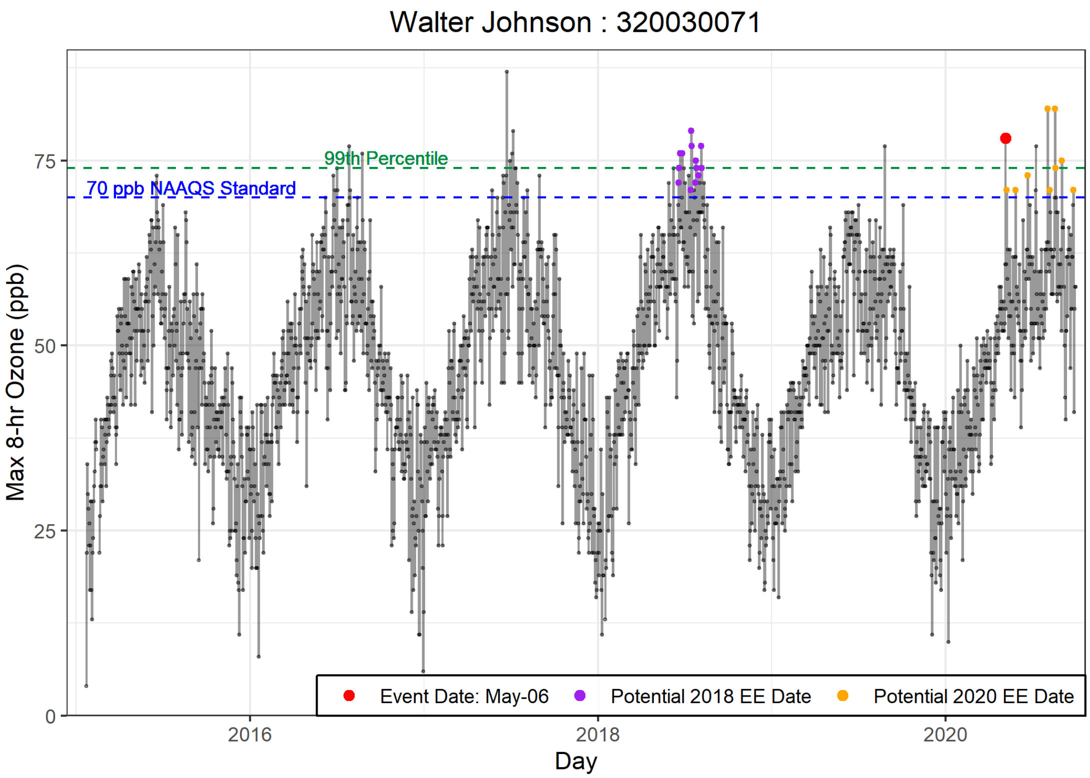

Figure 2-6. Time series of 2015-2020 ozone concentrations at the Walter Johnson site. May 6, 2020, is shown in red.

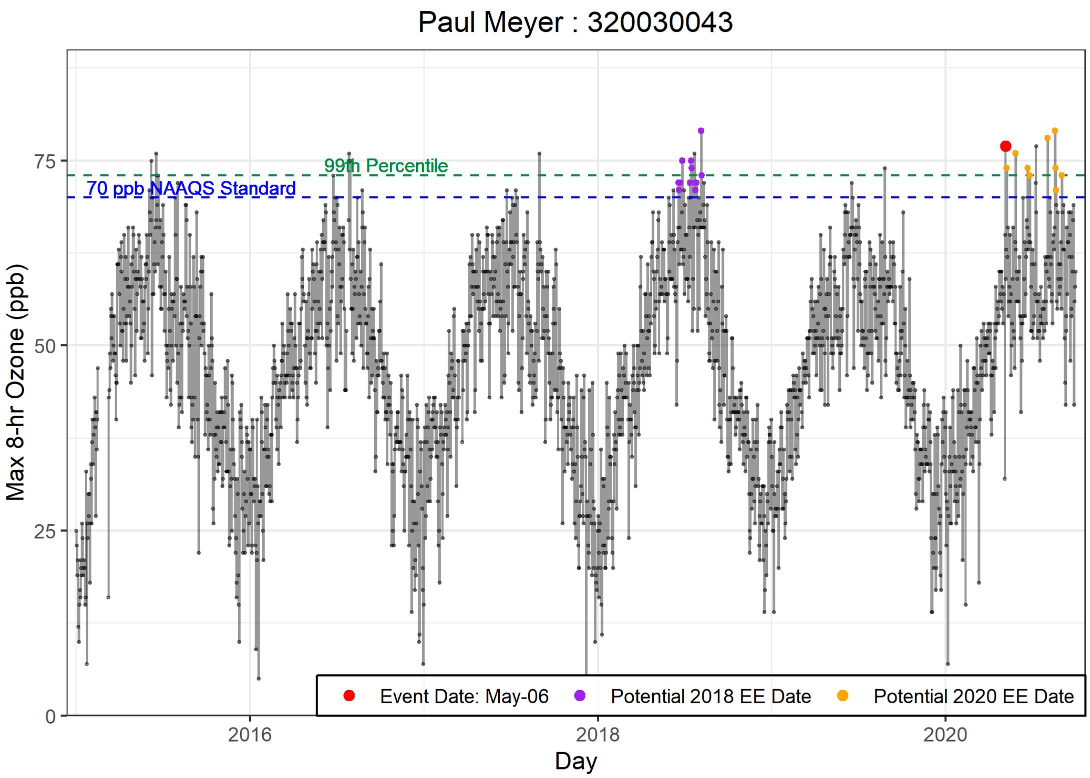

Figure 2-7. Time series of 2015-2020 ozone concentrations at the Paul Meyer site. May 6, 2020, is shown in red.

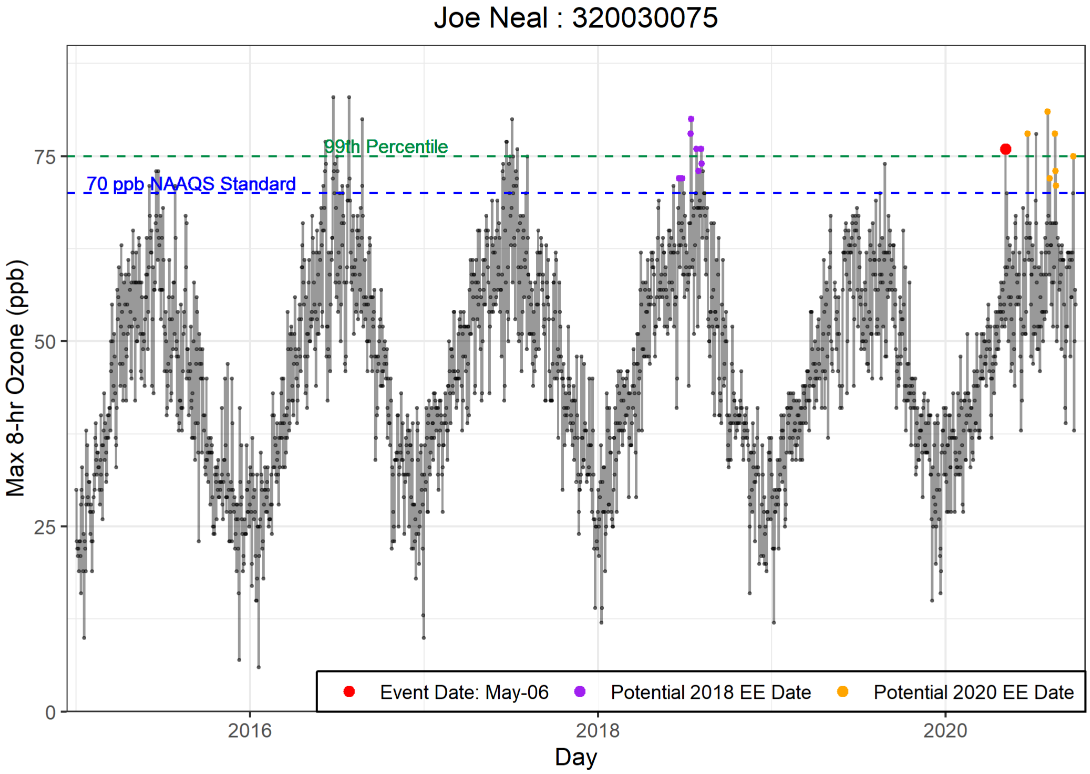

Figure 2-8. Time series of 2015-2020 ozone concentrations at the Joe Neal site. May 6, 2020, is shown in red.

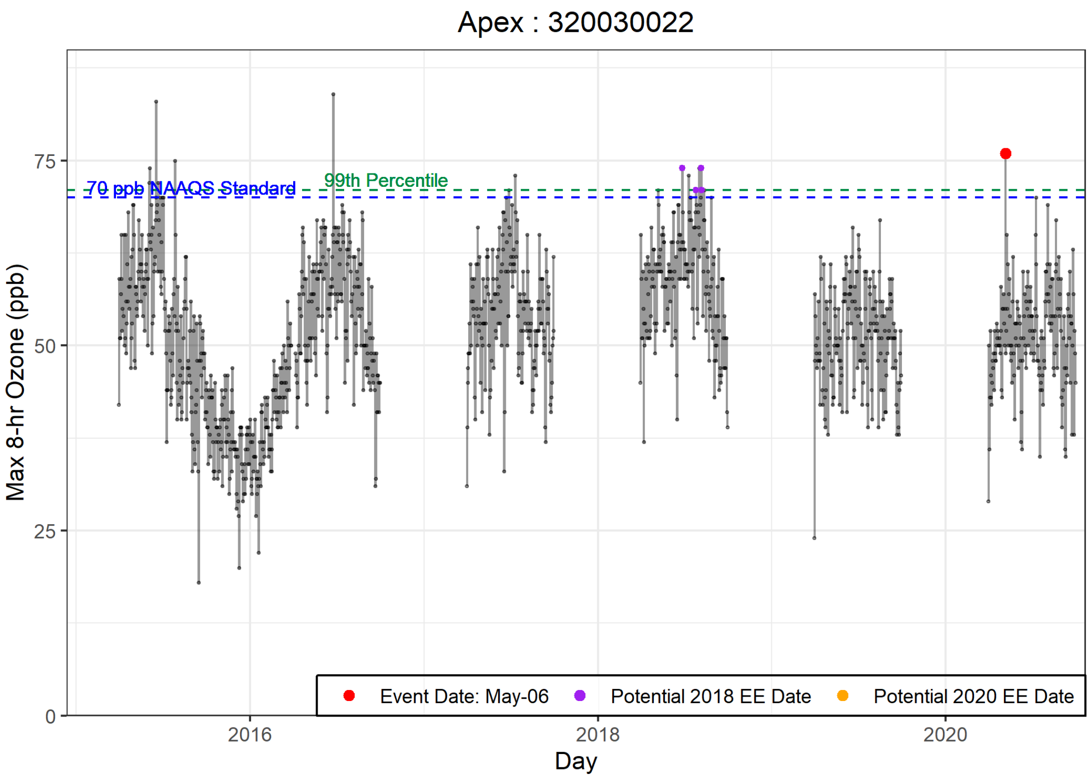

Figure 2-9. Time series of 2015-2020 ozone concentrations at the Apex site. May 6, 2020, is shown in red.

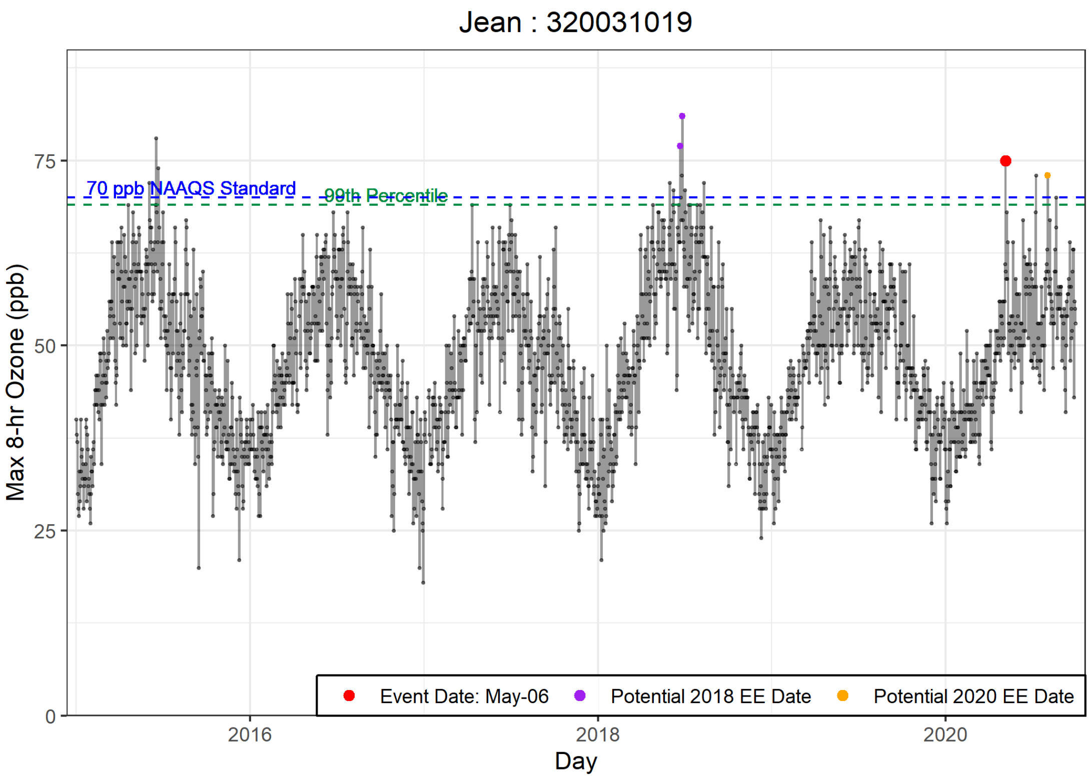

Figure 2-10. Time series of 2015-2020 ozone concentrations at the Jean site. May 6, 2020, is shown in red.

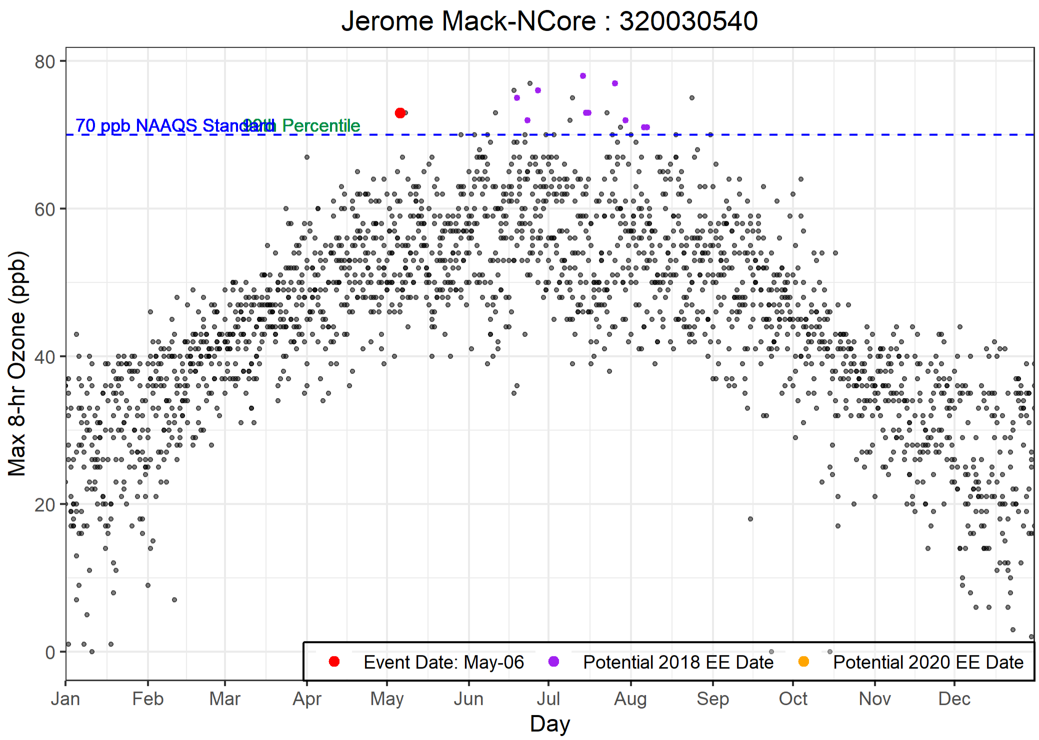

Figure 2-11. Seasonality of 2015-2020 ozone concentrations from the Jerome Mack-NCore site. May 6, 2020, is shown in red.

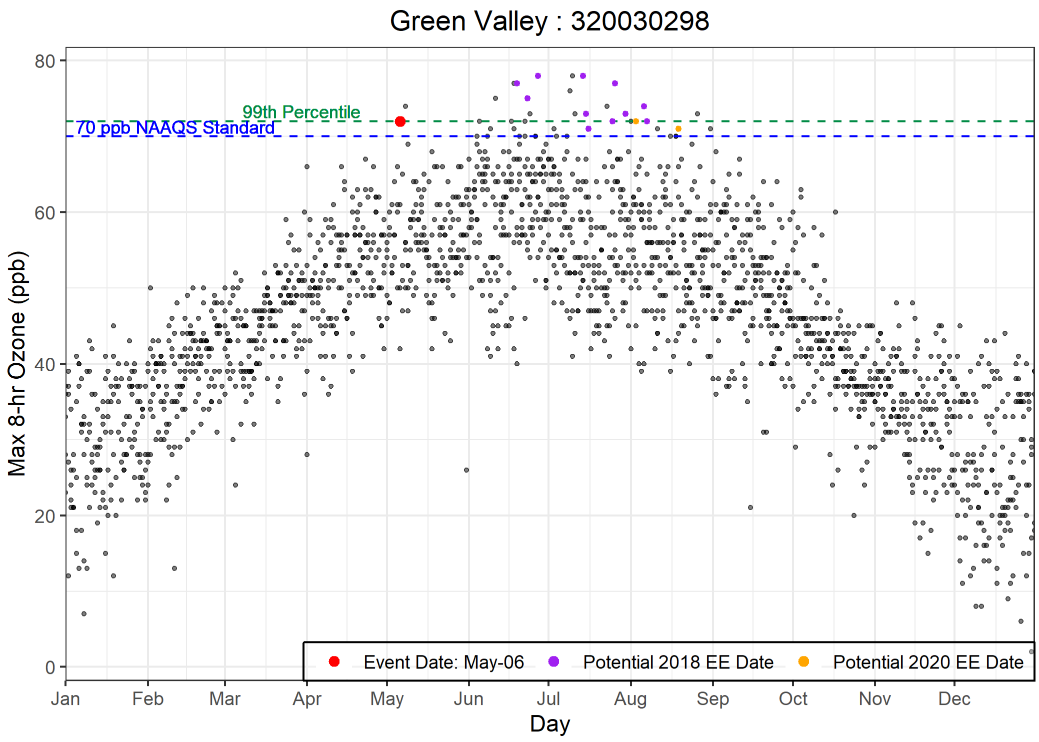

Figure 2-12. Seasonality of 2015-2020 ozone concentrations from the Green Valley site. May 6, 2020, is shown in red.

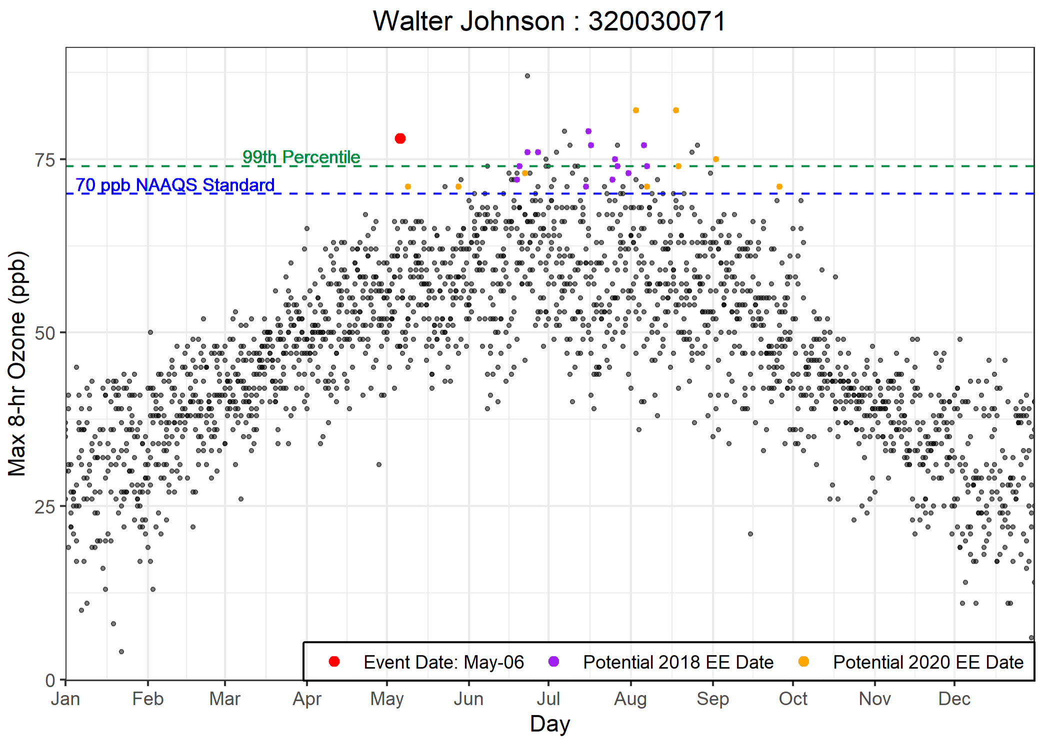

Figure 2-13. Seasonality of 2015-2020 ozone concentrations from the Walter Johnson site. May 6, 2020, is shown in red.

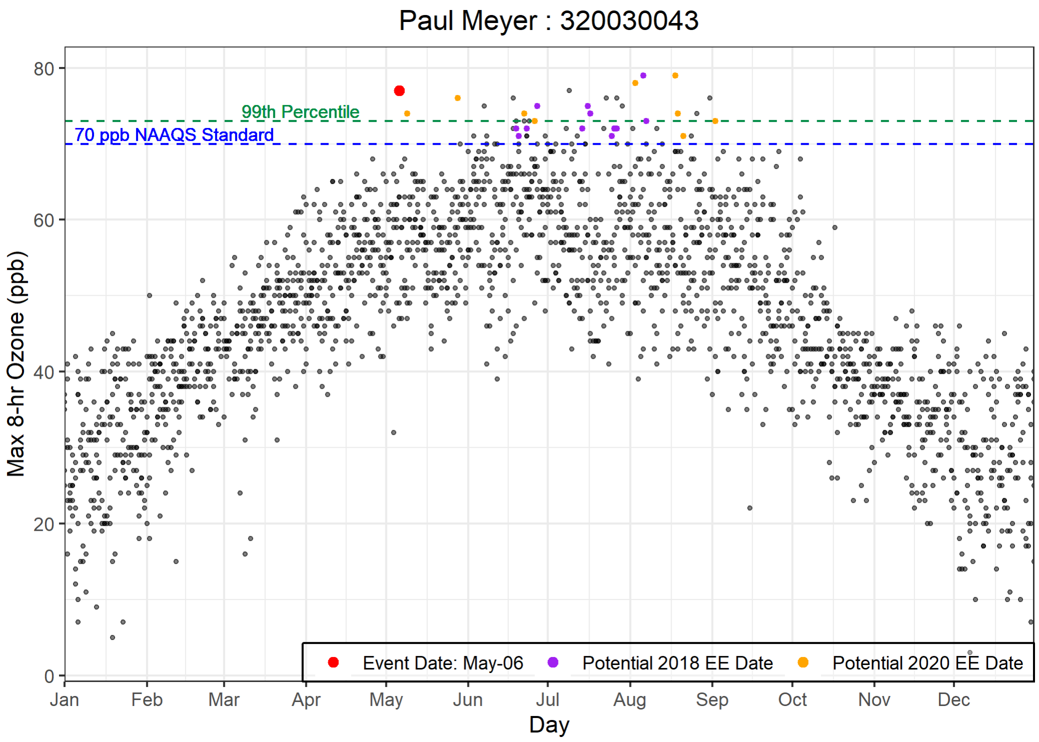

Figure 2-14. Seasonality of 2015-2020 ozone concentrations from the Paul Meyer site. May 6, 2020, is shown in red.

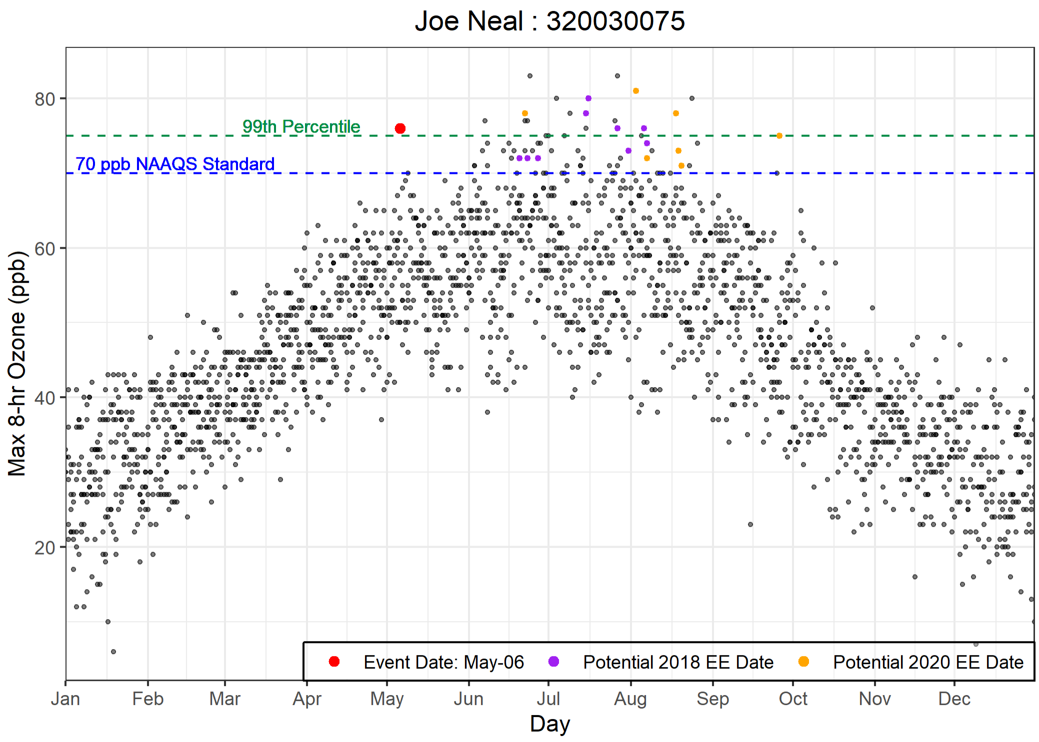

Figure 2-15. Seasonality of 2015-2020 ozone concentrations from the Joe Neal site. May 6, 2020, is shown in red.

Figure 2-16. Seasonality of 2015-2020 ozone concentrations from the Apex site. May 6, 2020, is shown in red.

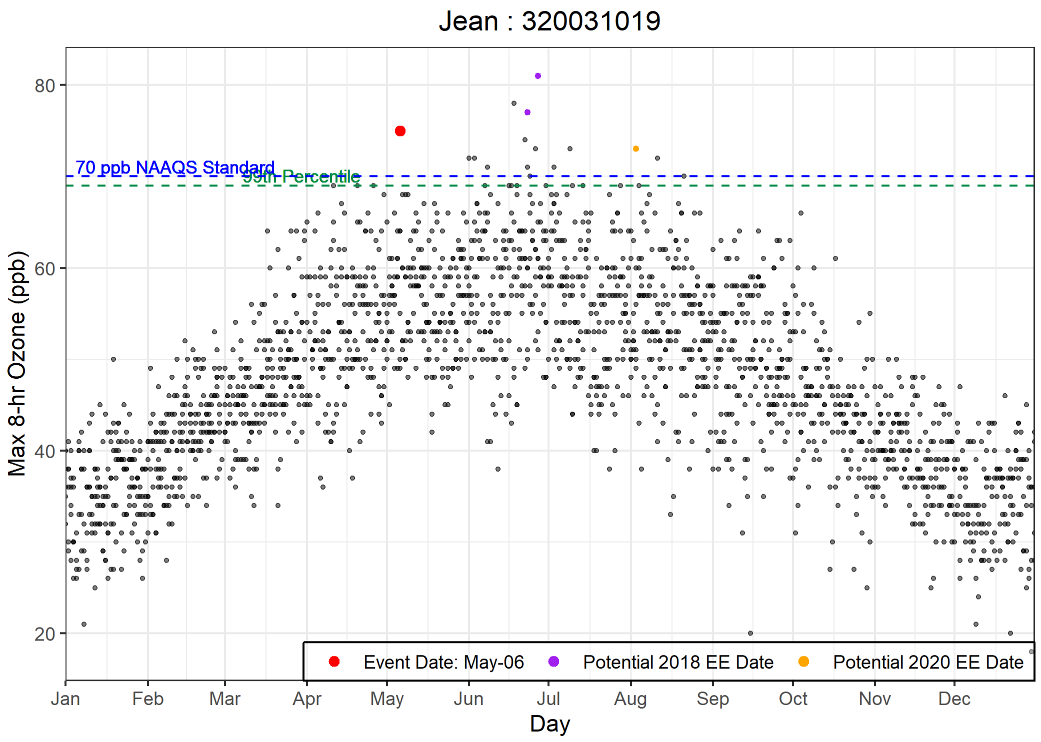

Figure 2-17. Seasonality of 2015-2020 ozone concentrations from the Jean site. May 6, 2020, is shown in red.

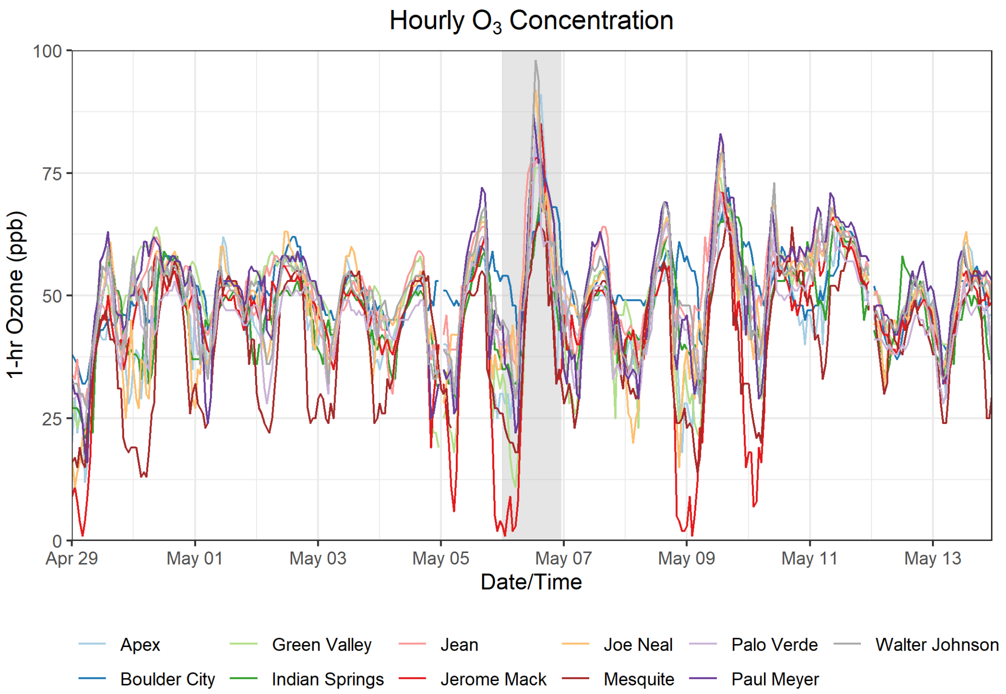

Figure 2-18. Time series of hourly ozone concentrations at all monitoring sites in Clark County for one week before and one week after the May 6, 2020, event. May 6 is shaded for reference.

2.4 Stratospheric Intrusion Event Description

Figure 2-19 shows a basic model of stratospheric-tropospheric mixing and transport of ozone-rich air downwind to an area like Clark County. The basic narrative for these events starts with a stratospheric intrusion of high ozone air into the troposphere, then transport and mixing of the stratospheric-tropospheric air into the free troposphere and PBL, which is eventually mixed to the surface. In this narrative, the city-measured ozone concentration—a combination of anthropogenic and background ozone—can thus be enhanced by the transport of stratospheric ozone into the area. On photochemically active days, the addition of even small quantities of stratospheric ozone can cause ozone concentrations to exceed the NAAQS standards. In order to trace stratospheric air, we can look for the key parameters identified in Figure 2-19. Stratospheric air usually has high ozone concentrations, high IPV, low concentrations of water vapor, and low CO concentrations, while tropospheric air has lower ozone concentrations, low IPV, and may exhibit higher concentrations of water vapor and CO. First, we identify where stratospheric intrusion occurred, as indicated by the above parameters, then show that the stratospheric-tropospheric air mass was transported and mixed to the surface. Table 2-2 identifies the analyses needed to confirm each step of the stratospheric intrusion and transport. Each piece of evidence described in the table is shown in Section 3 and is consistent with the EPA SOI demonstration requirement shown in Table 1-5.

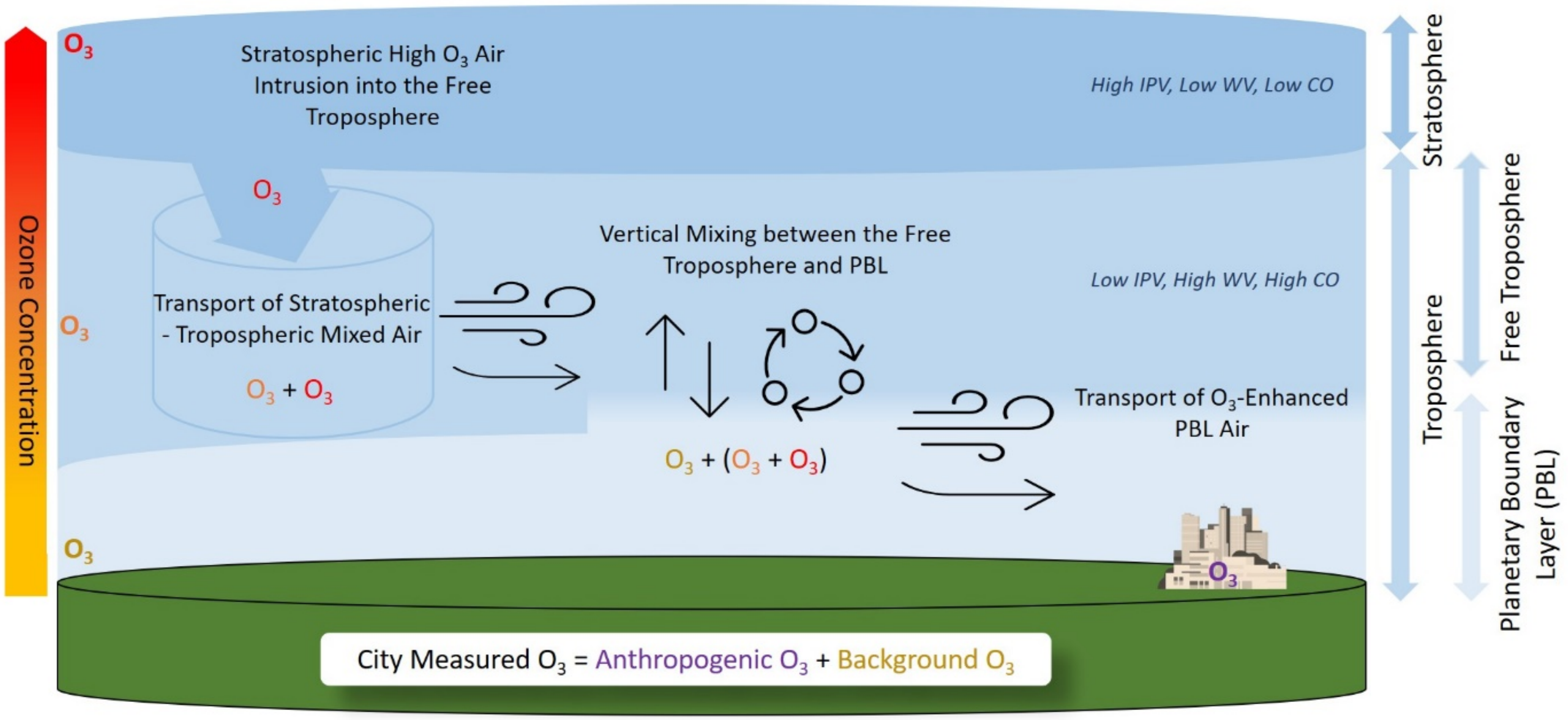

Figure 2-19. Stratospheric intrusion and transport example. Ozone concentration with height is shown on the left, and ozone is colored by each source region to illustrate transport. Tracers for stratospheric and tropospheric air are shown on the right, as well as labels for the different atmospheric layers.

Table 2-2. Transport mechanisms during a stratospheric ozone intrusion (as displayed in Figure 2-19) and evidence needed to determine transport.

Transport of Stratospheric Air	Evidence of Transport
Stratospheric High Ozone Air Intrusion into the Free Troposphere	Potential Vorticity Plots, High Ozone, Low Carbon Monoxide, Low Water Vapor
Transport of Stratospheric – Tropospheric Mixed Air	Upper-Level Meteorology Maps, HYSPLIT Modeling
Vertical Mixing between the Free Troposphere and PBL	Meteorology Maps, Skew-T Diagrams, PBL Height Maps
Transport of Ozone-Enhanced PBL Air	Surface-Level Meteorology Maps, HYSPLIT Modeling, Measured of Ozone, Water Vapor, and NO_X

In this report, we describe evidence of a stratospheric intrusion upwind of Clark County influencing already high ozone levels expected under the non-event conceptual model for May 6, 2020. We detail evidence for (1) stratospheric intrusion into the free troposphere, (2) transport of ozone-rich air in the free troposphere, (3) vertical mixing between the free troposphere and PBL, and (4) mixing into the PBL and surface in Clark County. The meteorological conditions on May 6 (explained in Sections 2.3 and 3.3.3) suggest that local and regional ozone production from surface pollutant precursors should be relatively high. Any additional free tropospheric ozone mixed into the PBL could increase surface concentrations over the 70 ppb NAAQS standard. The key differences between the observed SOI event-related concentration(s) and a typical non-SOI event ozone exceedance are detailed in Section 3.1.

Back trajectories from Clark County (Section 3.3.1) demonstrate that air was transported from the free troposphere over a region from the Pacific Ocean west of northern California to northern California and Oregon. We identified this source region for a possible stratospheric intrusion based on evidence for the exchange of stratospheric and tropospheric air. Specifically, there is evidence for this exchange based on IPV, water vapor mass mixing ratio at 250 hPa pressure level, enhanced ozone, and depleted CO levels in the upper troposphere. Values of water vapor below 0.1 g/kg, CO at or below 100 ppb, and ozone concentrations greater than 60 ppb in the mid-troposphere, can be indicative of stratospheric influence. IPV is a proxy for atmospheric rotation and is a critical indicator for detecting stratospheric intrusion events. Stratospheric air has values of greater than 1 potential vorticity unit (PVU), which are much greater than the IPV of tropospheric air; values remain above 1 even after stratospheric air enters the troposphere. In the source region on May 4 at 00:00 UTC, we see stratospheric air in the upper troposphere with modeled IPV greater than 1 and water vapor mixing ratio less than 0.1 g/kg (Section 3.2.2). High modeled ozone and low modeled CO concentrations are seen in the source region near the tropopause at this same time and location

(Section 3.2.2). The combination of high IPV and ozone concentrations, as well as low water vapor and CO concentrations, provides evidence for a stratospheric intrusion into the free troposphere off the coast of northern California and over northern California and Oregon at ~200-300 hPa level on May 4, 2020, between 00:00 and 23:00 UTC.

Meteorological conditions promoted transport from the source region through the free troposphere to the mixed layer and surface at Clark County. Forward trajectories indicate air was transported from an area to the west of northern California and Oregon at elevated heights over the eastern Pacific Ocean, across California and Nevada, and intersected with the Clark County area at 1000 m AGL (Section 3.3.1). Radiosonde profiles (skew-T diagrams) near the source region observed a relatively low tropopause height (~450 hPa) and upper-level dry air layers (Section 3.3.2). Upper level (500 hPa) and surface weather maps at 7:00 a.m. PST on May 4, 5, and 6 (Section 3.3.3) indicate that source region air masses were transported eastward along an upper-level high-pressure ridge over Oregon and northern Nevada, which promoted subsidence of free tropospheric air towards the deep mixed layers over the region (Section 3.3.2). Surface high pressure north of Clark County and surface low-pressure trough over Clark County were associated with enhanced vertical boundary layer mixing and surface level transport towards Clark County. The skew-T diagram on May 6 at 16:00 PST shows the air temperature profile follows the dry adiabatic lapse rate, indicating a well-mixed, dry layer from the surface up to 650 hPa, corresponding to a mixing height of ~3 km. This deep, well mixed layer over Clark County indicates the potential transport and mixing of ozone to the surface (Section 3.3.3).

The combination of a stratospheric intrusion source region—based on IPV, water vapor, ozone, and CO data—along with trajectories, upper-level and surface weather maps, radiosonde temperature profiles (skew-T diagrams), and modeled mixing heights, provide evidence that the air mass over Clark County on May 6, 2020, had contributions from a region of enhanced upper tropospheric ozone due to stratospheric origin. We cannot rule out contributions from enhanced local or regional photochemical ozone production due to surface precursor emissions in Clark County or upwind. However, statistical (GAM) modeling results provide a way to estimate ozone enhancements from outside sources (e.g., an SOI) and suggest that there was a significant enhancement of ozone concentrations on May 6 (i.e., MDA8 concentrations are predicted to be less than the NAAQS without outside sources). Further detailed meteorology, satellite imagery, and model simulation-based evidence are presented in detail in Section 3.

2.5 Analysis of COVID Restrictions on Ozone

Mobile emission sources decreased throughout the U.S. during the mobility restrictions for the COVID-19 pandemic beginning in mid-March 2020. Because decreases in NO_x emissions from these mobile sources could result in higher ozone concentrations, we evaluate the potential contribution and sensitivity of the COVID shutdown effects on ozone concentrations and MDA8 ozone on EE days. Ozone production has non-linear dependence on precursor emissions of NO_x and VOCs and meteorological conditions. Changes in precursors also can shift photochemical regimes. Thus, the effects of COVID-induced NO_x emission changes on ozone are complex and uncertain (Kroll et al., 2020). Recent studies have found variable ozone responses during lockdowns across countries ranging from −2 to +10% (Venter et al., 2020). Parker et al. (2020) found spatially disparate effects of higher ozone concentrations downwind of Los Angeles and lower concentrations in the western Los Angeles Basin. To evaluate the potential influence of COVID shutdown precursor emission decreases on increases in MDA8 ozone, we compared May 2020 ozone to the historical climatology and compared the GAM residuals during May 2020 with those for the same historical record.

Based on 2017 Las Vegas emission inventories, on-road mobile sources comprise 40% of NOx emissions, and total mobile (vehicle + aviation) emissions comprise 88% of total NO_x emissions for typical ozone season weekdays (Clark County Department of Environment and Sustainability, 2020). In contrast, only 11% of VOC emissions originate from on-road mobile sources. The effects of decreased mobility due to COVID restrictions has a significant effect on total NO_x emissions, but minimal effect on VOC emissions. To determine the time period for these effects, we compared 2020 daily traffic count data from the Nevada Department of Transportation with data from 2019 at 10 monitoring sites (two examples in **Figure 2-20**). On-road traffic activity was significantly reduced from mid-March through early-June 2020 in Clark County compared with 2019. Although aviation activity remained lower than pre-pandemic levels for a longer duration of 2020, commercial aviation represents only 12% of NO_x emissions in Clark County. Thus, the reduced aviation activity had a minimal influence on precursors available for ozone formation from mid-June 2020 onwards. Here we focus on May 2020, the first month of 2020 with EE days.

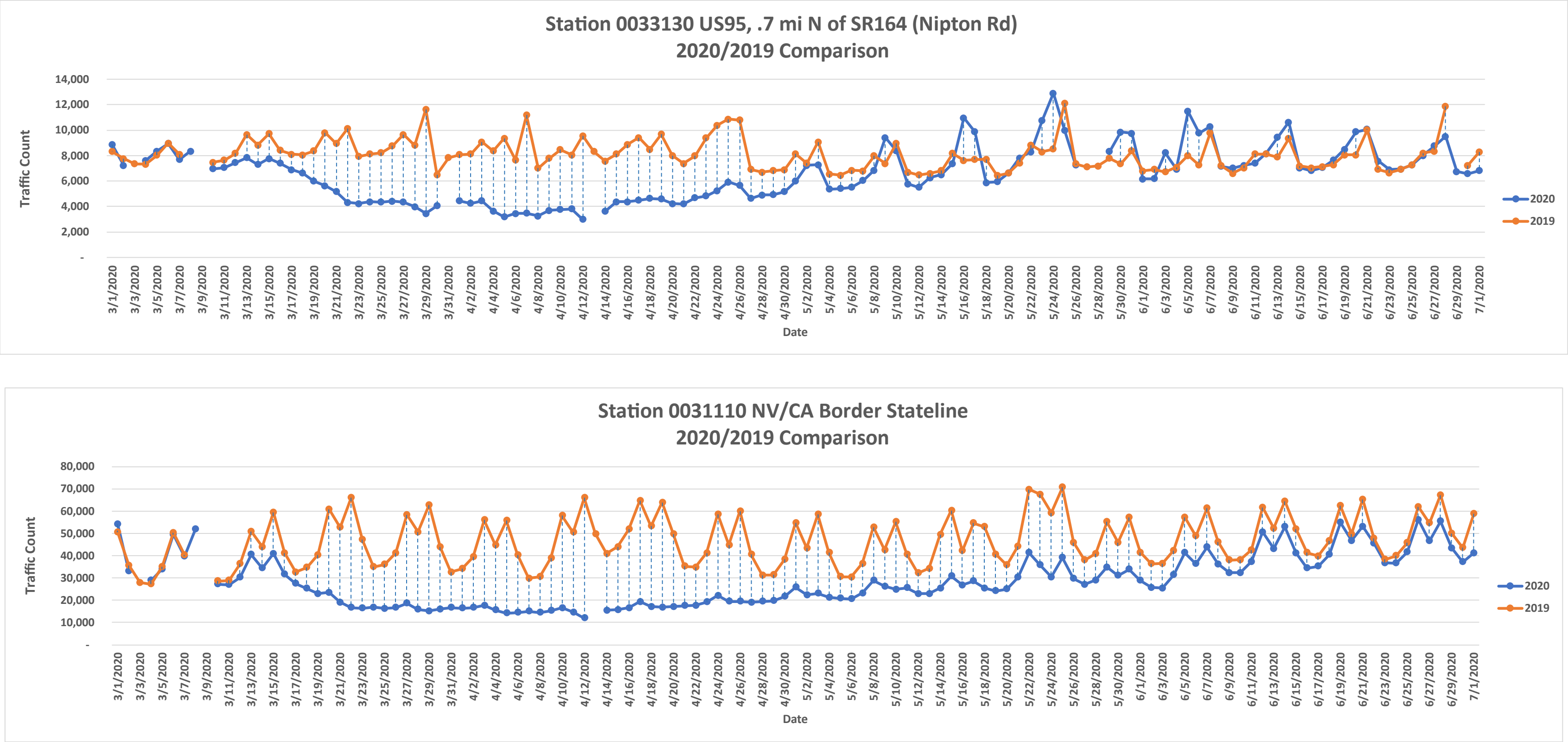
Station 0033130 US95, .7 mi N of SR164 (Nipton Rd)
2020/2019 Comparison

Station 0031110 NV/CA Border Stateline
2020/2019 Comparison

Figure 2-20. Time series of 2020 and 2019 traffic counts at two stations: US95 south of Las Vegas (top) and at the Nevada-California border west of Las Vegas (bottom). Data were provided by the Nevada Department of Transportation.

Two sub-analyses for the ozone comparison to historical climatology were performed. First, we compared the distribution of daily MDA8 ozone during May 2020 with values during each May in the previous five years. Across all EE sites, we found median 2020 MDA8 ozone was not statistically different than any of the previous five years. This is illustrated by the overlap in the 95th confidence intervals of the monthly medians of previous years and the monthly median for 2020 (**Figure 2-21**). Furthermore, monthly median MDA8 ozone during May 2020 was not particularly high (much less than 65 ppb) at all sites despite the EE days. This indicates that the EE day exceedances were extreme episodes that did not affect the monthly median. Thus, the observations do not suggest a month-long high ozone effect due to COVID emission precursor changes. Second, we compared the historical distribution of daily MDA8 ozone during May with the observations during May 2020 (**Figure 2-22**). Across all EE sites, MDA8 ozone on the exceedance days for a given site rank above the confidence interval of the historical daily median MDA8 ozone. Based on these sub-analyses, we conclude that although precursor NO_x emissions decreased during May 2020 due to COVID restrictions, MDA8 ozone concentrations were not statistically higher than previous years, and the EE days cannot be attributed to a consistent month-long increase in ozone concentrations due to the COVID shutdown.

To evaluate the GAM model residuals during the COVID shutdown period, Figure 3-73 provides a more in-depth look at April to May 2020, which were the most heavily affected months. The 95th confidence interval of the median GAM MDA8 residuals (shown by the notches in the box plots) overlap between 2020 and most other years (except 2015 and 2016). The May 2020 median residual with EE days (1.5 ppb) is lower than the typical GAM model uncertainty given by the range of confidence intervals for median residuals at comparable ozone concentrations (+2.9 to 5.3 ppb, Table 3-17). The median GAM residuals during May 2020 were within the typical GAM model error during the previous 5 years.

In summary, although mobile source precursor emissions of NO_x decreased during April and May 2020 due to COVID shutdown restrictions, we did not observe statistically higher ozone concentrations, nor a higher residual in the GAM model, during May 2020. We find consistent evidence across analyses that the EE day ozone concentrations cannot be attributed to an increase in ozone concentrations associated with COVID shutdown periods.

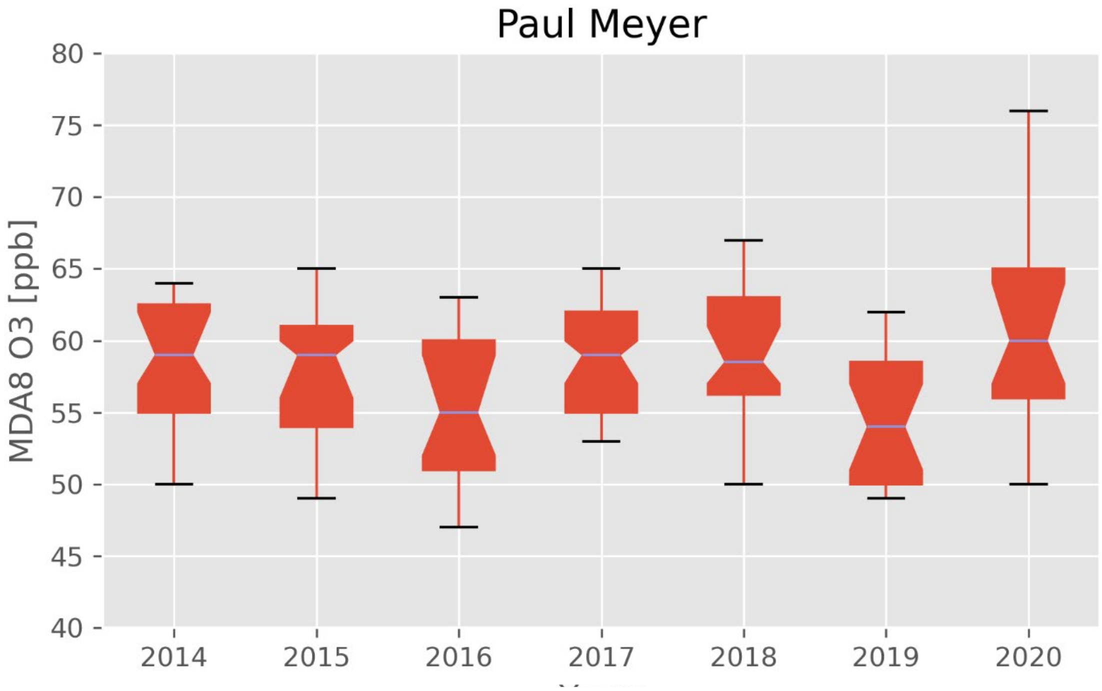

Paul Meyer

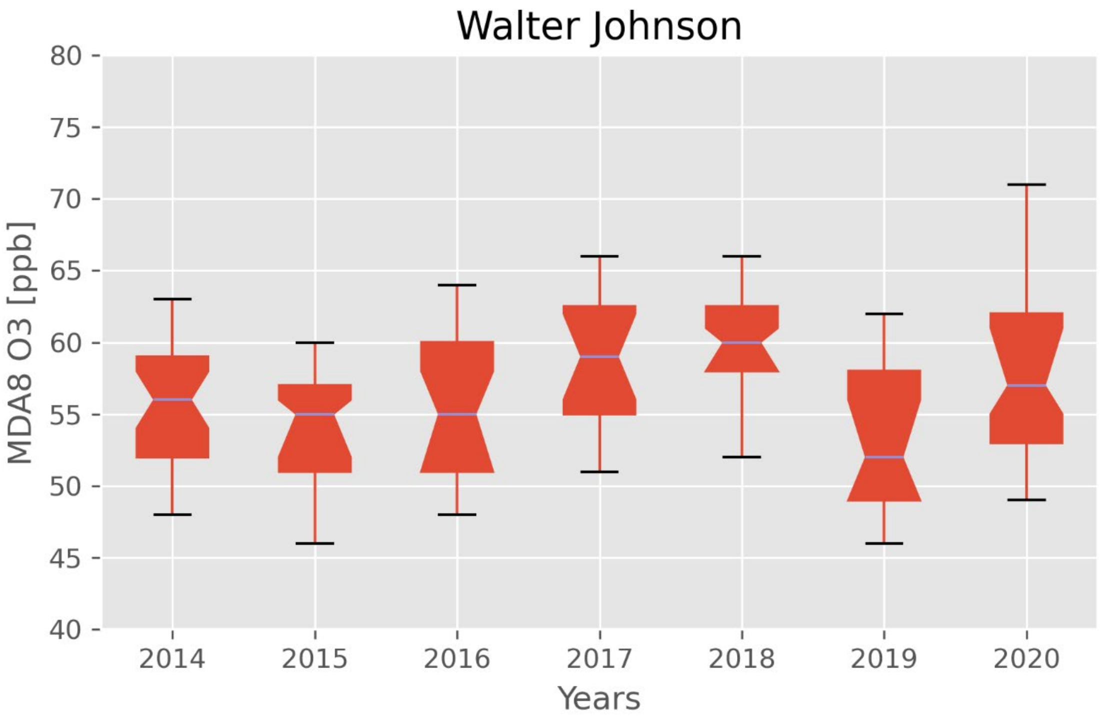

Walter Johnson

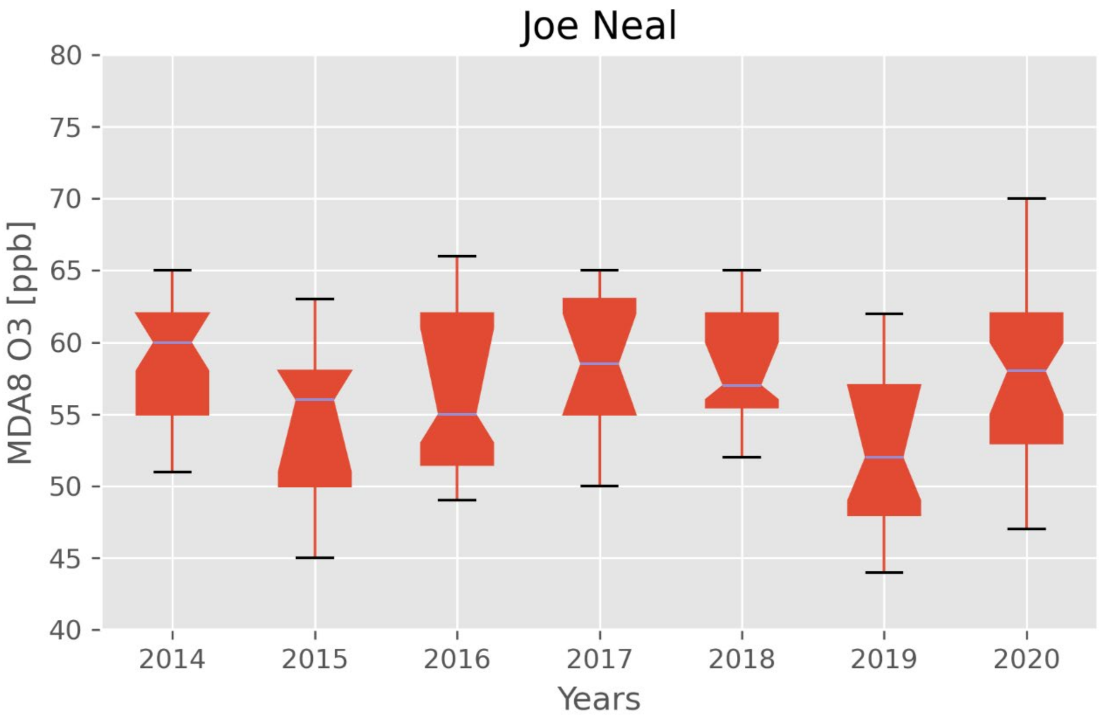
Joe Neal
80
75
70
65
60
55
50
45
40
MDA8 O3 [ppb]
2014
2015
2016
2017
2018
2019
2020
Years

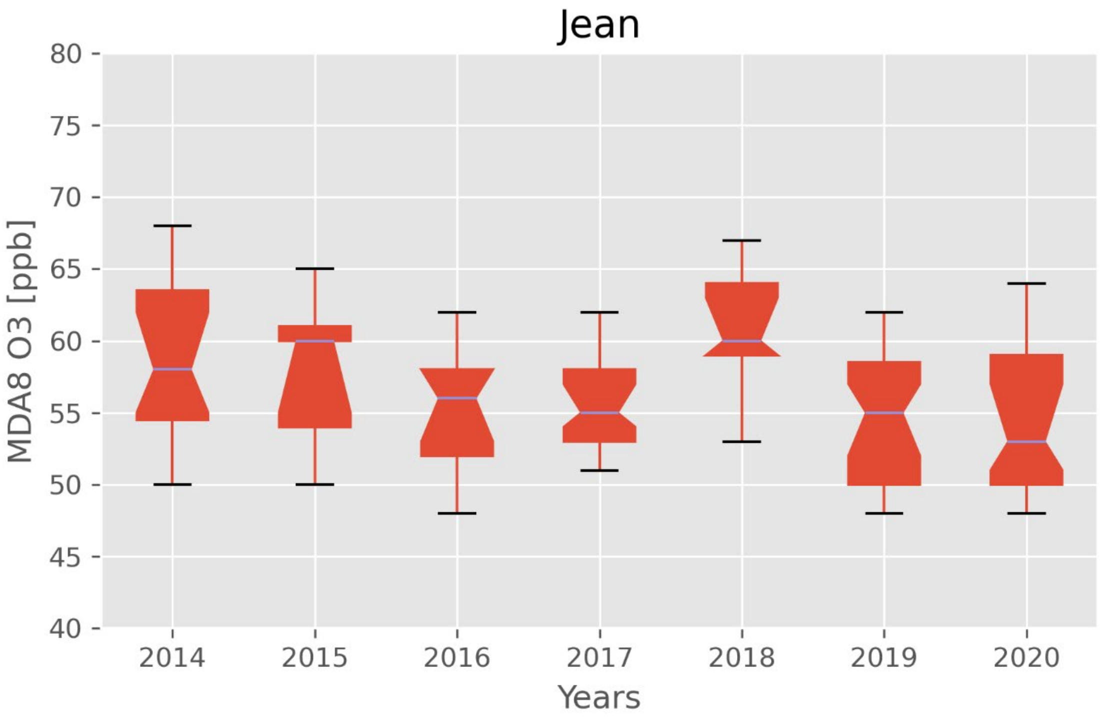
Jean
80
75
70
65
60
55
50
45
40
MDA8 O3 [ppb]
2014
2015
2016
2017
2018
2019
2020
Years

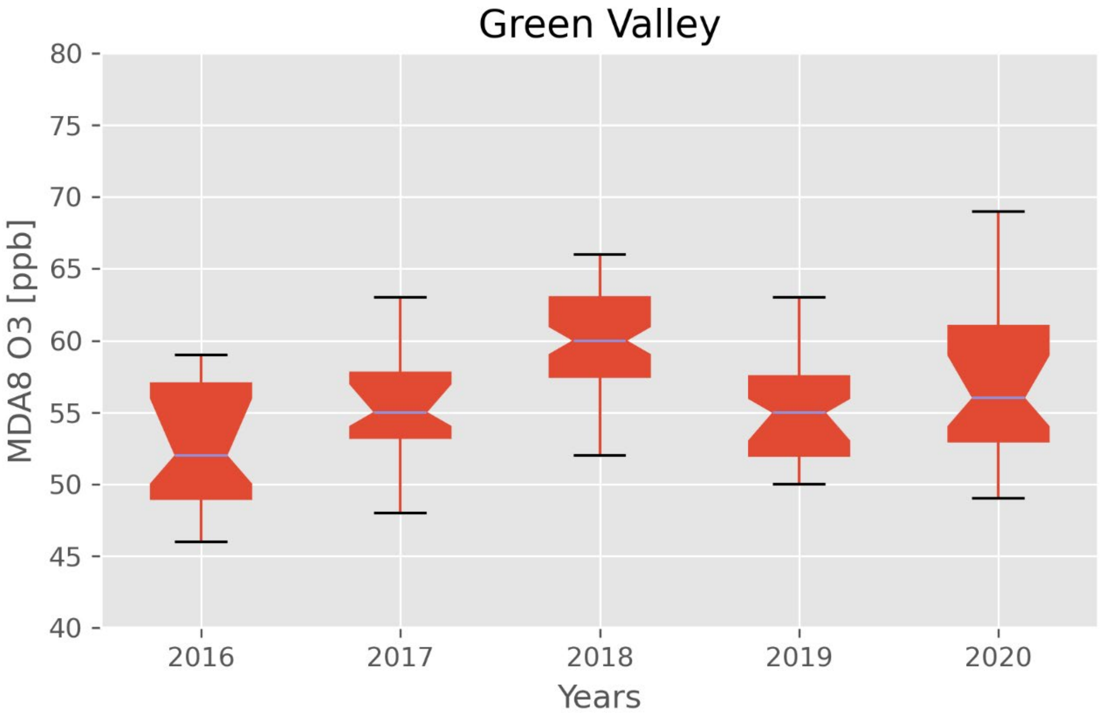

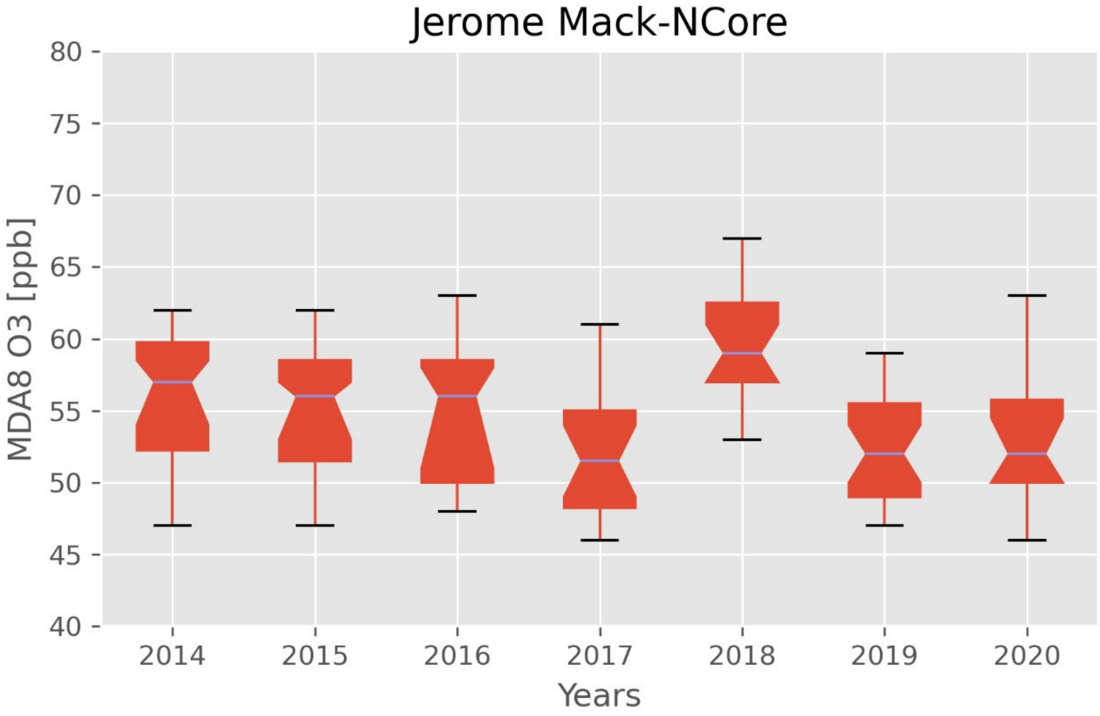

Figure 2-21. Annual May distributions of MDA8 ozone at sites with EEs during May 2020. Notches denote 95th confidence interval of the median, boxes are 25th, 50th, and 75th percentiles, and whiskers are 5th and 95th percentiles.

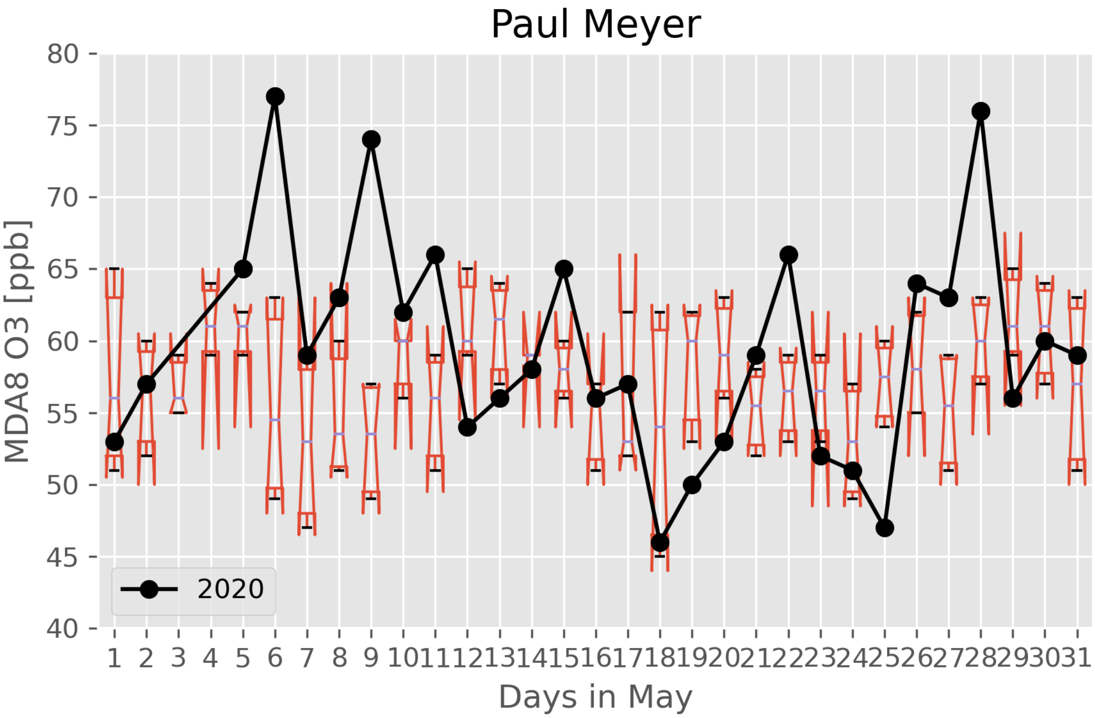
Paul Meyer
MDA8 O3 [ppb]
80
75
70
65
60
55
50
45
40
2020
1 2 3 4 5 6 7 8 9 10 11 12 13 14 15 16 17 18 19 20 21 22 23 24 25 26 27 28 29 30 31
Days in May

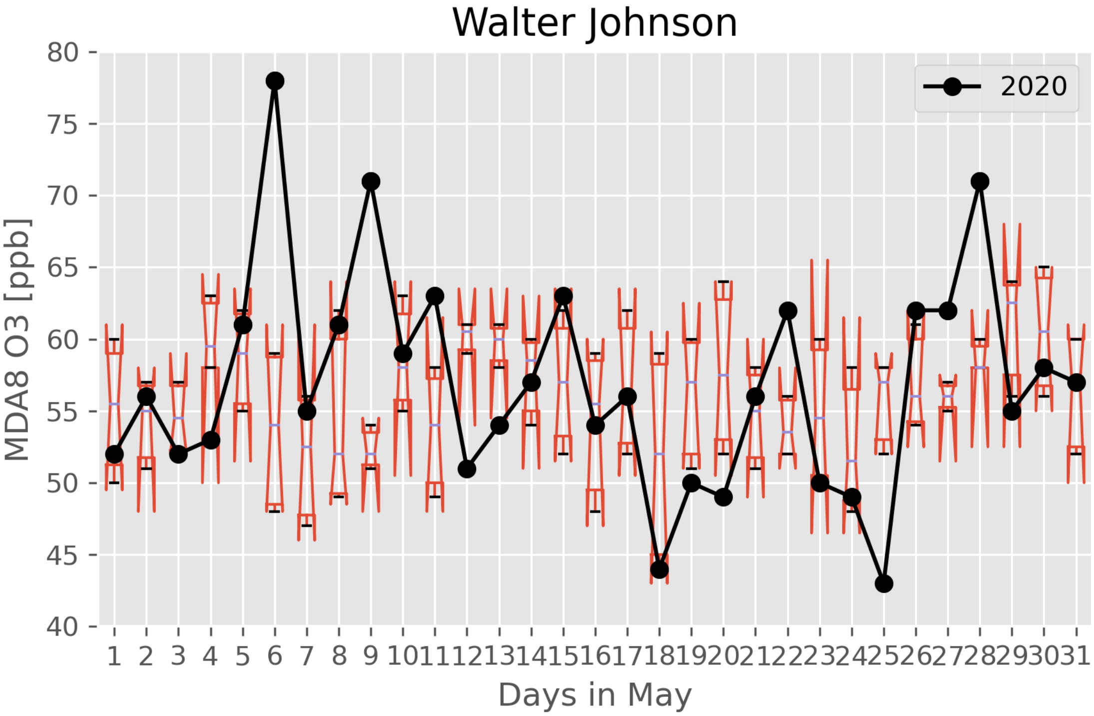
Walter Johnson
MDA8 O3 [ppb]
80
75
70
65
60
55
50
45
40
2020
1 2 3 4 5 6 7 8 9 10 11 12 13 14 15 16 17 18 19 20 21 22 23 24 25 26 27 28 29 30 31
Days in May

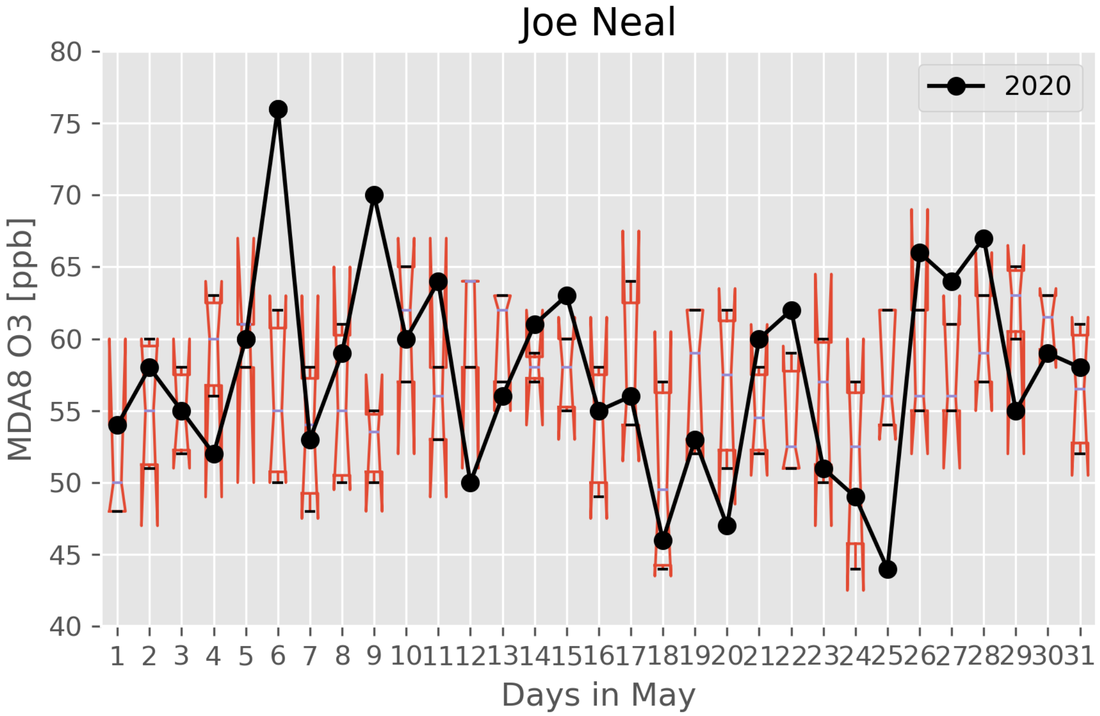
Joe Neal
2020
MDA8 O3 [ppb]
40
45
50
55
60
65
70
75
80
1 2 3 4 5 6 7 8 9 10 11 12 13 14 15 16 17 18 19 20 21 22 23 24 25 26 27 28 29 30 31
Days in May

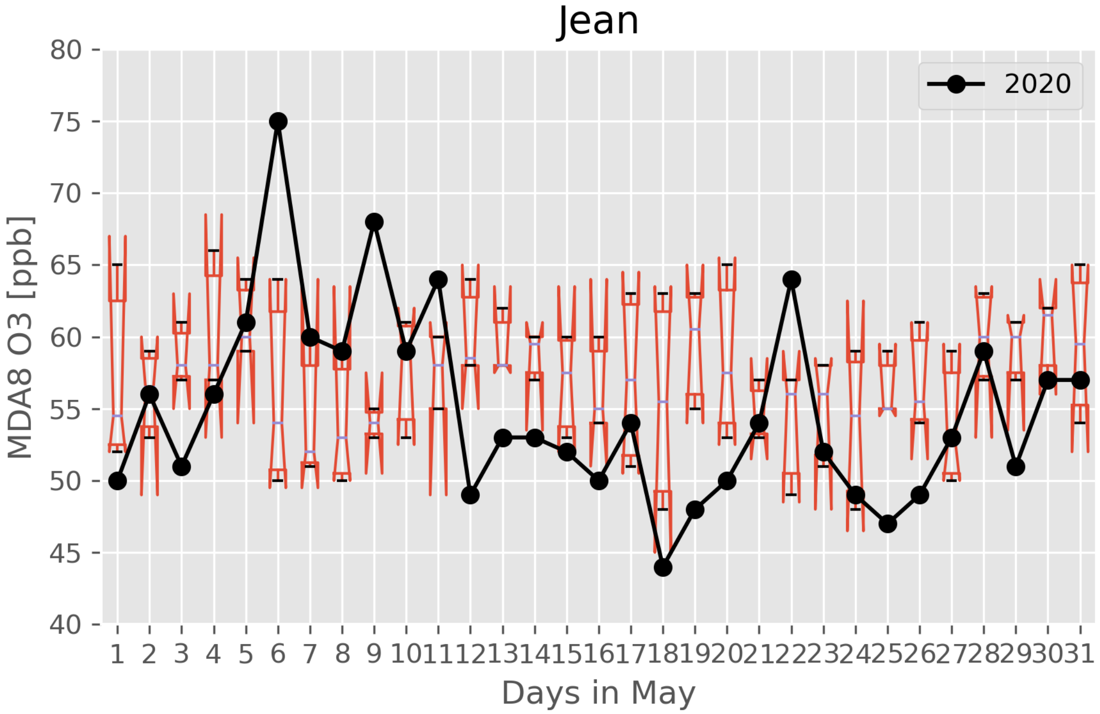
Jean
2020
MDA8 O3 [ppb]
40
45
50
55
60
65
70
75
80
1 2 3 4 5 6 7 8 9 10 11 12 13 14 15 16 17 18 19 20 21 22 23 24 25 26 27 28 29 30 31
Days in May

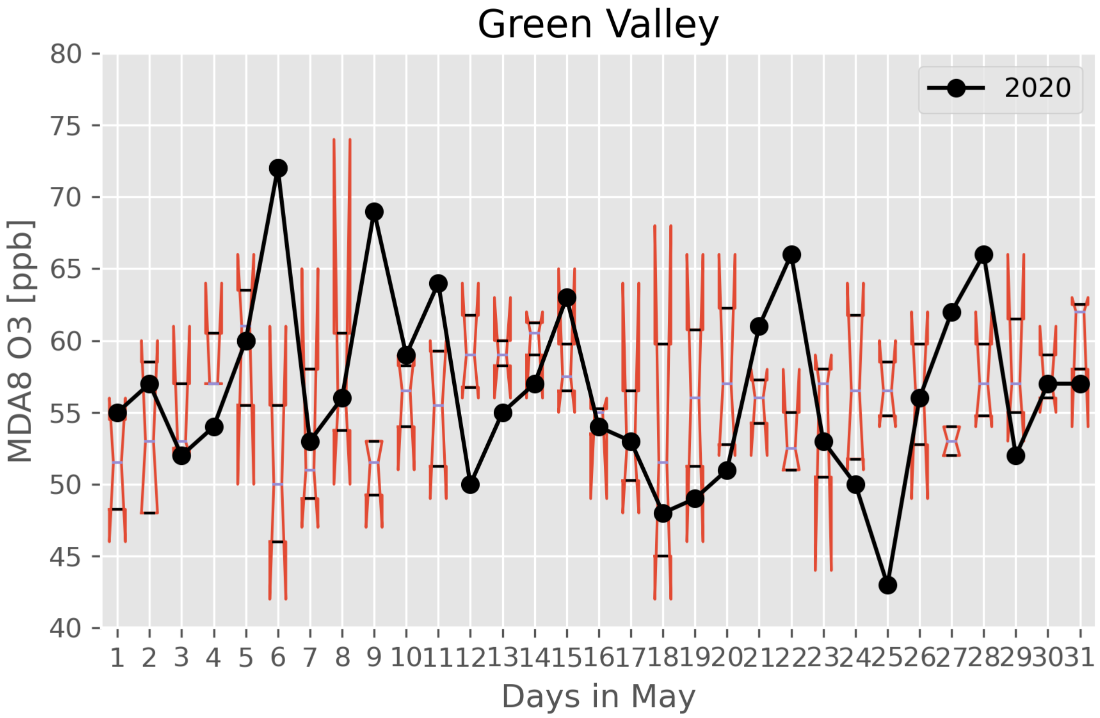

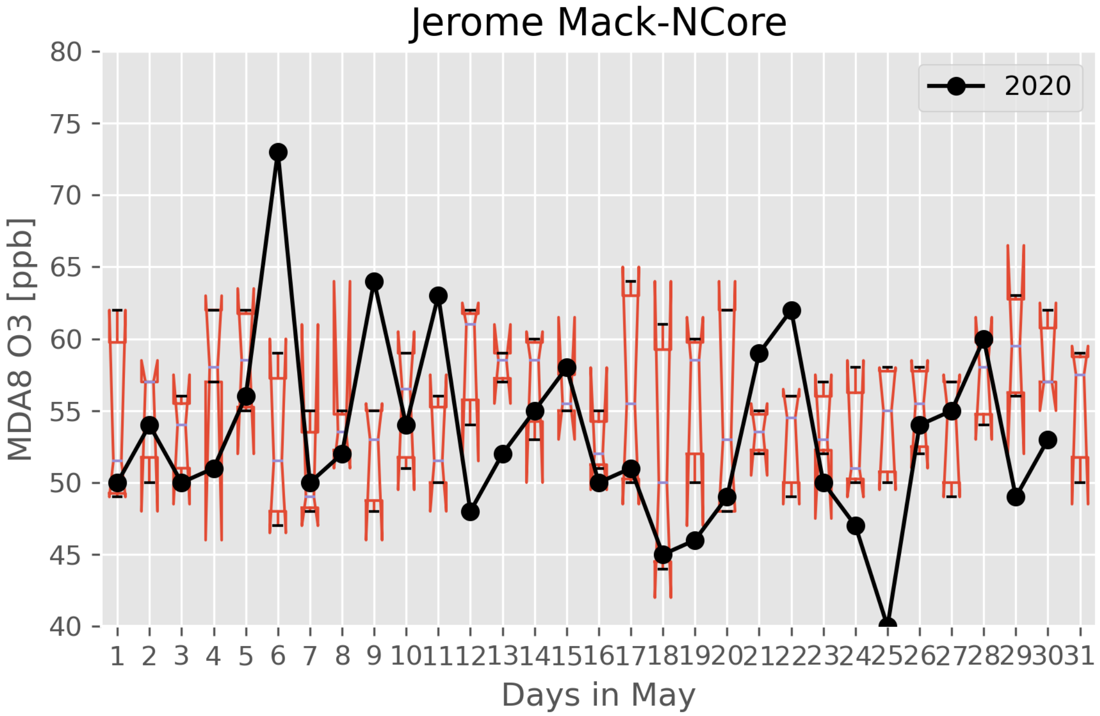

Figure 2-22. Daily time series of 2014-2019 MDA8 ozone distributions and 2020 MDA8 ozone at each site with proposed EE during May 2020. Notches denote 95th confidence interval of the median, boxes are 25th, 50th, and 75th percentiles, and whiskers are 5th and 95th percentile

3. Clear Causal Relationship Analyses

3.1 Comparison of Event Concentrations with Historical Concentrations

To address the Tier 1 EE criterion of comparison with historical ozone concentrations, we compared the May 6 EE ozone concentrations at each site with the 2020 ozone record, focusing mainly on the ozone season when highest ozone concentrations occur. **Figures 3-1 through 3-7** depict the 2020 daily maximum ozone record at each monitoring site, along with the 99th percentile over the past six years, and NAAQS criteria ozone concentrations. During 2020, May 6 ranks in the top 1% for daily maximum ozone concentrations at all EE-affected monitoring sites. The May 6 EE was in the top 1% of MDA8 ozone concentrations in the past five years at all EE-affected sites (**Table 3-1**). When compared with daily ozone rankings on May 6 over the six-year ozone record (Figures 2-11 through 2-17), the 2020 rankings indicate that May 6, 2020, was an extreme ozone event.

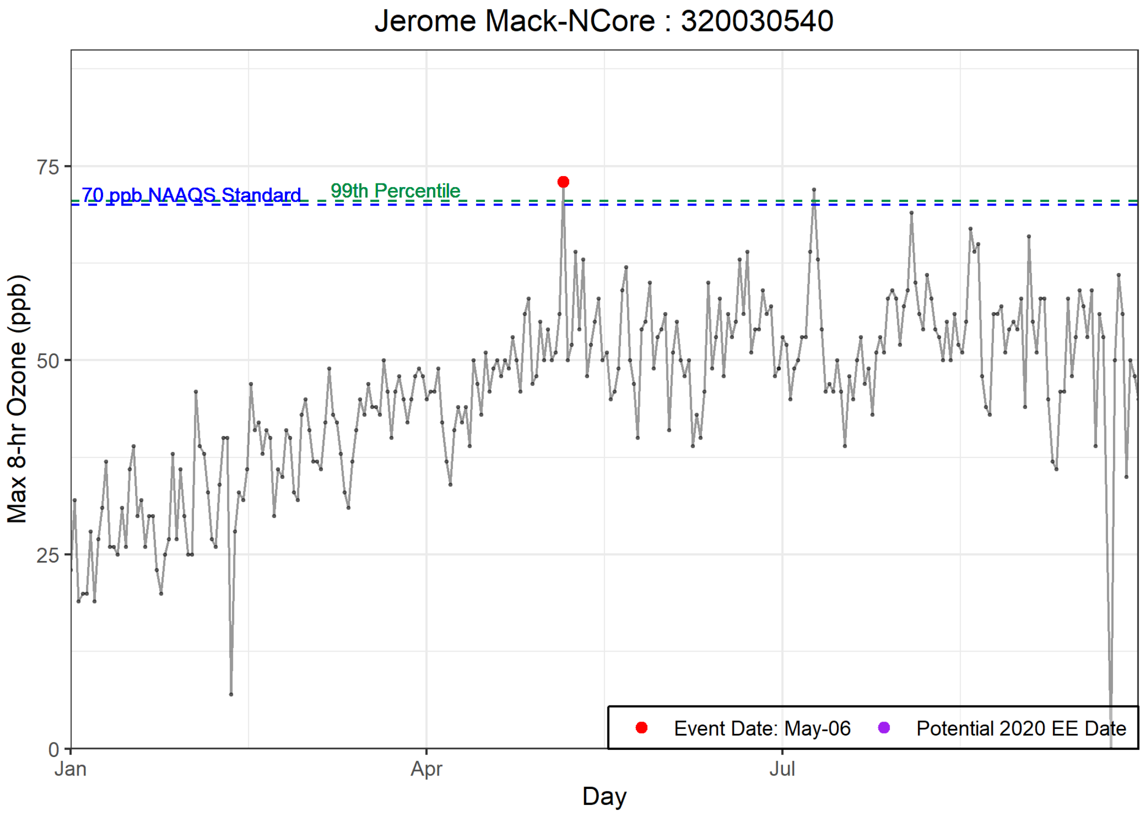

Figure 3-1. Time series of 2020 MDA8 ozone concentrations from the Jerome Mack-NCore site. May 6, 2020, is shown in red.

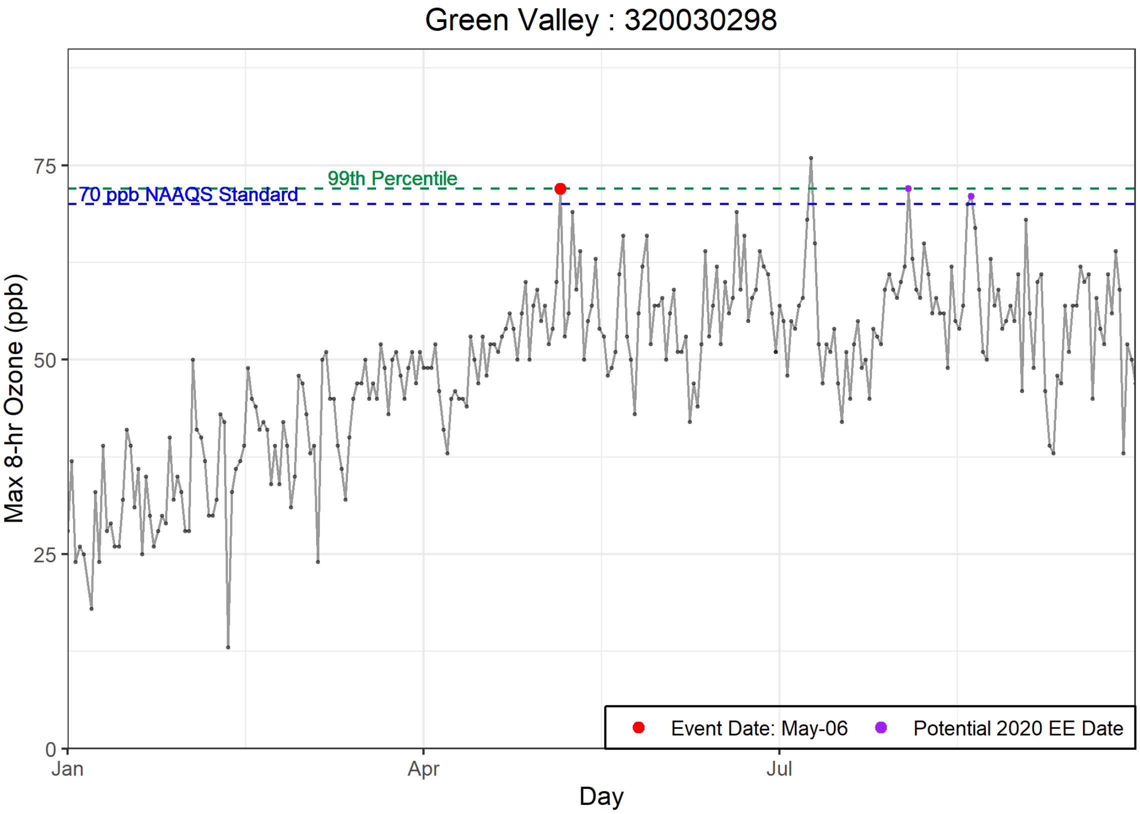

Figure 3-2. Time series of 2020 MDA8 ozone concentrations from the Green Valley site. May 6, 2020, is shown in red.

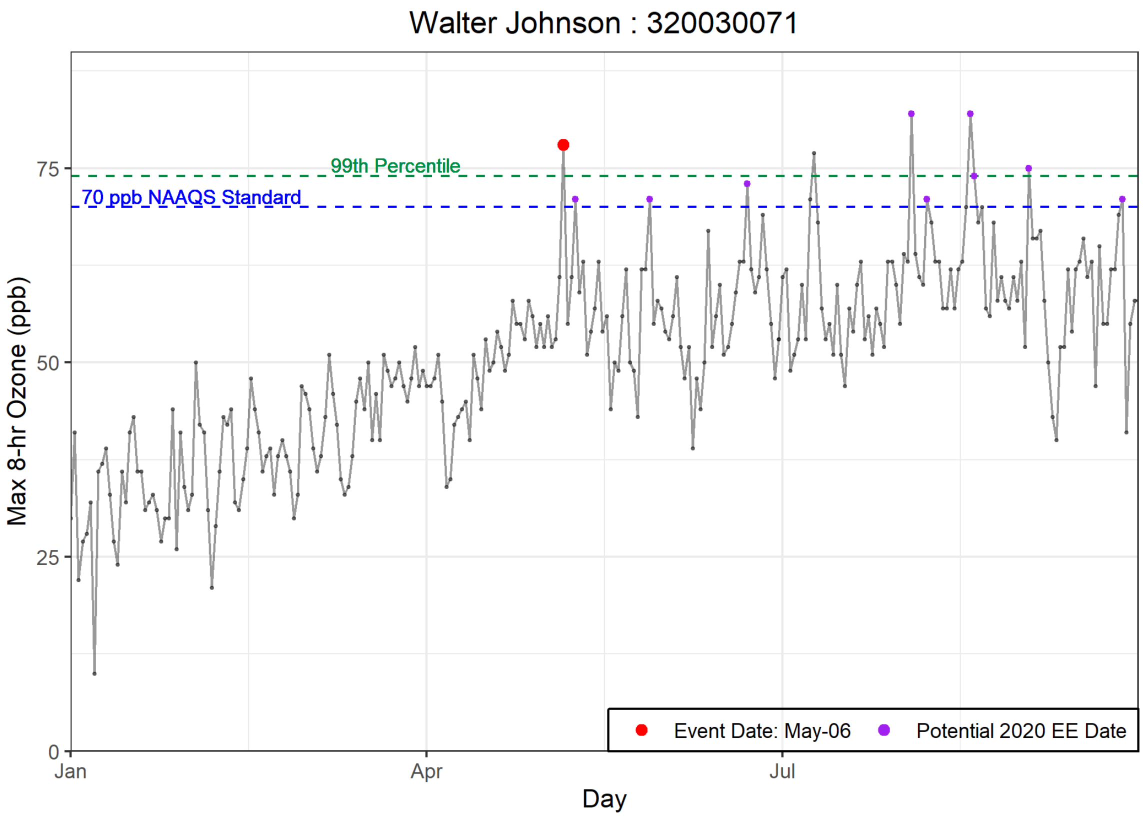

Figure 3-3. Time series of 2020 MDA8 ozone concentrations from the Walter Johnson site. May 6, 2020, is shown in red.

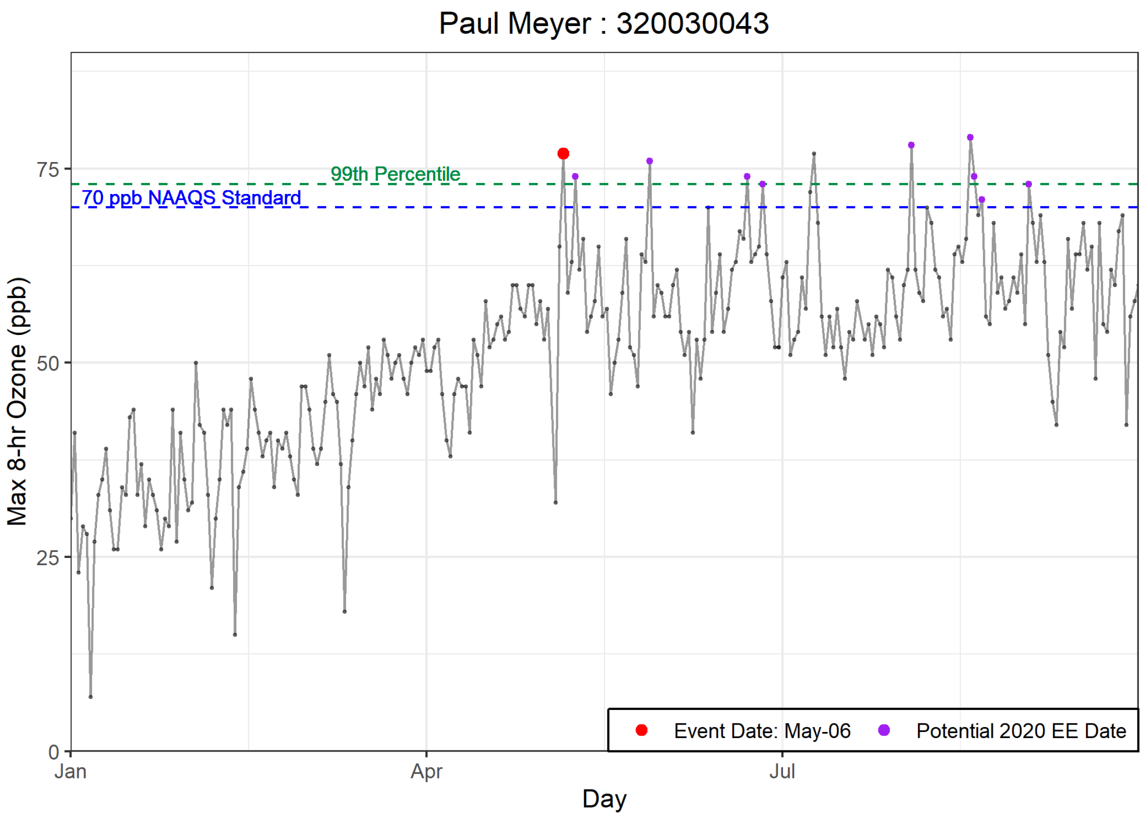

Figure 3-4. Time series of 2020 MDA8 ozone concentrations from the Paul Meyer site. May 6, 2020, is shown in red.

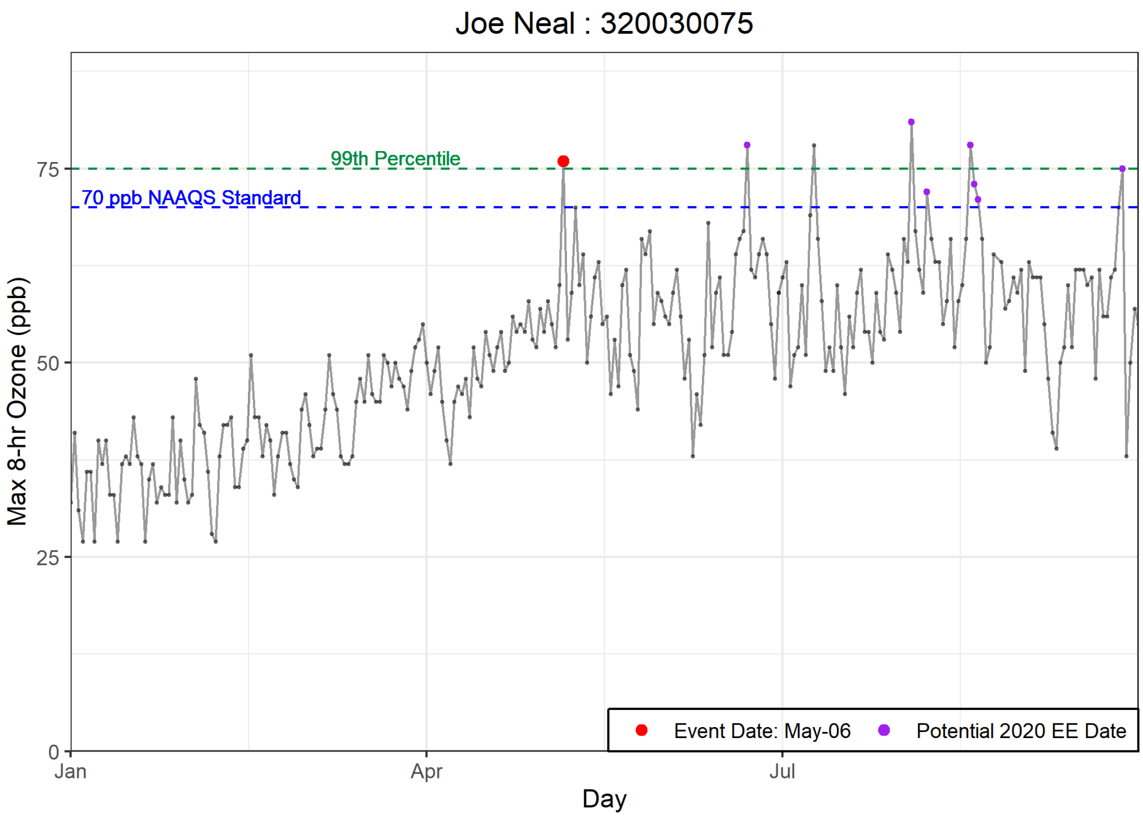

Figure 3-5. Time series of 2020 MDA8 ozone concentrations from the Joe Neal site. May 6, 2020, is shown in red.

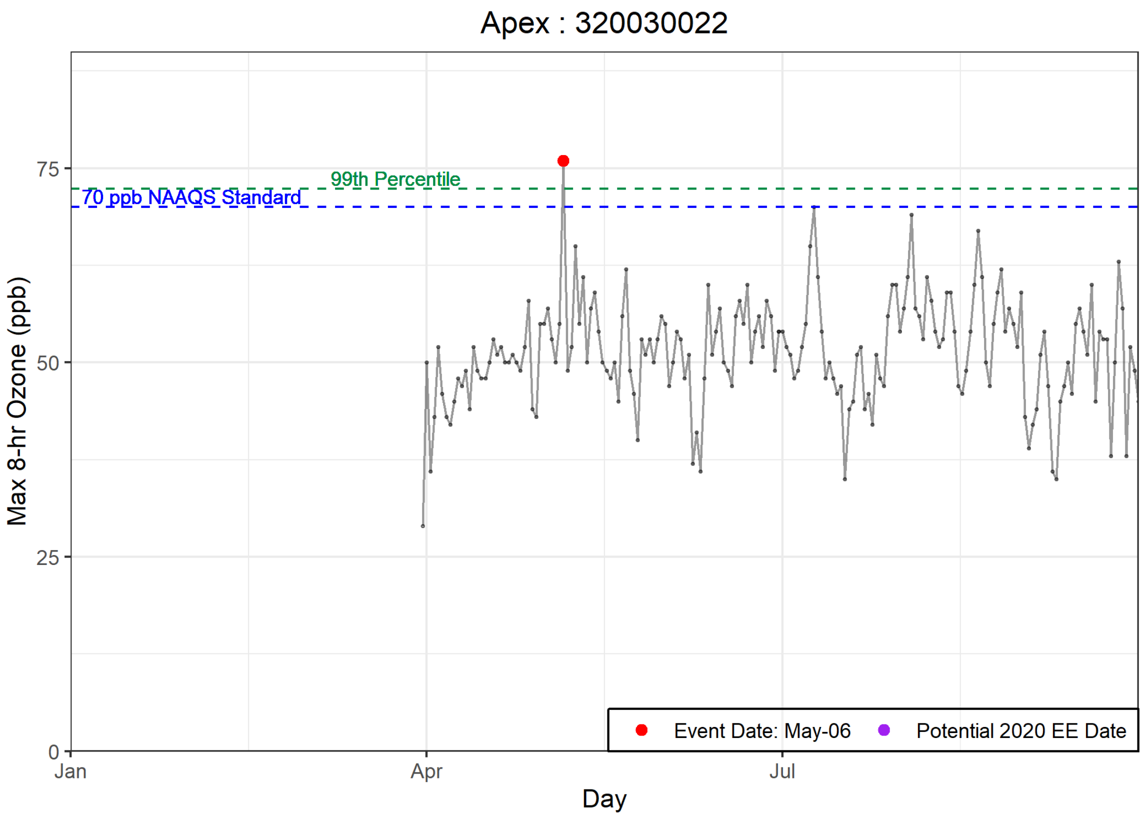

Figure 3-6. Time series of 2020 MDA8 ozone concentrations from the Apex site. May 6, 2020, is shown in red.

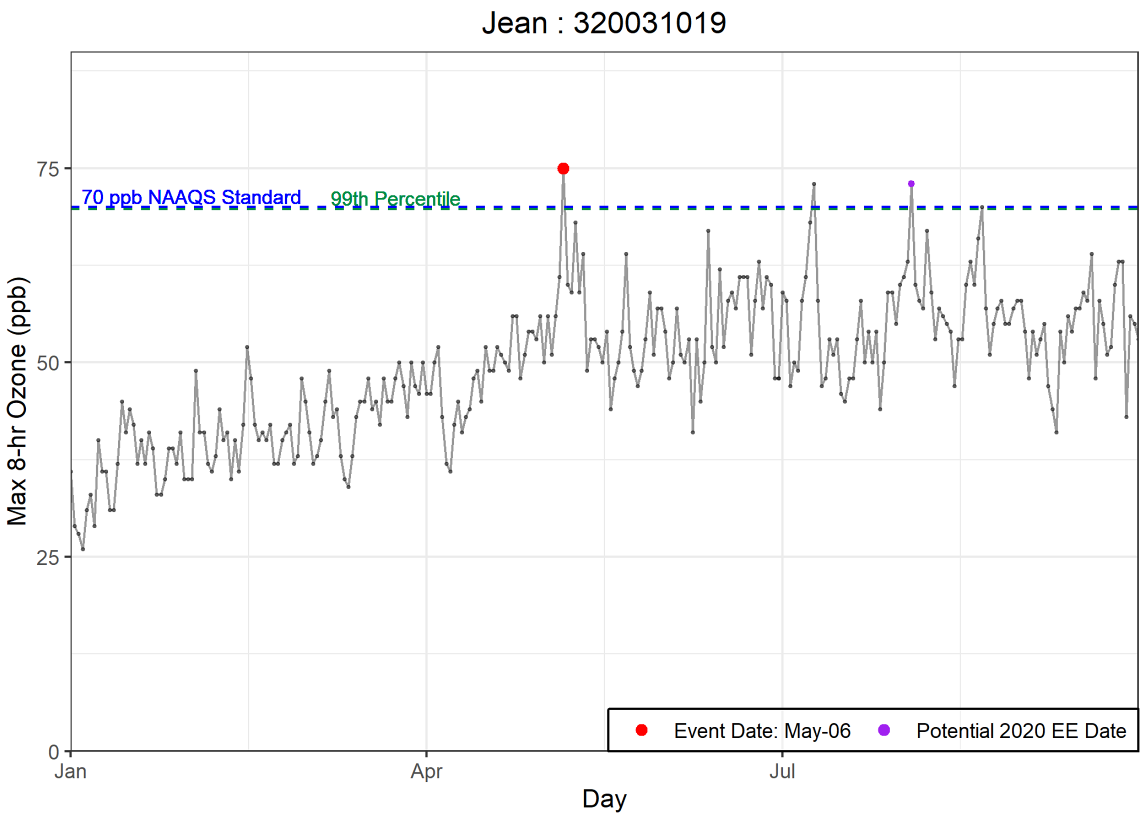

Figure 3-7. Time series of 2020 MDA8 ozone concentrations from the Jean site. May 6, 2020, is shown in red.

Table 3-1. Six-year percentile ozone. The May 6 EE ozone concentration at each site is calculated as a percentile of the last five years with and without other 2018 and 2020 EEs included in the historical record.

AQS Site Code	Site Name	6-Year Percentile	6-Year Percentile w/o EE Dates
320030071	Walter Johnson	99.8	*99.9*
320030043	Paul Meyer	99.9	*100.*
320030075	Joe Neal	99.3	*99.6*
320030298	Green Valley	99.1	*99.5*
320030022	Apex	99.8	*99.8*
320030540	Jerome Mack	99.6	*99.8*
320031019	Jean	99.9	*100.*

The May 6, 2020, ozone exceedance occurred during the typical ozone season, but MDA8 ozone concentrations on May 6 were the highest or second highest compared with daily ozone concentrations excluding potential EE days, depending on the monitoring site examined (Figures 3-1 through 3-7). Table 3-2 provides historical ozone season monitoring site statistics for each EE-affected site on May 6. The statistics shown are for May through September from 2015-2019; we do not exclude the dates with proposed 2018 EE ozone concentrations. The MDA8 ozone concentrations on May 6 were more than 10 ppb above the mean and median ozone concentrations for the historical ozone season at all EE-affected sites. In contrast, MDA8 ozone concentrations were 3-8 ppb above the 95th percentile of non-event day historical ozone concentrations at EE-affected sites. Because May 6 is during the normal ozone season and MDA8 ozone concentrations at the two EE-affected sites could not be clearly distinguished from the 95th percentile ozone concentration during the non-event historical ozone season, further analysis (Tier 2) is required.

To address the Tier 2 EE criterion to determine whether the May 6, 2020, exceedance event is exceptional, we compare event ozone concentrations with non-event concentrations via percentile and rank-order analysis. Table 3-1 shows May 6 concentrations as a percentile in comparison with the last six years of data (with and without the other proposed 2018 and 2020 EE days). For all monitoring sites that show a NAAQS standard exceedance on May 6, all of the exceedances are greater than the 99th percentile when compared to the last six years of data, with or without all other proposed 2018 and 2020 EE days included. To confirm that the calculated percentiles are not biased by non-ozone season data, Table 3-3 shows the May 6 percentile ranks for all monitoring sites around Clark County in comparison with the last six years of ozone season (May to September) data. The May 6 ozone concentration percentile over the last six ozone seasons (with all proposed 2018 and 2020 EE days included) ranks above the 98th percentile at all EE-affected sites. When the other possible EE days are excluded, the percentile rank of ozone season concentrations increases to >99th percentile. Although not all of the sites ranked above the 99th percentile of ozone season concentrations on May 6, this analysis confirms that the May 6 EE included unusually high concentrations of ozone when compared with ozone concentrations across both the last six years and the last six ozone seasons.

We also compared the rank-ordered concentrations at each site for 2020. As shown in Figures 2-4 through 2-10, ozone concentrations across 2020 were not atypically low, which might bias our rank-ordered analysis for May 6. Tables 3-4 through 3-10 show the rank-ordered ozone concentrations for 2018 through 2020 and the design values for 2020, with the proposed 2018 and 2020 EEs included. Based on the concentration rankings, May 6 is in the top five ozone concentrations of 2020 at all EE-affected sites when including all other proposed EE events. The May 6 ozone concentrations are the highest recorded in 2020 at the Jerome Mack, Apex, and Jean monitoring sites.

For further comparison with non-event ozone concentrations, Table 3-11 shows five-year (2015-2019, proposed 2018 EE events included) MDA8 ozone statistics for one week before and after May 6, 2020. This two-week window analysis shows that each affected monitoring site exhibited MDA8 ozone concentrations on May 6 that were greater than 10 ppb above the mean or median, and 7-12 ppb above the 95th percentile of ozone concentrations over the two-week window in the last five years.

The percentile, rank-ordered analyses, and the two-week window analysis indicate that all affected monitoring sites on May 6 showed atypically high ozone concentrations compared with non-event concentrations. This conclusion supports Tier 1 and 2 criteria, suggesting that May 6 was an EE in Clark County.

Table 3-2. Ozone season (May-September) non-event comparison. May 6, 2020, MDA8 ozone concentrations for each affected site are shown in the top row. Five-year (2015-2019) average MDA8 ozone statistics for May-September are shown for each affected site around Clark County to compare with the event ozone concentrations.

	Apex 320030022	Green Valley 320030298	Jean 320031019	Jerome Mack 320030540	Joe Neal 320030075	Paul Meyer 320030043	Walter Johnson 320030071
May. 6	76	72	75	73	76	77	78
Mean	54	56	55	54	57	57	57
Median	54	56	55	54	57	58	57
Mode	52	52	57	50	62	58	57
St. Dev	8	8	8	8	9	8	9
Minimum	18	21	20	0	23	22	21
95 %ile	68	69	67	67	72	70	71
99 %ile	73	74	72	73	78	76	77
Maximum	84	78	81	78	83	79	87
Range	66	57	61	78	60	57	66
Count	917	877	914	915	912	911	917

Table 3-3. Six-year ozone-season percentile ozone. The May 6 EE ozone concentration at each site is calculated as a percentile of the last five years' ozone season (May-September) with and without other 2018 and 2020 EEs included in the historical record.

AQS Site Code	Site Name	6-Year Percentile	6-Year Percentile w/o EE Dates
320030071	Walter Johnson	99.5	*99.8*
320030043	Paul Meyer	99.7	*100.*
320030075	Joe Neal	98.5	*99.0*
320030298	Green Valley	98.1	*99.0*
320030022	Apex	99.8	*99.8*
320030540	Jerome Mack	99.1	*99.6*
320031019	Jean	99.7	*99.9*

Table 3-4. Site-specific ozone design values for the Jerome Mack monitoring site. The top five highest ozone concentrations for 2018-2020 at Jerome Mack are shown, and proposed EE days in 2018 and 2020 are included.

Jerome Mack-NCore Rank	2018	2019	2020
Highest	78	69	73
Second Highest	77	68	72
Third Highest	76	67	69
Fourth Highest	75	67	67
Fifth Highest	75	66	66
Design Value		69	

Table 3-5. Site-specific ozone design values for the Green Valley monitoring site. The top five highest ozone concentrations for 2018-2020 at Green Valley are shown, and proposed EE days in 2018 and 2020 are included.

Green Valley Rank	2018	2019	2020
Highest	78	73	76
Second Highest	78	72	72
Third Highest	78	71	72
Fourth Highest	77	70	71
Fifth Highest	77	70	70
Design Value		72	

Table 3-6. Site-specific ozone design values for the Walter Johnson monitoring site. The top five highest ozone concentrations for 2018-2020 at Walter Johnson are shown, and proposed EE days in 2018 and 2020 are included.

Walter Johnson Rank	2018	2019	2020
Highest	79	77	82
Second Highest	77	69	82
Third Highest	77	69	78
Fourth Highest	76	68	77
Fifth Highest	76	68	75
Design Value		73	

Table 3-7. Site-specific ozone design values for the Paul Meyer monitoring site. The top five highest ozone concentrations for 2018-2020 at Paul Meyer are shown, and proposed EE days in 2018 and 2020 are included.

Paul Meyer Rank	2018	2019	2020
Highest	79	74	79
Second Highest	76	72	78
Third Highest	75	70	77
Fourth Highest	75	69	77
Fifth Highest	74	69	76
Design Value		73	

Table 3-8. Site-specific ozone design values for the Joe Neal monitoring site. The top five highest ozone concentrations for 2018-2020 at Joe Neal are shown, and proposed EE days in 2018 and 2020 are included.

Joe Neal Rank	2018	2019	2020
Highest	80	74	81
Second Highest	78	70	78
Third Highest	76	69	78
Fourth Highest	76	68	78
Fifth Highest	74	67	76
Design Value	74		

Table 3-9. Site-specific ozone design values for the Apex monitoring site. The top five highest ozone concentrations for 2018-2020 at Apex are shown, and proposed EE days in 2018 and 2020 are included.

Apex Rank	2018	2019	2020
Highest	74	67	76
Second Highest	74	66	70
Third Highest	74	65	69
Fourth Highest	73	63	67
Fifth Highest	71	62	65
Design Value	67		

Table 3-10. Site-specific ozone design values for the Jean monitoring site. The top five highest ozone concentrations for 2018-2020 at Jean are shown, and proposed EE days in 2018 and 2020 are included.

Jean Rank	2018	2019	2020
Highest	81	67	75
Second Highest	77	67	73
Third Highest	73	66	73
Fourth Highest	72	66	70
Fifth Highest	72	65	68
Design Value	69		

Table 3-11. Two-week non-event comparison. May 6, 2020, MDA8 ozone concentrations for each affected site are shown in the top row. Five-year (2015-2019) average MDA8 ozone statistics for April 29 through May 13 are shown for each affected site around Clark County to compare with the event ozone concentrations.

	Apex 320030022	Green Valley 320030298	Jean 320031019	Jerome Mack 320030540	Joe Neal 320030075	Paul Meyer 320030043	Walter Johnson 320030071
May. 6	76	72	75	73	76	77	78
Mean	55	56	57	54	56	57	56
Median	56	56	58	54	57	58	56
Mode	55	57	59	50	58	59	61
St. Dev	7	6	6	6	7	7	7
Minimum	38	42	43	39	37	32	41
95 %ile	68	65	67	64	67	66	66
99 %ile	71	73	68	73	70	74	71
Maximum	76	74	75	73	76	77	78
Range	38	32	32	34	39	45	37
Count	96	75	95	96	93	95	96

3.2 Evidence of Stratospheric-Tropospheric Exchange

3.2.1 Satellite Imagery

Satellite retrievals can help identify signatures of a stratospheric intrusion event, such as ozone-rich and extremely dry air. We examined maps of true color visible imagery from the Moderate Resolution Imaging Spectroradiometer (MODIS) instruments onboard the Terra satellite, water vapor imagery from Geostationary Operational Environmental Satellite (GOES)-East, and total column ozone from the Ozone Mapping and Profiling Suite (OMPS) Nadir-Mapper (NM) instrument onboard the Suomi NPP satellite and from Modern-Era Retrospective analysis for Research and Applications, Version 2

(MERRA-2). These maps provide evidence to support the transport of dry ozone-rich stratospheric air from an area to the west of northern California and Oregon around May 4, 00:00 UTC, over the eastern Pacific Ocean, and into Clark County, Nevada on the May 6 EE date.

True color visible satellite imagery can be used to identify areas of very dry and cloudless air that may be indicative of the effects from a stratospheric intrusion. True color visible satellite imagery from the MODIS instruments onboard the Terra satellite shows a lack of extensive cloud cover over California and Nevada (Figures 3-8 through 3-10). On May 5 and 6, Clark County was almost entirely devoid of cloud cover (except upper-level cirrus), which can be a characteristic of dry stratospheric air.

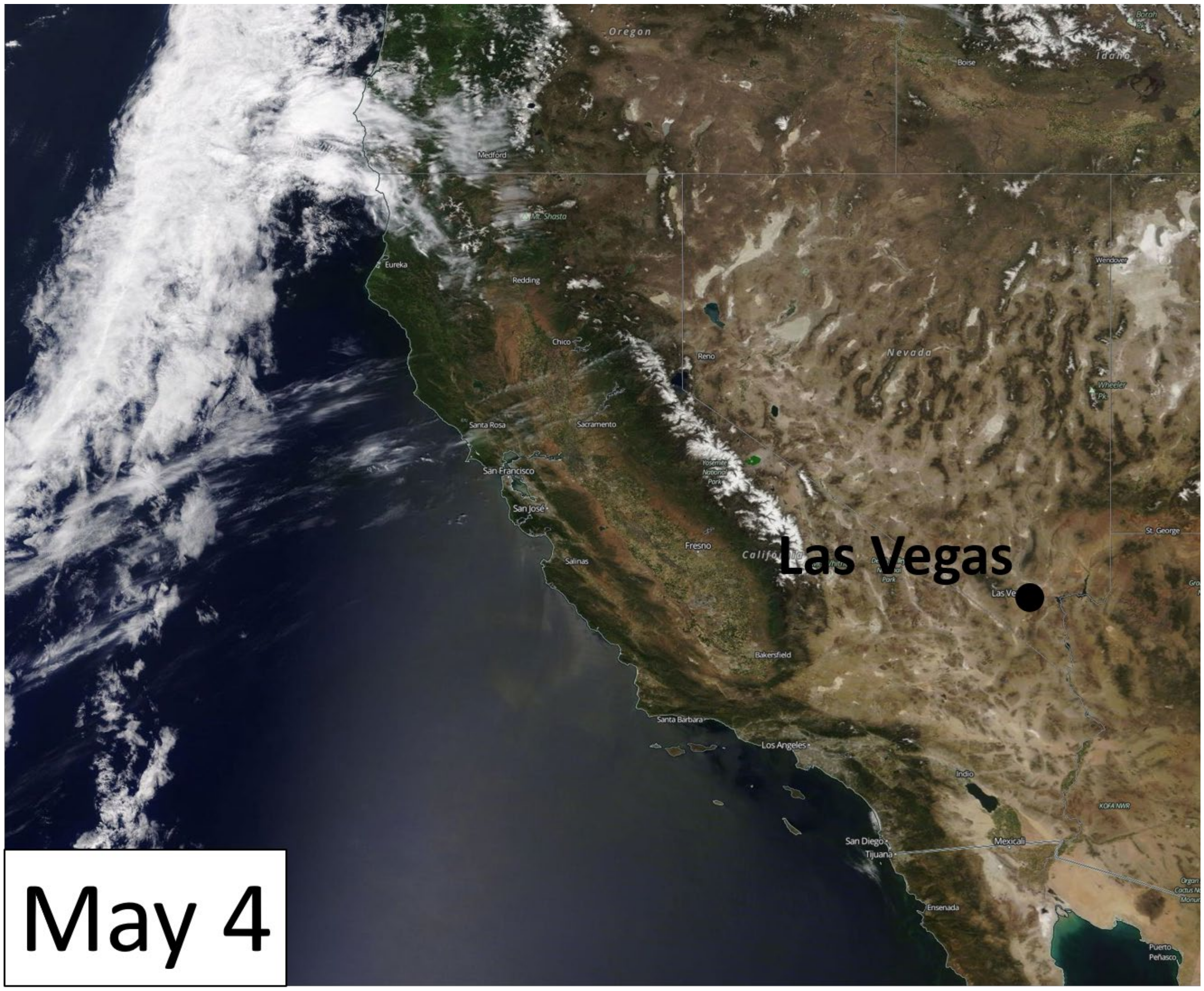

Figure 3-8. Visible Satellite Imagery from over the eastern Pacific Ocean, California, and Nevada on May 4, 2020. Source: NASA Worldview

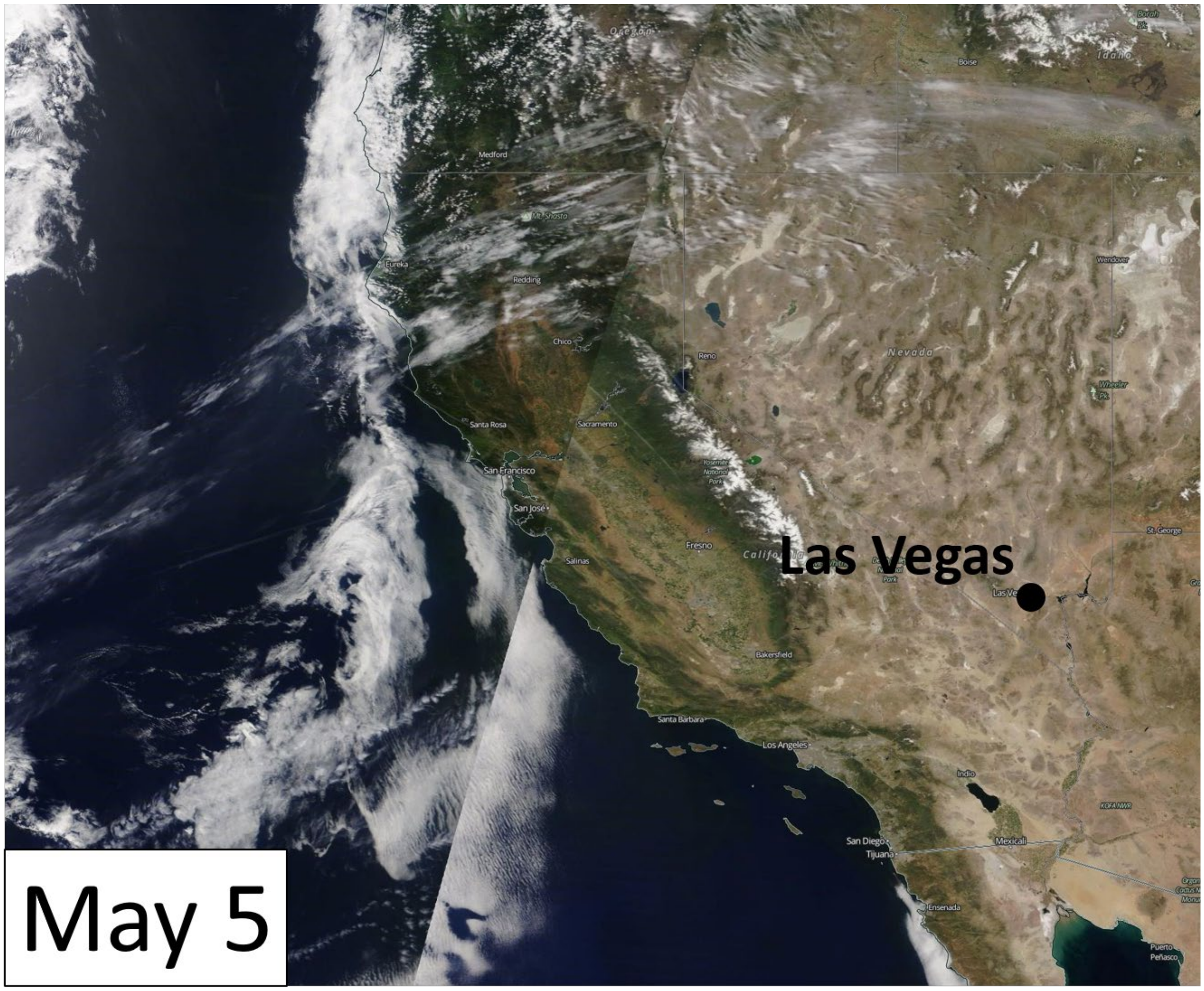

Figure 3-9. Visible Satellite Imagery from over the eastern Pacific Ocean, California, and Nevada on May 5, 2020. Source: NASA Worldview

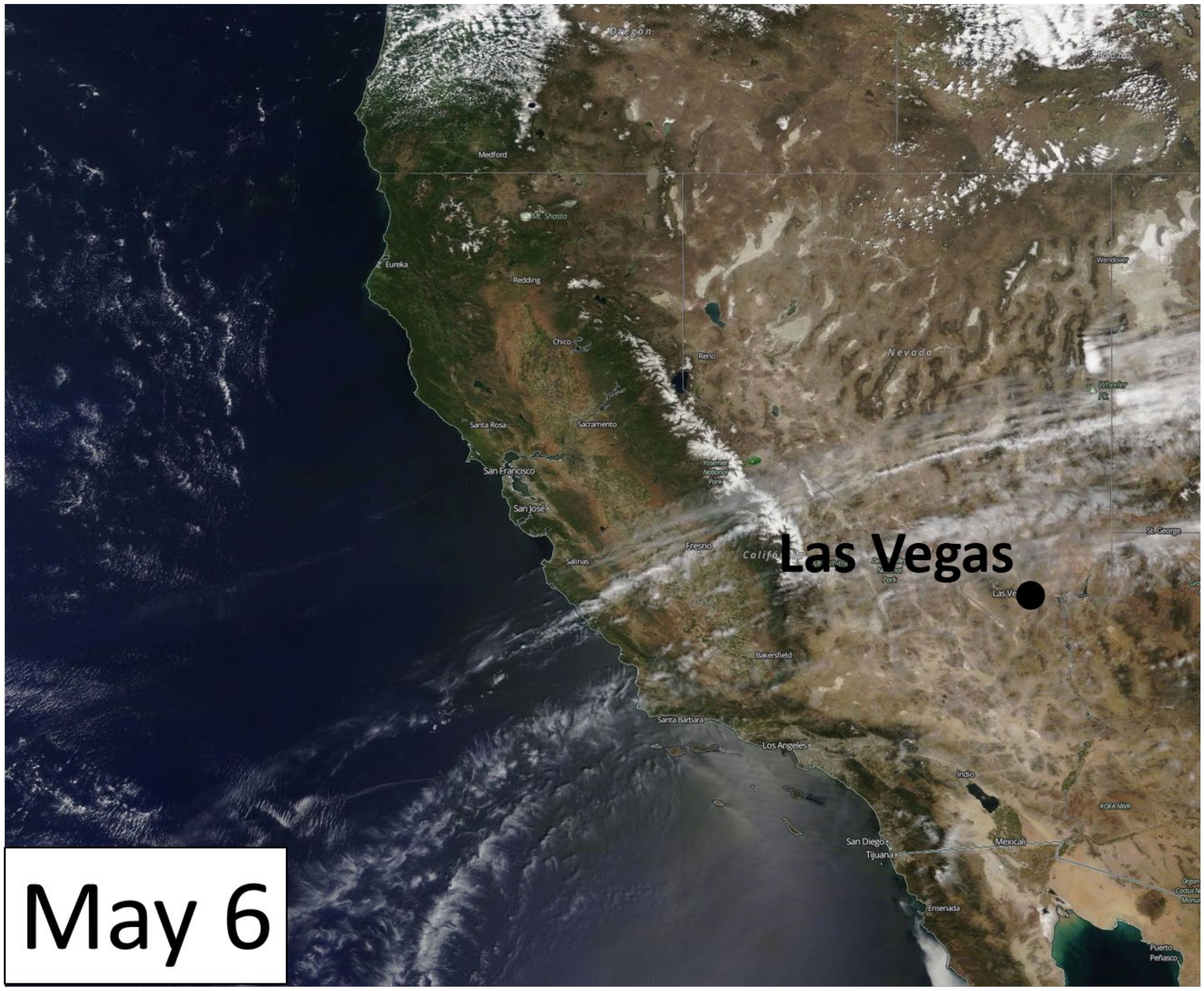

Figure 3-10. Visible Satellite Imagery from over the eastern Pacific Ocean, California, and Nevada on May 6, 2020. Source: NASA Worldview

The stratosphere's lack of water vapor relative to that of the troposphere is a key characteristic when tracing stratospheric air. Because stratospheric intrusion events will lead to the drying of tropospheric air, satellite imagery of total column water vapor can be used to highlight areas of dry and potentially stratospheric air. Water vapor imagery from the GOES-East satellite shows water vapor was present over the eastern Pacific Ocean—as shown by shades of blue—from May 4 to May 7 (Figures 3-11 through 3-14). However, the moisture over the eastern Pacific Ocean is at lower altitude in the troposphere and likely below the approximate region and altitude of the stratospheric intrusion, as low-altitude clouds with a large amount of water vapor are indicated by dark shades of blue.

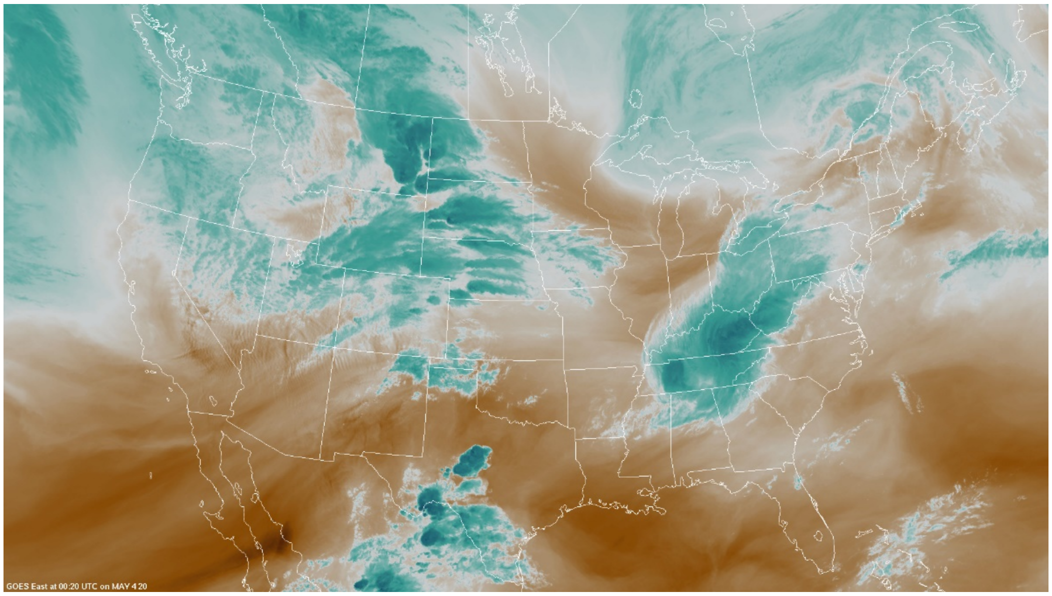

Figure 3-11. Water vapor imagery from the GOES-East Satellite on May 4, 2020, at 00:20 UTC. Bright blue and white areas indicate the presence of high water vapor or moisture content, whereas dark orange and brown areas indicate little or no moisture present.

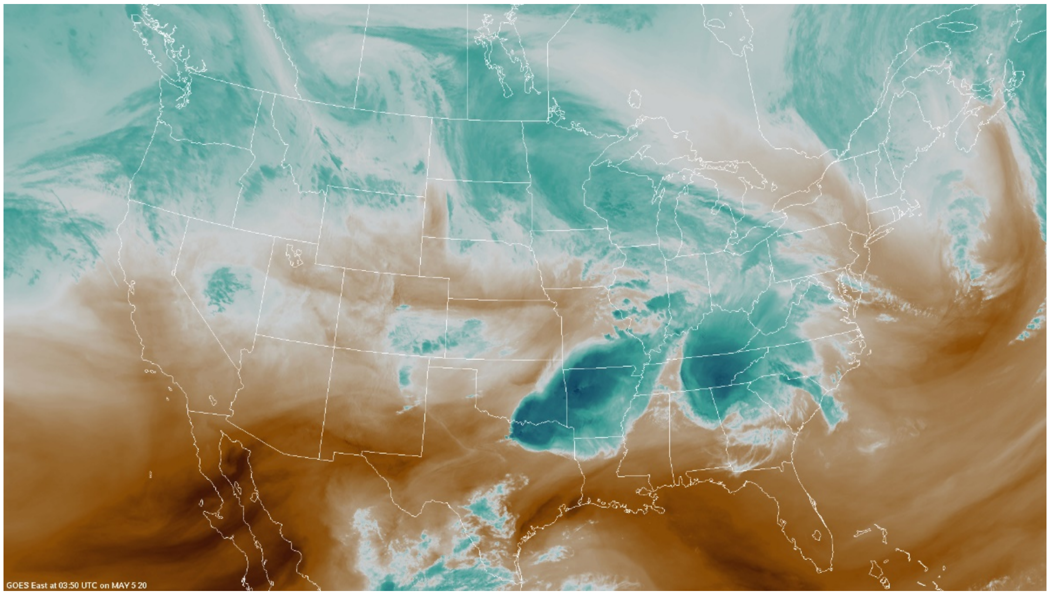

Figure 3-12. Water vapor imagery from the GOES-East Satellite on May 5, 2020, at 03:50 UTC. Bright blue and white areas indicate the presence of high water vapor or moisture content, whereas dark orange and brown areas indicate little or no moisture present.

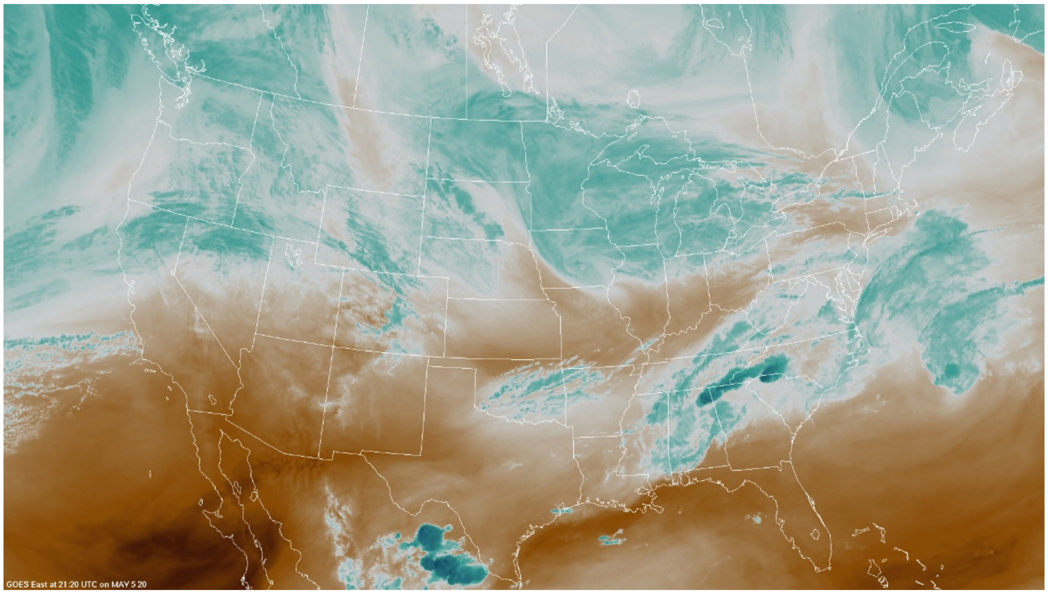

Figure 3-13. Water vapor imagery from the GOES-East Satellite on May 5, 2020, at 21:20 UTC. Bright blue and white areas indicate the presence of high water vapor or moisture content, whereas dark orange and brown areas indicate little or no moisture present.

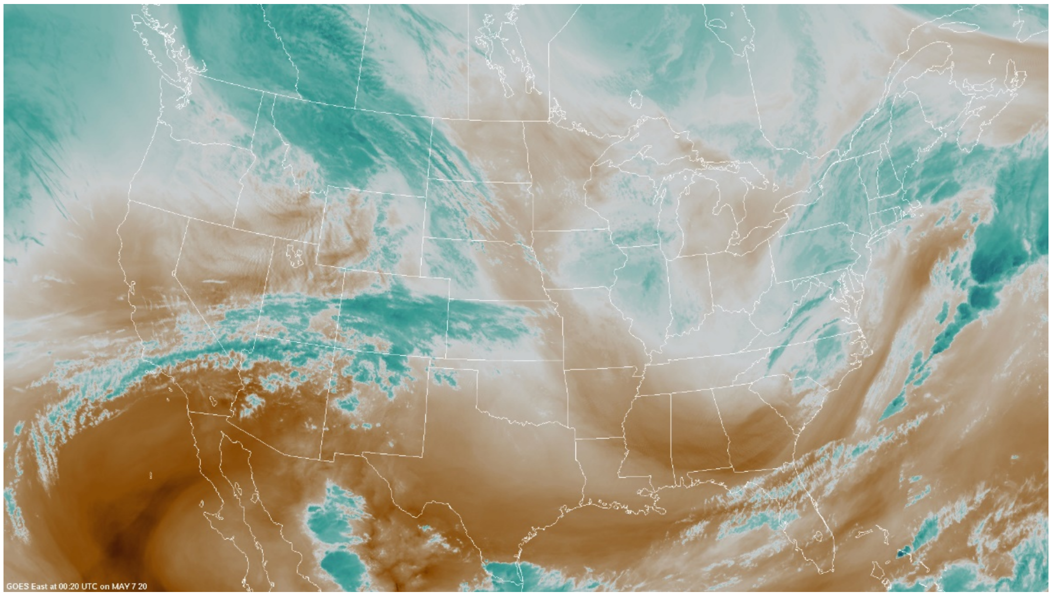

Figure 3-14. Water vapor imagery from the GOES-East Satellite on May 7, 2020, at 00:20 UTC. Bright blue and white areas indicate the presence of high water vapor or moisture content, whereas dark orange and brown areas indicate little or no moisture present.

Satellite retrievals of total column ozone are useful in identifying areas with high ozone concentrations that may be associated with stratospheric intrusion events. Maps of total column ozone from OMPS on May 4, 5, and 6 are shown in Figure 3-15. On May 4, total column ozone concentrations were elevated—as shown by shades of yellow and orange—over the area to the west of northern California and Oregon over the eastern Pacific Ocean to approximately 315 Dobson Units (DU) to 350 DU. This area remained elevated in ozone on May 5 and May 6. Additionally, we examined a map of total column ozone from MERRA-2 for May 5 at 00:00 UTC (**Figure 3-16**). The map shows that total column ozone was elevated over an area to the west of northern California and Oregon to approximately 364 DU and above. This area of high ozone is a feature of a much larger area of high ozone over the northeastern Pacific Ocean. These maps provide evidence that total column ozone was elevated in the area of the stratospheric intrusion.

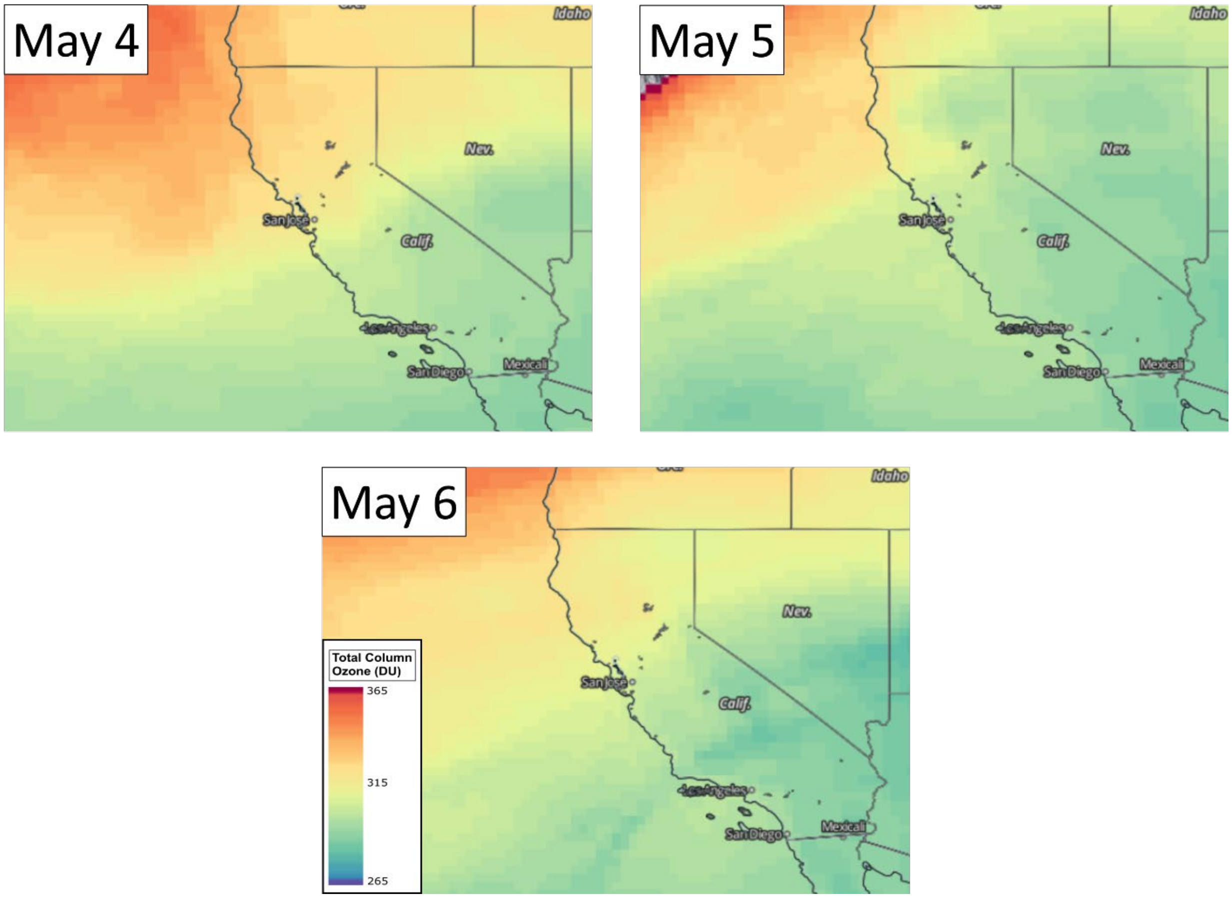

Figure 3-15. Maps of satellite-estimated total column ozone from May 4 to May 6 from the OMPS instrument on the Suomi NPP satellite. Data source: NASA Worldview.

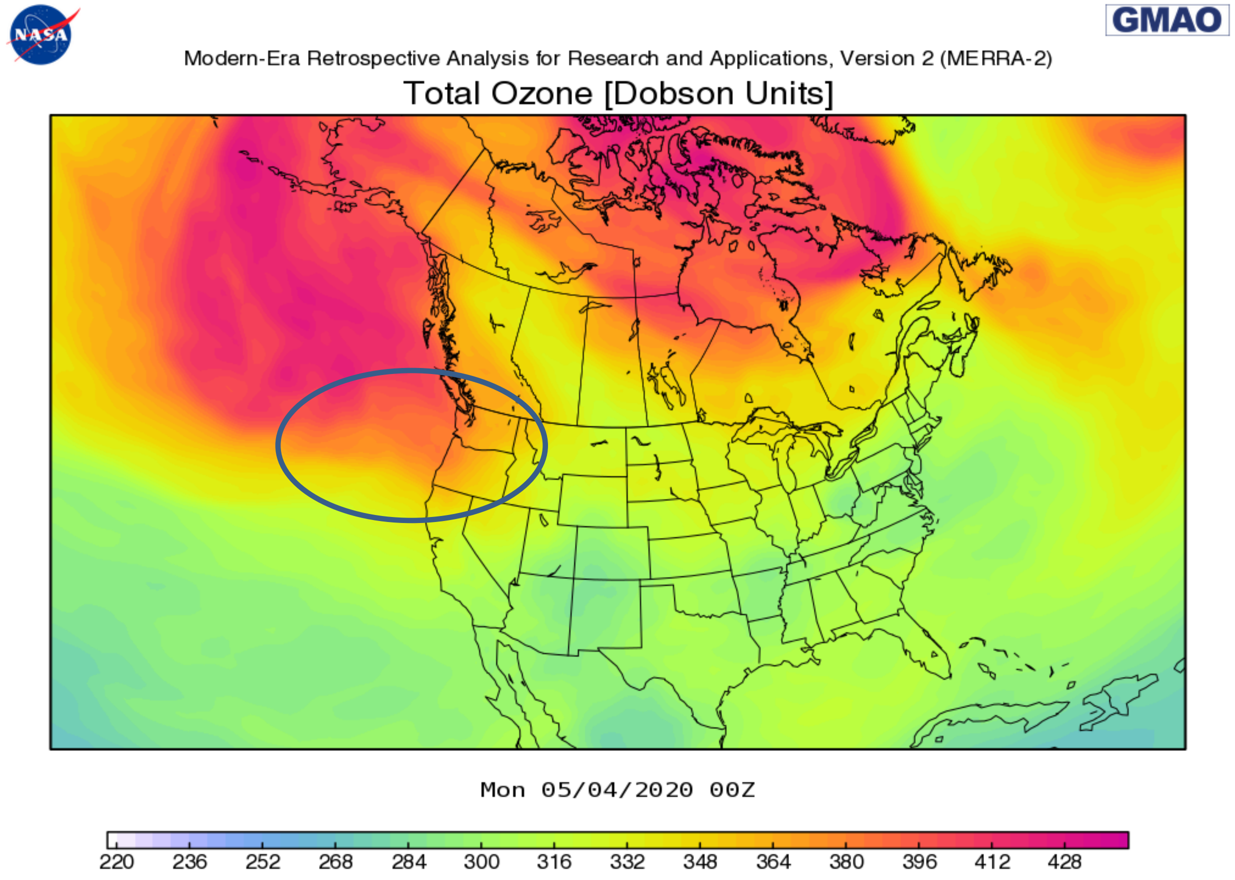

Figure 3-16. Maps of satellite-estimated total column ozone from May 4 at 00:00 UTC from Modern-Era Retrospective analysis for Research and Applications, Version 2 (MERRA-2). The approximate area of the SOI is shown by the circle.

3.2.2 Model Results

Modeled analysis of IPV, ozone, and CO can provide supporting evidence of the suspected stratosphere-to-troposphere mixing northwest of Clark County that likely contributed to the ozone exceedance on May 6. Stratospheric air is characterized by high IPV, low moisture, high concentrations of ozone, and low concentrations of CO compared to tropospheric air. Therefore, these four measurements can act as tracers for the penetration of stratospheric air into the troposphere. The Real-time Air Quality Modeling System (RAQMS), Global Forecast System (GFS), Whole Atmosphere Community Climate Model (WACCM), and MERRA-2 data are utilized in this section to provide evidence of stratosphere-to-troposphere exchange through the examination of IPV, ozone, and CO levels. Animations and stratospheric ozone tracer figures to accompany the images in this section are provided in Appendix A.

As noted in Sections 2.4 and 3.2.1, the air mass over Clark County on May 6 originated from a source region over the northwest U.S. and eastern Pacific on May 4, 00:00 UTC. Figure 3-17 shows the GFS model analysis of IPV at the 250 mb level at 00:00 UTC on May 4. Stratospheric IPV values are typically much higher than in the troposphere, so a region where stratospheric-tropospheric mixing occurs is marked by elevated levels of IPV. The region of elevated IPV is represented by the colored contours in Figure 3-17. This provides supporting evidence of stratospheric-tropospheric exchange in this area. The boxed area in Figure 3-17 encompasses the approximate area of the SOI that was transported to Clark County on May 6 (see Section 3.3.1 for HYSPLIT trajectories), indicating that air with high IPV values was transported to Clark County on the EE day.

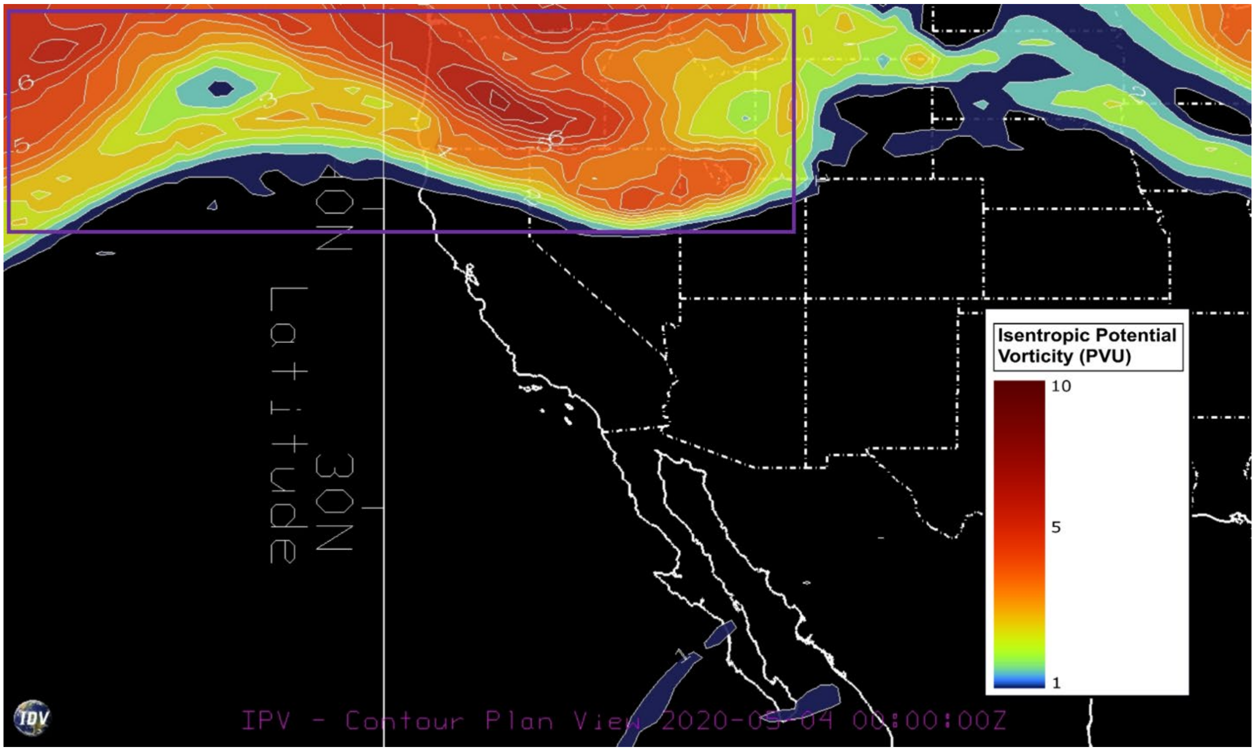

Figure 3-17. GFS-modelled isentropic potential vorticity (IPV) at 0:00 UTC on May 4 at the 250 hPa geopotential height, plotted with Unidata's Integrated Data Viewer (IDV). The region of elevated IPV, where stratosphere-to-troposphere exchange is suspected, is highlighted in purple.

Figure 3-18 shows the GFS model analysis of the water vapor mixing ratio at 250 mb at 00:00 UTC on May 4. Stratospheric air is drier than tropospheric air, so regions with stratospheric-tropospheric mixing are often marked by low water vapor mixing ratios. The modeled water vapor mixing ratio confirms this characteristic in the northwest U.S. and west into the Pacific. Water vapor mixing ratios are low within the region of elevated IPV, shown in Figure 3-17. The approximate origin of air crossing Clark County on May 6 is boxed in red.

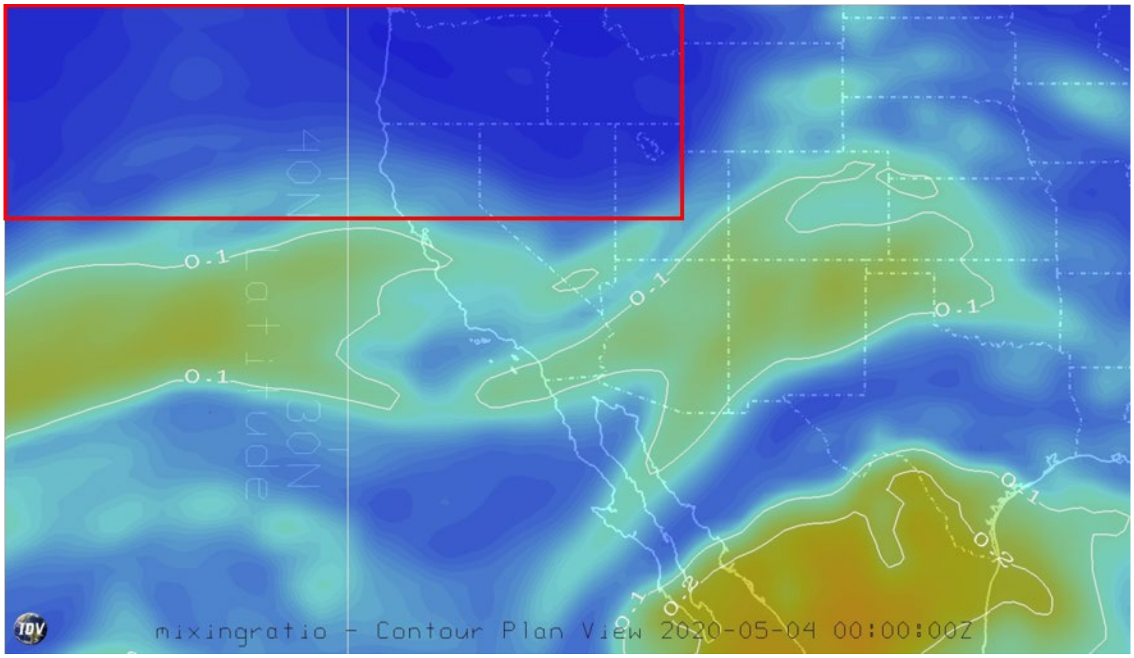

Figure 3-18. Mixing ratio contour map at 250 hPa geopotential height based on GFS model simulations for 00:00 UTC on May 4 (May 3 at 16:00 PST). Each contour above 0.1 g/kg represents 0.1 g/kg increments. The suspected origin of air crossing Clark County on May 6 is boxed in red. This region aligns with the region of elevated IPV shown in Figure 3-17.

Stratospheric air is characterized by high ozone concentrations, as ozone is produced naturally and efficiently in the stratosphere. The mid-troposphere, on the other hand, typically has much lower ozone concentrations. Figure 3-19 shows the modeled ozone concentration from RAQMS. A region of enhanced tropospheric ozone can be seen in the northwest corner of the U.S. at approximately the 400 mb level (circled in gray).

Figure 3-20 further explores the source of the region of elevated ozone shown in Figure 3-19. Longitudinal cross sections from RAQMS are available at 60-degrees, 90-degrees, and 120-degrees W. Figure 3-20 shows a vertical cross section from RAQMS along 120 degrees W, which passes through the stratosphere-to-troposphere exchange area in the northwest U.S. This figure shows high ozone concentrations from the stratosphere penetrating downwards to the 600 mb level in the mid-troposphere (circled in black) near 40-degrees N, with ozone concentrations above 70 ppb seen at the 500-m level. This provides evidence that ozone-rich air originating in the stratosphere was mixed downwards to mid-tropospheric levels prior to being transported to Clark County on May 6.

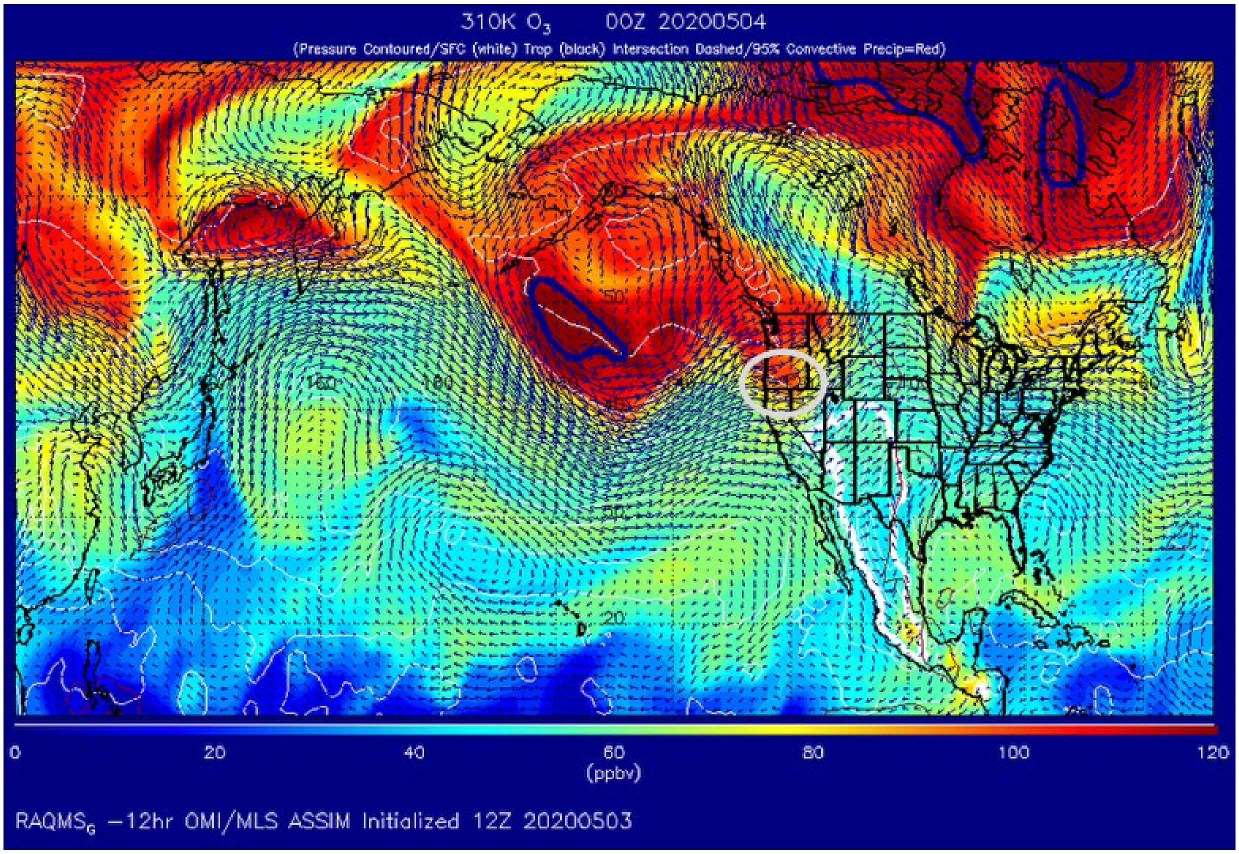

Figure 3-19. RAQMS-modelled ozone at the 310 K isentrope level at 0:00 UTC on May 4. The model was initialized at 12:00 UTC on May 3. The region with suspected stratosphere-to-troposphere mixing, and corresponding elevated ozone levels, is circled in gray.

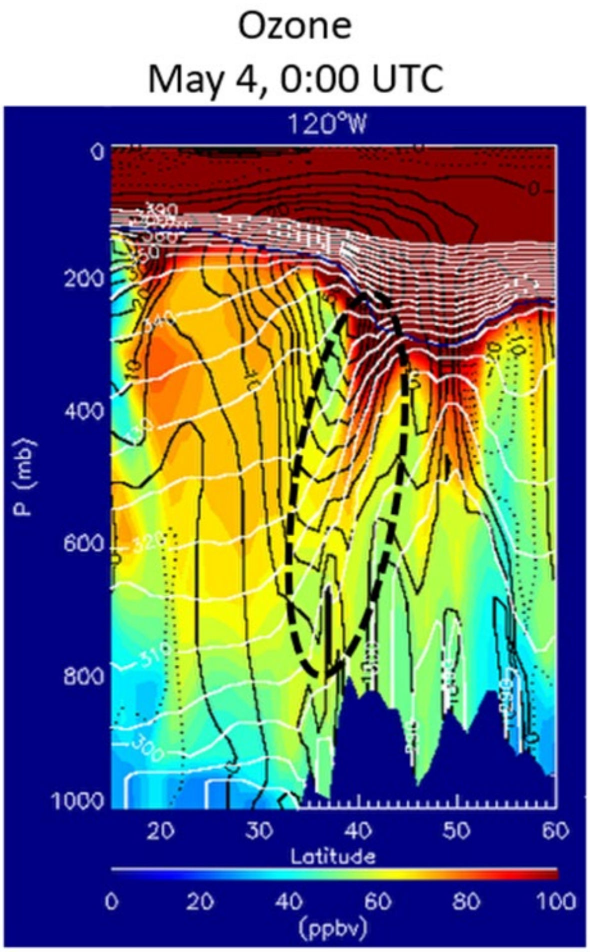

Figure 3-20. RAQMS-modelled cross-section of ozone along the 120 degrees west longitude line on May 4 at 0:00 UTC. The model was initialized at 12:00 UTC on May 3. The "tongue" of elevated ozone extending from the stratosphere into the mid-to-lower troposphere near 40-degrees N is circled in black.

The WACCM model analysis of ozone on May 4 at 00:00 UTC also provides supporting evidence for stratosphere-to-troposphere mixing northwest of Clark County. Figure 3-21 shows modelled ozone in the mid-troposphere at the 500 mb level. At this height, a similar area of elevated ozone, circled in red, is visible near 120 degrees west longitude. This agrees with the RAQMS vertical cross section of ozone at 120 degrees west longitude, showing ozone concentrations of 70-80 ppb.

Figures 3-22 and 3-23 show MERRA-2 modeled ozone concentrations for the May mean (2014–2020) and for May 4 at 00:00 UTC over the western United States at 488 hPa and 288 hPa. During the hours of the stratospheric intrusion that led to the May 6 ozone exceedance in Las Vegas, ozone concentrations over northern California, Oregon, and Nevada in the upper troposphere were well above the May average. On May 4 at 00:00 UTC at 488 hPa and 288 hPa, ozone concentrations at the area of stratospheric intrusion, were well above the mean May ozone concentrations over the same area. Figures 3-22 and 3-23 are consistent with Figures 3-19 and 3-21, which also show elevated ozone in the upper troposphere over the area of stratospheric intrusion.

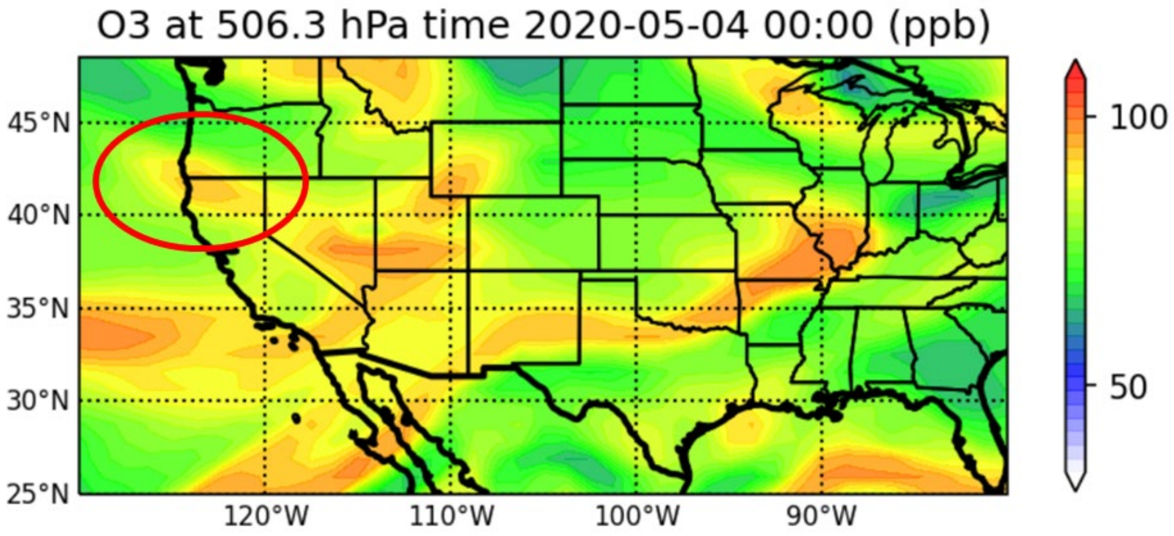

Figure 3-21. WACCM-modelled ozone at the 500 mb level on May 4 at 0:00 UTC. The region with suspected stratosphere-to-troposphere mixing, and corresponding increased O_3 levels, is circled in red.

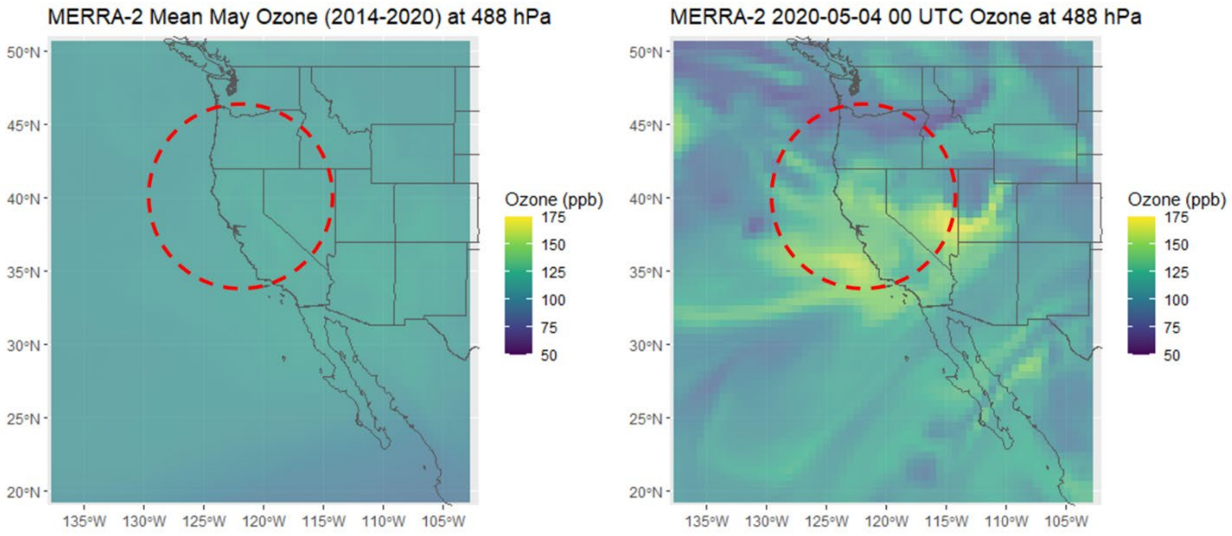

Figure 3-22. MERRA-2 mean May ozone concentrations at the 488 hPa level based on data from 2014-2020 (left). MERRA-2 ozone concentrations at the 488 hPa level at 00:00 UTC (right). The red oval represents the area of stratospheric intrusion.

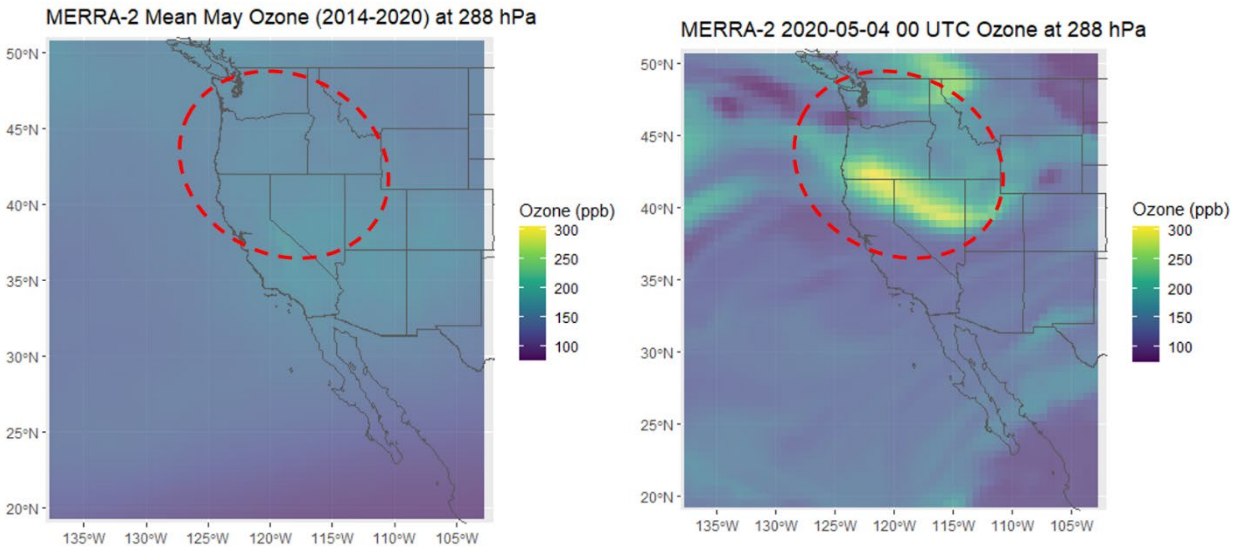

Figure 3-23. MERRA-2 mean May ozone concentrations at the 288 hPa level based on data from 2014-2020 (left). MERRA-2 ozone concentrations at the 288 hPa level at 00:00 UTC (right). The red oval represents the area of stratospheric intrusion.

The ozone "tongue" extending from the stratosphere modelled by RAQMS, shown in Figure 3-20, can also be seen in the modelled cross-section along 120-degrees W from the WACCM model. Figure 3-24 shows the injection of stratospheric ozone into the troposphere over 120-degrees W longitude on May 4 at 00:00 UTC that extended to 500 mb near 40-degrees N. Over the next 18 hours, the remnants of this ozone "tongue" are visible further eastward at 117.5-degrees and 116.2-degrees W longitude. The elevated ozone layer that results from the intrusion drops further into the atmosphere over 18 hours, reaching 800 mb by May 4 at 18:00 UTC.

Figures 3-25 through 3-28 show the progression of ozone-rich air from the suspected source region to Clark County between May 5 at 00:00 UTC to the event date, May 7, 00:00 UTC (May 6, 16:00 local time). Modelled ozone profiles on May 5 at 00:00 UTC are displayed in Figure 3-25 along three longitudes that align with HYSPLIT transport trajectories between the source region and Clark County (see Section 3.3.1). On May 5, each longitudinal cross section shows the ozone "tongue" shifting southward to 35-degrees N and extending further into the mid-troposphere. By 00:00 UTC on May 6, this ozone rich air mixes into the free troposphere, expanding downward in altitude as shown in the top panel of Figure 3-26. Vertical mixing is represented by black arrows in this figure. On the morning of the event date (May 6, 12:00 UTC), this layer of elevated ozone persists in the lower troposphere between 30-degrees to 40-degrees N latitude (bottom panel of Figure 3-26). A longitudinal cross section over Clark County is shown in Figure 3-27 on the event date, May 7, at 00:00 UTC (May 6, 18:00 local time). By this time, the layer of enhanced ozone has descended to surface-level over 36-degrees N latitude, the approximate location of Las Vegas.

An additional view of transport is displayed in Figure 3-28, which shows a progression of latitudinal cross sections along the southward trajectory between May 4 at 00:00 UTC and May 6 at 00:00 UTC. This progression displays the southward and westward shift in ozone-rich air from the source region towards Clark County. On May 4, a tropospheric fold (boxed in black) is visible in the source region near 43-degrees N latitude. On May 5 at 00:00 UTC, a pocket of enhanced ozone exists in the mid-troposphere (600 mb) at 37.2-degrees N latitude (boxed in black), confirming southward transport of ozone-rich air from the source region. Twenty-four hours later, the latitudinal cross section over the Las Vegas region (36.3-degrees N latitude) shows a deep plume of higher ozone between the surface and 600 mb (boxed in black), lending evidence to the assertion that the layer of enhanced ozone aloft mixed toward the surface by the event date. The progressions of modeled ozone displayed in Figures 3-25 through 3-28 and consistency of results across modeling platforms provide evidence of ozone-rich, stratospheric air mixing into the mid-troposphere and transporting southward towards Clark County, according to the HYSPLIT trajectories shown in Section 3.3.1. This movement of the high concentration ozone pocket indicates that the stratospheric intrusion in the Pacific Northwest could have contributed to high surface-level ozone concentrations on May 6 in Clark County.

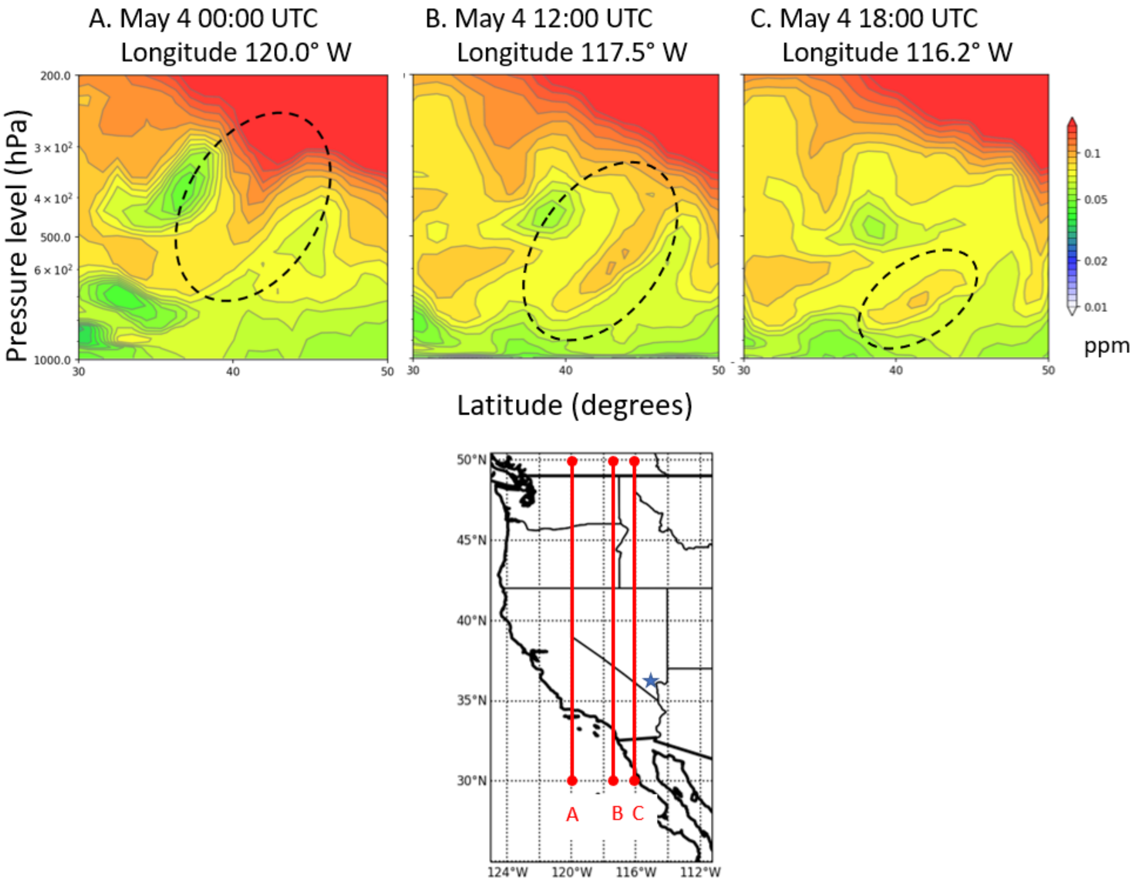

Figure 3-24. WACCM-modelled cross-section of ozone along the (A) 120-degrees W longitude line on May 4 at 00:00 UTC, (B) 117.5-degrees W longitude line on May 4 at 12:00 UTC, and (C) 116.2-degrees W longitude line on May 4 at 18:00 UTC. Ozone injected from the proposed source of stratospheric ozone on May 4, 00:00 UTC is circled in black in each plot. The extent of the cross-section is represented by the red line on the map (bottom). Las Vegas is represented by a blue star.

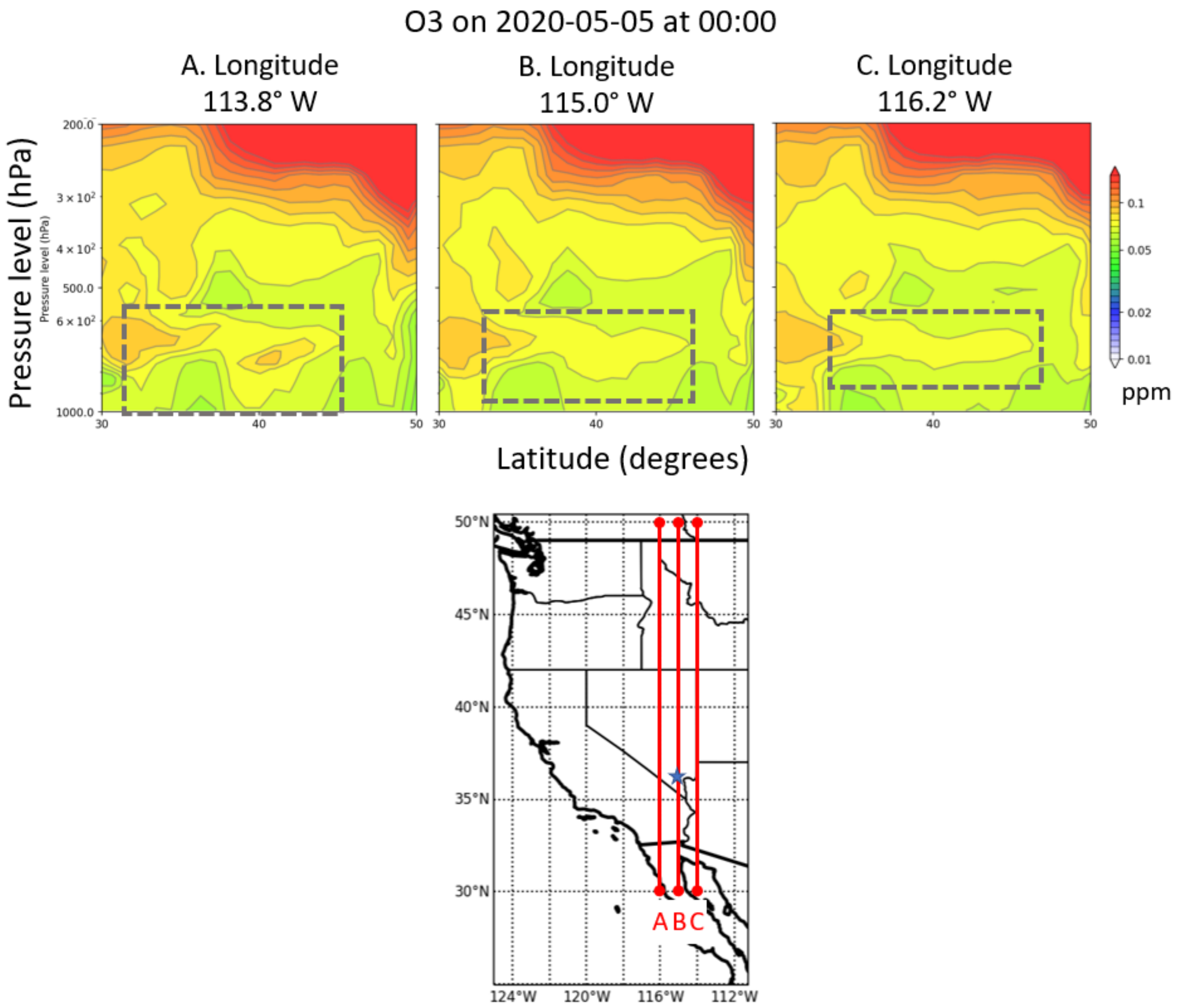

Figure 3-25. WACCM-modelled cross-section of ozone along the (A) 113.8-, (B) 115.0, and (C) 116.2-degrees W longitude line on May 5 at 00:00 UTC. The layer of ozone injected from the stratosphere is boxed in gray. The extent of each cross-section is represented by the red lines (labelled by letter) on the map (bottom). Las Vegas is represented by a blue star.

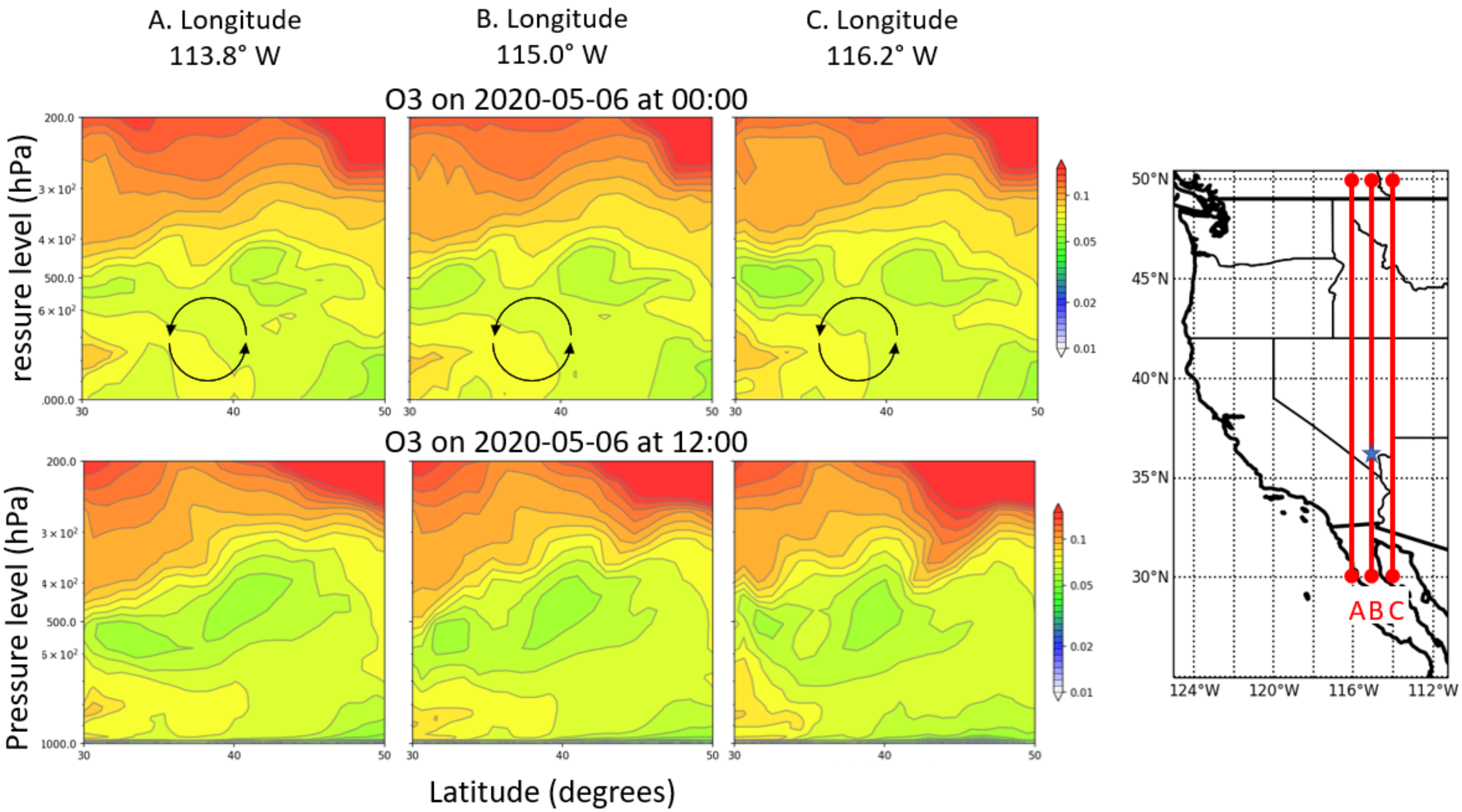

Figure 3-26. WACCM-modelled cross-section of ozone along the (A) 113.8-, (B) 115.0, and (C) 116.2-degrees W longitude line on May 6 at 00:00 UTC (top panel) and May 6 at 12:00 UTC (bottom panel). Vertical mixing is represented by black arrows. The extent of each cross-section is represented by the red lines (labelled by letter) on the map (right). Las Vegas is represented by a blue star.

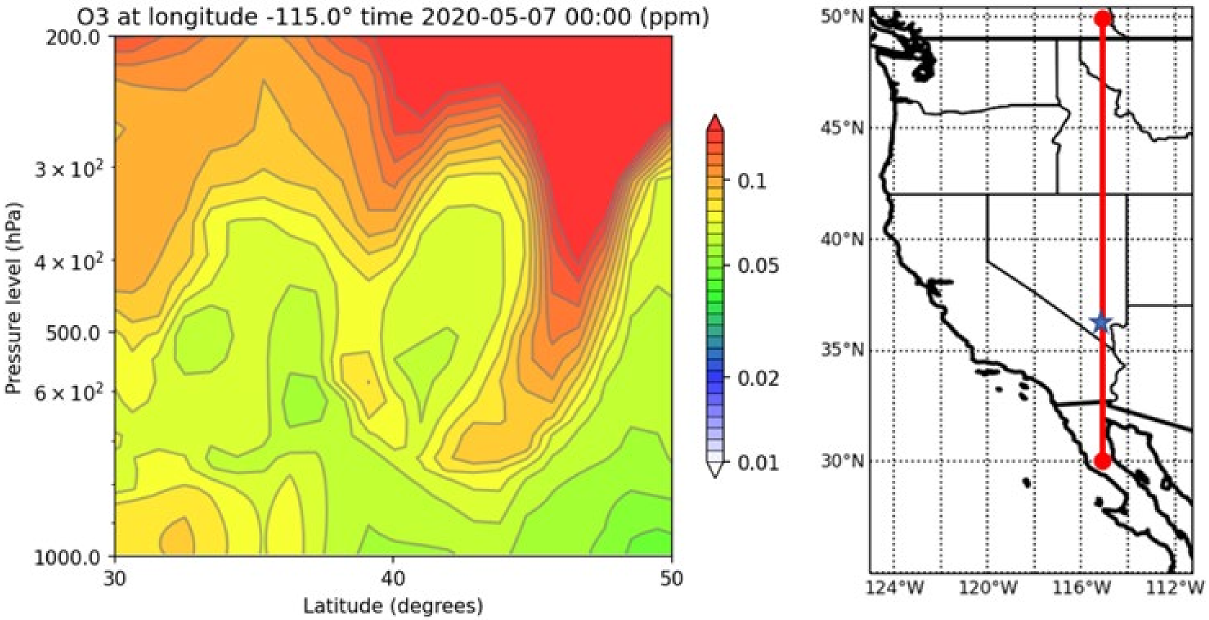

Figure 3-27. WACCM-modelled cross-section of ozone along the 115-degrees W longitude line on May 7 at 00:00 UTC, the exceedance event date (May 6, 16:00 local time). The extent of the cross-section is represented by the red line on the map (right). Las Vegas is represented by a blue star.

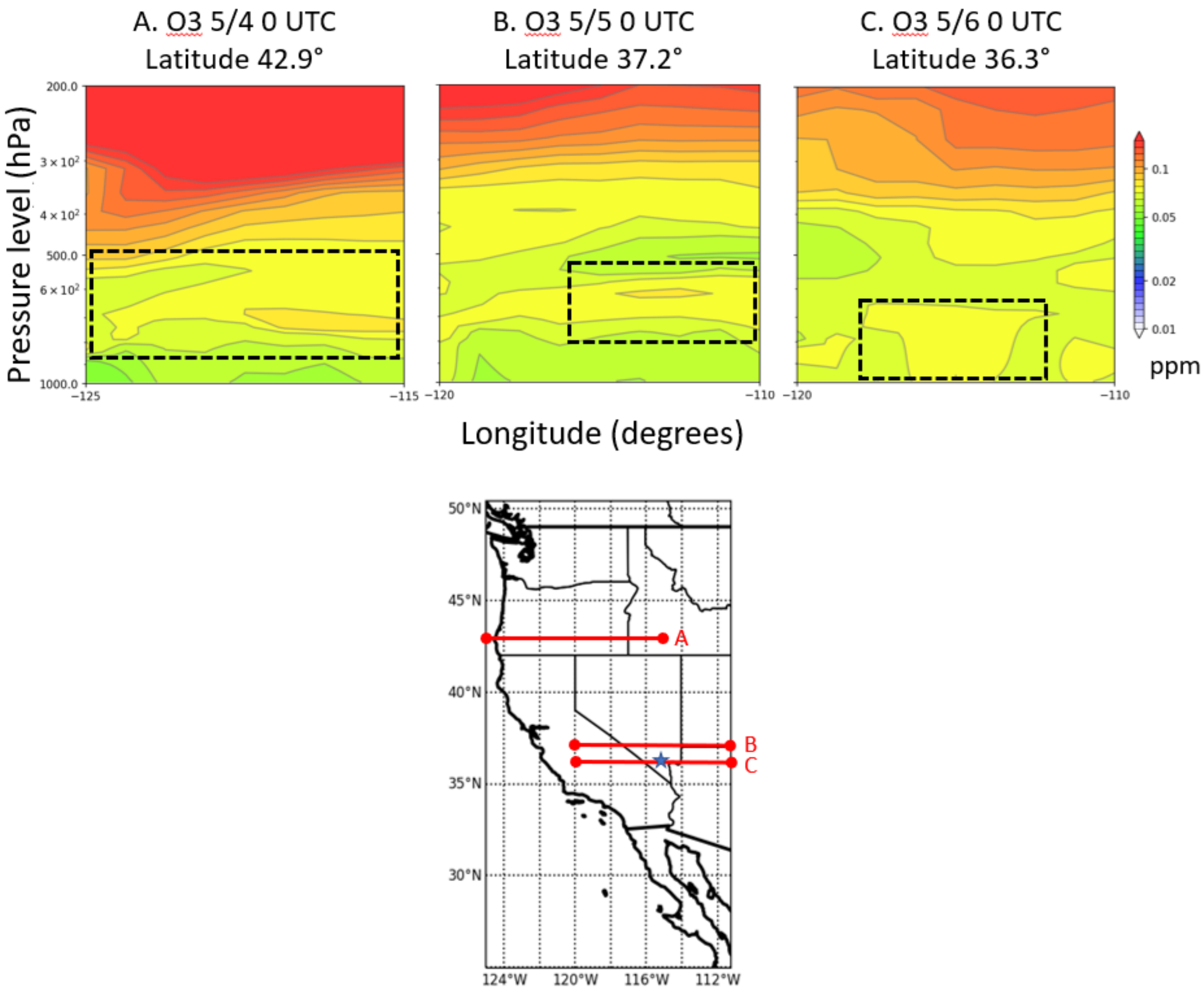

Figure 3-28. WACCM-modelled cross-section of ozone along the (A) 42.9-, (B) 37.2, and (C) 36.3-degrees N latitude lines on May 4, 5, and 6 respectively at 00:00 UTC. The extent of each cross-section is represented by the red lines (labelled by letter) on the map (right). Las Vegas is represented by a blue star. The boxed layer in A shows a tropospheric fold and elevated ozone in the mid-troposphere over the source region. The boxed layer in B shows elevated mid-tropospheric ozone in the transport path between the source region and Clark County. The boxed area in C shows a deep layer of elevated ozone between the surface and 600 mb.

The May 7 00:00 UTC RAQMS model similarly shows the suspected source ozone "tongue" expanding deeper into the atmosphere, as shown in Figure 3-29. On May 7, ozone concentrations as high as 75 ppb are seen at the 700 mb level between 30- and 40-degrees N.

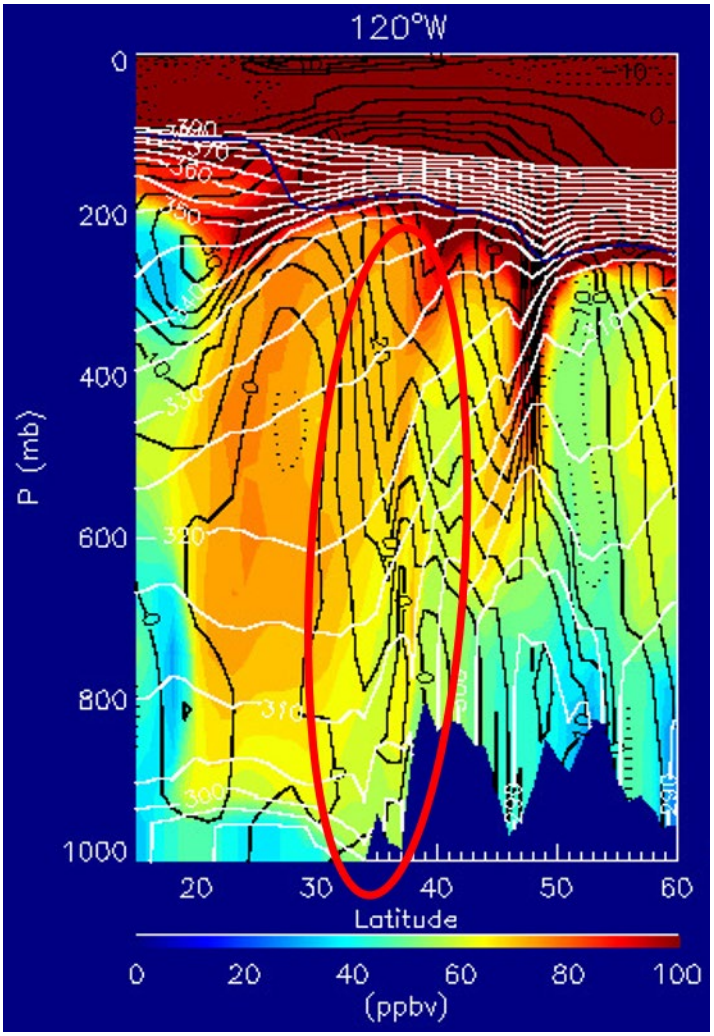

Figure 3-29. RAQMS-modelled cross section of ozone along the 120 degrees west longitude line on May 7 at 0:00 UTC (May 6 at 4:00 p.m. local time). The model was initialized at 12:00 UTC on May 6. The "tongue" of elevated ozone extending from the stratosphere into the mid-to-lower troposphere between 35- and 40- degrees N is circled in red.

Stratospheric air is also characterized by low CO concentrations. Therefore, an instance of stratosphere-to-troposphere mixing may be indicated by the presence of low concentrations of CO in the troposphere. Figure 3-30 shows the modeled CO concentration from RAQMS on May 4 at 0:00 UTC. Low CO can be seen in the region of suspected stratosphere-to-troposphere mixing in the northwestern United States (circled in red). Similarly, the WACCM-modelled CO concentrations for the same time also show relatively low CO concentrations (at or below 100 ppb) in the northwestern U.S. at the 300 mb level (**Figure 3-31**).

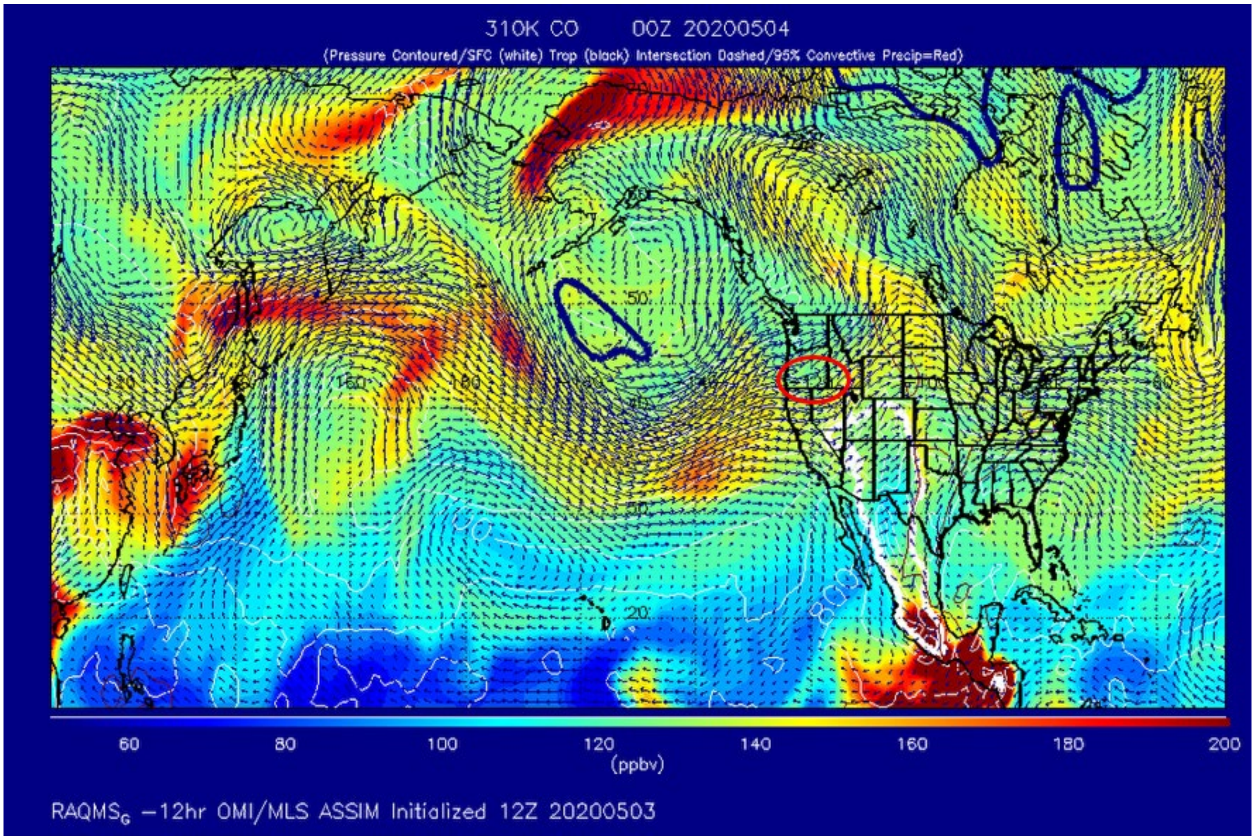

Figure 3-30. RAQMS-modelled CO at the 310 K isentrope level at 00:00 UTC on May 4. The model was initialized at 12:00 UTC on May 3. The region with suspected stratosphere-to-troposphere mixing, and corresponding reduced CO levels, is circled in red.

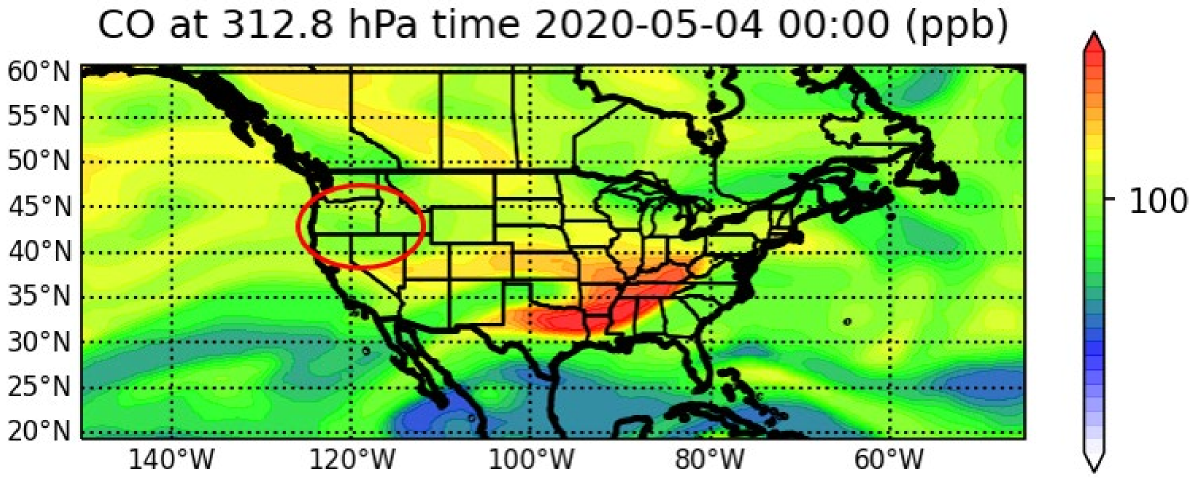

Figure 3-31. WACCM-modelled CO at the 300 mb level on May 4 at 0:00 UTC. The region with suspected stratosphere-to-troposphere mixing, and corresponding reduced CO levels, is circled in red.

A vertical cross section of modelled CO concentrations from the RAQMS is shown in Figure 3-32. The figure shows an intrusion of low-CO air from the stratosphere into the upper troposphere (circled in black) that aligns with the position of the ozone-rich "tongue" displayed at the same timestamp in Figure 3-20.

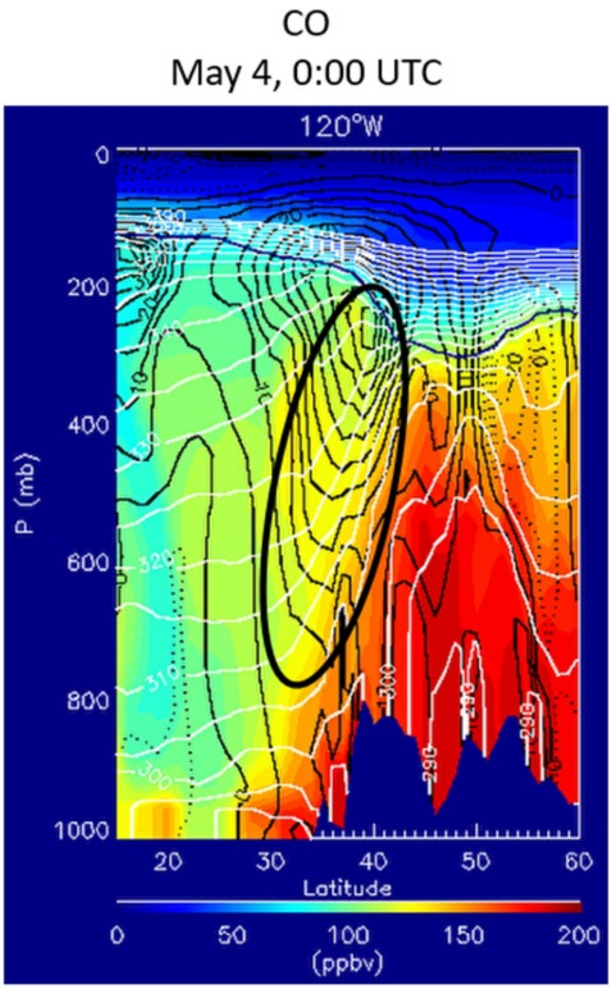

Figure 3-32. RAQMS-modelled cross-section of CO along the 120 degrees west longitude line on May 4 at 0:00 UTC. The model was initialized at 12:00 UTC on May 3. The "tongue" of reduced CO concentrations extending from the stratosphere into the upper near 40-degrees N is circled in black.

Maps of modelled CO from WACCM and RAQMS on the event date, seen in **Figures 3-33 and 3-34** respectively. Figures 3-33 and 3-34 show reduced CO concentrations over Clark County (circled in red), relative to surrounding regions, on the event date, May 7 at 00:00 UTC (4:00 p.m. PST on May 6), near the 900 mb level.

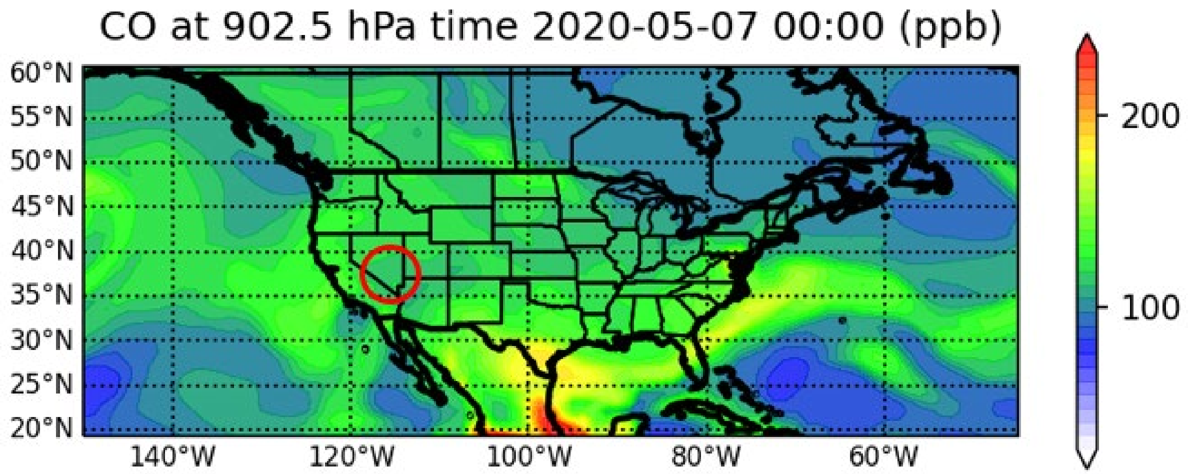

Figure 3-33. WACCM-modelled CO at the 900 mb level on May 7 at 00:00 UTC (May 6 at 4:00 p.m. PST, the event date). The region of relatively low CO concentrations over Clark County is circled in red.

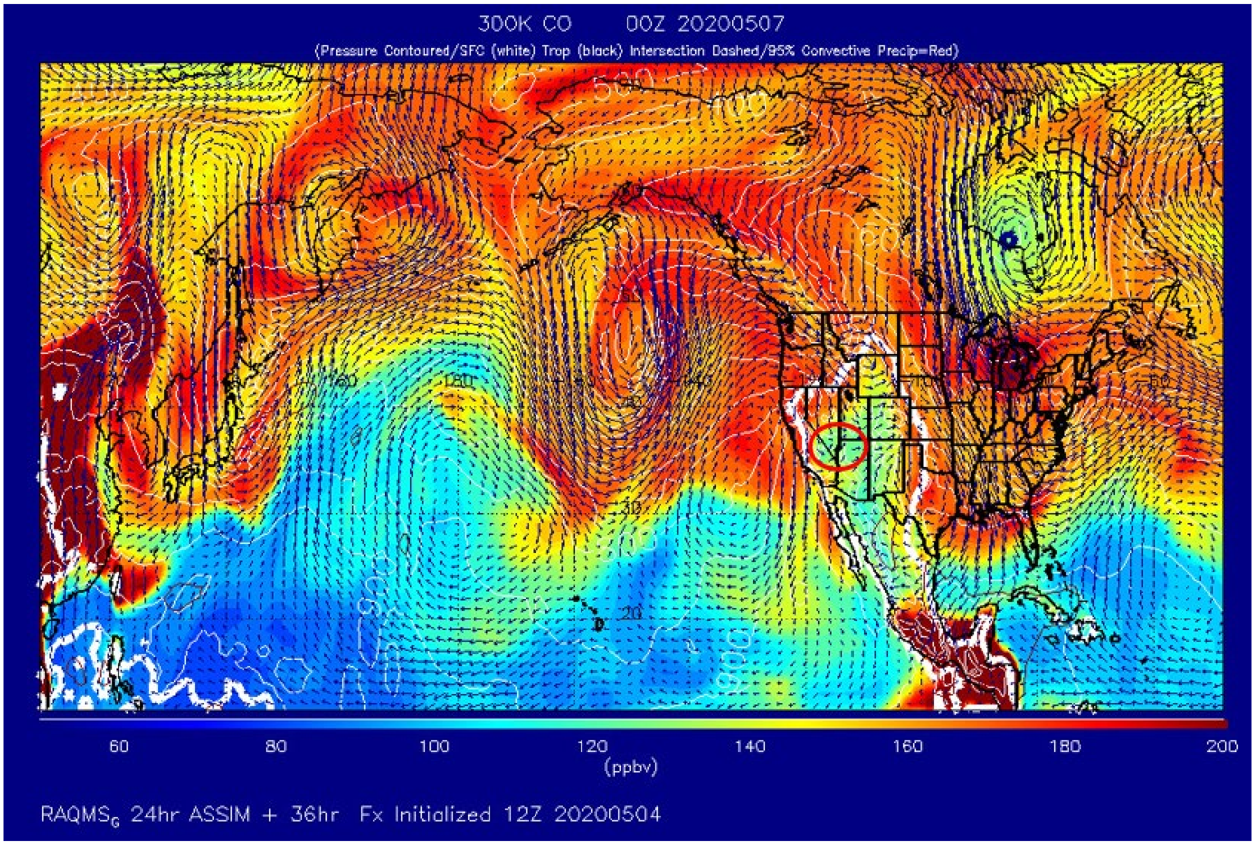

Figure 3-34. RAQMS-modelled CO at the 300 K isentrope level at 00:00 UTC on May 7 (May 6 at 4:00 p.m. PST, the event date). The region of relatively low CO concentrations over Clark County is circled in red. The model was initialized at 12:00 UTC on May 4.

Figure 3-35 shows MERRA-2 modeled CO concentrations for the May mean (2014 – 2020) and 00:00 UTC on May 4 over the western United States at 288 hPa. During the hours of the stratospheric intrusion that led to the May 6 ozone exceedance in Las Vegas, CO concentrations over California, Nevada, and Oregon at the 288 hPa level were lower than average. This low CO area is consistent with modeled CO in the upper troposphere shown in Figures 3-30 and 3-31 and the high ozone area from MERRA-2 in Figure 3-23 at the same date, time, and pressure level. Near the surface at the 985 hPa level on the event date, May 6, CO concentrations over the Las Vegas area were average to slightly below average (Figure 3-36), as indicated by darker shades of blue and purple.

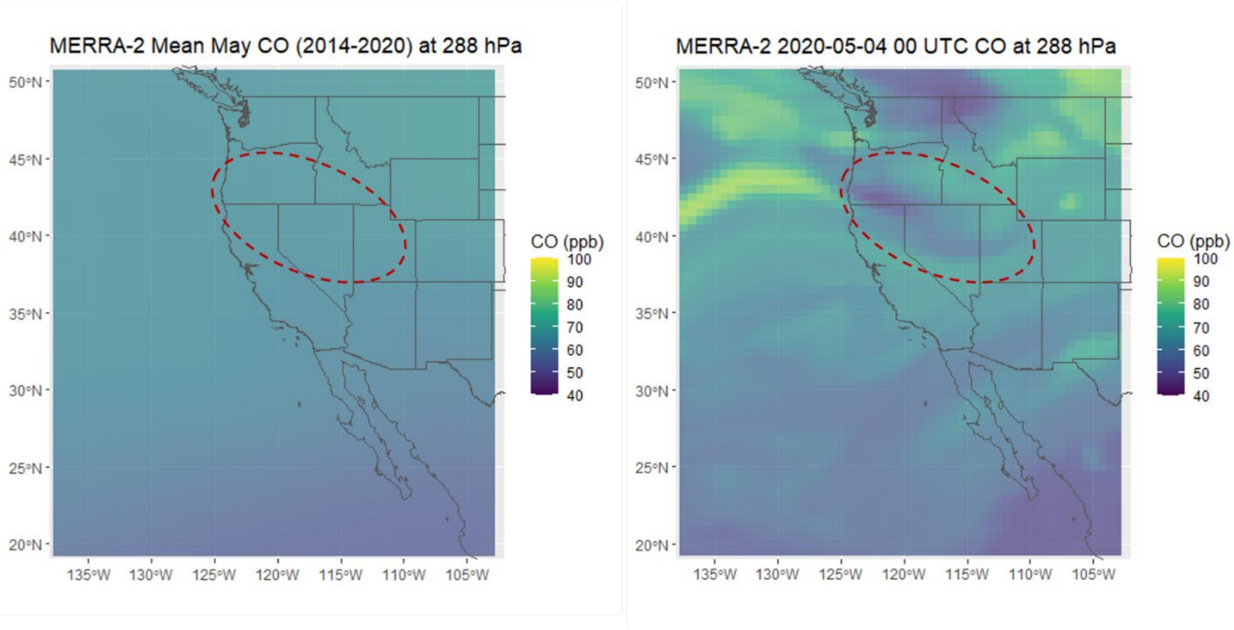

Figure 3-35. MERRA-2 mean May CO concentrations at the 288 hPa level based on data from 2014-2020 (left). MERRA-2 CO concentrations at the 288 hPa level at 00:00 UTC on May 4 show low CO at the stratospheric intrusion (right).

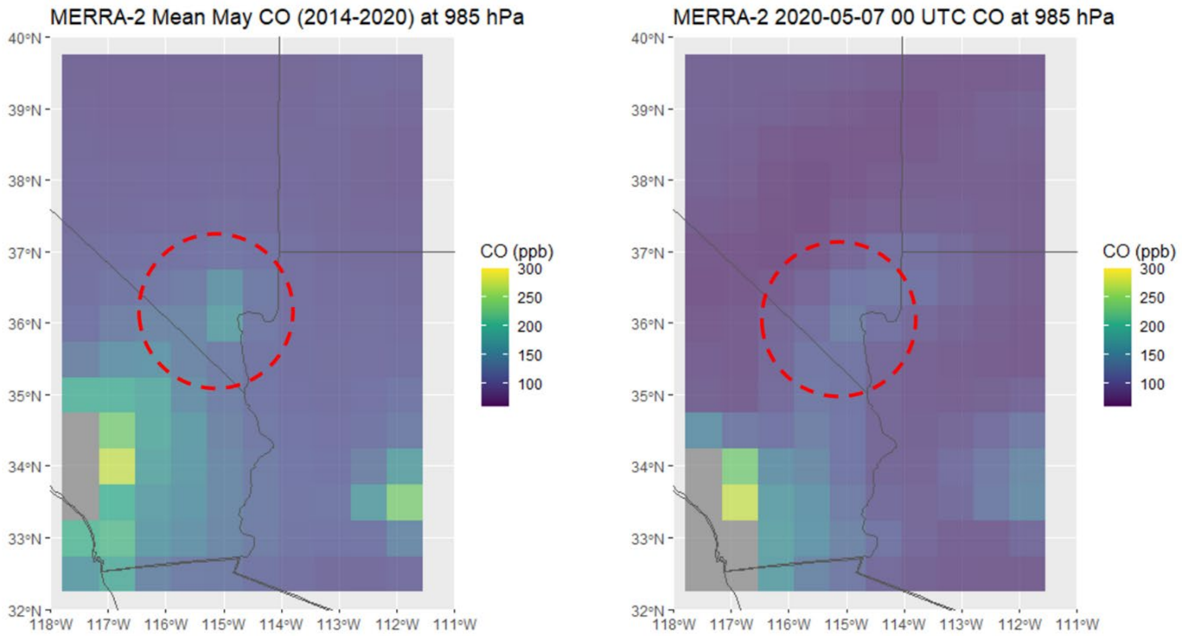

Figure 3-36. MERRA-2 mean May CO concentrations near the surface at the 985 hPa level based on data from 2014-2020 (left). MERRA-2 CO concentrations at the 985 hPa level (right) at 00:00 UTC on May 7 (4:00 p.m. local standard time on May 6). The red circle represents the Las Vegas area.

Modelled values of IPV, water vapor, and ozone and CO concentrations show that stratosphere-to-troposphere mixing occurred in the northwestern U.S. and off the coast on May 4 at 00:00 UTC. This region saw relatively high IPV, reduced water vapor, enhanced ozone throughout the upper- and mid-troposphere, and reduced CO levels in the upper troposphere, which are all markers of stratospheric air. Furthermore, a series of modeled ozone in mid-troposphere from May 4 through the event date indicates transport of air from the source region in the northwestern U.S. downward in altitude and southeastward toward Clark County. The following section will provide further evidence of the transport of air from the northwestern United States over Clark County that aligns with this timeline.

3.3 Evidence of Stratospheric Air Reaching the Surface

3.3.1 HYSPLIT Trajectory Analysis

HYSPLIT trajectories were run to demonstrate the transport of air from a stratospheric intrusion to Clark County. In the days prior to the event on May 6, 2020, these trajectories show that air was transported from the stratospheric intrusion, generally located in northern California and Oregon and over the eastern Pacific Ocean to Clark County. Combined with satellite observations and modeled analyses described in Sections 3.2.1 and 3.2.2, these trajectories provide evidence that stratospheric ozone was transported to Las Vegas, Nevada.

NOAA's online HYSPLIT model tool was used for the trajectory modeling (http://ready.arl.noaa.gov/HYSPLIT.php). HYSPLIT is a commonly used model that calculates the path of a single air parcel from a specific location and height above the ground over a period of time; this path is the modeled trajectory. HYSPLIT trajectories can be used as evidence that high-ozone stratospheric air was transported to an air quality monitor. This type of analysis is important for meeting both Tier 1 and 2 requirements.

The model options used for this study are summarized in Table 3-12. The meteorological data from the North American Mesoscale Forecast System (NAM, 12-km resolution) model were used (ready.noaa.gov/archives.php). These data are high in spatial resolution, are readily available for HYSPLIT modeling over the desired lengths of time, and are expected to capture fine-scale meteorological variability. The backward trajectory start time was selected to be in the afternoon at 00:00 UTC (i.e., 16:00 PST) when daily ozone concentrations peak. As suggested in the EPA's EE guidance (U.S. Environmental Protection Agency, 2016), a backward trajectory length of 72 hours was selected to assess whether stratospheric air from the current day or from the previous two days may have been transported over a long distance to the monitoring sites. Trajectories were initiated at 50 m and 1000 m to capture transport to the lower and upper mixed boundary layer, as stratospheric ozone may be transported aloft and influence concentrations at the surface through vertical mixing. Three backward trajectory approaches available in the HYSPLIT model were used in this analysis, including site-specific trajectories, trajectory matrix, and trajectory frequency. Site-specific back trajectories were run to show direct transport from the SOI to the affected site(s). This analysis is useful in linking air quality and meteorological impacts at a single location (i.e., an air quality monitor) to an SOI. Matrix back trajectories were run to show the general air parcel transport patterns from the Las Vegas area to the SOI. Similarly, matrix forward trajectories were run to show air parcel transport patterns from the SOI region to the Las Vegas area. Matrix trajectories are useful in analyzing air transport over areas larger than a single air quality site. Trajectory frequency analysis show the frequency with which multiple trajectories initiated over multiple hours pass over a grid cell on a map. Trajectory frequencies are useful in estimating the temporal and spatial patterns of air transport from a source region to a specific air quality monitor. Additionally, a forward trajectory matrix was run for the area to the west of northern California and Oregon (over the eastern Pacific Ocean) to examine the transport from the stratospheric intrusion region in the direction of Clark County.

Table 3-12. HYSPLIT run configurations for each analysis type, including meteorology data set, time period of run, starting location(s), trajectory time length, starting height(s), starting time(s), vertical motion methodology, and top of model height.

HYSPLIT Parameters	Back Trajectory Analysis – Matrix	Backward Trajectory Analysis – Frequency	Forward Trajectory Analysis – Matrix	Backward Trajectory Analysis – High Resolution
Meteorology	12-km NAM	12-km NAM	12-km NAM	3-km HRRR
Time Period	May 4 – May 7, 2020	May 4 – May 7, 2020	May 4 – May 7, 2020	May 4 – May 7, 2020
Starting Location	Evenly spaced grid covering Las Vegas, Nevada	36.1475 N, 115.1773 W, Apex, Jean	Evenly spaced grid covering area west of California, U.S.A., in the eastern Pacific Ocean	36.1475 N, 115.1773 W, Apex, Jean
Trajectory Time Length	72 hours	72 hours	72 hours	72 hours
Starting Heights (AGL)	1,000 m	50 m	5,000 m	50 m
Starting Times	00:00 UTC	00:00 UTC	00:00 UTC	00:00 UTC
Vertical Motion Method	Model Vertical Velocity	Model Vertical Velocity	Model Vertical Velocity	Model Vertical Velocity
Top of Model	10,000 m	10,000 m	10,000 m	10,000 m

Site-specific backward trajectories were calculated from the Las Vegas Valley (36.1475 N, 115.1773 W), the Apex site, and the Jean site on May 6, 2020. We chose to model all trajectories for sites within the Las Vegas metropolitan area using the Las Vegas Valley location. The Apex and Jean sites are far enough away from the Las Vegas metropolitan area to warrant their own backward trajectories. The hour of 00:00 UTC (i.e., 16:00 PST) was chosen as the model starting time, since ozone concentrations are usually the highest in the afternoon. The NAM-based backward trajectories from the Las Vegas Valley are shown in Figures 3-37 through 3-39. All three trajectories follow a similar backward path from the Las Vegas Valley, Apex, and Jean sites originating at elevated heights over the area to the west of California and Oregon in the eastern Pacific Ocean.

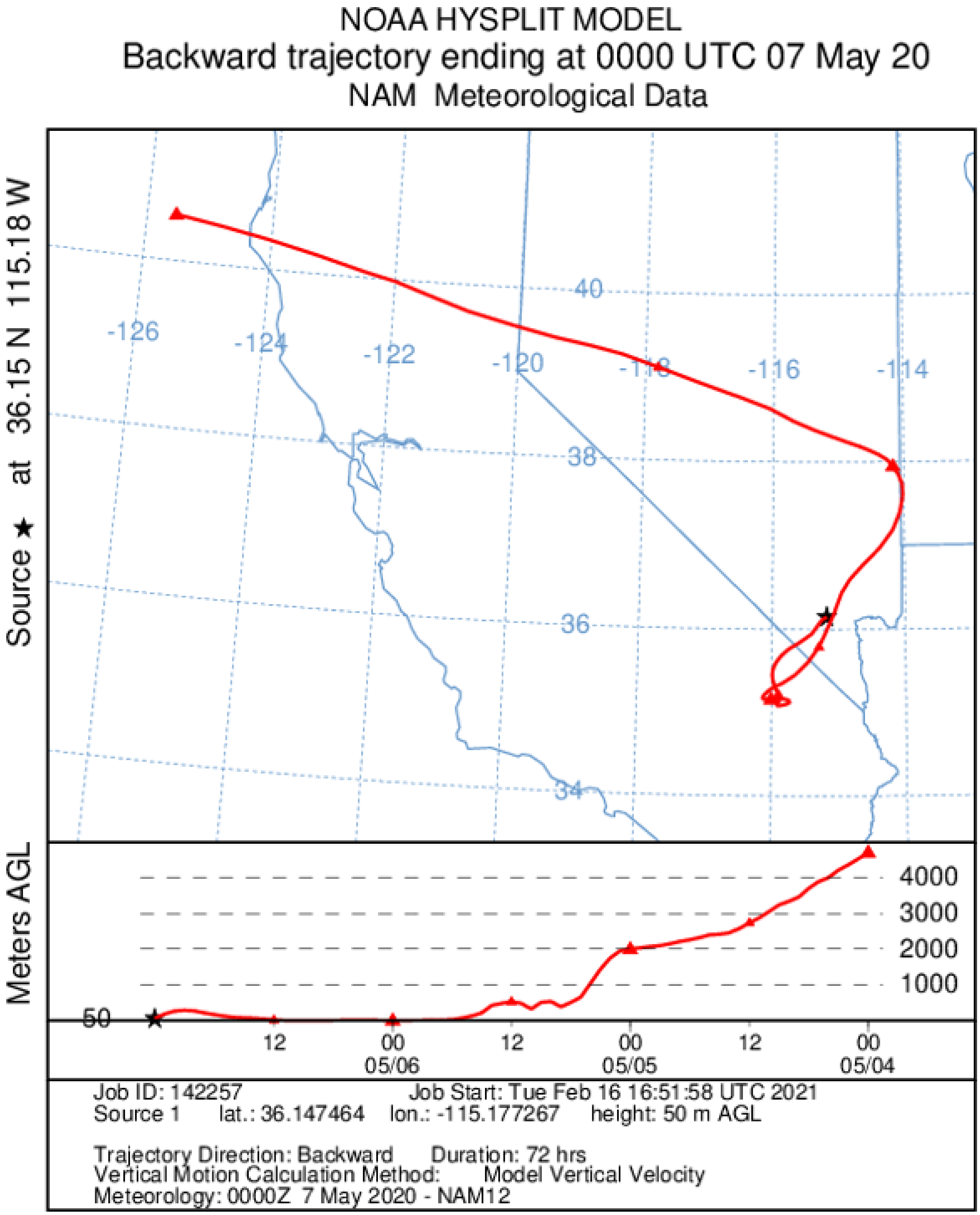

Figure 3-37. 72-hour HYSPLIT back trajectories from Las Vegas Valley, ending on May 7, 2020. NAM 12-km back trajectories are shown for 50 m (red) above ground level.

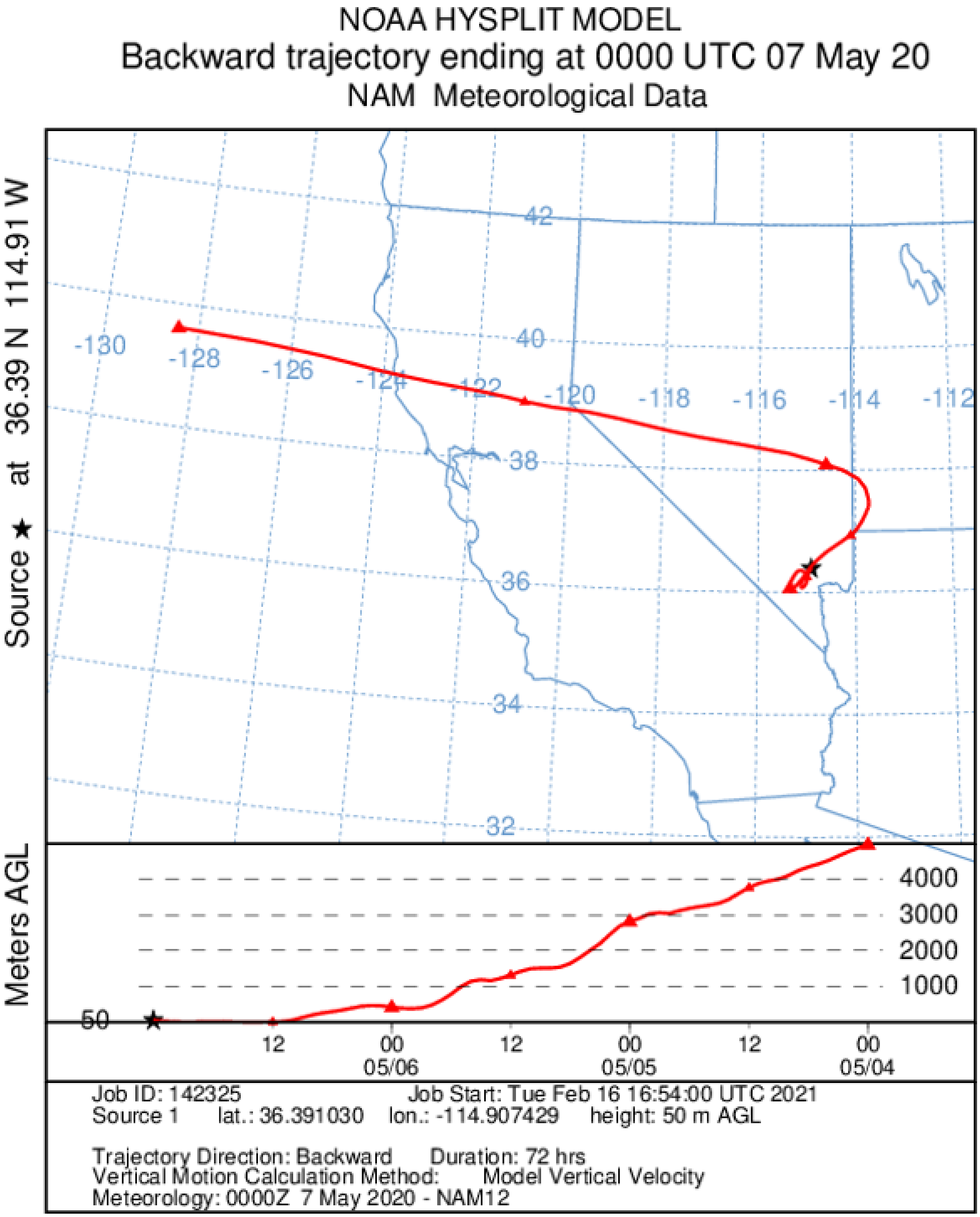

Job ID: 142325 Job Start: Tue Feb 16 16:54:00 UTC 2021
Source 1 lat.: 36.391030 lon.: -114.907429 height: 50 m AGL

Trajectory Direction: Backward Duration: 72 hrs
Vertical Motion Calculation Method: Model Vertical Velocity
Meteorology: 0000Z 7 May 2020 - NAM12

Figure 3-38. 72-hour HYSPLIT back trajectories from the Apex station, ending on May 7, 2020. NAM 12 -km back trajectories are shown for 50 m (red) above ground level.

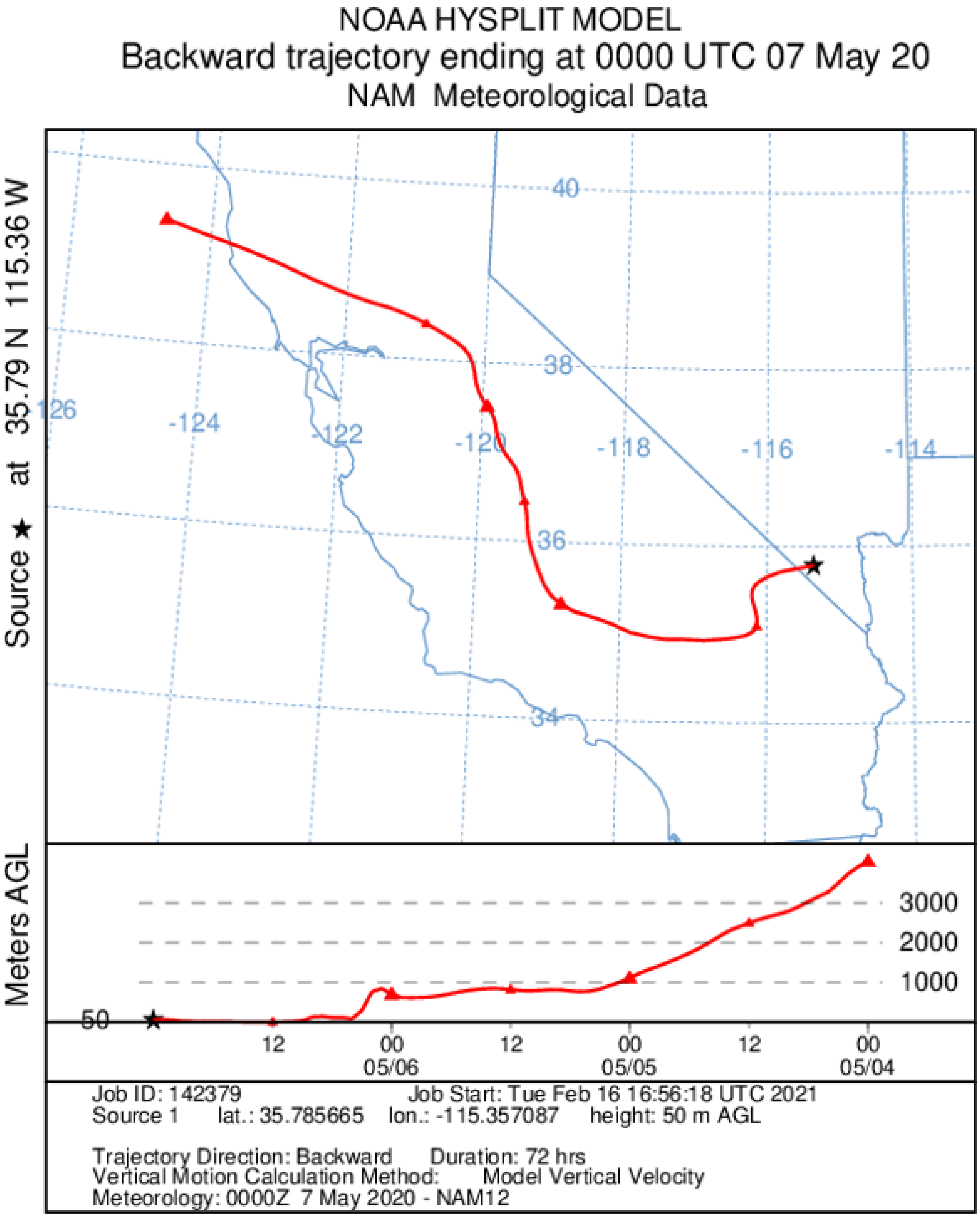

Figure 3-39. 72-hour HYSPLIT back trajectories from the Jean station, ending on May 7, 2020. NAM 12-km back trajectories are shown for 50 m (red) above ground level.

To identify variations in meteorological patterns of transported air to Las Vegas, we generated a HYSPLIT trajectory matrix. For this approach, trajectories are run in an evenly spaced grid of source locations. **Figure 3-40** shows a 72-hour backward trajectory matrix with source locations encompassing Clark County. The backward trajectories were initiated during late afternoon at 00:00 UTC on May 7, 2020 (i.e., May 6 at 16:00 PST), at a starting height of 1000 m agl. Consistent with the trajectories depicted in Figures 3-37 through 3-39, a major subset of air parcels is transported from an area to the west of northern California at elevated heights over the eastern Pacific Ocean, across California and Nevada, and finally intersected Las Vegas at 1000 m agl.

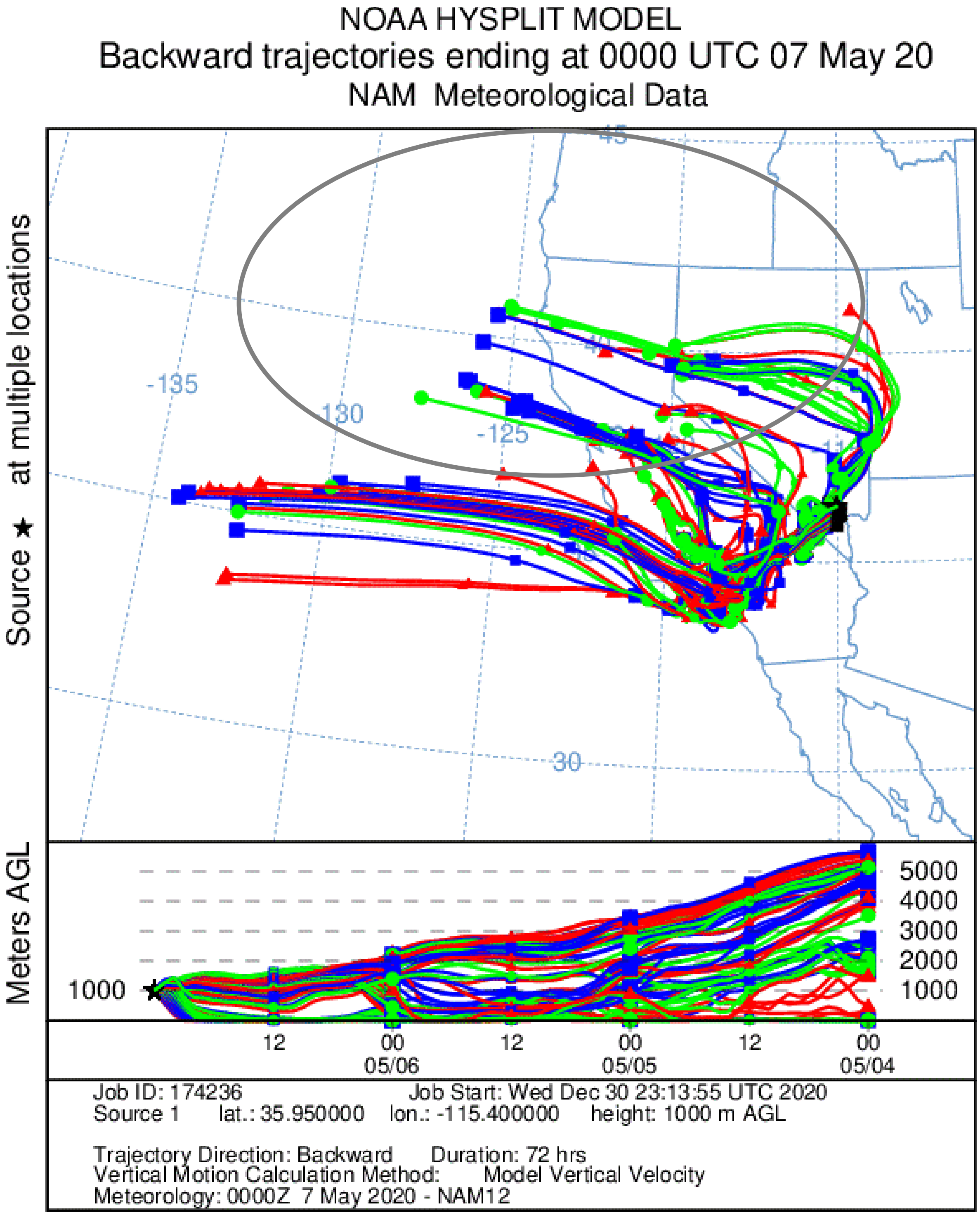

Figure 3-40. 72-hour HYSPLIT back trajectory matrix from Las Vegas Valley, ending on May 7, 2020. NAM 12 km-back trajectories are shown for 1000 m above ground level. The approximate area of the SOI is shown by the gray circle.

The third trajectory approach used in this analysis was HYSPLIT trajectory frequency. In this option, a trajectory from a single location and height starts every three hours. Using a continuous 0.25-degree grid, the frequency of trajectories passing through each grid cell is totaled and then normalized by the total number of trajectories. **Figures 3-41 through 3-43** show 72-hour backward trajectory frequency plots starting from the Las Vegas Valley, Apex site, and Jean site at 50 m agl during the afternoon of May 6, 2020. The trajectory frequency plot yields similar results as those from the back trajectory matrix; transported air impacting the Las Vegas Valley, Apex site, and Jean site on May 6 partly came from the eastern Pacific Ocean bordering California.

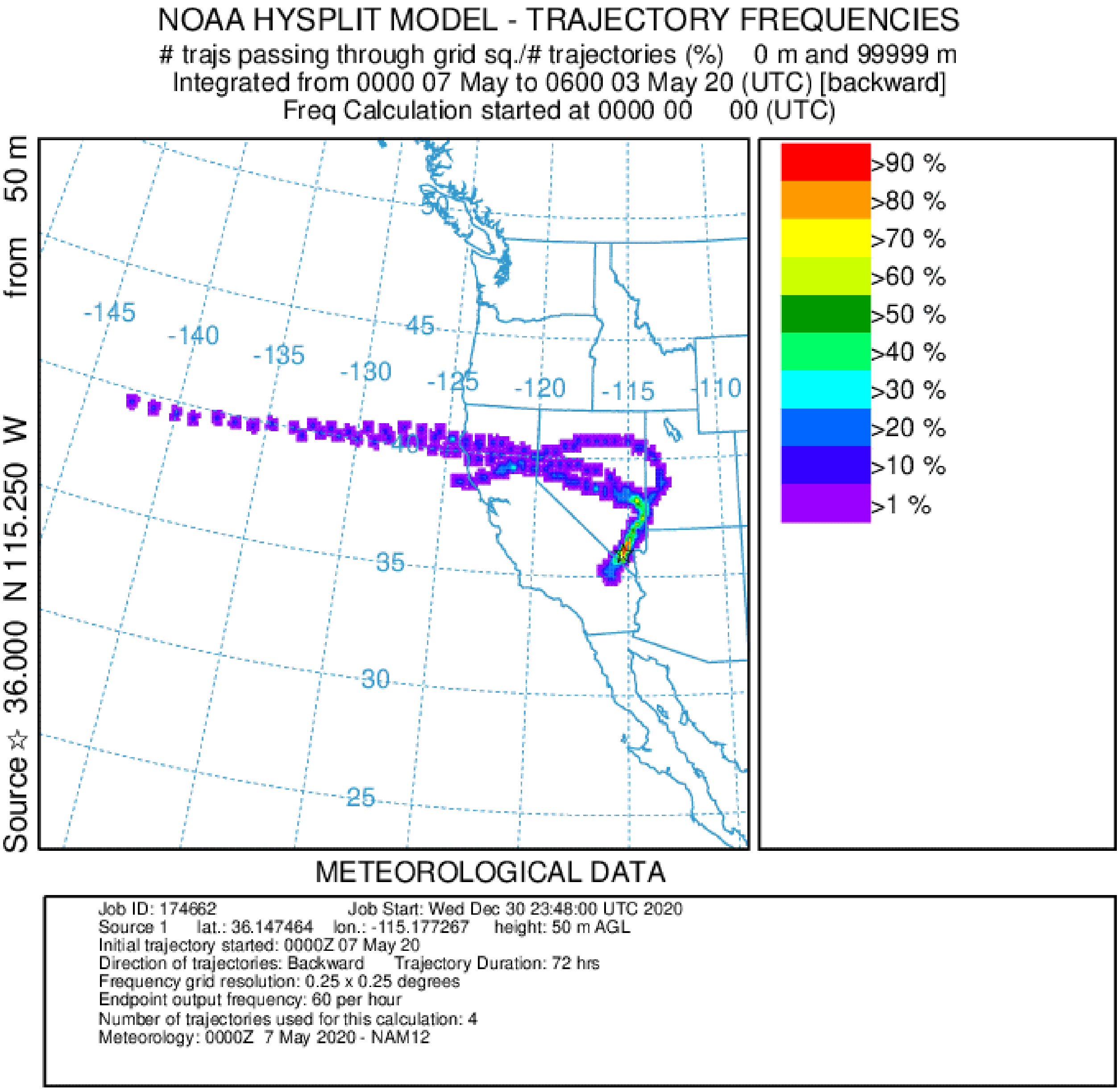

Job ID: 174662   Job Start: Wed Dec 30 23:48:00 UTC 2020
Source 1   lat.: 36.147464   lon.: -115.177267   height: 50 m AGL
Initial trajectory started: 0000Z 07 May 20
Direction of trajectories: Backward   Trajectory Duration: 72 hrs
Frequency grid resolution: 0.25 x 0.25 degrees
Endpoint output frequency: 60 per hour
Number of trajectories used for this calculation: 4
Meteorology: 0000Z 7 May 2020 - NAM12

Figure 3-41. 72-hour HYSPLIT back trajectories frequency from Las Vegas Valley, ending on May 7, 2020. NAM 12-km back trajectories are shown for 1,000 m above ground level. The colors within the frequency plot indicate the percent of trajectories that pass through a grid square.

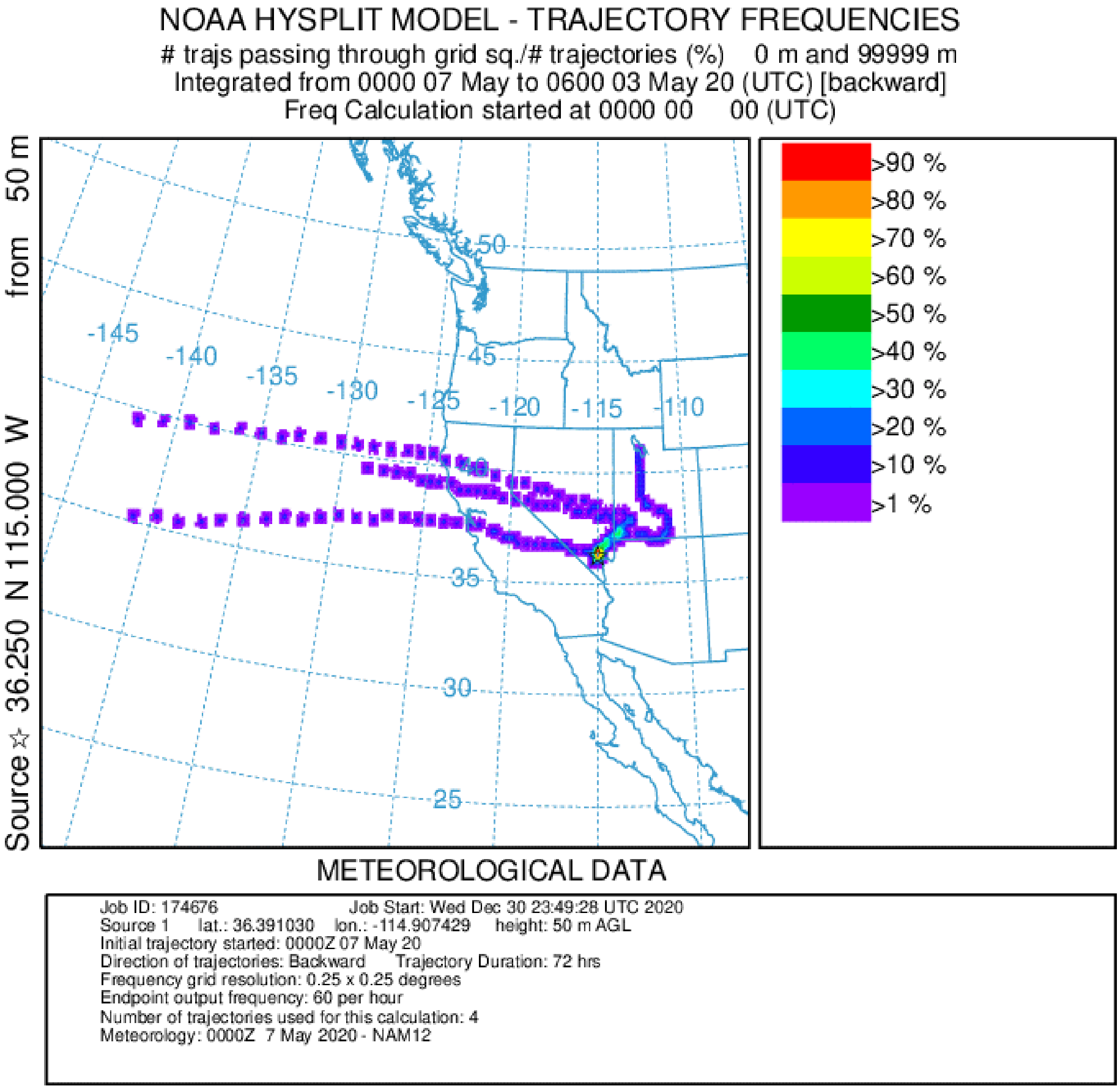

Job ID: 174676 Job Start: Wed Dec 30 23:49:28 UTC 2020
Source 1 lat.: 36.391030 lon.: -114.907429 height: 50 m AGL
Initial trajectory started: 0000Z 07 May 20
Direction of trajectories: Backward Trajectory Duration: 72 hrs
Frequency grid resolution: 0.25 x 0.25 degrees
Endpoint output frequency: 60 per hour
Number of trajectories used for this calculation: 4
Meteorology: 0000Z 7 May 2020 - NAM12

Figure 3-42. 72-hour HYSPLIT back trajectories frequency from the Apex site, ending on May 7, 2020. NAM 12-km back trajectories are shown for 1,000 m above ground level. The colors within the frequency plot indicate the percent of trajectories that pass through a grid square.

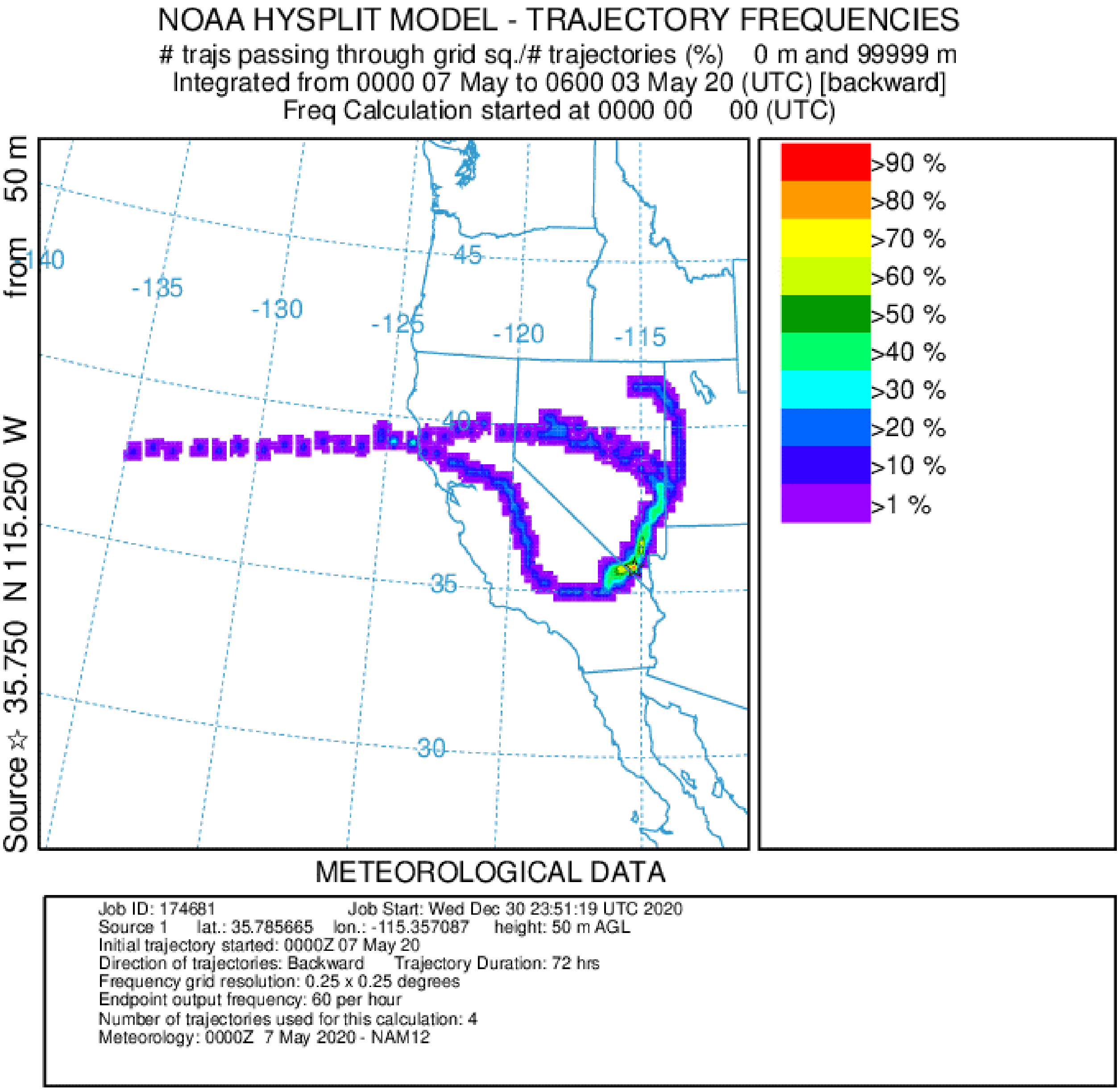

Job ID: 174681 Job Start: Wed Dec 30 23:51:19 UTC 2020
Source 1 lat.: 35.785665 lon.: -115.357087 height: 50 m AGL
Initial trajectory started: 0000Z 07 May 20
Direction of trajectories: Backward Trajectory Duration: 72 hrs
Frequency grid resolution: 0.25 x 0.25 degrees
Endpoint output frequency: 60 per hour
Number of trajectories used for this calculation: 4
Meteorology: 0000Z 7 May 2020 - NAM12

Figure 3-43. 72-hour HYSPLIT back trajectories frequency from Jean site, ending on May 7, 2020. NAM 12-km back trajectories are shown for 1,000 m above ground level. The colors within the frequency plot indicate the percent of trajectories that pass through a grid square.

Forward trajectories were initiated from the approximate area of the stratospheric intrusion starting at a height of 5,000 m agl at 00:00 UTC on May 4 (**Figure 3-44**). These trajectories show that stratospheric air was transported from the approximate area of the stratospheric intrusion, and air descended along the path into Clark County. These forward trajectories, combined with the back trajectories shown above, further support the transport of stratospheric air from the eastern Pacific Ocean bordering California to Clark County, Nevada. The backward and forward trajectories presented in this section all describe high altitude air over the eastern Pacific, northern California, and Oregon being transported and descending into Clark County between May 4 and the May 6 EE day.

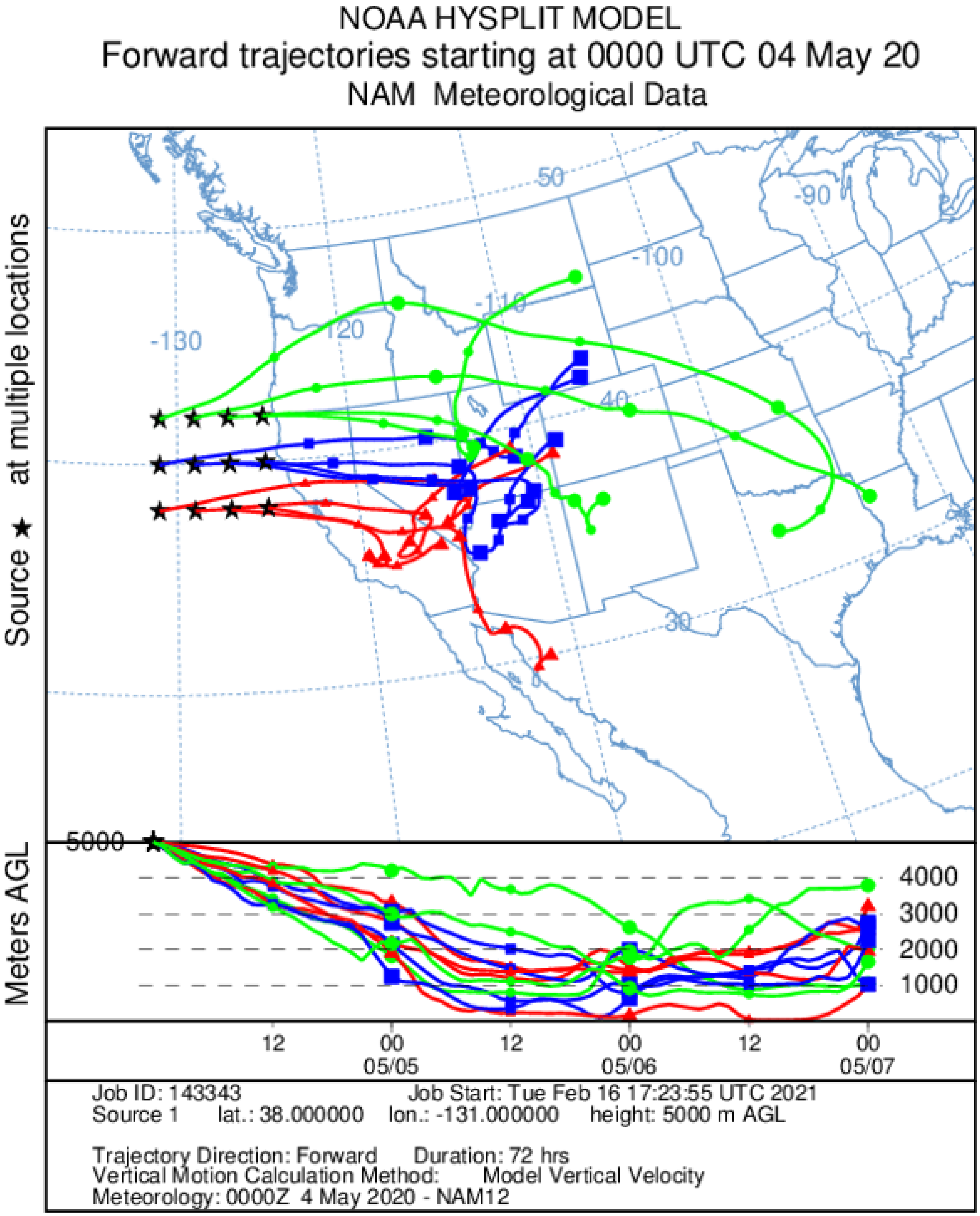

Figure 3-44. 72-hour HYSPLIT forward trajectories from the stratospheric intrusion source region initiated on May 4, 2020, at 00:00 UTC. NAM 12-km forward trajectories were initiated at 5,000 m above ground level.

3.3.2 Measurements of Tropospheric Mixing

Atmospheric soundings in the form of skew-T diagrams can provide an initial view into the extent of vertical mixing between the stratosphere and the troposphere. Some indications of stratospheric intrusion revealed by a sequence of these atmospheric soundings include the transport of dry, stratospheric air to lower elevations, a lowering of the tropopause, and favorable conditions for mixing between the surface and higher altitudes. An example of a skew-T diagram, shown in Figure 3-45, shows the change in air temperature (T) and dewpoint temperature (T_d) as a function of altitude and corresponding pressure level. Drier air is indicated by a separation between T and T_d (e.g. orange-boxed region). The tropopause is indicated by temperatures reaching a minimum before increasing with height and represents the boundary between the troposphere and the stratosphere. The air temperature profile follows the dry adiabatic lapse rate (green curve), indicating a well-mixed, dry layer from the surface up to 550 hPa. Dry adiabats identify the slope at which the temperature lapse rate is absolutely or conditionally unstable. Moist adiabats are drawn in blue and identify the slope at which the temperature lapse rate indicates conditionally unstable or absolutely stable air.

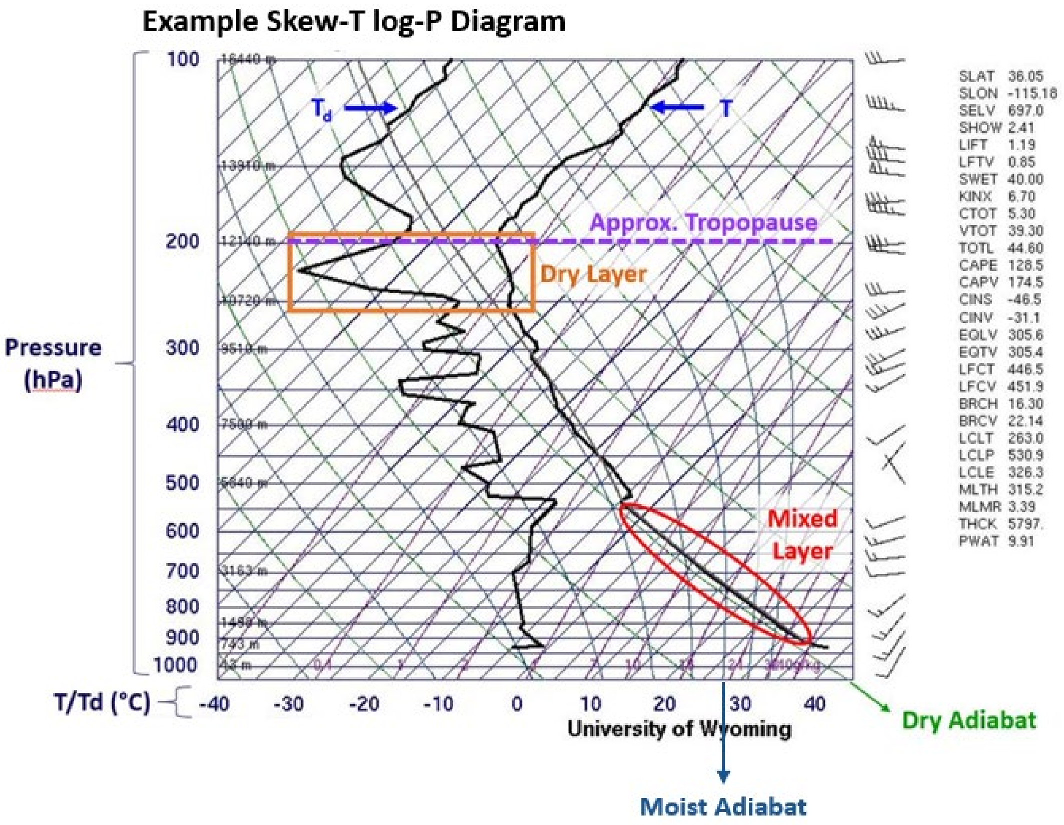

Figure 3-45. An example skew-T diagram with labelled features. Red circle denotes deep mixed layer. Orange box denotes relatively dry layer of air. The approximate (cold-point temperature) tropopause is denoted by the dashed purple line. Dry and moist adiabats are drawn as green and blue lines at a range of initial surface temperatures.

Our analysis of atmospheric soundings during the May 6 event period was guided by an example included in the EPA SOI Guidance that displayed skew-T diagrams from a documented stratospheric intrusion over Grand Junction, Colorado, in 2017. This example included two skew-T diagrams, shown in **Figure 3-46** of this report, with particular characteristics that suggest viable tropospheric mixing to facilitate vertical transport of ozone injected into the mid-troposphere to the surface. The two skew-T diagrams are characterized primarily by the large, very dry layer at a height greater than approximately 5 km above mean sea level or 3.5 km above ground level. A temperature inversion, observed from the 00:00 UTC sounding, likely prevented the dry air above from mixing down into the lower troposphere. During the 12:00 UTC sounding, 12 hours after the 00:00 UTC sounding and 12 hours before the exceedances occurred, it is clear from the widening of the gap between the dewpoint temperature (Td) and the temperature (T) profile that dry air mixed into the lower troposphere. The base of the very dry mixed layer also moved down into the atmosphere by about 500 m. Furthermore, the temperature lapse rate of the lower troposphere was approximately dry-adiabatic, indicating that the lower PBL was well-mixed. In this EPA-provided Grand Junction example, the SOI affected surface ozone concentrations and caused an exceedance of the ozone NAAQS. Skew-T diagrams for the May 6 event show very similar characteristics to this documented example of an SOI event, suggesting that a similar pathway of vertical mixing in the troposphere to transport SOI-injected ozone towards the surface existed on May 6.

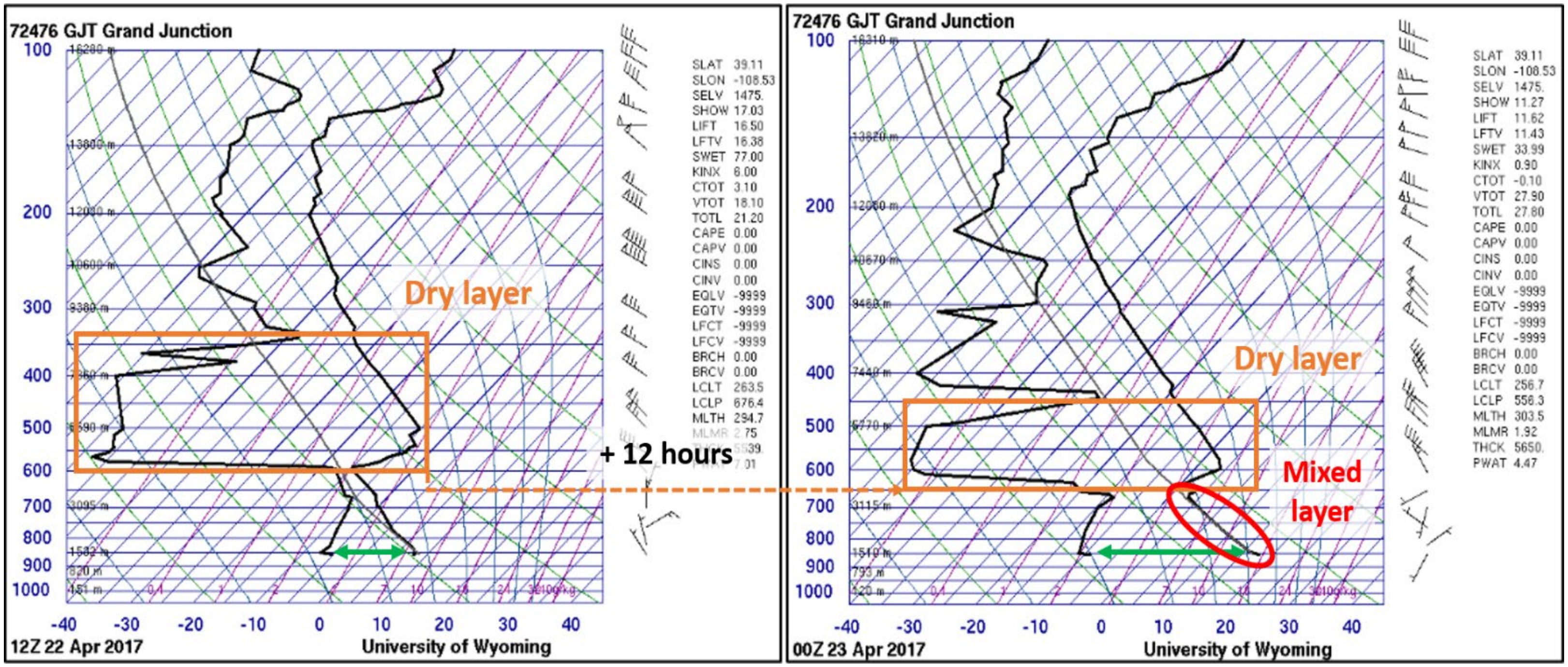

Figure 3-46. Skew-T diagrams for 12:00 UTC (left) on April 22, 2017, and 00:00 UTC (right) on April 23, 2017, at Grand Junction, Colorado. Orange boxes denote the very dry layer. The red circle denotes the mixed layer. Green arrows indicate the intrusion of very dry air to the surface. The figures were collected directly from EPAs "Guidance on the Preparation of Exceptional Events Demonstrations for Stratospheric Ozone Intrusions".

We examined skew-T diagrams from four National Weather Service (NWS) forecasting offices in the western U.S.: Medford, Oregon (MFR), Oakland, California (OAK), Reno, Nevada (REV), and Las Vegas, Nevada (VEF). The approximate location of each office along with the location of Clark County (shaded in yellow) is shown in Figure 3-47.

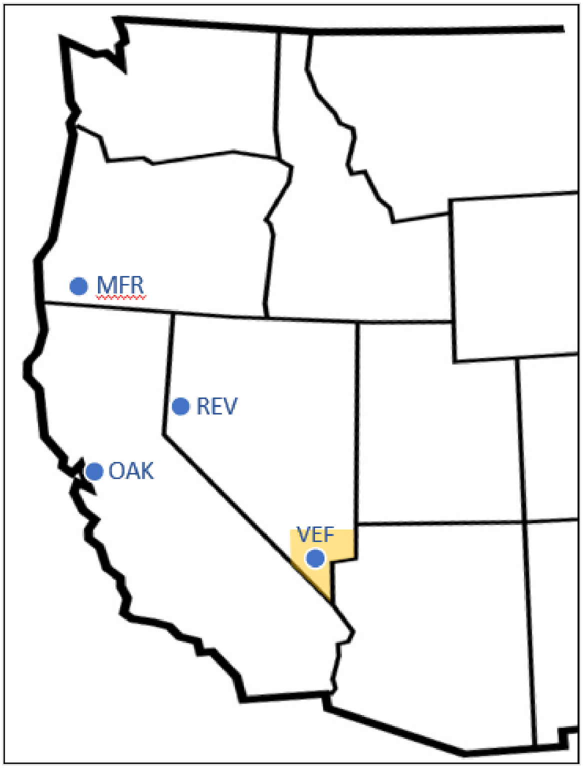

Figure 3-47. The locations of four National Weather Service offices in the western U.S. MFR and OAK are located in the suspected region of stratosphere-to-troposphere exchange on May 3. OAK and REV lie along possible trajectories of air to Clark County between May 3 and May 6 modelled using HYSPLIT (see Figure 3-40). VEF is located in Las Vegas, near the sites that measured ozone exceedances on May 6. Clark County is shaded in yellow.

MFR is just north of the modelled source region but well within the region of suspected stratosphere-to-troposphere mixing. The skew-T diagram from May 4, 00:00 UTC is shown in Figure 3-48. This sounding shows a relatively low tropopause at about 450 hPa and a layer of dry air in the upper troposphere. This provides supporting evidence of stratospheric intrusion, as the reduced altitude of the tropopause and low measured water content indicate penetration of dry stratospheric air into lower layers of the atmosphere.

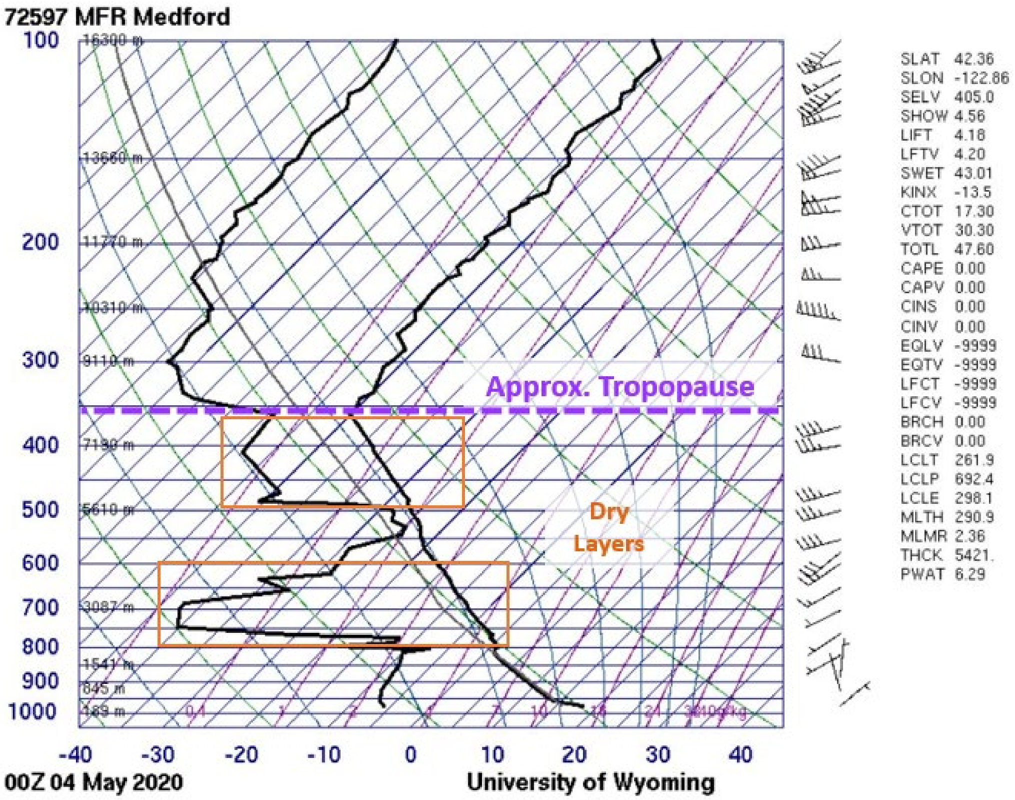

Figure 3-48. Skew-T sounding launched from the Medford (MFR) National Weather Service office on May 4, 2020, at 0:00 UTC (4:00 p.m. May 3, local time). The approximate (cold-point temperature) tropopause is denoted by the dashed purple line. A dry layer of air is boxed and labeled in orange.

Based on the HYSPLIT trajectories presented in Figure 3-40, Oakland, CA (OAK), is near the source region and lies along the pathway between the source region and Clark County on the days leading up to the ozone exceedance on May 6. Skew-T soundings from OAK on May 4 at 00:00 UTC and May 5 at 00:00 UTC are shown in Figure 3-49. These dates align with trajectories presented in Figure 3-40 showing transport from the SOI source region in the eastern Pacific and northwestern U.S. to Clark County between May 4 and May 6. Both of these skew-T soundings, taken 24 hours apart, exhibit dry layers of air near the tropopause and within the mid-to-lower troposphere, as well as a descending tropopause. These dry layers and a descending tropopause provide supporting evidence that dry, stratospheric air penetrated downwards into the lower atmosphere in this region.

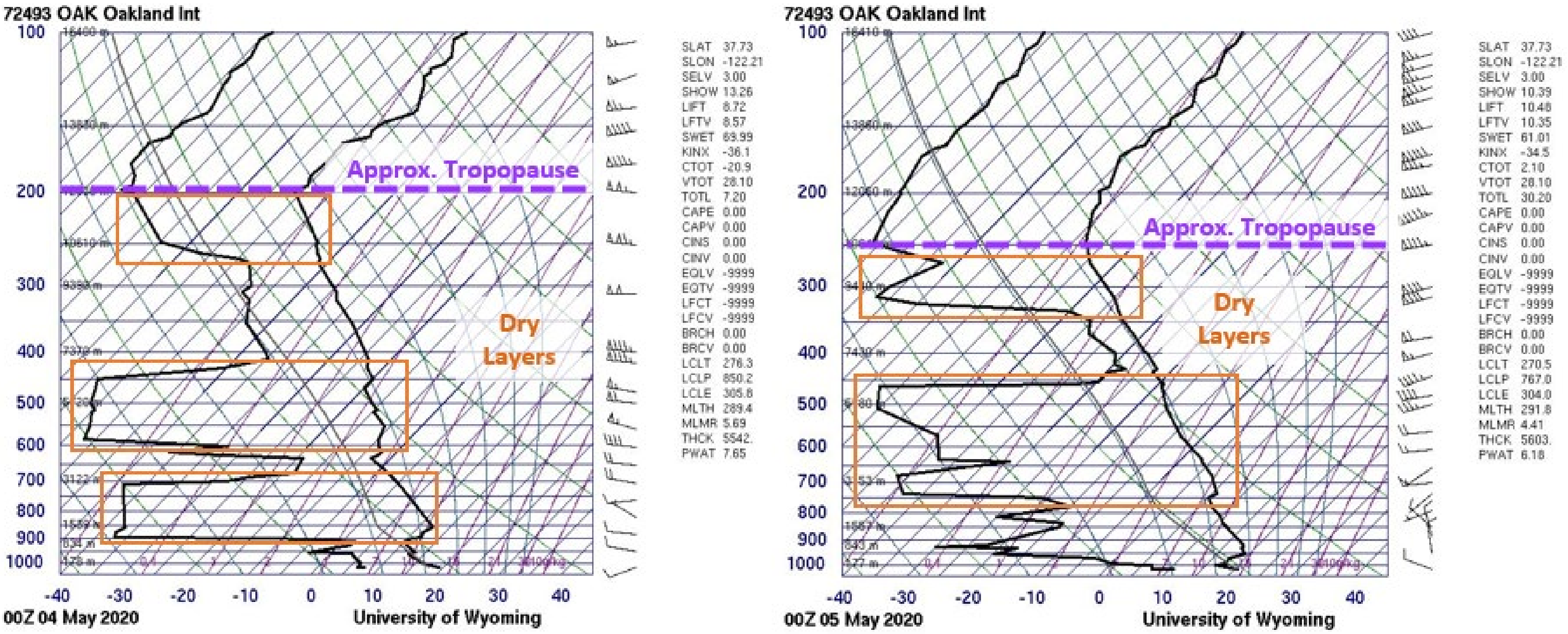

	00Z 04 May 2020	00Z 05 May 2020
SLAT	37.73	37.73
SLON	-122.21	-122.21
SELV	3.00	3.00
SHOW	13.26	10.39
LIFT	8.72	10.48
LFTV	8.57	10.35
SWET	63.99	61.01
KINX	-36.1	-34.5
CTOT	-20.9	2.10
VTOT	28.10	28.10
TOTL	7.20	30.20
CAPE	0.00	0.00
CAPV	0.00	0.00
CINS	0.00	0.00
CINV	0.00	0.00
EQLV	-9999	-9999
EQTV	-9999	-9999
LFCT	-9999	-9999
LFCV	-9999	-9999
BRCH	0.00	0.00
BRCV	0.00	0.00
LCLT	276.3	270.5
LCLP	850.2	767.0
LCLE	305.8	304.0
MLTH	289.4	291.8
MLMR	5.69	4.41
THCK	5542.	5603.
PWAT	7.65	6.18

Figure 3-49. Skew-T soundings launched from the Oakland (OAK) National Weather Service office on May 4 and 5, 2020, at 0:00 UTC (4:00 p.m. May 3 and 4 local time). The approximate (cold-point temperature) tropopause is denoted by the dashed purple line. Dry layers of air are boxed and labeled in orange.

The HYSPLIT matrix presented in Figure 3-40 shows REV along multiple possible pathways of air towards Clark County between May 4, 00:00 UTC and May 7, 00:00 UTC (the afternoon of the May 6 EE date). Skew-T soundings from REV between May 5 at 00:00 UTC and May 6 at 00:00 UTC are shown in **Figure 3-50**. Vertical transport of the proposed stratospheric injection can be tracked by following the descent of a dry layer over the course of 24 hours. On May 5 at 00:00 UTC, this dry layer is seen at 300 hPa. Twelve hours later, the dry layer has expanded deeper into the atmosphere and sunk closer to the surface. By May 6 at 00:00 UTC, the very dry air has descended to the 600 hPa level, which provides supporting evidence that dry, stratospheric air has mixed deeper into the troposphere by this date. This dry layer is situated at the top of a mixed layer that reached from the surface to 600 hPa. The temperature lapse rate in a mixed layer follows a dry adiabatic lapse rate (shown in the red circle where the slope of the temperature lapse rate parallels the dry adiabatic lapse rate [green curve]). A mixed layer facilitates the exchange of air from its upper boundary to its lower boundary, providing a mechanism for transporting stratospheric air entrained into the free troposphere towards lower altitudes.

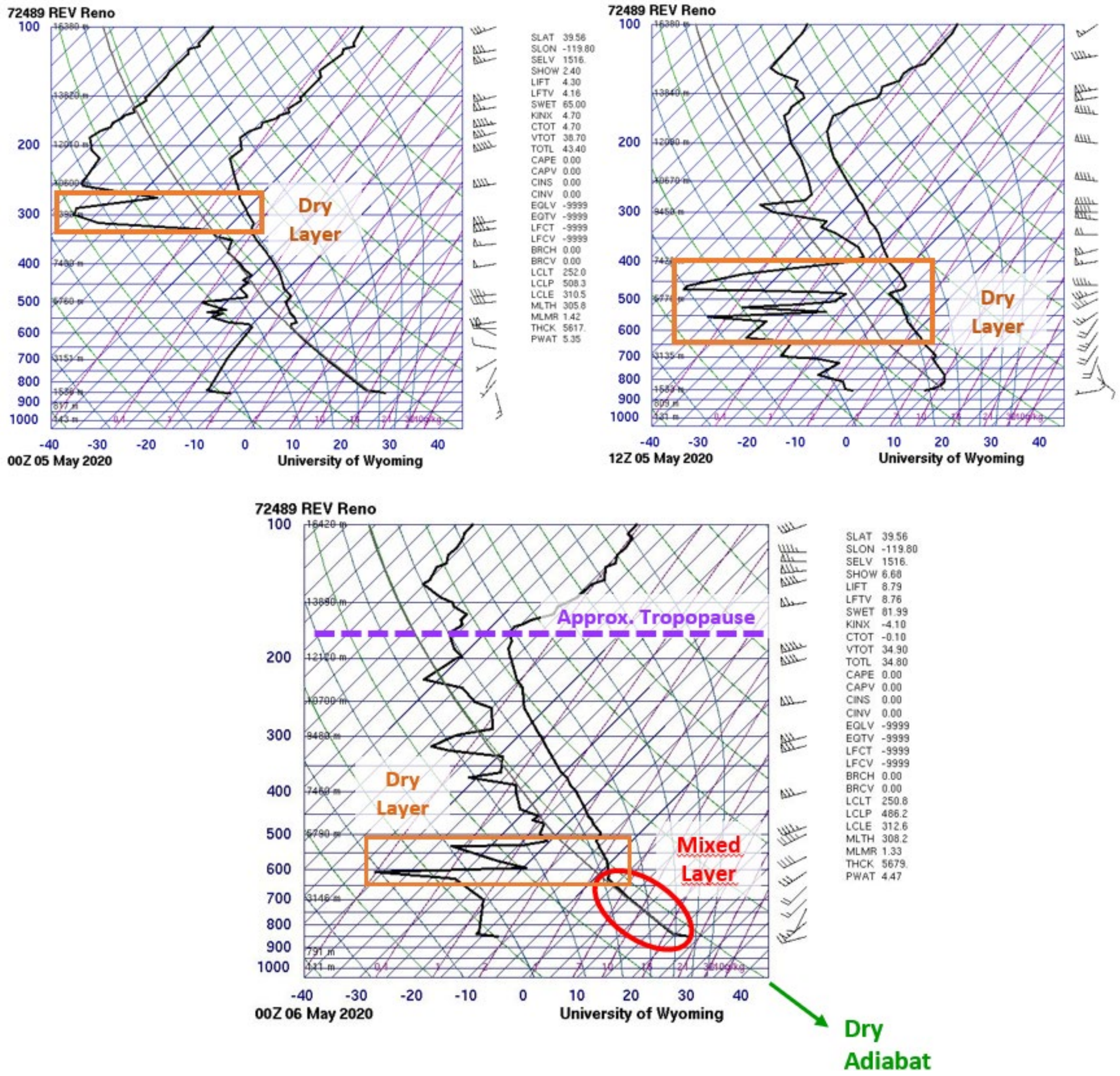

Figure 3-50. Skew-T sounding launched from the REV National Weather Service office on May 5, 2020, at 0:00 UTC (top left), May 5, 2020, at 12:00 UTC (top right) and May 6, 2020, at 0:00 UTC (4:00 p.m. May 5, local time, bottom). The approximate (cold-point temperature) tropopause is denoted by the dashed purple line. A dry layer of air is boxed and labeled in orange. The red circle denotes a mixed layer to 650 hPa.

Figure 3-51 shows the skew-T soundings launched from Las Vegas on the night before the exceedance event at 12:00 UTC, May 7, and for the observation closest to the exceedance event, 0:00 UTC, May 7 (May 6, 16:00 PST). The existence atypically dry overnight air, like the deep dry air mass over Las Vegas the night before the exceedance event (boxed in orange), can mark the presence of transported stratospheric air in the troposphere. The comparison of the temperature lapse rate against the moist adiabatic lapse rate (navy) and the dry adiabatic lapse rate (green) reveals conditions that are well-suited to vertical mixing on the event date (May 7 at 0:00 UTC) from the surface up to the 300 hPa level. In two different layers in the troposphere, from the surface to 650 hPa (circled in red) and from 500 hPa to 300 hPa (circled in yellow), the temperature follows a dry adiabatic lapse rate, which is characteristic of a well-mixed layer. This suggests that air entrained from higher altitudes into these layers could be mixed toward lower altitudes (including the very dry region around 500 hPa). Between these two well-mixed layers is a region of conditional stability (labeled in blue), where the slope of the temperature lapse rate is between the dry adiabatic lapse rate and the moist adiabatic lapse rate (navy blue curve). Given that air is relatively dry in this layer, the motion of downward moving air is likely uninhibited, allowing for entrainment between the upper mixed layer to the lower mixed layer.

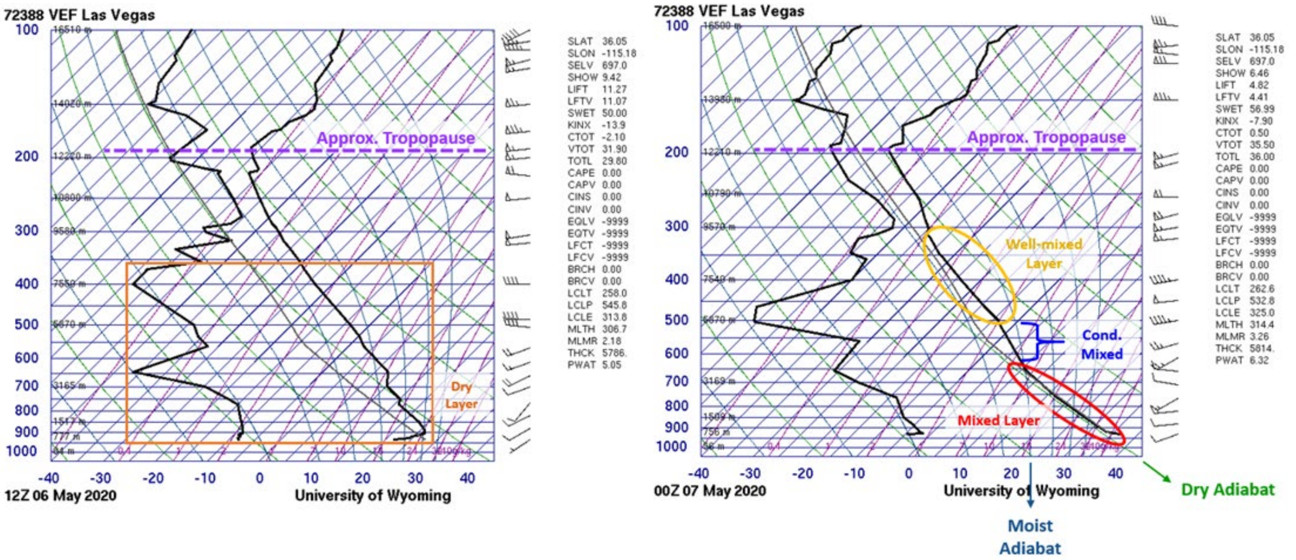

Figure 3-51. Skew-T soundings launched from the Las Vegas (VEF) National Weather Service office on May 6, 2020, at 12:00 UTC and May 7, 2020, at 0:00 UTC (4:00 p.m. May 6, local time). The approximate (cold-point temperature) tropopause is denoted by the dashed purple line. The red and yellow circles denote a mixed layers, and the blue label marks a conditionally mixed layer. A notable overnight dry layer is boxed in orange.

Vertical profiles of ozone were available from NOAA's Chemical Sciences Laboratory site at Boulder, CO, for the day after the May 6 EE event in Clark County. The Chemical Science Laboratory collects routine vertical measurements of ozone via the TOPAZ lidar, which collects data up to 8 km. HYSPLIT back trajectories initialized on May 7 at 23:00 UTC from Boulder (**Figure 3-52**) show the northwestern U.S. as the origin of the airmass over Boulder on May 7, within the region and time frame of stratosphere-to-troposphere exchange identified in Section 3.2. **Figure 3-53** shows the TOPAZ ozone profile from May 7, 2020. Starting at 16:00 MST (22:00 UTC), a layer of ozone is observed between 4 and 8 km ASL that is above 100 ppb in concentration. This high concentration ozone "tongue" extends towards the surface, with ozone concentrations between 70 and 80 ppb seen as low as 2 km above sea level (asl) (near ground level in Boulder, CO). This vertical profile of ozone demonstrates a clear instance of stratosphere-to-troposphere exchange along the trajectory of this air mass, with mixing of ozone-rich air to lower altitudes.

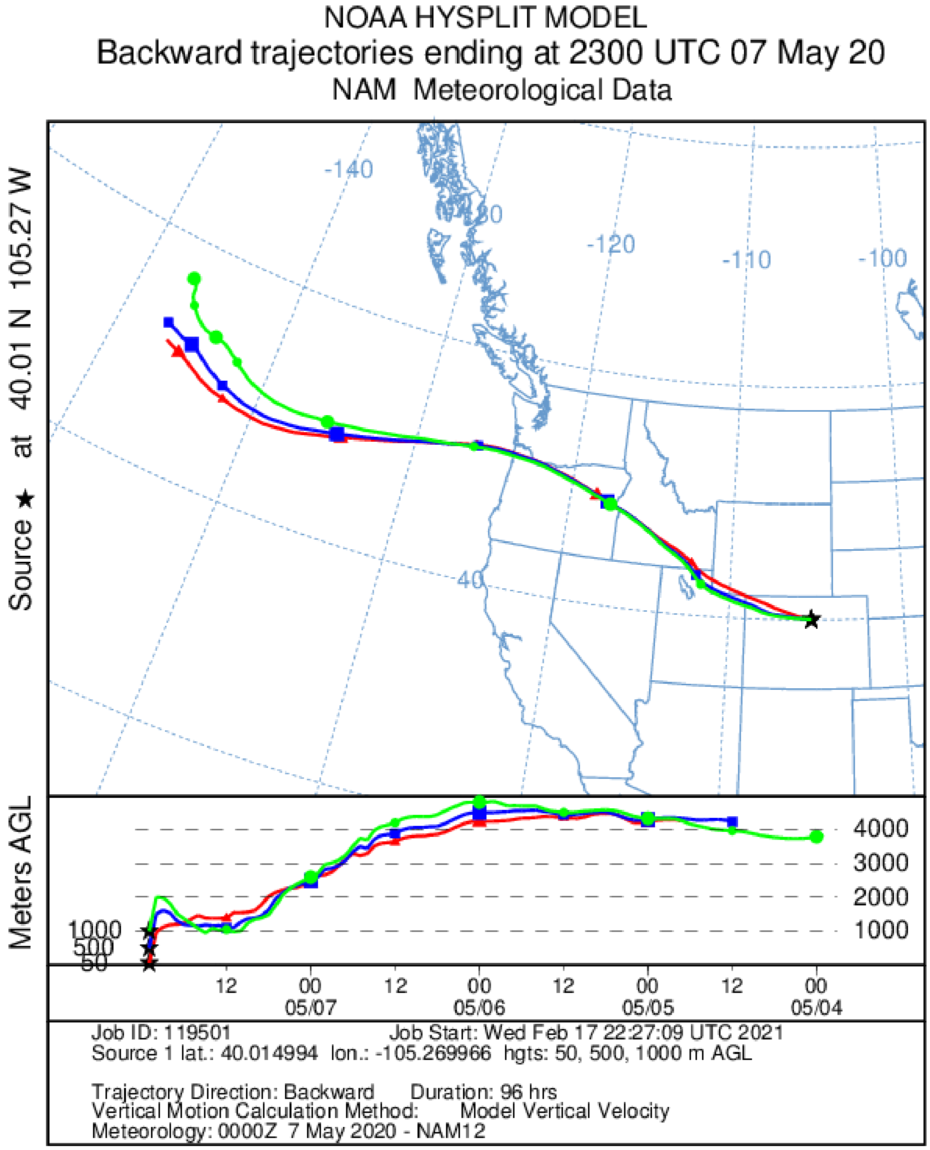

Figure 3-52. 96-hour HYSPLIT back trajectories from Boulder (40.01 degrees N, 105.27 degrees W), ending on May 7, 2020, at 23:00 UTC. NAM 12-km back trajectories are shown for 50 m (red), 500 m (blue), and 1000 m (blue) above ground level.

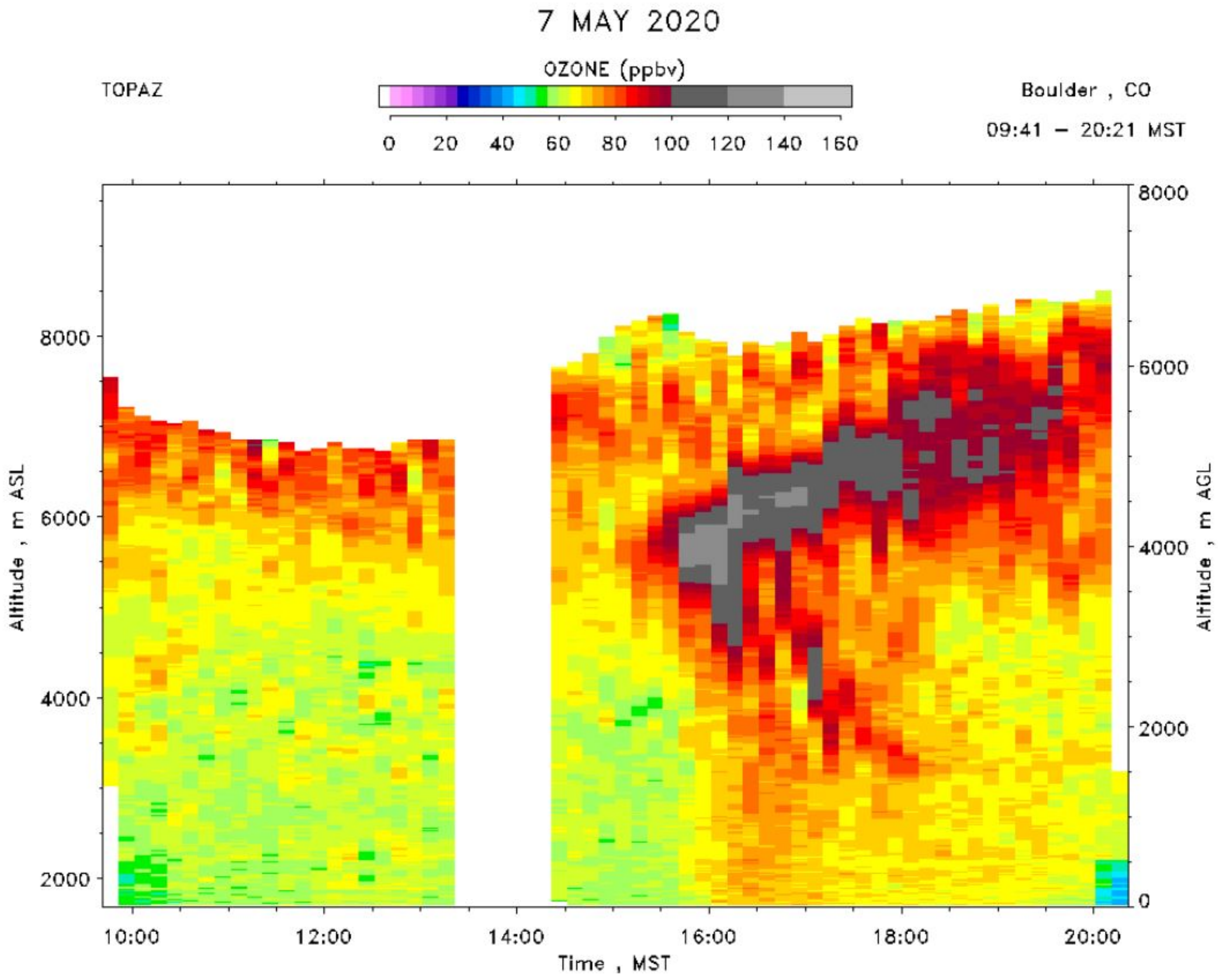

Figure 3-53. Vertical profile of ozone captured at NOAA's Chemical Sciences Laboratory in Boulder, CO on May 7, 2020, between 10:00 and 20:00 MST (May 7 at 16:00 UTC to May 8 at 2:00 UTC). Data was collected by The Tunable Optical Profiler for Aerosol and Ozone lidar (TOPAZ). The left y-axis shows altitude above sea level. The right y-axis shows altitude above ground level.

The combination of the skew-T diagrams, LIDAR analysis, and trajectories to and from a suspected source region to Clark County provide evidence for the free tropospheric transport of ozone enhancements towards the deep mixed layer and the surface at Clark County on May 6, 2020.

3.3.3 Model Results of Meteorological Conditions

The mesoscale and local meteorological conditions from May 4 to May 6 provide evidence for transport of vertically mixed air from the eastern Pacific and northwestern U.S. to Clark County, Nevada. The upper-level wind direction indicates that air from the SOI region moved northeast into Oregon along an upper-level ridge, identified by the downward 'v' shape of the brown height contours, on May 4 (**Figure 3-54**). There is an influx of sinking air to the west of a ridge, where slowing upper-level winds induce convergence. This scenario provides synoptic conditions that are favorable to allow for ozone-rich stratospheric air to mix from the upper-level to lower levels. Upper-level air flows towards the east in the western U.S. on May 6.

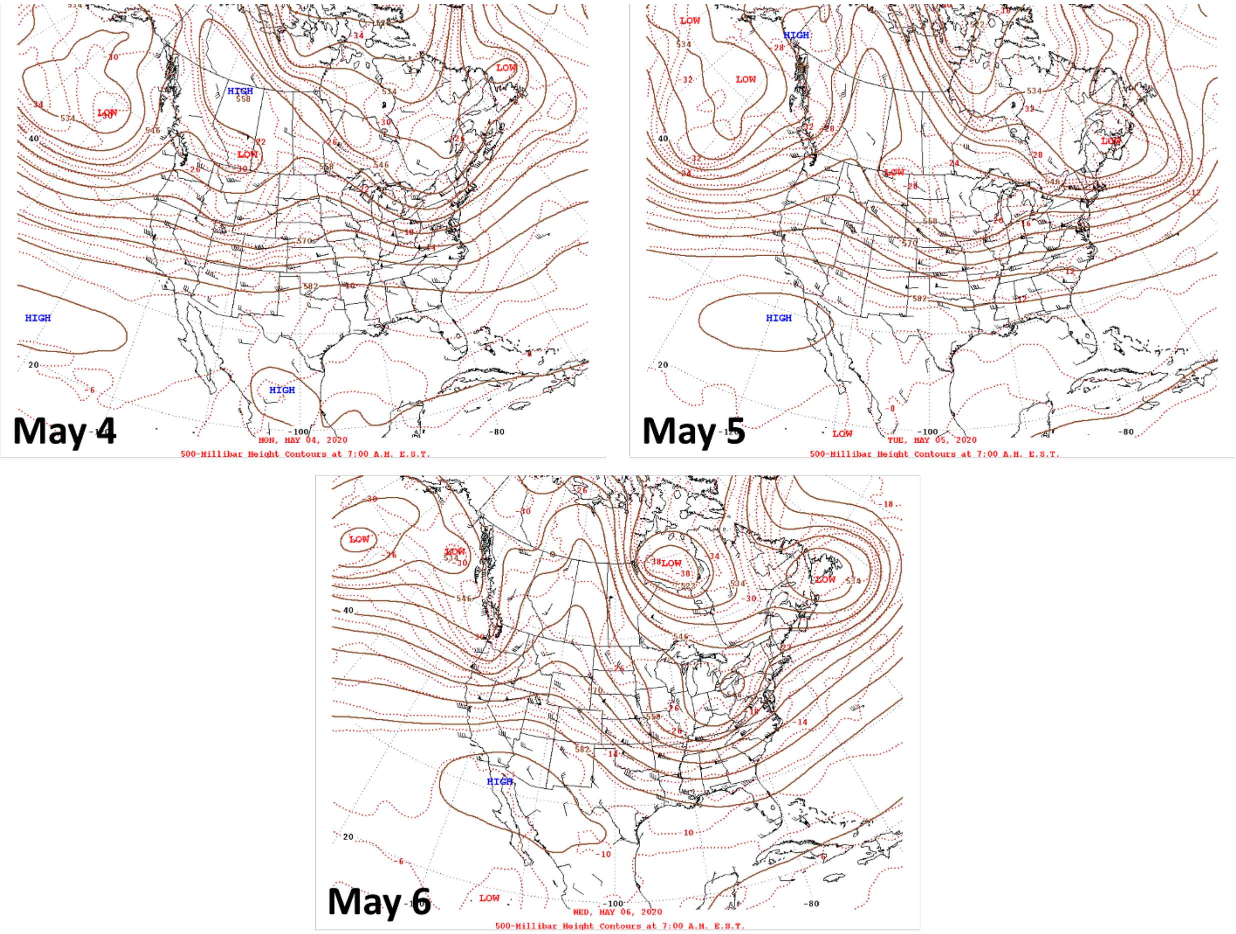

Figure 3-54. Daily upper-level meteorological maps for the two days leading up to the EE and during the May 6 EE.

The surface high- and low-pressure centers over Oregon and Washington on May 4 are indicative of strong vertical mixing between the upper free troposphere and the surface (**Figure 3-55**). The large distance between pressure contours (1,016 hPa and 1,020 hPa) and the north-south orientation indicates southerly to southwesterly winds into Clark County, NV, on May 5 and May 6 (consistent with the trajectories looping into Clark County from the southwest on May 5-6). This is also consistent with the surface wind barbs shown in the vertical atmospheric profiles in Section 3.3.2. The surface low pressure, as seen on May 6, can induce vertical mixing between the surface and upper levels. In addition, at high surface temperatures, air becomes buoyant and further enhances vertical mixing between upper and lower atmosphere over Clark County.

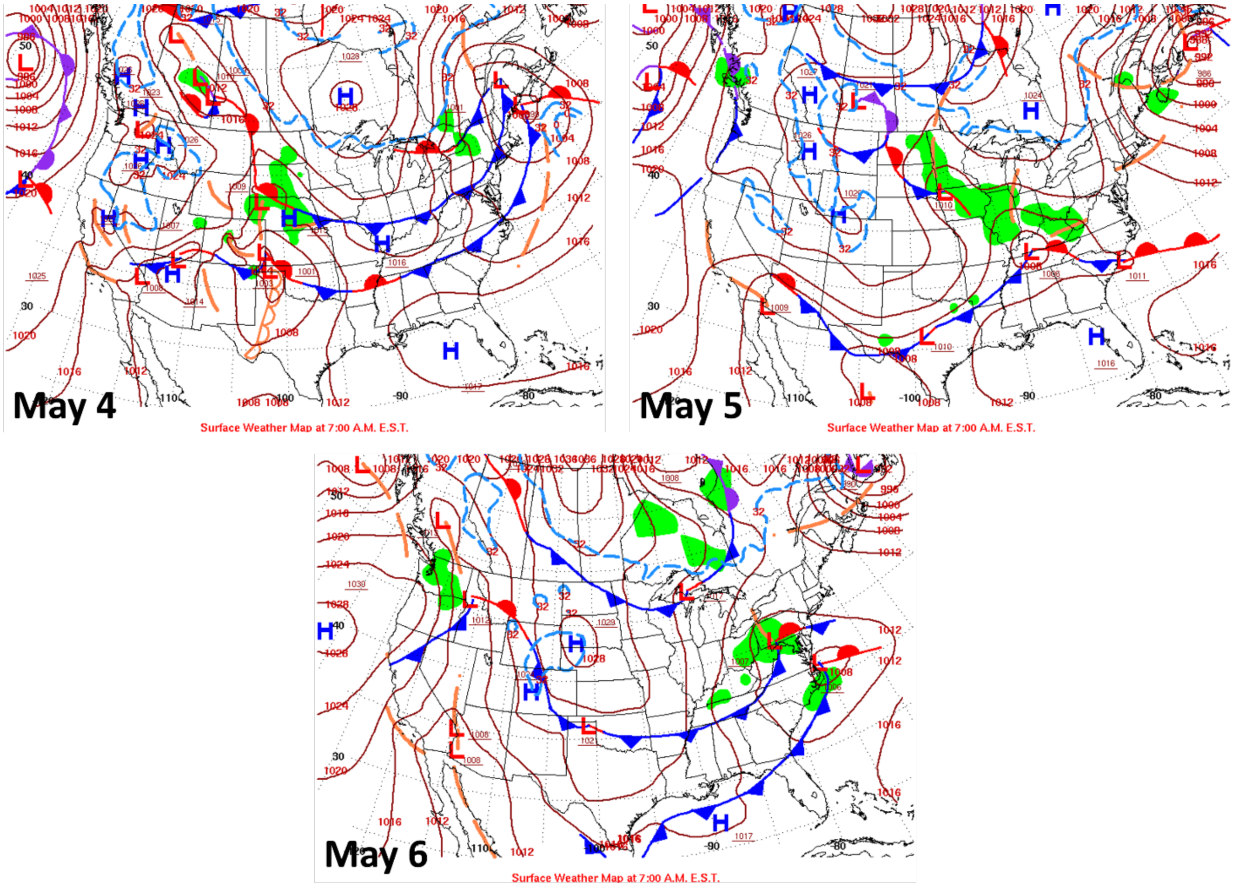

Figure 3-55. Daily surface meteorological maps for the two days leading up to the EE and during the May 6 EE.

The planetary boundary layer denotes the atmospheric layer closest to the surface. On May 5, the planetary boundary layer height was approximately 3 km over Oregon, indicating a deep mixed layer, which is defined by consistent air characteristics from the surface to approximately 650 hPa (Figure 3-56). The deep mixed layer heights blanketed Oregon, Nevada, and Arizona and shifted southeast on May 6. The planetary boundary layer height for the southern region of Clark County, Nevada, on May 6 was between 2 to 3 km in altitude, consistent with the skew-T 650 hPa mixed layer shown in Section 3.3.2. The modeled planetary boundary layer height for the southern region of Clark County, Nevada, on May 6 was approximately 2 km in altitude, which is less than the height as shown in the skew-T shown in Section 3.3.2. The modeled planetary boundary layer was likely underestimated by NAM because it was approximately 1,000 m lower than the observed planetary boundary layer indicated by the skew-T. The regional deep mixed layer and southeast shift is consistent with air transport from the stratosphere to the troposphere over Oregon and subsequent transport into the deep mixed layer over Clark County, Nevada (Figure 3-57).

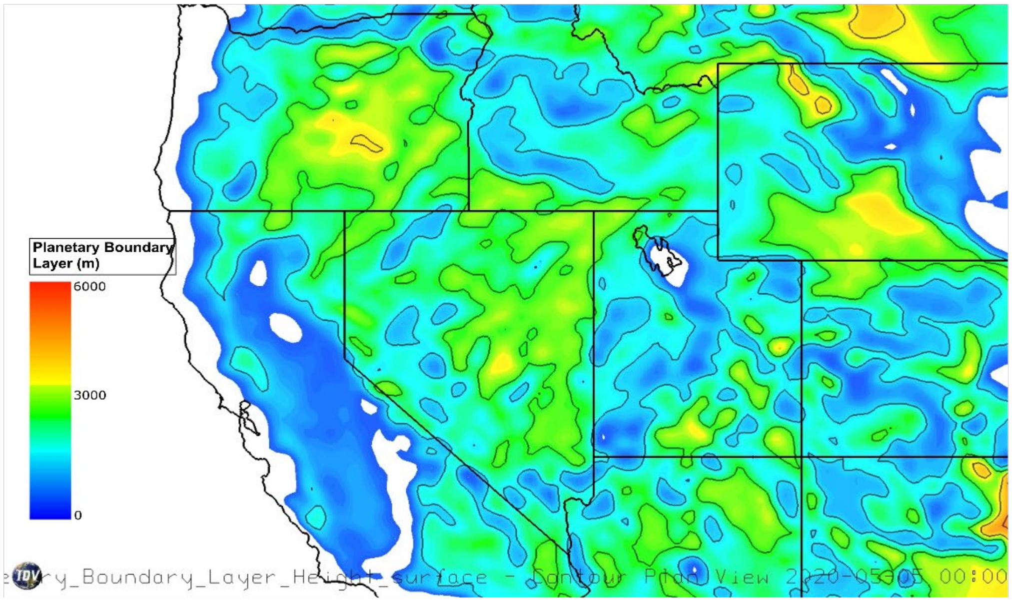

Figure 3-56. Planetary boundary layer (PBL) height contour map based on the NAM model for May 5, 2020, at 16:00 PST. The gray lines denote PBL heights above 2-km altitude in 1-km increments.

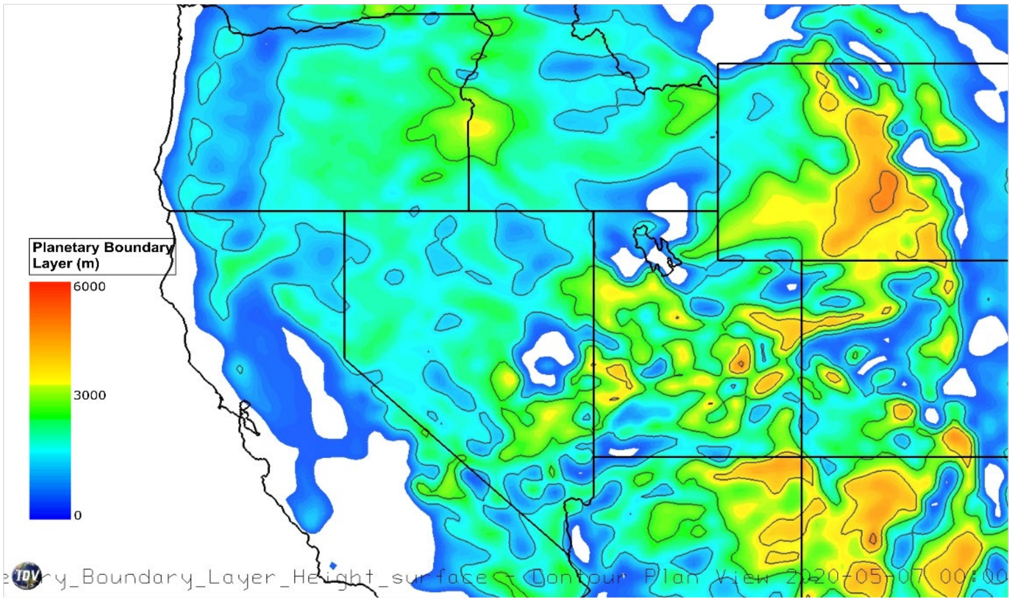

Figure 3-57. Planetary boundary layer (PBL) height contour map based on the NAM model for May 6, 2020, at 16:00 PST. The gray lines denote PBL heights above 2-km altitude in 1-km increments.

Ozone-rich stratospheric air originating along the coast of the California Oregon border moved eastward along an upper-level high-pressure ridge on May 4 into Oregon. Enhanced vertical mixing over Oregon on May 4 into May 5 is evident from the surface high pressure and a deep well-mixed planetary boundary layer. The high-pressure system moving air clockwise from the North Pacific Ocean transported the well-mixed layer south into the low-pressure centered over Clark County, Nevada, on May 6. The relatively high planetary boundary layer heights are consistent on May 5 over the entire Oregon, Nevada, and Arizona region, and shifted southeast on May 6. This shows that stratospheric ozone-rich air originating near the coastal California Oregon border was transported eastward to Oregon on May 4, and may have become well-mixed within the planetary boundary layer on May 5, then transported at the lower level to Clark County, Nevada, on May 6. Although photochemical production of ozone occurred on May 6, this analysis provides evidence that meteorological conditions were favorable for vertical mixing of ozone to the surface on May 6 in the Las Vegas area.

3.4 Impacts of the Intrusion at the Surface

As stated in Sections 3.2.1, 3.2.2, and 3.3.2, stratospheric air is characterized by high ozone and low water vapor content relative to tropospheric air. Therefore, stratospheric intrusion and subsequent transport of stratospheric air to the surface should cause meteorological variables at the surface, such as ozone concentrations and relative humidity, to have characteristics similar to stratospheric air.

Figure 3-58 shows observations from May 6 and a typical diurnal profile of ozone concentrations, absolute humidity, and temperature observed at the Jerome Mack station for May 2015-2019. Absolute humidity has a relatively constant diurnal profile in May, hovering between 5 to 7 grams per cubic meter with a slight dip in the afternoon. The diurnal profile of temperature shows a trough in the early morning and is followed by a peak throughout the afternoon with a gradual decrease into the evening. The diurnal profile of ozone is similar to temperature, reaching a maximum in the afternoon and minimum in the early morning. Temperature on May 6 was high compared to the 5-year May average, reaching a magnitude just above the 95th percentile at its daily maximum. Absolute humidity, rather than relative humidity, is displayed in Figure 3-58 to decouple the measurement of humidity from temperature. Throughout the day on May 6, absolute humidity values were lower than the five-year May average, reaching magnitudes below the lowest 5th percentile of May observations between 5:00 a.m. and midnight. Absolute humidity values on May 6 were below 1 gram per cubic meter for much of the afternoon. During the late afternoon on May 6, ozone concentrations were higher than the highest 95th percentile of May observations and higher than the 5-year May average. The extremely low absolute humidity values and high ozone concentrations provide evidence that stratospheric air reached the lower troposphere in Las Vegas on May 6.

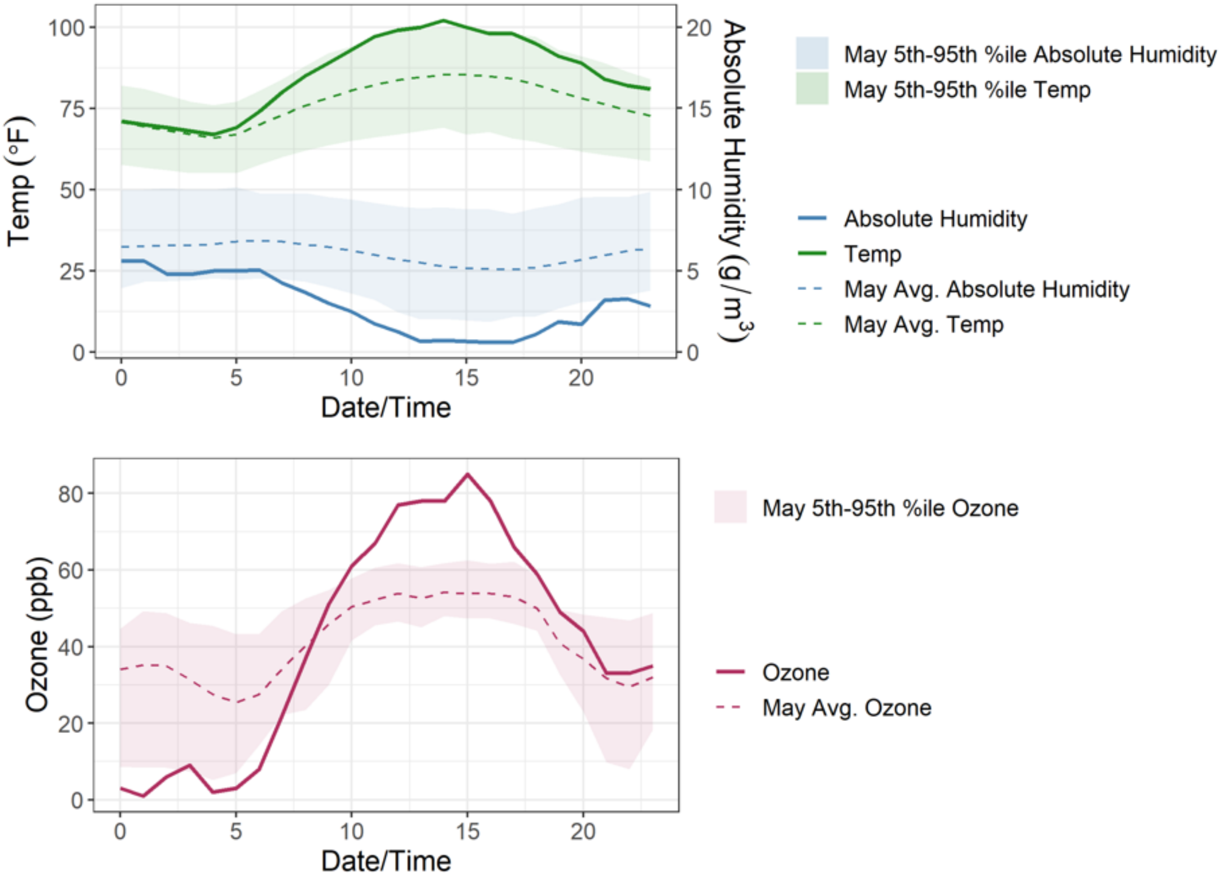

Figure 3-58. (Top plot) Diurnal profile of temperature (green) and absolute humidity (blue) at Jerome Mack, including temperature and absolute humidity values on May 6 and the 5-year May averages (dotted lines). (Bottom plot) Diurnal profile of ozone at Jerome Mack on May 6. Shaded ribbons represent the five-year 5^{th}-95^{th} percentile range.

Figures 3-59 through 3-63 show NO and nitrogen dioxide NO_2 concentration observations from May 6 and a typical diurnal profile of ozone concentrations from the Walter Johnson, Paul Meyer, Joe Neal, Jerome Mack, and Green Valley stations. Ozone data at each site is available for 2015-2020. NO_2 observations are available from the Jerome Mack and Joe Neal stations for 2017-2020 and 2015-2020 respectively. Diurnal profiles of NO_2 are included on the plots for Jerome Mack and Joe Neal below. NO observations are available from the Jerome Mack site only for 2015-2020. A diurnal profile of NO is included on the plot for Jerome Mack. NO_2 concentrations usually reach a peak in the early to mid-morning and gradually decrease throughout the day, followed by a gradual increase into the later evening. The diurnal profile of NO is similar to NO_2 but does not have a distinct increase into the late evening. NO_x (NO + NO_2) is an important ingredient (in addition to VOCs and sunlight) in the creation of ozone in the troposphere. To determine whether the May 6 event was predominately due to photochemical processes at the surface, we examine whether NO_x was abnormally high during this event. During the afternoon on May 6, ozone concentrations at all stations were higher than the highest 95th percentile and higher than the average of May. During this time, NO_2 concentrations at Jerome Mack and Joe Neal, and NO concentrations at Jerome Mack were approximately average relative to the seasonal average. The average NO and NO_2 concentrations at Jerome Mack provide evidence that abnormally high local photochemical ozone production alone was unlikely to be responsible for the EE in Clark County on May 6.

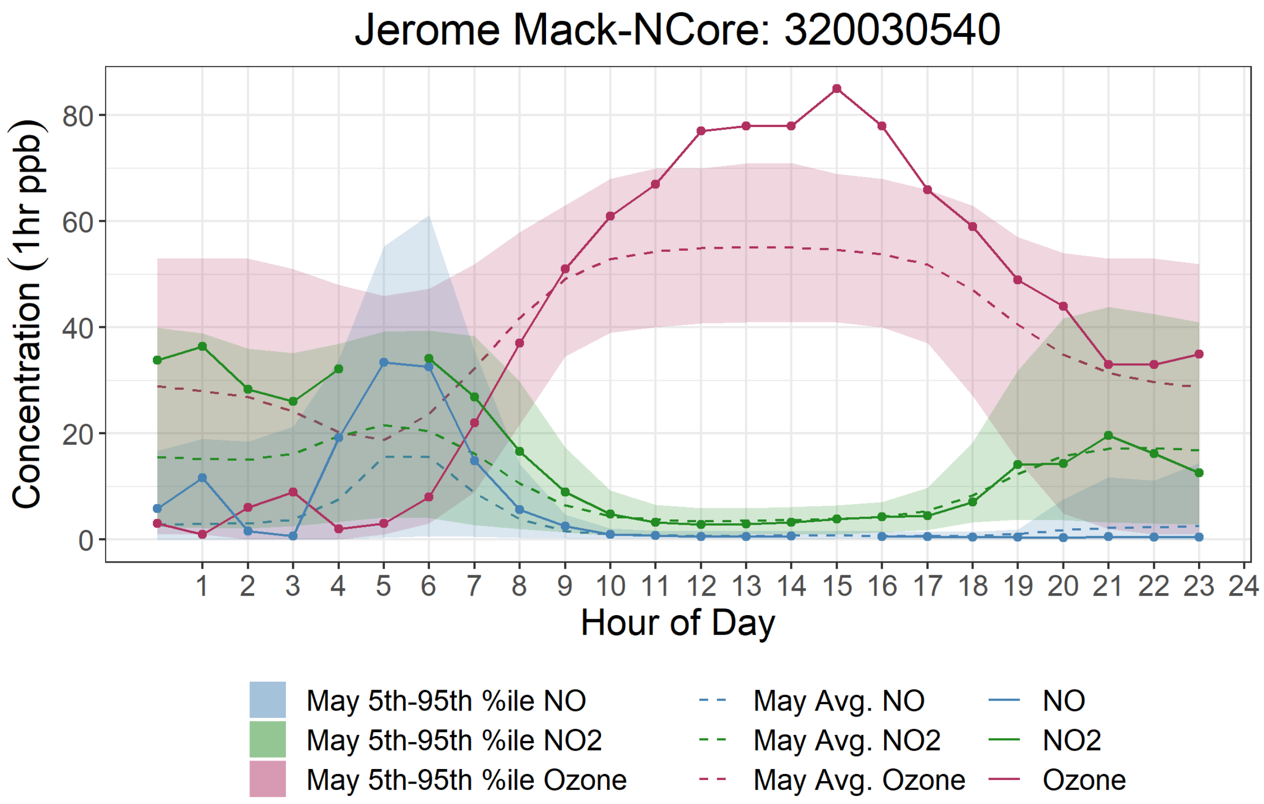

Figure 3-59. Diurnal profile of ozone concentrations (red), NO (blue), and NO_2 at Jerome Mack and the 5-year seasonal averages (dotted lines). Shaded ribbons represent the five-year 5th-95th percentile range.

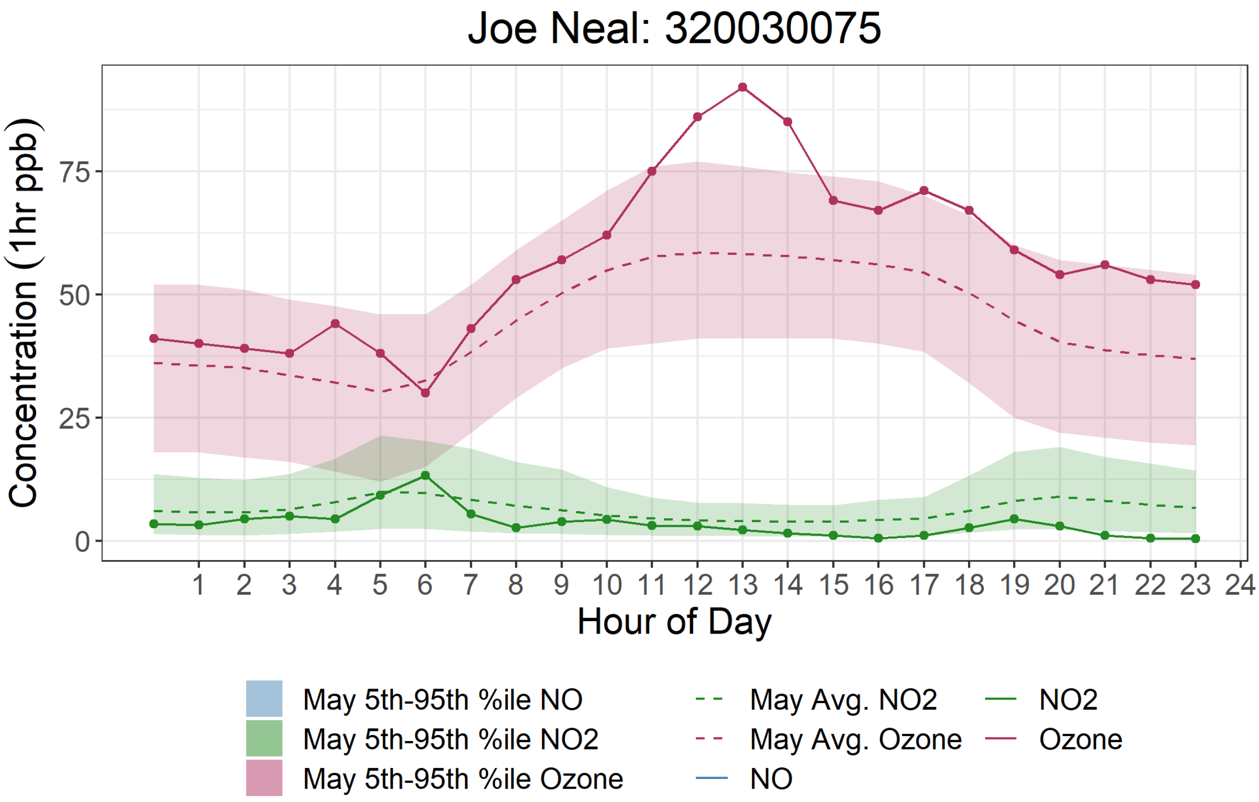

Figure 3-60. Diurnal profile of ozone concentrations (red) and NO_2 concentrations (green) at Joe Neal on May 6 and the 5-year seasonal averages (dotted lines). Shaded ribbons represent the five-year 5th-95th percentile range. Nitric oxide data are unavailable from Joe Neal.

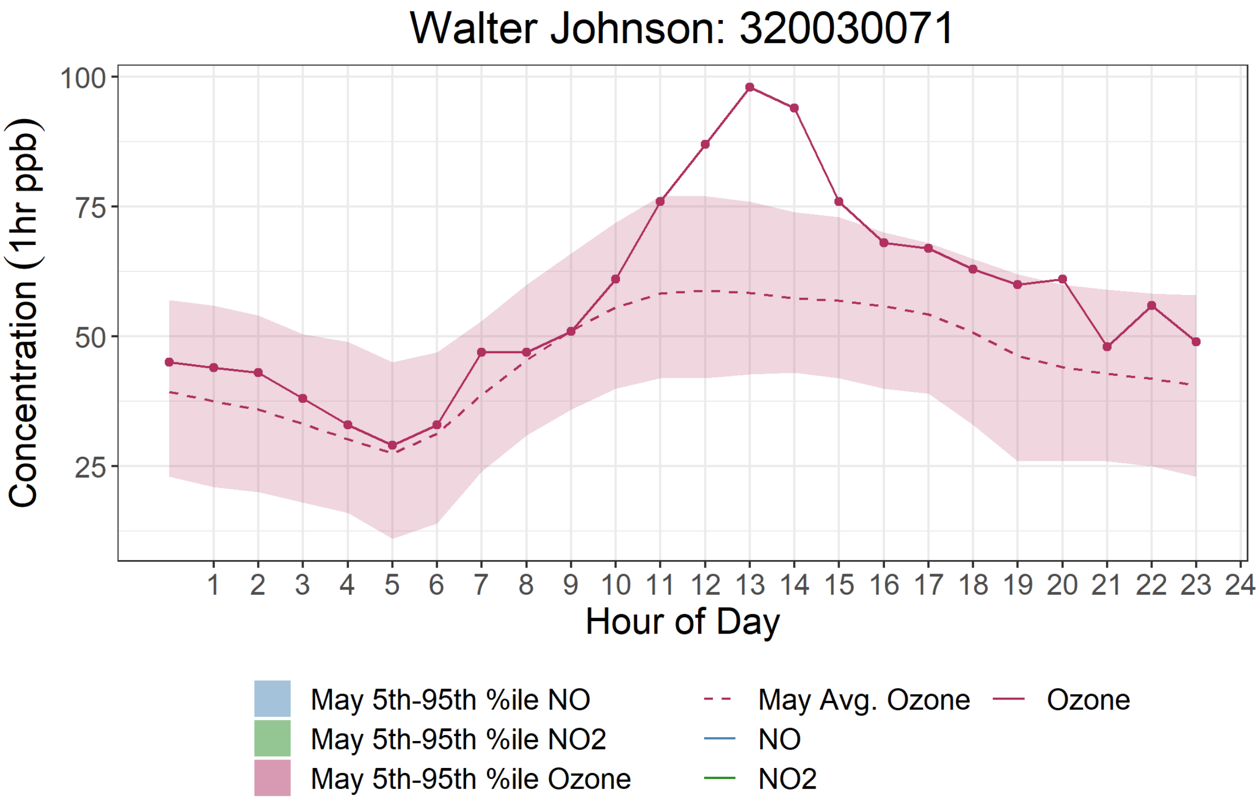

Figure 3-61. Diurnal profile of ozone concentrations (red) at Walter Johnson on May 6 and the 5-year seasonal averages (dotted lines). Shaded ribbons represent the five-year 5th-95th percentile range. NO and NO_2 data are unavailable from Walter Johnson.

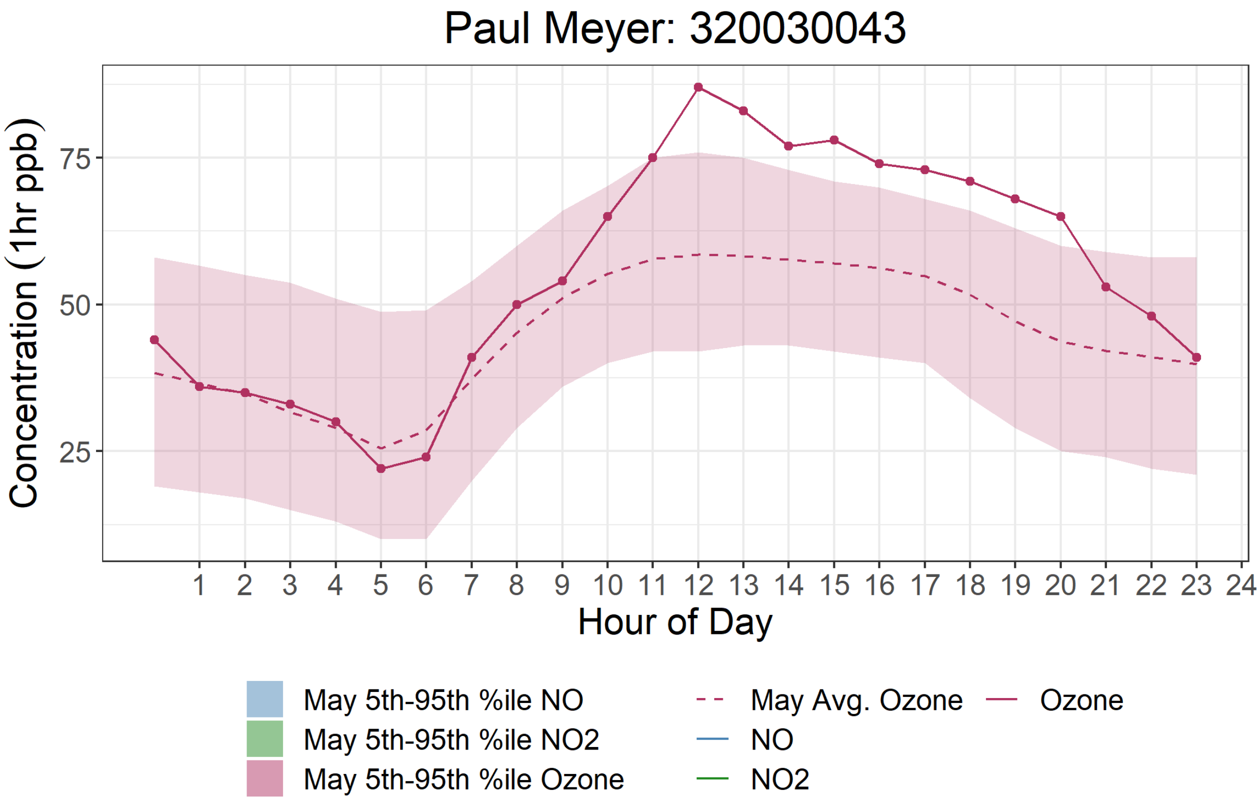

Figure 3-62. Diurnal profile of ozone concentrations (red) at Paul Meyer on May 6 and the 5-year seasonal averages (dotted lines). Shaded ribbons represent the five-year 5th-95th percentile range. NO and NO_2 data are unavailable from Paul Meyer.

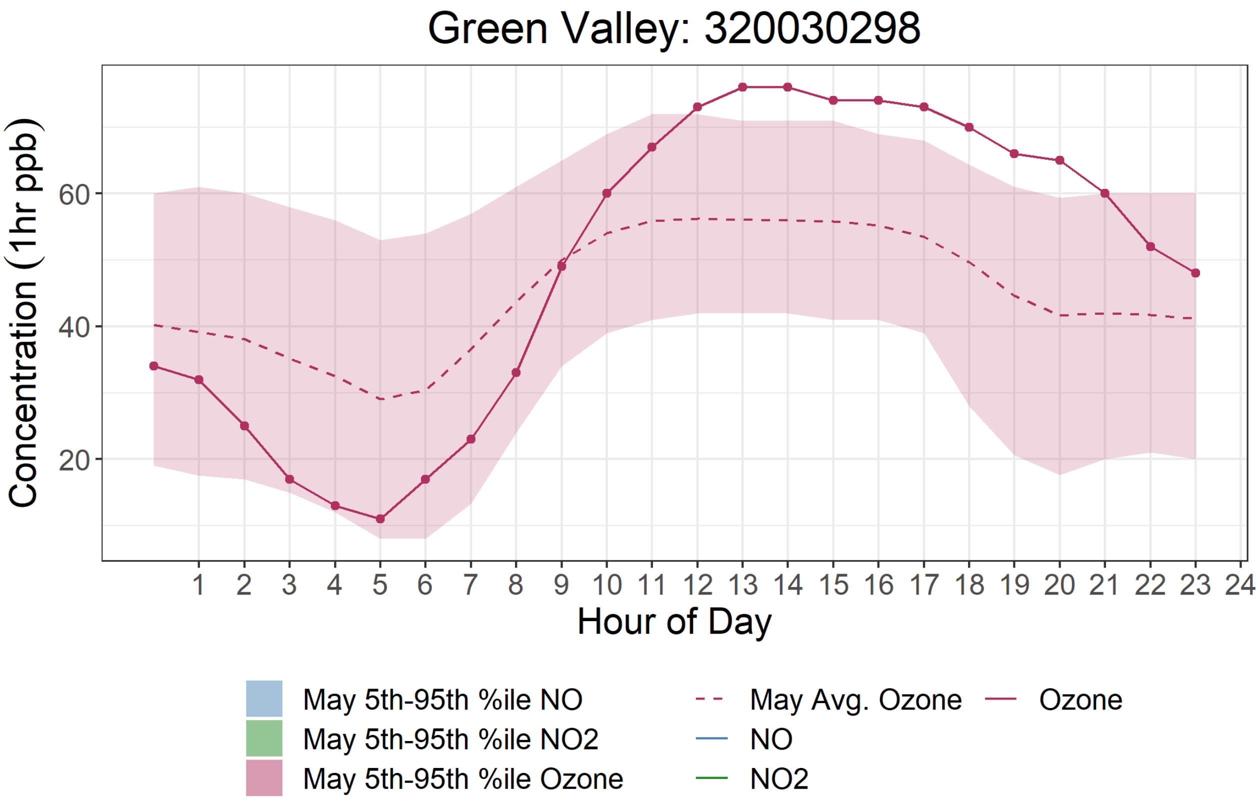

Figure 3-63. Diurnal profile of ozone concentrations (red) at Green Valley on May 6 and the 5-year seasonal averages (dotted lines). Shaded ribbons represent the five-year 5th-95th percentile range. NO and NO_2 data are unavailable from Green Valley.

A map of observed MDA8 ozone concentrations shows elevated ozone levels throughout southern California to the east of Los Angeles, in the Central Valley, and southern Nevada within the Clark County border (Figure 3-64). Stations with recorded NAAQS ozone exceedances are colored orange or red. 12 stations located in southern California reached MDA8 ozone concentrations between 86 – 106 ppb. In Clark County, the Walter Johnson, Paul Meyer, Joe Neal, Jerome Mack, Green Valley, Jean, and Apex monitoring sites exceeded the 2015 ozone NAAQS of 70 ppb on May 6, 2020. These stations were surrounded by stations that observed elevated MDA8 ozone concentrations (55 – <71 ppb) but did not exceed NAAQS. In Clark County, the highest observed value of 78 ppb was recorded at the Walter Johnson station. The Jean and Indian Springs stations often act as indicators of background ozone concentrations because they are not within the Las Vegas metropolitan area. As mentioned above, the Jean site exceeded NAAQS with a concentration of 75 ppb. Although the Indian Springs station did not exceed NAAQS on May 6, it reached a moderate concentration of 63 ppb. Regionally high ozone concentrations, along with enhanced background ozone recorded at the Indian Springs and Jean stations, provides more evidence that suggests stratospheric ozone enhanced surface ozone on May 6, 2020.

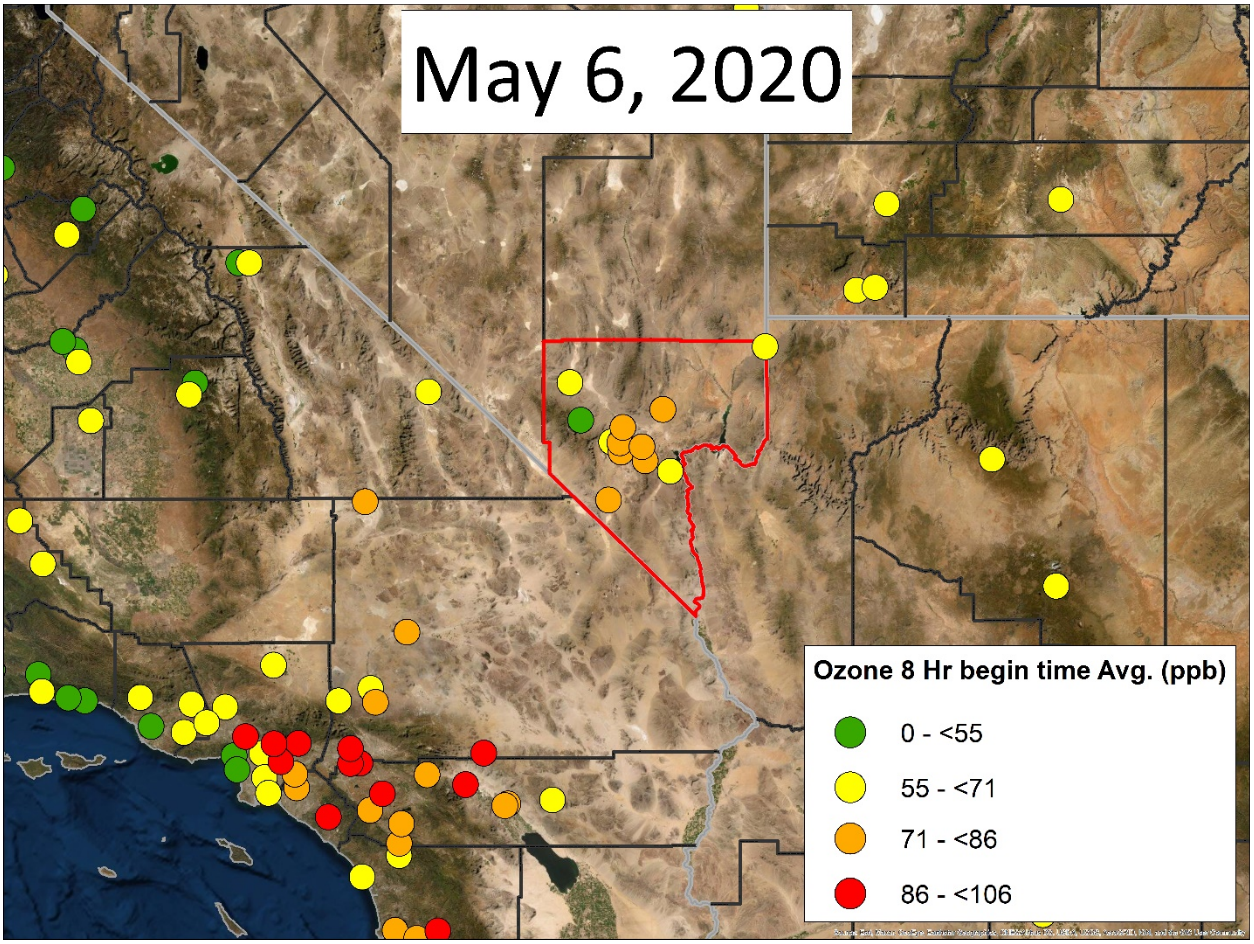

Figure 3-64. Observed maximum daily 8-hour average (MDA8) ozone at stations in southern California, southern Nevada, western Arizona, and southwestern Utah.

We also produced maps of daily ozone Air Quality Index (AQI) for the two days leading up to the May 6 event and the day of the event. These maps show moderate and unhealthy ground-level AQI values (indicated by yellow, orange, and red area) across the southwestern United States, with unhealthy levels expanding between May 4 and May 6 (Figure 3-65). Again, regionally high ozone/AQI can be indicative of stratospheric ozone influence. While we cannot rule out photochemical production or transport of anthropogenic ozone/ozone precursors, based on low water vapor, regionally high ozone concentrations, and typical concentrations of NO_x, ozone concentrations on May 6 were clearly enhanced by an upwind SOI event and not purely due to photochemical production.

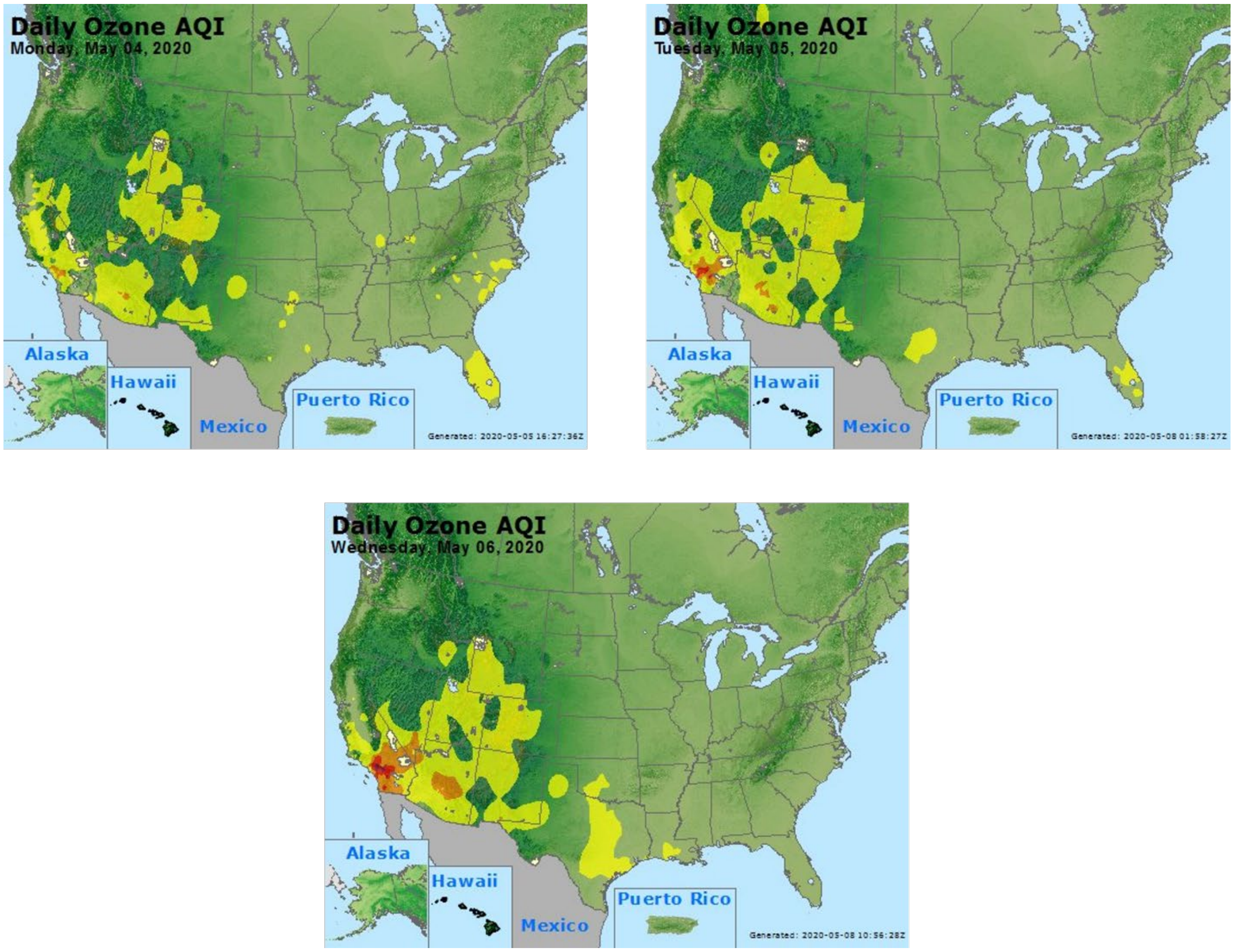

Figure 3-65. Daily ozone AQI for the two days before the May 9 event and the day of the event.

3.5 Additional Evidence

3.5.1 Matching Day Analysis

Ozone production and transport strongly depend on regional and local meteorological conditions. A comparison of ozone concentrations on suspected exceptional event days with non-event days that share similar meteorology can help identify periods when ozone production was affected by an atypical source. Given that similar meteorological days are likely to have similar ozone concentrations, noticeable differences in levels of ozone between the event date and meteorologically similar days can lend evidence to a clear causal relationship between a stratospheric intrusion and elevated ozone concentration.

Identify Meteorologically Similar Days

In order to identify the best matching meteorological days, both synoptic and local conditions were examined from ozone-season days (April 1 through September 30) between 2014 and 2020. Excluded from this set are days with suspected EEs in the 2018 and 2020 seasons, as well as dates within 5 days of the event date, to ensure that lingering effects of smoke transport or stratospheric intrusion did not appear in the data.

To best represent similar air transport, twice daily HYSPLIT trajectories (initiated at 18:00 and 22:00 UTC) from Clark County for 2014-2020 were clustered by total spatial variance. The calculation, based on the difference between each point along a trajectory, provides seven distinct pathways of airflow into Clark County. The cluster that best represents the trajectory on the EE day was chosen, and ozone-season days within the cluster were then subset for regional meteorological comparison to the EE day.

For the meteorological comparison, a correlation score was assigned to each day from the cluster subset. The National Centers for Environmental Prediction (NCEP) reanalysis data were compiled for the ozone seasons in 2014-2020. Daily average wind speed, geopotential height, relative humidity, and temperature were considered at 1000 mb and 500 mb. At the surface, daily average atmospheric pressure, maximum temperature, and minimum temperature were utilized. Pearson product-moment coefficient of linear correlation (pattern correlation) was calculated between the EE date and each cluster-subset ozone-season day in 2014-2020 for each parameter. The pattern correlation calculates the similarity between two mapped variables at corresponding grid locations within the domain. The statistic was calculated using a regional domain of 30 °N-45 °N latitude and 125° W-105° W longitude. The correlation score for each day was defined as the average pattern correlation of all parameters at each height level. The correlation scores were then ranked by the highest correlation for 1000 mb, surface, and finally 500 mb. Dates within 5 days of the EE were removed from the similar day analysis to ensure the data are mutually exclusive. The 50 dates with the highest rank correlation scores were then chosen as candidate matching days for further analysis.

Local meteorological conditions for the subset of candidate matching days were then compared to conditions on May 6, 2020, and filtered to identify five or more days that best matched the event date. Meteorological maps at the surface and 500 mb, and local meteorological data describing temperature, wind, moisture, instability, mixing layer height, and cloud cover were examined. The data source for each parameter is summarized in Table 3-13.

Table 3-13. Local meteorological parameters and their data sources.

Meteorological Parameter	Data Source
Maximum daily temperature	Jerome Mack - NCore Monitoring Site
Average daily temperature	Jerome Mack - NCore Monitoring Site
Resultant daily wind direction	Jerome Mack - NCore Monitoring Site (calculated vector average)
Resultant daily wind speed	Jerome Mack - NCore Monitoring Site (calculated vector average)
Average daily wind speed	Jerome Mack - NCore Monitoring Site
Average daily relative humidity (RH)	Jerome Mack - NCore Monitoring Site
Precipitation	Jerome Mack - NCore Monitoring Site
Total daily global horizontal irradiance (GHI)	UNLV Measurement and Instrumentation Data Center (MIDC) in partnership with NREL (https://midcdmz.nrel.gov/apps/daily.pl?site=UNLV&start=20060318&yr=2021&mo=4&dy=29)
4:00 p.m. local standard time (LST) mixing layer mixing ratio	Upper air soundings from KVEF (http://weather.uwyo.edu/upperair/sounding.html)
4:00 p.m. LST lifted condensation level (LCL)	Upper air soundings from KVEF (http://weather.uwyo.edu/upperair/sounding.html)
4:00 p.m. LST convective available potential energy (CAPE)	Upper air soundings from KVEF (http://weather.uwyo.edu/upperair/sounding.html)
4:00 p.m. LST 1000-500 mb thickness	Upper air soundings from KVEF (http://weather.uwyo.edu/upperair/sounding.html)
Daily surface meteorological map	NOAA's Weather Prediction Center Daily Weather Maps (https://www.wpc.ncep.noaa.gov/dailywxmap/index.html)
Daily 500 mb meteorological map	NOAA's Weather Prediction Center Daily Weather Maps (https://www.wpc.ncep.noaa.gov/dailywxmap/index.html)

Matching Day Analysis – Results

The meteorological conditions on May 6, 2020, were normal for the region at this time of year. Table 3-14 displays that the percentile ranking of each examined meteorological parameter other than wind speed at the Jerome Mack-NCore site falls within the 5th to 95th percentile range among 7 years of observations for the 30-day period surrounding May 6 (April 21 through May 21). Measurement summaries over this 30-day period best represent the expected conditions on the event date. The maximum temperature on May 6 was near the median measurement, but wind speeds were very low. The resultant wind speed is at the 7th percentile, and the average scalar wind speed is at the 2nd percentile. As is typical for Clark County during this period, there was no precipitation.

Table 3-14. Percentile rank of meteorological parameters on May 6, 2020, compared to the 30-day period surrounding May 6 over seven years (April 21 through May 21, 2014-2020). The percentile ranking of a directional degree value is irrelevant and has been marked NA.

Date	Max Temp (°F)	Avg Temp (°F)	Resultant Wind Direction (°)	Resultant Wind Speed (mph)	Avg Wind Speed (mph)	Avg RH (%)	Precip (in)	Total GHI (kWh/m^2)	Mixing Layer Mixing Ratio (g/kg)	LCL (mb)	CAPE (J/kg)	500-1,000 mb Thickness (m)
2020-05-06	40	13	NA	7	2	45	NA	18	15	24	62	22

The subset of synoptically similar days identified according to the methodology above was further filtered based on parameters listed in Table 3-13 to match local meteorological conditions that existed on the event date. A priority was placed on matching wind speeds rather than direction since the low scalar and resultant wind speeds indicate that wind direction was variable. **Table 3-15** shows the eight days that best match the meteorological conditions that existed on May 6, 2020, as well as the MDA8 ozone concentration at each site that experienced an ozone exceedance on May 6, 2020. Three days from 2020 are included in Table 3-15, May 26, May 27, and June 2. May 26, 2020, May 27, 2020, and June 2, 2020, are valuable dates to include in this analysis, since they occurred under comparable abnormal anthropogenic emissions to the event date due to Covid-19 restrictions. Surface maps for May 6, 2020, and each date listed in Table 3-15 show highly consistent conditions, with a surface low-pressure system over Clark County. Most dates also had an upper-level ridge to the north, and upper-level high pressure to the south. Surface and upper-level maps are included in **Appendix B**.

Table 3-15 shows the average MDA8 ozone concentration across these eight days with a range defined by one standard deviation, a conservative estimate given the small sample size. The expected MDA8 ozone concentration, given similar meteorological conditions to those on the event date, is well below the 70-ppb ozone standard at each site, ranging from 57 to 64 ppb. Further, the upper end of the provided range at each site also falls below the ozone standard. None of these dates except May 8, 2018, which is discussed further below, reached the 70-ppb ozone standard on any of the identified meteorologically similar days. Several similar dates with higher photochemical potential than May 6 (lower wind speeds, higher temperatures, and greater solar irradiance) did not exceed the ozone standard. Thus, an ozone exceedance on May 6, 2020, was unexpected based on meteorological conditions alone. If meteorology were the sole cause of the ozone exceedance on May 6, 2020, we would expect to see similarly high ozone levels on each of the similar days listed in Table 3-15, especially those with even warmer temperatures than experienced on May 6, 2020, alongside other similar conditions.

Though an ozone exceedance did occur on one meteorologically similar day, May 8, 2018, this exceedance exhibits a gradient in ozone concentrations across sites that differs from the event on May 6, 2020. Though wind speeds were low, westerly resultant winds ultimately prevailed on both May 6, 2020, and May 8, 2018, indicating that net movement of air across Las Vegas was from west to east. On May 8, 2018, those sites downwind of downtown Las Vegas (Jerome Mack and Green Valley) experienced exceedances while those upwind (Joe Neal, Walter Johnson and Paul Meyer) did not. An additional upwind site, Indian Springs, was also examined and reported MDA8 ozone values of 66 ppb on May 8, 2018, compared to 63 ppb on May 6, 2020. These pieces of evidence show that the event on May 8, 2018, was a localized photochemical event where anthropogenic emissions from Las Vegas fueled increased ozone production. In contrast, on May 6, 2020, a site's position relative to downtown did not determine whether an exceedance occurred or not (a characteristic typical with SOI events). In fact, sites upwind from downtown Las Vegas (Paul Meyer and Walter Johnson) showed the highest levels of ozone compared to downwind sites. The distribution of elevated ozone concentrations across Clark County sites on May 6, 2020, shows that this was a regional rather than a local event. The resultant wind direction did not align with a gradient of MDA8 ozone concentrations across monitoring sites as it did on May 8, 2019. Further, the meteorologically similar days from 2020 (Table 3-15) provide a better reference for how altered conditions due to COVID-19 restrictions might affect ozone production (see (see Section 2.5) during meteorological conditions similar to those that existed on May 6, 2020. None of these three 2020 matching days show an unusually high MDA8 ozone concentration. This lends evidence to an additional source of ozone on May 6, 2020, other than local emissions and photochemical production. Therefore, the May 8, 2018, exceedance during similar meteorological conditions to those that existed on May 6, 2020, does not detract from the assertion that meteorological conditions alone did not cause the ozone exceedance across Clark County's monitoring network on May 6, 2020.

Table 3-15. Top eight matching meteorological days to May 6, 2020. WJ, PM, JN, JM, and GV refer to monitoring sites Walter Johnson, Paul Meyer, Joe Neal, Jerome Mack and Green Valley respectively. Average MDA8 ozone concentration of meteorologically similar days is shown plus-or-minus one standard deviation rounded to the nearest ppb.

Date	Max Temp (°F)	Avg Temp (°F)	Resultant Wind Direction (°)	Resultant Wind Speed (mph)	Avg Wind Speed (mph)	Avg RH (%)	Precip (in)	Total GHI (kWh/m^2)	Mixing Layer Mixing Ratio (g/kg)	LCL (mb)	CAPE (J/kg)	500-1,000 mb Thickness (m)	MDA8 Ozone Concentration (ppb)				
													PM	WJ	JN	JM	GV
2020-05-06	102	85.46	277.21	0.77	2.05	10.79	0	7.98	3.26	532	0	5814	77	78	76	73	72
2015-05-29	98	88.33	147.89	1.86	2.92	13.25	0	8.62	3.89	553	0	5800	65	62	64	62	NA
2017-05-21	98	83.92	58.32	1.28	2.51	17.42	0	8.43	3.06	534	0	5765	59	62	64	54	55
2017-05-30	101	88.08	228.54	1.66	2.88	10.71	0	7.26	4.1	553	130	5804	60	62	64	57	57
2017-06-03	106	92.21	135.33	0.96	2.90	11.5	0	8.51	4.73	553	0	5846	66	70	69	60	64
2018-05-08	103	88.83	221.49	0.66	2.00	9.75	0	8.21	3.12	521	0	5836	68	66	69	73	74
2019-08-21	110	94.88	104.27	1.19	2.82	9.33	0	7.69	5.31	543	0	5914	64	63	64	54	56
2020 Dates																	
2020-05-26	103	88.33	117.17	0.76	1.80	13.17	0	8.65	4.39	556	0	5835	64	62	66	54	56
2020-05-27	108	94.38	117.85	0.54	1.44	10.25	0	8.49	4.69	539	40	5874	63	62	64	55	62
2020-06-02	103	91.21	131.12	0.87	2.07	13.04	0	6.07	5.22	580	29	5828	56	53	55	41	50
Average MDA8 Ozone Concentration of Meteorologically Similar Days													**63** ± 4	**62** ± 4	**64** ± 4	**57** ± 8	**59** ± 7

These findings show that an external source of ozone contributed to the ozone exceedance on May 6, 2020. All examined meteorological parameters besides wind speed fall between the 10th and 90th percentile. Our analysis expanded on methods shown in the EPA guidance and a previously concurred EE to identify eight days that are meteorologically similar to May 6, 2020 (Arizona Department of Environmental Quality, 2018). An exceedance occurred on only one of these eight days across the monitoring sites that experienced an ozone exceedance on May 6, 2020, though the exceedance on May 8, 2018, showed a gradient of MDA8 ozone concentrations across the monitoring network that indicates local photochemical production, a characteristic not shared by the May 6, 2020, event. Additionally, the May 6, 2020, exceedance occurred under a significantly different pollutant regime than May 8, 2018 (see Section 2.5), and compared with the meteorologically similar days in 2020 that occurred under the same altered anthropogenic emissions due to COVID-19 restrictions, none had an exceedance at any site. The expected MDA8 ozone concentration at each site is over 10 ppb below the concentrations measured at each site on May 6, 2020. Based on this evidence, it is unlikely that meteorology alone enhanced photochemical production of ozone enough to cause an exceedance on May 6, 2020. This validates the existence of an extrinsic ozone source on May 6, 2020.

3.5.2 GAM Statistical Modeling

Generalized additive models (GAM) are a type of statistical model that allows the user to predict a response based on linear and non-linear effects from multiple variables (Wood, 2017a). These models tend to provide a more robust prediction than Eulerian photochemical models or simple comparisons of similar events (Simon et al., 2012; Jaffe et al., 2013; U.S. Environmental Protection Agency, 2016). Camalier et al. (2007) successfully used GAM modeling to predict ozone concentrations across the eastern United States using meteorological variables with r^2 values of up to 0.8. Additionally, previous concurred EE demonstrations and associated literature, i.e., Sacramento Metropolitan Air Quality Management District (2011), Alvarado et al. (2015), LDEQ (2018), ADEQ (2016), and Pernak et al. (2019) used GAM modeling to predict ozone events that exceed the NAAQS standards, some in EE cases. By comparing the GAM-predicted ozone values to the actual measured ozone concentrations (i.e., residuals), we can determine the effect of outside influences, such as wildfires or stratospheric intrusions, on ozone concentrations each day (Jaffe et al., 2004). High, positive residuals suggest a non-typical source of ozone in the area but cannot specifically identify a source. Gong et al. (2017) and McClure and Jaffe (2018b) used GAM modeling, in addition to ground and satellite measurements of wildfire pollutants, to estimate the enhancement of ozone during wildfire smoke events. Similar to other concurred EE demonstrations, we used GAM modeling of meteorological and transport variables to estimate the MDA8 ozone concentrations at multiple sites across Clark County for 2014-2020. To estimate the effect of wildfire smoke on ozone concentrations, we can couple the GAM residual results (observed MDA8 ozone–GAM-predicted MDA8 ozone) with the other analyses to confirm that the non-typical enhancement of ozone is due to a stratospheric intrusion on May 6, 2020.

Using the same GAM methodology as prior concurred EE demonstrations and the studies mentioned above, we examined more than 30 meteorological and transport predictor variables, and through testing, compiled the 16 most important variables to estimate MDA8 ozone each day at eight monitoring sites across Clark County, Nevada (Paul Meyer, Walter Johnson, Joe Neal, Green Valley, Boulder City, Jean, Indian Springs, and Jerome Mack). As suggested by EPA guidance (U.S. Environmental Protection Agency, 2016), we used meteorological variables measured at each station (the previous day's MDA8 ozone, daily min/max temperature, average temperature, temperature range, wind speed, wind direction, or pressure), if available (see Table 2-1). If meteorological variables were not available at a specific site, we supplemented the data with National Centers for Environmental Prediction (NCEP) reanalysis meteorological data to fill any data gaps. We also tested filling data gaps with Jerome Mack meteorological data and found results had no statistical difference. We used sounding data from KVEF (Las Vegas Airport) to provide vertical meteorological components; soundings are released at 00:00 and 12:00 UTC daily. Variables such as temperature, relative humidity, wind speed, and wind direction were averaged over the first 1000 m above the surface to provide near-surface, vertical meteorological parameters. Other sounding variables, such as Convective Available Potential Energy (CAPE), Lifting Condensation Level (LCL) pressure, mixing layer potential temperature, mixed layer mixing ratio, and 500-1,000 hPa thickness provided additional meteorological information about the vertical column above Clark County. We also initiated HYSPLIT GDAS 1°x1° 24-hour back trajectories from downtown Las Vegas (36.173° N, -115.155° W, 500 m agl) at 18:00 and 22:00 UTC (10:00 a.m. and 2:00 p.m. local standard time) each day to provide information on morning and afternoon transport during critical ozone production hours. We clustered the twice per day back trajectories from 2014-2020 into seven clusters. Figure 3-66 shows the clusters, percentage of trajectories per cluster, and heights of each trajectory cluster. We identified a general source region for each cluster: (1) Northwest U.S., (2) Stagnant Las Vegas, (3) Central California, (4) Long-Range Transport, (5) Northern California, (6) Southern California, and (7) Baja Mexico. Within the GAM, we use the cluster value to provide a factor for the distance traveled by each back trajectory. Additionally, day of year (DOY) was used in the GAM to provide information on season and weekly processes. The year (2014, 2015, etc.) was used a factor for the DOY parameter to distinguish interannual variability.

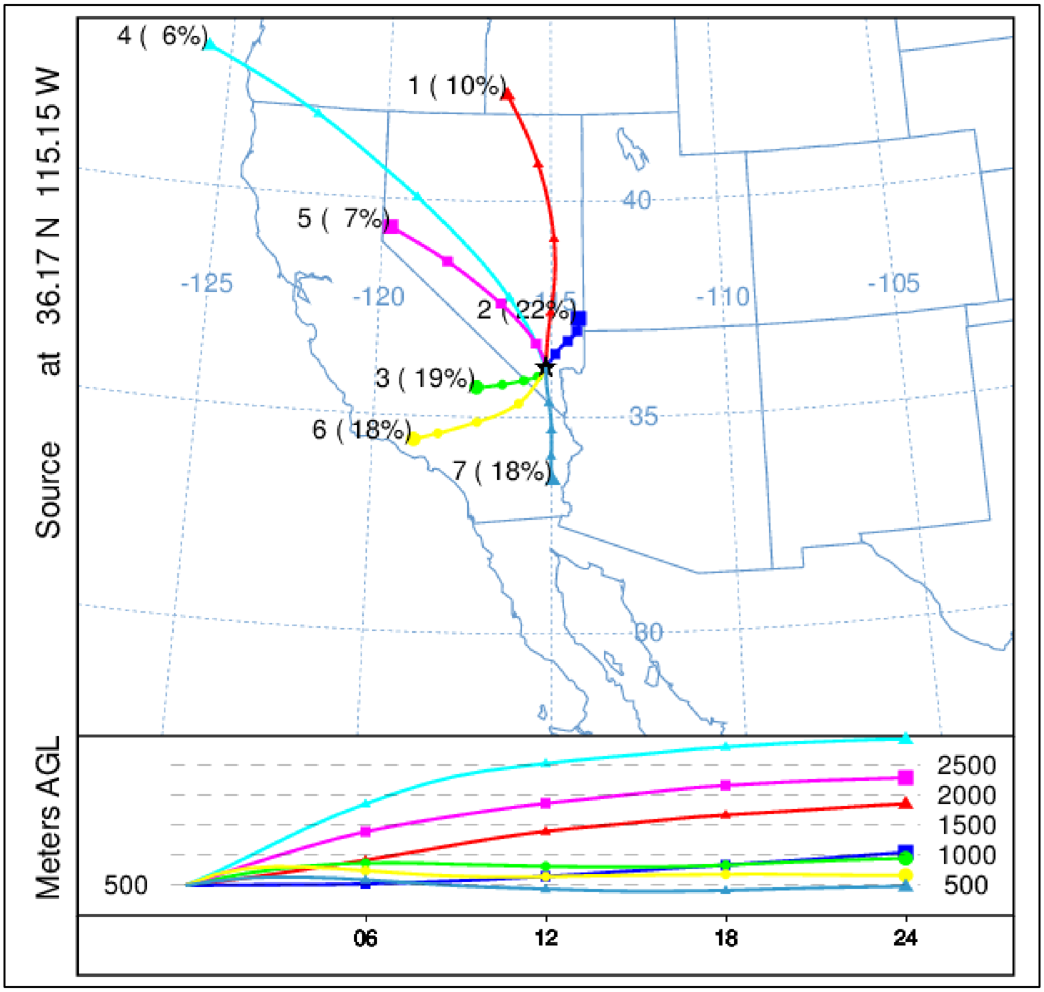

Figure 3-66. Clusters for 2014-2020 back trajectories. Seven unique clusters were identified for the twice daily (18:00 and 22:00 UTC) back-trajectories for 2014-2020 initiated in the middle of the Las Vegas Valley. The percentage of trajectories per cluster is shown next to the cluster number. The height of each cluster is shown below the map.

Once all the meteorological and transport variables were compiled, we inserted them into the GAM equation to predict MDA8 ozone:

$$g\left(MDA8\ O_{3,i}\right) = f_1(V1_i) + \ f_2(V2_i) + \ f_3(V3_i) + \cdots + residual_i$$

where f_i are fit functions calculated from penalized cubic regression splines of observations (allowing non-linearity in the fit), Vi are the variables, and *i* is the daily observation. All variables were given a cubic spline basis except for wind direction, which used a cyclic cubic regression spline basis. For DOY and back trajectory distances, we used year factors (i.e., 2014-2020) and cluster factors (i.e., 1-7) to distinguish interannual variability and source region differences. The factors provide a different smooth function for each category (Wood, 2017b). For example, the GAM smooth of DOY for 2014 can be different than 2015, 2016, etc. In order to optimize the GAM, we first must adjust knots or remove any variables that are over-fitting or under-performing. We used the “mgcv” R package to summarize and check each variable for each monitoring site (Wood, 2020). A single GAM equation (using the same variables) was used for each monitoring site for consistency. During the initial optimization process, we removed the proposed 2018 and 2020 EE days from the dataset. We also ran 10 cross-validation tests by randomly splitting data 80/20 between training/testing for each monitoring site to ensure consistent results. All cross-validation tests showed statistically similar results with no large deviations for different data splits. We used data from each site during the April-September ozone seasons for 2014 through 2020, which is consistent with other papers modeling urban ozone (e.g., Pernak et al., 2019; McClure and Jaffe, 2018b; Solberg et al., 2019; Solberg et al., 2018) and ozone concentrations during the periods with exceptional events are within the representative range of ozone in the GAM model.

Table 3-16 shows the variables used in the GAM and their F-value. The F-value suggests how important each variable is (higher value = more important) when predicting MDA8 ozone. Any bolded F-values had a statistically significant correlation ($p < 0.05$). R^2, the positive 95th quantile of residuals, and normalized mean square residual values for each monitoring site are listed at the bottom of the table.

Table 3-16. GAM variable results. F-values per parameter used in the GAM model are shown for each site. Units and data source for each parameter in the GAM model are shown on the right of the table. 95th quantile, R^2, and normalized mean square residual information is shown at the bottom of the table.

Parameters	Paul Meyer	Walter Johnson	Joe Neal	Green Valley	Jerome Mack	Boulder City	Jean	Indian Springs	Unit	Source
Day of Year (DOY) factored by Year (2014-2020)	**8.11**	**7.09**	**7.65**	**11.8**	**7.94**	**7.11**	**8.68**	**7.53**	--	--
Previous Day MDA8 Ozone	**37.9**	**22.7**	**41.5**	**18.1**	**27.9**	**31.3**	**105.5**	**123.8**	ppb	Monitor Data
Average Daily Temperature	1.92	**2.90**	**4.80**	0.05	1.83	2.13	0.12	1.83	K	Monitor Data/NCEP Reanalysis
Maximum Daily Temperature	1.37	**2.74**	**2.48**	0.16	0.38	0.02	1.30	1.52	K	
Temperature Range (TMax - TMin)	**4.12**	2.13	1.38	1.74	1.77	1.51	0.50	0.54	K	
Average Daily Pressure	**5.54**	**6.42**	**6.74**	**4.64**	**2.94**	0.22	2.17	0.24	hPa	
Average Daily Wind Speed	**11.1**	**5.03**	**7.49**	**5.02**	**15.3**	0.07	0.49	2.19	knots	
Average Daily Wind Direction	0.47	**1.04**	0.24	**1.35**	**2.43**	0.69	0.11	**2.48**	deg	
18 UTC HYSPLIT Distance factored by Cluster	1.70	1.82	1.69	0.92	2.52	2.97	1.66	1.03	km	HYSPLIT Back-Trajectories
22 UTC HYSPLIT Distance factored by Cluster	1.03	0.74	1.47	1.47	1.20	1.26	1.19	0.50	km	
00 UTC Convective Available Potential Energy	3.50	0.13	0.37	1.17	1.16	0.57	**5.71**	**6.49**	J/kg	Sounding Data
00 UTC Lifting Condensation Level Pressure	1.36	**2.78**	2.29	2.41	**3.76**	0.38	1.43	0.38	hPa	
00 UTC Mixing Layer Potential Temperature	0.65	0.79	1.72	0.10	1.23	0.97	1.09	2.53	K	
00 UTC Mixed Layer Mixing Ratio	**2.10**	**2.76**	**2.85**	**3.09**	**3.07**	**2.42**	0.69	1.04	g/kg	
00 UTC 500-1000 hPa Thickness	**2.91**	0.43	1.70	1.60	1.69	**4.11**	**2.18**	1.83	m	
12 UTC 1km Average Relative Humidity	**12.4**	**14.6**	**17.8**	**21.3**	**37.5**	**26.0**	**11.1**	2.18	%	
95th Quantile of Positive Residuals (ppb)	10	10	10	10	9	9	9	10		
R^2	0.55	0.58	0.60	0.58	0.61	0.58	0.57	0.55		
Normalized Mean Square Residual	3.6E-06	7.3E-04	6.1E-05	1.3E-04	3.1E-05	1.3E-04	1.2E-04	1.5E-04		

Table 3-17 provides GAM residual and fit results for all sites for the ozone season of 2014 through 2020. Overall, the residuals are low for all data points, and similarly low for all non-EE days. However, the 2018 and 2020 EE day residuals are significantly higher than the non-EE day results, meaning there are large, atypical influences on these days. Figure 3-67 shows non-EE vs EE median residuals with the 95th confidence intervals denoted as notches in the boxplots. We show the data in both ways to provide specific values, as well as illustrate the difference in non-EE vs EE residuals. Since the 95th confidence intervals for median EE residuals are above and do not overlap with those for non-EE residuals at any site in Clark County, we can state that the median residuals are higher and statistically different ($p<0.025$). The R^2 for each site ranged between 0.55 and 0.61, suggesting a good fit for each monitoring site, and similar to the results in prior studies and EE demonstrations mentioned previously (r^2 range of 0.4-0.8). We also provide the positive 95th quantile MDA8 ozone concentration, which is used to estimate a “No Fire” MDA8 ozone value based on the EPA guidance (U.S. Environmental Protection Agency, 2016). We also provide the median residuals (and confidence interval) for all non-EE days with observed MDA8 at or above 60 ppb; this threshold was needed to build a sufficient sample size with a representative distribution, and derive the median and 95% confidence interval. It should be noted that four out of the seven years modeled by the GAM were high wildfire years, and these values likely include a significant amount of wildfire days. We were not able to systematically remove wildfire influence by subsetting the Clark County ozone data based on HMS smoke, HMS smoke and $PM_{2.5}$ concentrations, and low wildfire years. These methods produced a significant number of false positives and negatives, and yielded datasets that were still affected by wildfire smoke. Therefore, these values should be considered an upper estimate of residuals for high ozone days. We see that the median residuals for 2018 and 2020 EE days are significantly higher than those on non-EE high observed ozone days since their confidence intervals do not overlap (or are comparable for the Jerome Mack station). The non-EE day residuals on days where observed MDA8 was at or above 60 ppb were determined to be normally distributed with a slight positive skew (median skewness = 0.39).

Table 3-17. Overall 2014-2020 GAM median residuals and 95% confidence interval range in square brackets for each site modeled. Sample size is shown in parentheses below the residual statistics. For sample sizes less than ten, we include a range of residuals in square brackets instead of the 95% confidence interval. Residual results are split by non-EE days and the 2018 & 2020 EE days. R^2 for each site is also shown along with the positive 95th quantile result.

Site Name	All Residuals (ppb)	Non-EE Day Residuals (ppb)	2018 & 2020 EE Day Residuals (ppb)	R^2	Positive 95th Quantile (ppb)	Non-EE Day Residuals when MDA8 ≥ 60 ppb (ppb)
Boulder City	0.22 [-0.04, 0.48] (1,132)	0.22 [-0.04, 0.48] (1,130)	12.05 [10.38-13.72] (2)	0.58	9	4.05 [3.55, 4.55] (200)
Green Valley	0.17 [-0.15, 0.48] (948)	0.10 [-0.21, 0.41] (934)	7.38 [5.40, 9.36] (14)	0.58	10	3.76 [3.28, 4.23] (271)
Indian Springs	0.13 [-0.18, 0.44] (1,014)	0.08 [-0.22, 0.38] (1,010)	12.30 [9.37-17.19] (4)	0.55	10	4.79 [4.26, 5.32] (201)
Jean	0.21 [-0.06, 0.48] (1,149)	0.20 [-0.07, 0.47] (1,146)	12.57 [9.59-13.90] (3)	0.57	9	3.40 [2.94, 3.85] (290)
Jerome Mack	0.09 [-0.19, 0.36] (1,152)	0.05 [-0.22, 0.32] (1,141)	6.83 [4.21, 9.45] (11)	0.61	9	3.83 [3.32, 4.33] (242)
Joe Neal	0.23 [-0.08, 0.54] (1,113)	0.17 [-0.13, 0.47] (1,097)	7.77 [5.79, 9.75] (16)	0.60	10	3.32 [2.92, 3.71] (377)
Paul Meyer	0.21 [-0.08, 0.50] (1,159)	0.10 [-0.19, 0.39] (1,137)	8.11 [6.34, 9.88] (22)	0.55	10	3.58 [3.19, 3.97] (388)
Walter Johnson	0.27 [-0.03, 0.57] (1,163)	0.19 [-0.10, 0.48] (1,141)	7.16 [5.11, 9.21] (22)	0.58	10	3.53 [3.13, 3.93] (379)

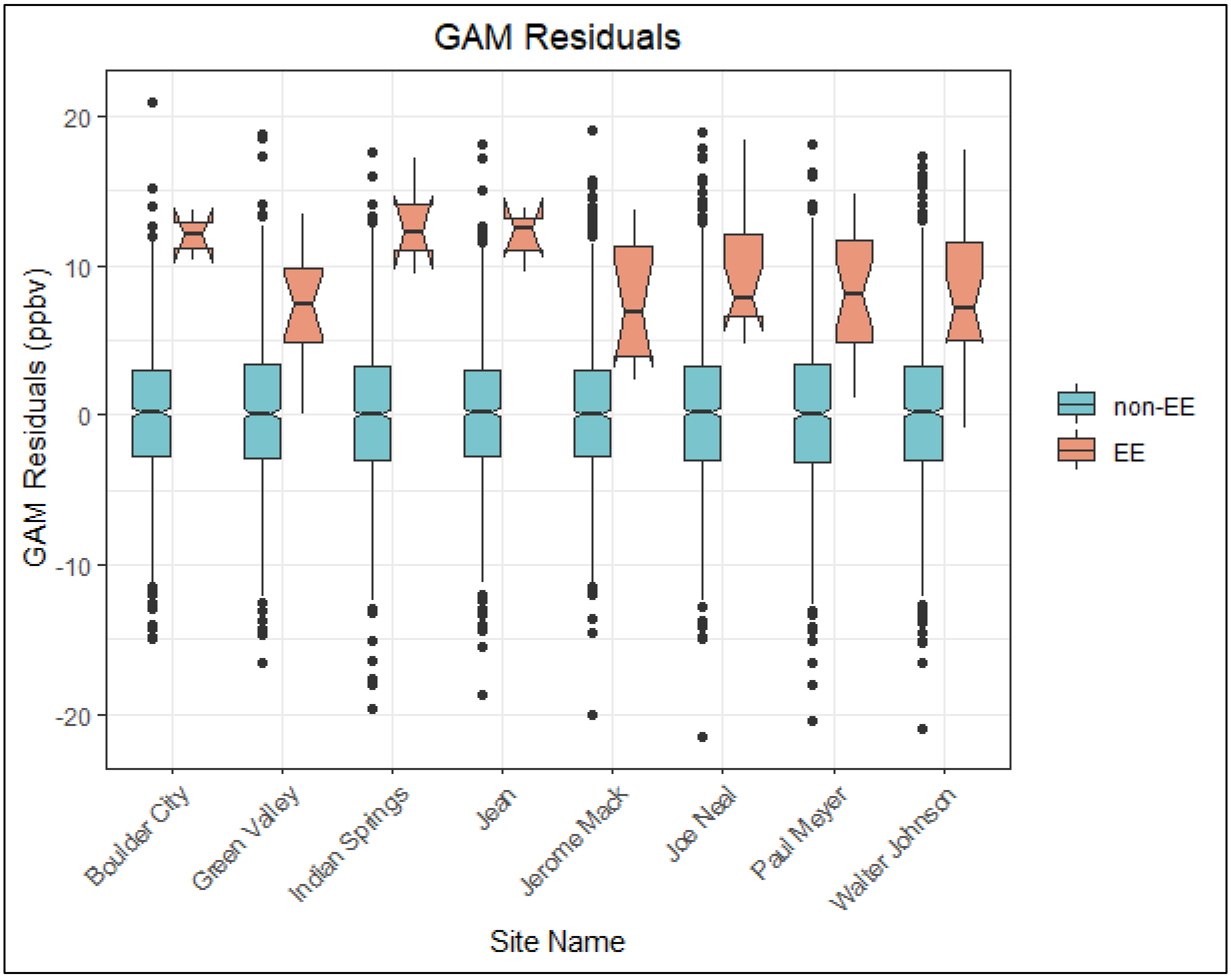

Figure 3-67. EE vs. non-EE residuals. Non-EEs (non-EE in blue) and EEs (EE in orange) residuals are shown for each site modeled in Clark County. The notches for each box represent the 95th confidence interval. This figure illustrates the information in Table 3-17.

Overall, the GAM results show low bias and consistently significantly higher residuals on EE days compared with non-EE days. We also evaluated the GAM performance on verified high ozone, non-smoke days by looking at specific case studies. This was done assess whether high-ozone days, such as the EE days, have a consistent bias that is not evident in the overall or high ozone day GAM performance. Out of the seven years used in the GAM model, four were high wildfire years in California (2015, 2017, 2018, and 2020). Since summer winds in Clark County are typically out of California (44% of trajectories originate in California according to the cluster analysis [not including transport through California in the Baja Mexico cluster]), wildfire smoke is likely to affect a large portion of summer days and influence ozone concentrations in Clark County. We identified specific case studies where most monitoring sites in Clark County had an MDA8 ozone concentration greater than or equal to 60 ppb and had no wildfire influence; “no wildfire influence” was determined by inspecting HMS smoke plumes and HYSPLIT back trajectories for each day and confirming no smoke was over, near, or transported to Clark County. We found one to two examples from each year used in the GAM modeling, and required that at least half of the case study days needed to include an exceedance of the ozone NAAQS. Table 3-18 shows the results of these case studies. Most case study days, including NAAQS exceedance days, show positive and negative residuals even when median ozone is greater than or equal to 65 ppb in Clark County, similar to the results for the entire multi-year dataset. GAM residuals on non-EE days when MDA8 is at or above 60 ppb have a median of 3.69 [95% confidence interval: 3.47, 3.88] (see Table 3-17). The high ozone, non-smoke case study days all show median residuals within or below the confidence interval of the high ozone residuals (from Table 3-17), meaning that the GAM model is able to accurately predict high ozone, non-smoke days within a reasonable range of error. Two additional factors indicate the GAM has good performance on normal, high ozone days: (1) the median residuals for the case studies are mostly lower than the 95% confidence interval of high ozone residuals (i.e., includes non-EE wildfire days), and (2) the case study days were verified as non-smoke days. Thus, residuals above the 95th confidence interval of the median residuals, such as those on the EE days, are statistically higher than on days with comparable high ozone concentrations, and not biased high because of the high ozone concentrations on these days.

Table 3-18. GAM high ozone, non-smoke case study results. Median GAM residuals for ten days in 2014-2020 are shown where most monitoring sites had MDA8 ozone concentrations of 60 ppb or greater. Sites used to calculate the MDA8 and GAM residual median/range are listed in the Clark County AQS Site Number column by site number.

Date	Clark County AQS Site Number	Median (Range) of Observed MDA8 Ozone (ppb)	Median (Range) GAM Residual (ppb)
5/17/2014	0601, 0075, 1019, 0540, 0043, 0071	66 (64-71)	1.66 (-0.53-4.28)
6/4/2014	0601, 0075, 0540, 1019, 0043, 0071	69 (66-72)	3.46 (1.70-4.80)
6/3/2015	1019, 0043, 0075, 0540, 7772, 0601, 0071	71 (65-72)	3.01 (-0.34-5.77)
6/20/2015	0601, 0298, 7772, 1019, 0540, 0075, 0043, 0071	65 (63-70)	1.40 (-6.20-5.28)
6/3/2016	0298, 1019, 0075, 0540, 0043, 0071	65 (63-71)	3.89 (1.89-5.26)
7/28/2016	0075, 0071, 0298, 0540, 0043	70 (63-72)	0.24 (-5.95-3.67)
6/17/2017	0601, 0075, 0071, 1019, 0540, 0298, 0043	66 (63-72)	1.85 (-1.94-7.01)
6/4/2018	0601, 0298, 7772, 1019, 0540, 0075, 0043, 0071	65 (60-67)	3.06 (-0.91-3.60)
5/5/2019	0601, 0298, 7772, 1019, 0540, 0075, 0043, 0071	65 (62-67)	1.28 (-2.00-3.42)
5/15/2020	0298, 0043, 0075, 0071	63 (63-65)	1.52 (1.09-3.49)

We also evaluate the bias of GAM residuals versus predicted MDA8 ozone concentrations in Figure 3-68. Residuals (i.e., observed ozone minus GAM-predicted MDA8 ozone) should be independent of the GAM-predicted ozone value, meaning that the difference between the actual ozone concentration on a given day and the GAM output should be due to outside influences and not well described by meteorological or seasonal values (i.e., variables used in the GAM prediction). Therefore, in a well-fit model, positive and negative residuals should be evenly distributed across all

GAM-predicted ozone concentrations and on average zero. In Figure 3-68, we see daily GAM residuals at all eight monitoring sites in Clark County from 2014-2020, the residuals are evenly distributed across all GAM-predicted ozone concentrations, with no pattern or bias at high or low MDA8 fit concentrations. This evaluation of bias in the model is consistent with established literature and other EE demonstrations (Gong et al., 2017; McVey et al., 2018; Pernak et al., 2019; Texas Commission on Environmental Quality, 2021), and indicate a well-fit model. In **Figure 3-69**, we also provide a histogram of the residuals at each monitoring site modeled in Clark County. This analysis shows that residuals at each site are distributed normally around a median near zero, and none of the distributions shows significant tails at high or low residuals (median skew = 0.05 with 95% confidence interval [-0.03, 0.12]). This analysis of error in the model and our results are consistent with previously concurred EE demonstrations (Arizona Department of Environmental Quality, 2016) and previous literature (Jaffe et al., 2013; Alvarado et al., 2015; Gong et al., 2017; McClure and Jaffe, 2018a; Pernak et al., 2019). **Appendix C** provides GAM residual analysis from the concurred ADEQ and submitted TCEQ demonstrations that compare well with our GAM residual results. Based on these analysis methods, bias in the model is low throughout the range of MDA8 prediction values and confirms that the GAM can be used to predict MDA8 ozone concentrations in Clark County.

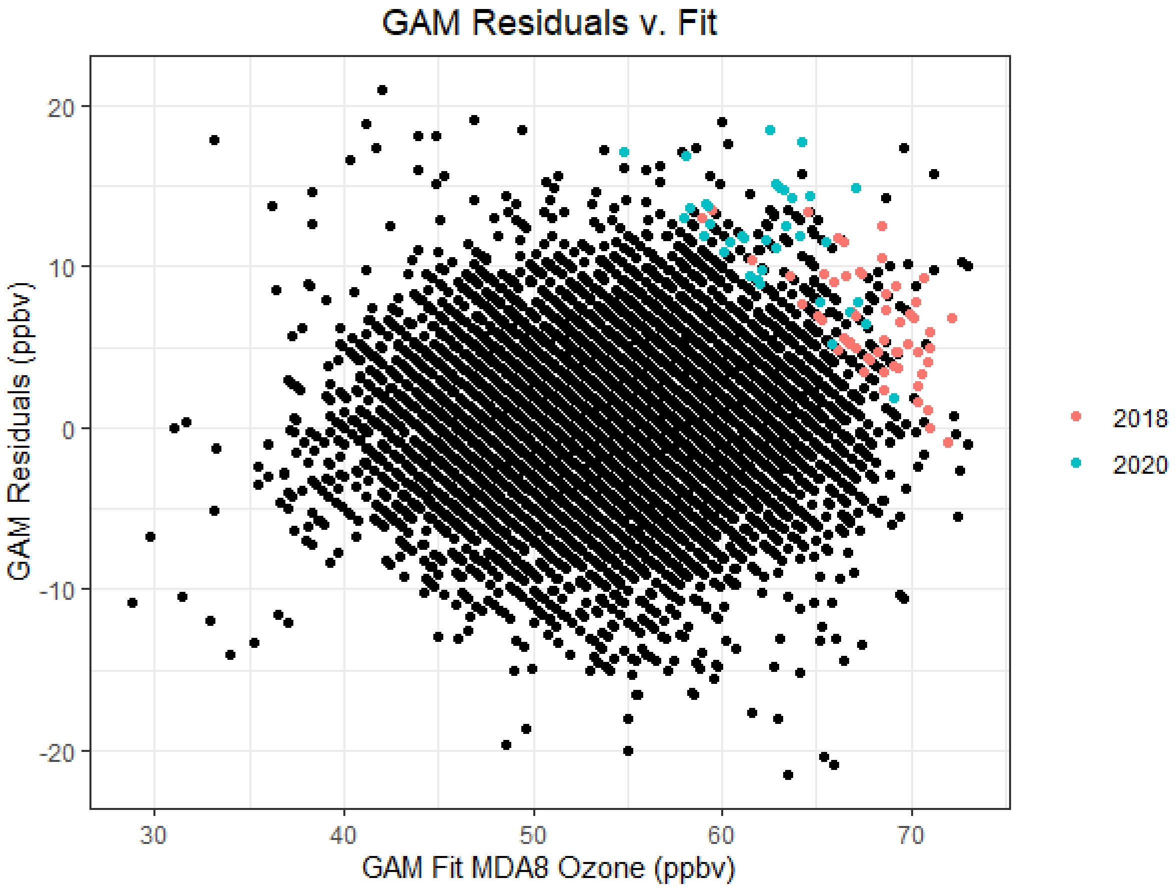

Figure 3-68. Daily GAM residuals for 2014-2020 vs GAM Fit (Predicted) MDA8 Ozone values. 2018 and 2020 EEs residuals are shown in red and blue.

Change color to black

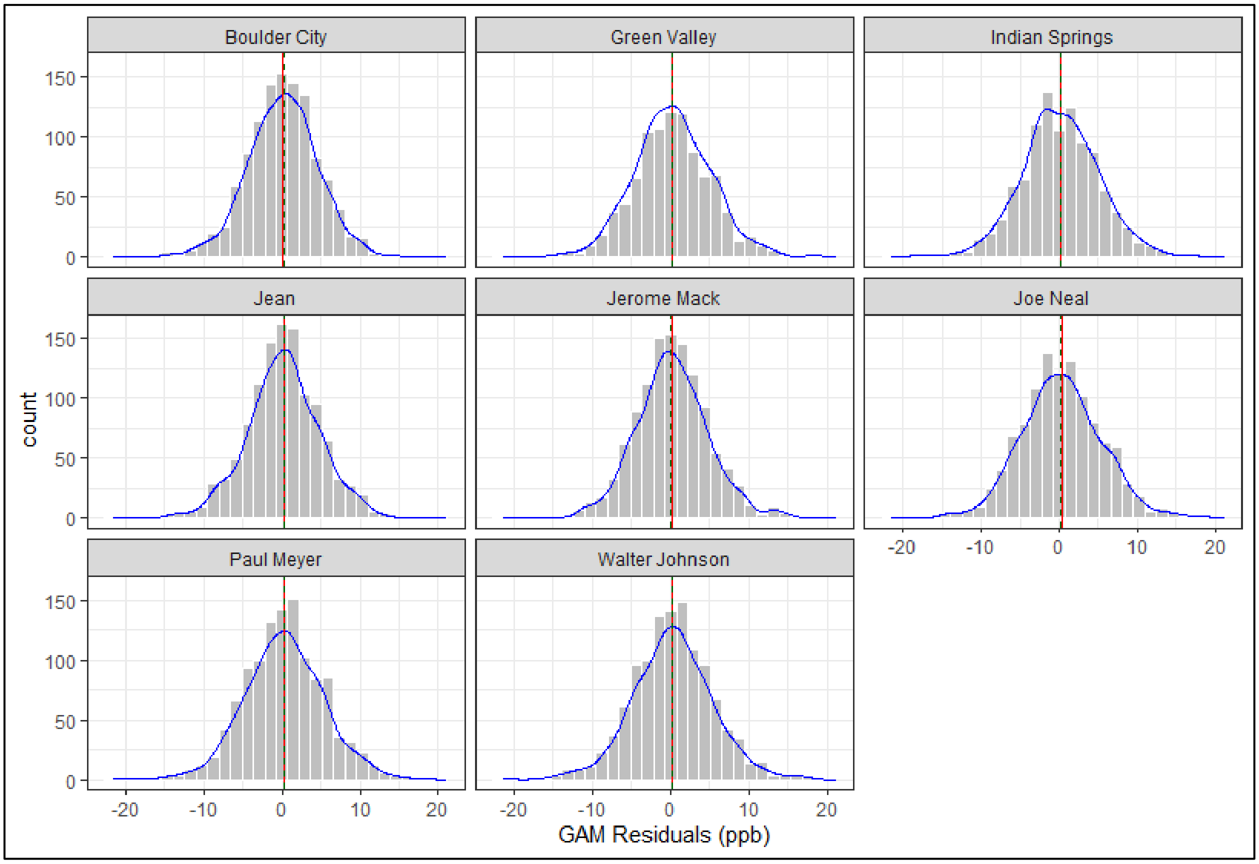

Figure 3-69. Histogram of GAM residuals at all modeled Clark County monitoring sites. The red line indicates the mean, and the green dashed line indicates the median. The blue line provides the density distribution.

Within the GAM model, we include HYSPLIT 24-hour distance values, which are factored by cluster, to provide source region and stagnation information into the algorithm. A major upwind pollution source for Las Vegas is the Los Angeles Basin (see the Southern California cluster), which is around 400 km away. Since the GAM model uses source region and distance traveled information to help predict daily MDA8 ozone concentrations, contributions from LA should be accounted for in the algorithm. Based on this, we can assess whether GAM residuals on LA-source region days were significantly different from other source regions. In Figures 3-70 and 3-71, we subset the GAM results by removing any potential EE days. From these results, we find that both morning (18:00 UTC) and afternoon (22:00 UTC) trajectory data have similar distributions for all clusters. The notches in the box plots (representing the 95th confidence interval) provide an estimate of statistical difference and show that the median of residuals is near zero for all clusters. The Northwest U.S. cluster at 18:00 UTC shows slightly negative residuals, while the Long-Range Transport cluster shows slightly positive residuals for both 18:00 and 22:00 UTC. The Southern California cluster shows a median residual of around zero for both 18:00 and 22:00 UTC trajectories, with significant overlap between the 95th confidence intervals of most other clusters (not statistically different). Additionally, the number of data points per cluster (bottom of each figure) corresponds well with transport from California being dominant for the April through September time frame. Overall, this analysis provides evidence that even when the Los Angeles Basin (Southern California cluster) is upwind of Las Vegas, the GAM model performs well (low median residuals), and the results are statistically similar to most of the other clusters. This implies that when residuals are large, the Los Angeles Basin influence is unlikely to be the only contributor to enhancements in MDA8 ozone.

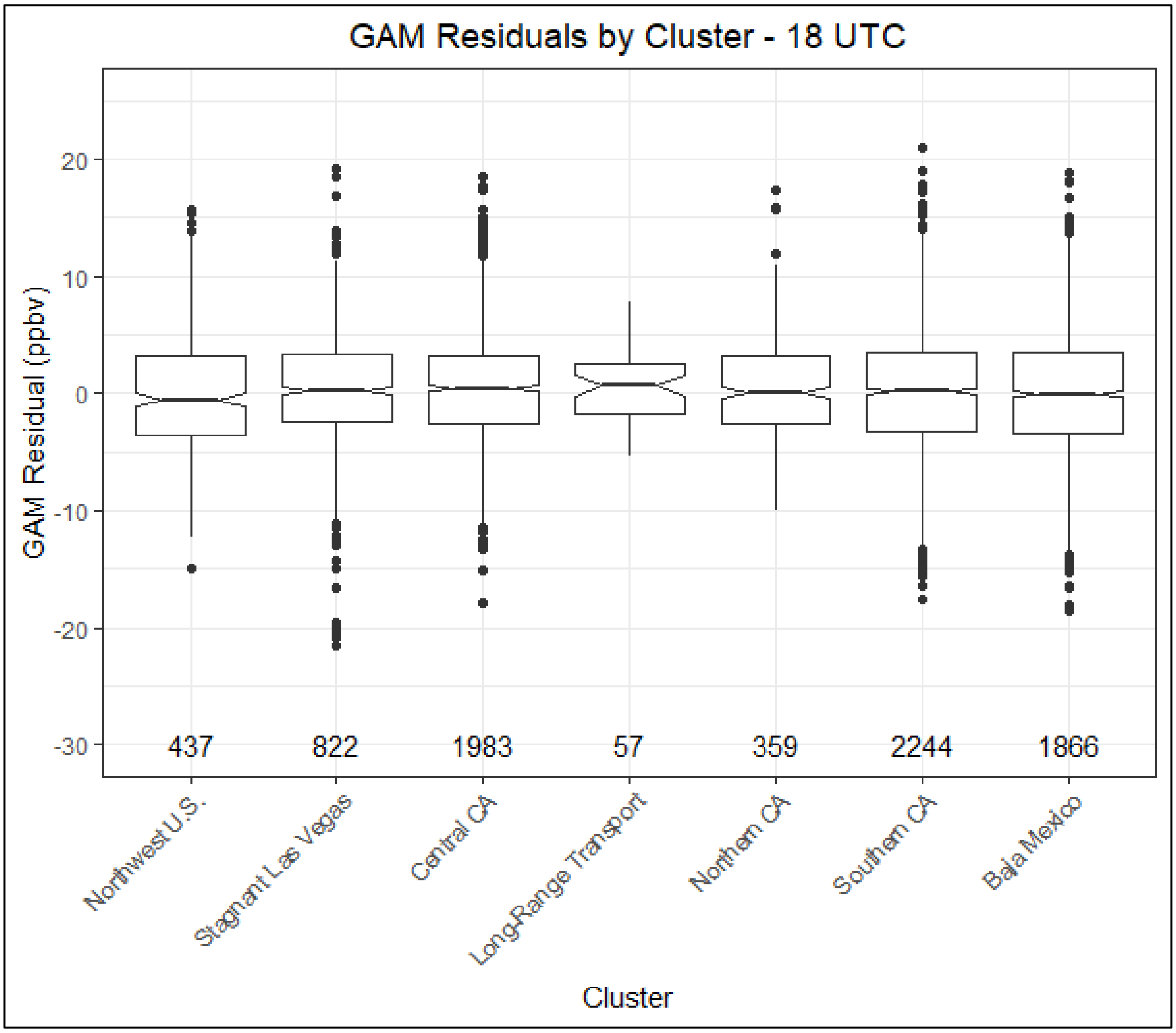

Figure 3-70. GAM cluster residual results for 18:00 UTC. The cluster is determined by grouping 24-hour back trajectories from Las Vegas based on their path. Clusters were created by using back trajectory results from Clark County between 2014 and 2020 were used (removed EE days).

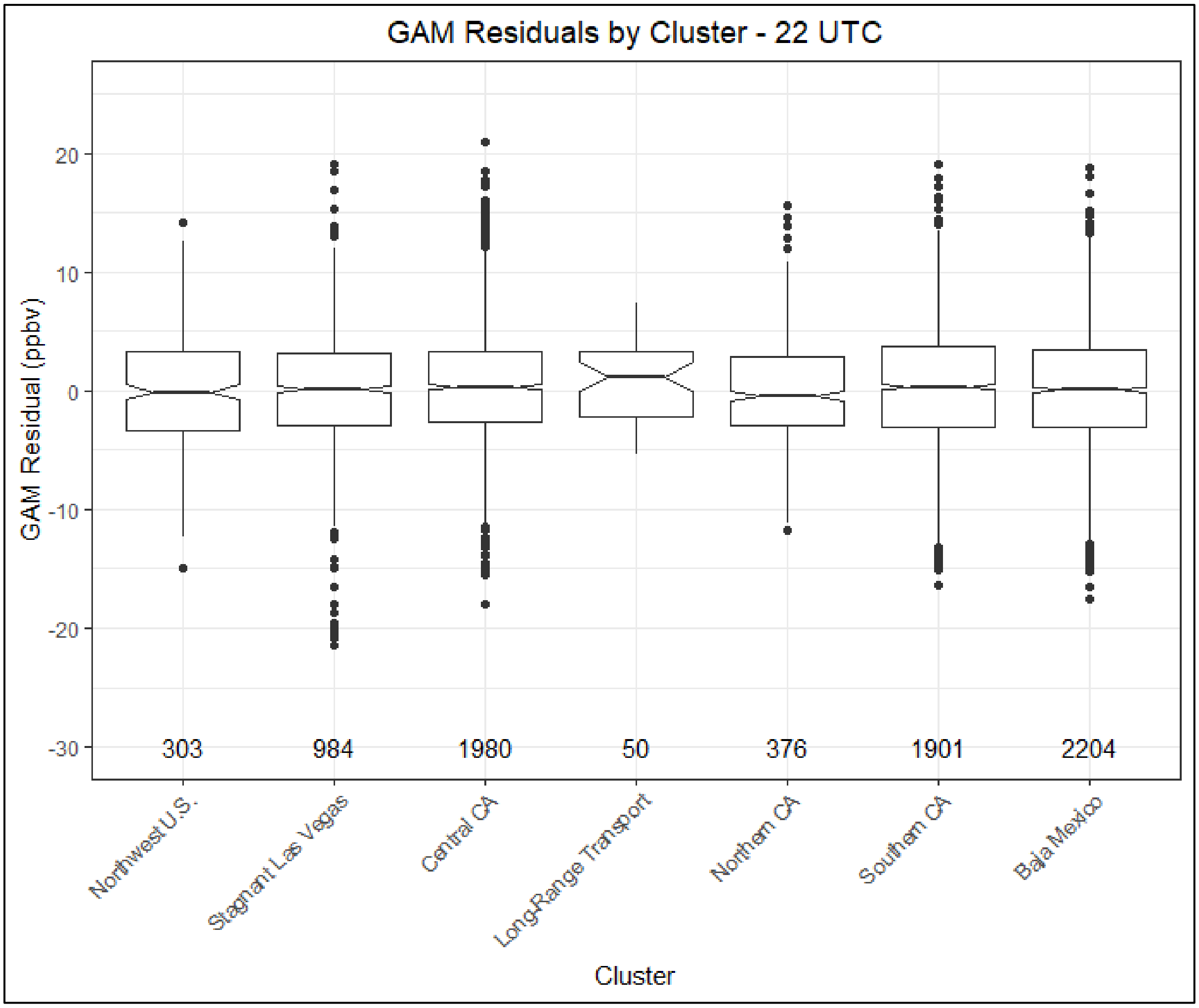

Figure 3-71. GAM cluster residual results for 22:00 UTC. The cluster is determined by grouping 24-hour back trajectories from Las Vegas based on their path. Clusters were created by using back trajectory results from Clark County between 2014 and 2020 were used (removed EE days).

Mobile emissions sources decreased throughout the U.S. after COVID restrictions went into place in March 2020. Based on emission inventories from Las Vegas, on-road emissions make up a significant portion of the NO_x emissions inventory (see Sections 2.3 and 2.5 for more details). Based on traffic data from the Nevada Department of Transportation, on-road traffic in Clark County in 2020 was significantly different than 2019 through early to mid-June (depending on the area where traffic volume was measured [see Section 2.5 for more details]). Figure 3-72 provides a scatter plot of MDA8 ozone observed versus GAM fit for all eight monitoring sites, separated by year. The linear regression fit, slope, and intercept do not show large difference between 2020 and other modeled years. Figure 3-73 provides a more in-depth look at the most heavily affected months due to COVID restrictions and traffic changes (April-May, 2020). The 95th confidence interval (shown as a notch in the box plots) show overlap between 2020 and most other years (except 2015 and 2016). The May 6, 9, and 28 EE days are included in the 2020 box. This analysis shows that there was not a statistically different GAM response in 2020 compared with other years; this is confirmed in the COVID analysis section (Section 2.5) where we show that MDA8 ozone during April-May 2020 in Las Vegas was not statistically different from previous years. Overall, ozone in Clark County did not change significantly and, similarly, GAM results were not significantly affected.

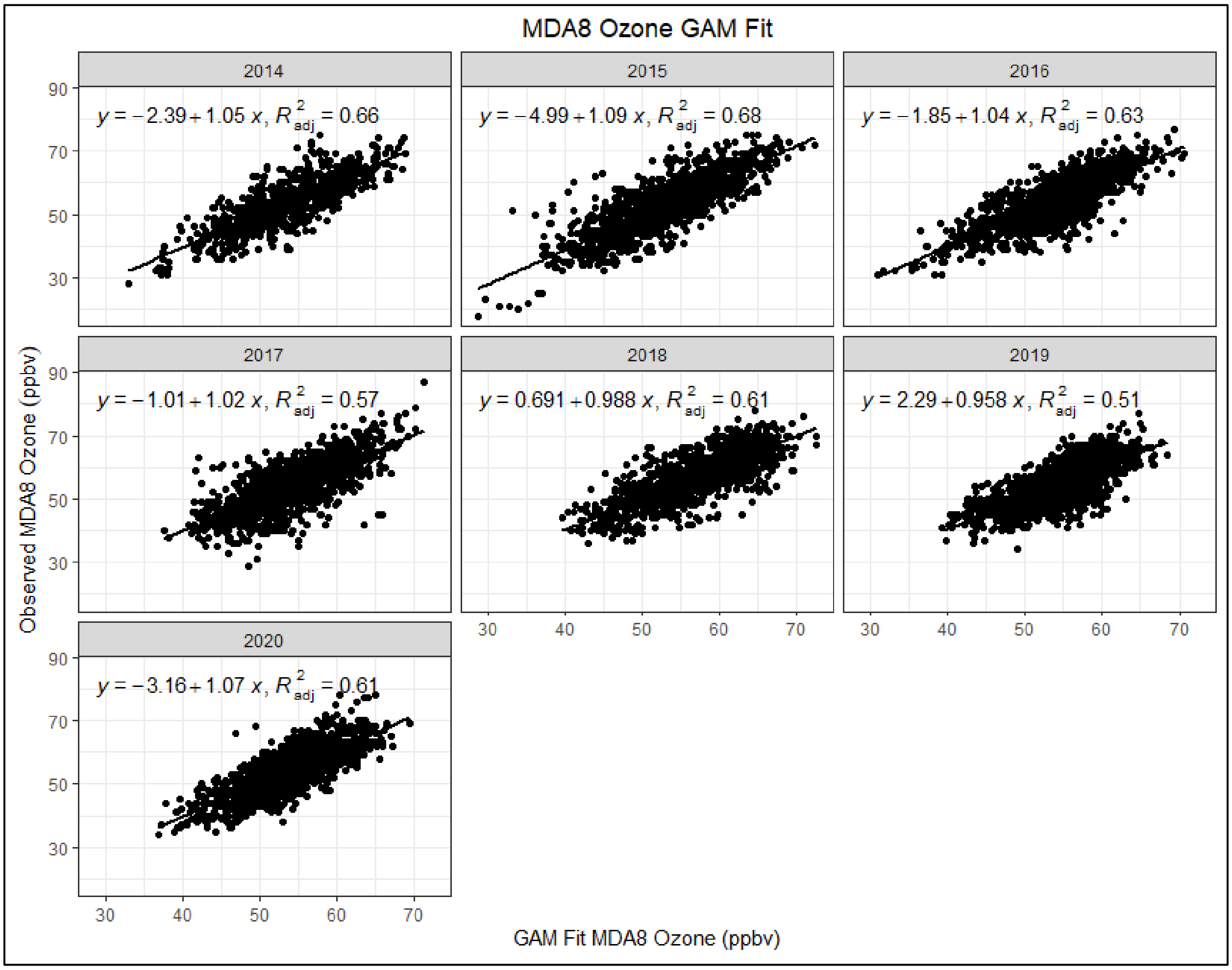

Figure 3-72. Observed MDA8 ozone vs GAM fit ozone by year. The relationship between observed MDA8 ozone and GAM fit ozone at all eight modeled monitoring sites in Clark County is broken out by year with linear regression and fit statistics shown (slope, intercept, and R^2 [R^2_{adj} is the same as R^2]). EE days are not included in the regression equations.

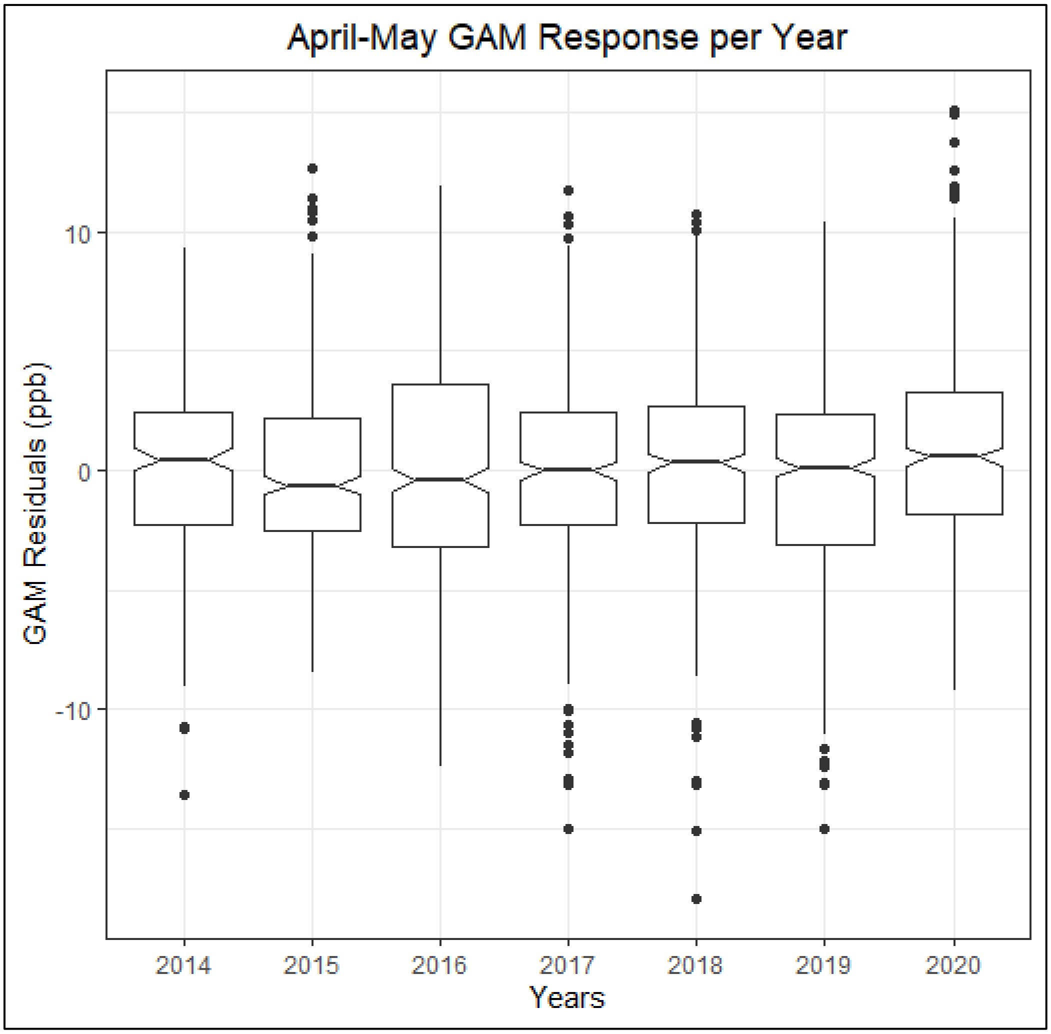

Figure 3-73. April-May Interannual GAM Response. April-May residuals per year (2014-2020) are plotted for all eight modeled monitoring sites in Clark County. May 6, 9, and 28 potential EE days are included.

Figure 3-74 provides the observed MDA8 ozone versus GAM Fit MDA8 from 2014 through 2020 for the sites affected on May 6 (Green Valley, Jean, Jerome Mack, Joe Neal, Paul Meyer, and Walter Johnson). We marked the possible 2020 (red), 2018 (blue), and other (purple) EE days to show that observed MDA8 ozone on these days is higher than those predicted by the GAM. The other (purple) points are from 2014-2016 suspected wildfire events, as indicated in the EPA AQS record. We also highlight the May 6, 2020, EE day as a large red triangle in each figure. Linear regression statistics (slope, intercept, and R^2) are also provided for context. Both linear regressions show a slope near unity and a low intercept value (around 2-4 ppb) with a good fit R^2 value.

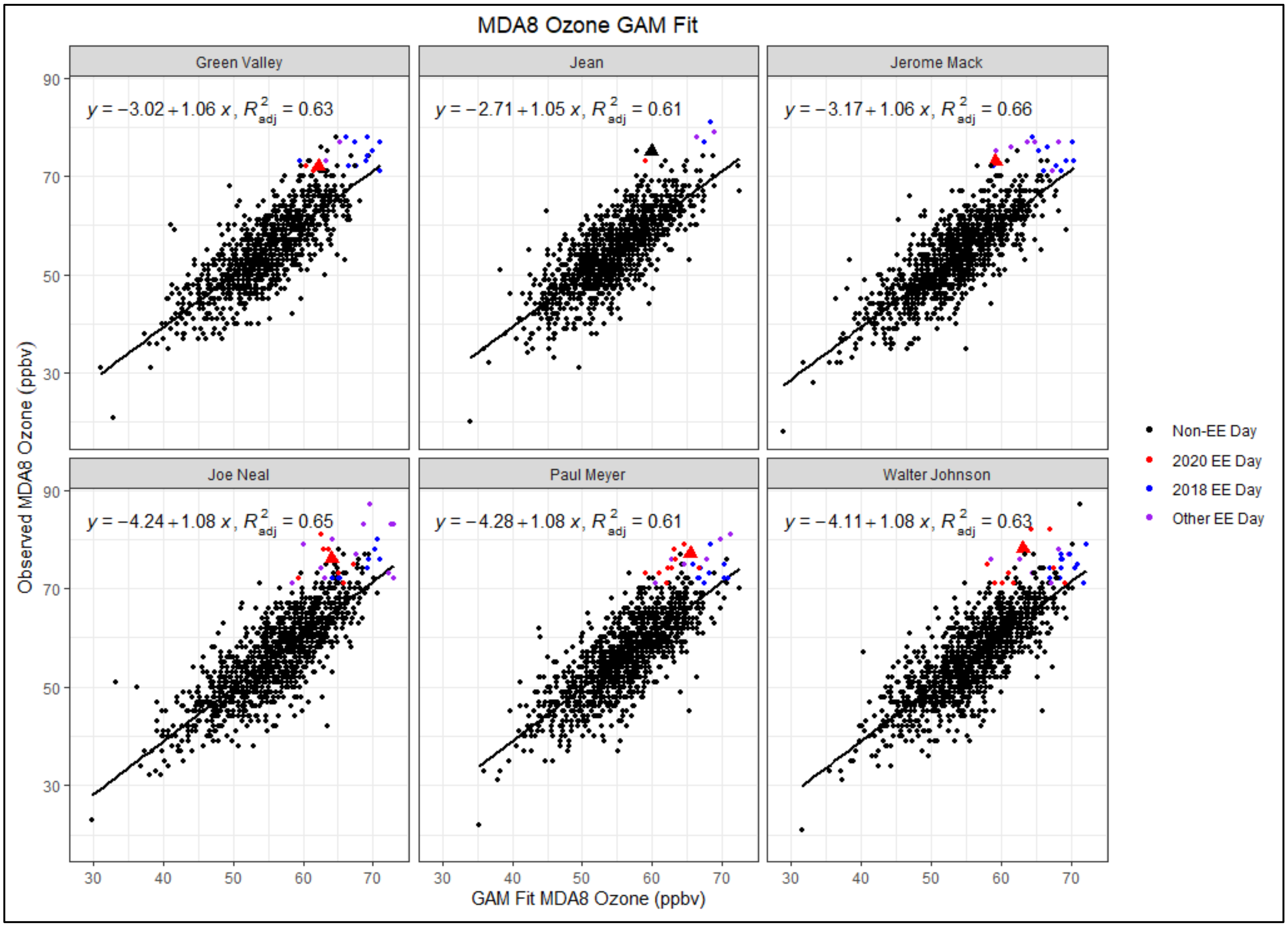

Figure 3-74. GAM MDA8 Fit versus Observed MDA8 ozone for EE affected sites on May 6, 2020. Black circles indicate data not associated with the 2018 or 2020 EE days, red circles indicate 2020 EE days, blue circles indicate 2018 EE days, and purple circles indicate 2014-2016 EE days. May 6 is shown as a red triangle. The black line is linear regression of the data and statistics (equation and R^2 value [R^2_{adj} is the same as R^2]) are shown in the top of each sub-figure.

Table 3-19 provides the GAM results for May 6, 2020, at each monitoring site affected by the EE. GAM residuals show a modeled wildfire impact of 10-16 ppb for all monitoring sites, with MDA8 GAM prediction values well below the 0.070 ppm standard. These values suggest that there was a significant, non-typical enhancement in MDA8 ozone concentrations at the affected Clark County monitoring sites on May 6, 2020.

Table -3-19. May 6 GAM results and residuals for each site. The GAM residual is the difference between observed MDA8 ozone and the GAM Prediction. We also estimate the minimum predicted fire influence based on the positive 95th quantile and GAM prediction value.

Site Name	MDA8 O_3 Concentration (ppm)	MDA8 GAM Prediction (ppm)	GAM Residual (ppm)
Paul Meyer	0.077	0.065	0.012
Walter Johnson	0.078	0.063	0.015
Joe Neal	0.076	0.064	0.012
Green Valley	0.072	0.062	0.010
Jerome Mack	0.073	0.059	0.014
Jean	0.075	0.059	0.016

Finally, Figure 3-75 shows a two-week time series of observed MDA8 ozone values across Clark County and GAM prediction values at those sites. May 6, 2020 (and May 9, 2020-another EE filed concurrently with this one), shows the large gap between observed MDA8 ozone and GAM-predicted values. Outside of the possible EE days, the GAM prediction values are close to the observed values (with the exception of May 11 which could have had an outside influence on MDA8 ozone less than 70 ppb), suggesting that immediately before and after the event, we are able to accurately predict typical fluctuations in ozone on non-event days.

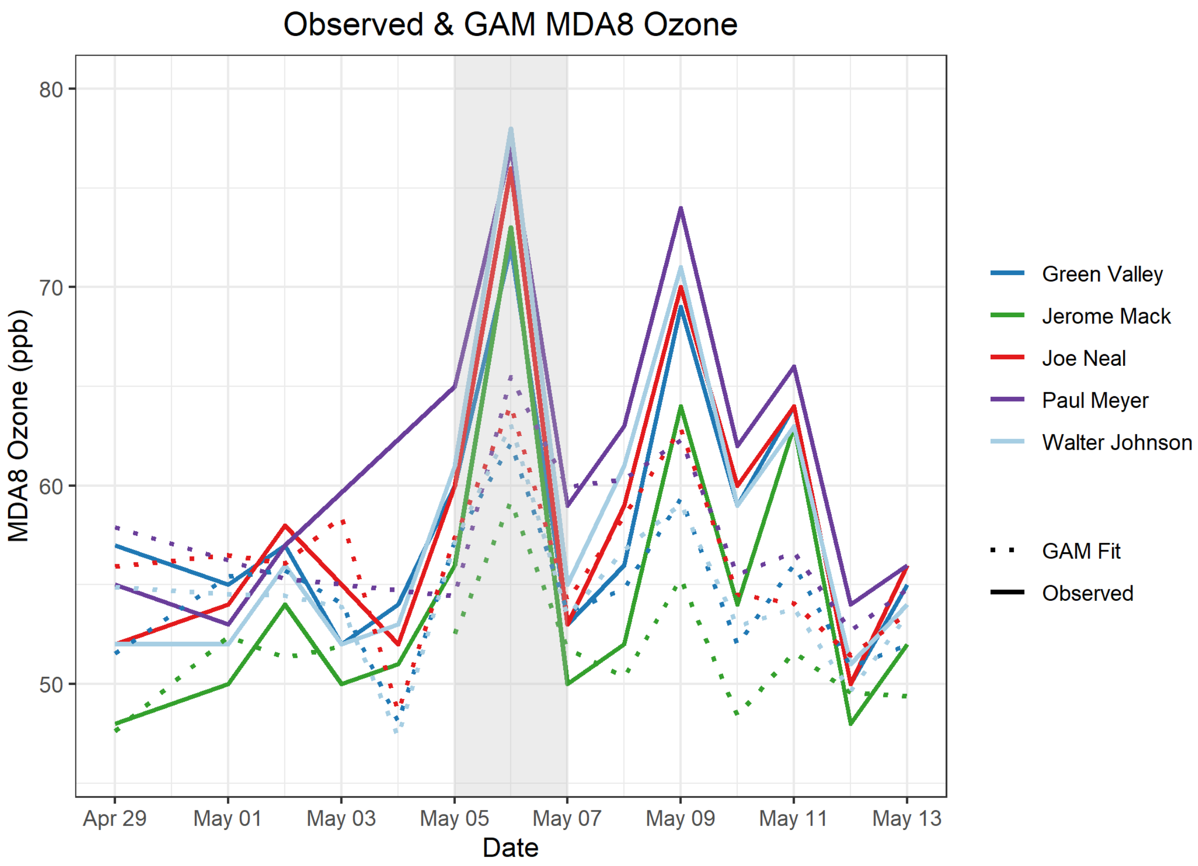

Figure 3-75. GAM time series showing observed MDA8 ozone for two weeks before and after the May 6 EE (solid lines). The GAM MDA8 ozone fit value is also shown for two weeks before and after May 6 (dotted line).

Overall, the GAM evidence clearly demonstrates that a non-typical source of ozone significantly impacted concentrations on May 6, 2020, at all EE-affected Clark County sites. Additionally, based on evidence in Figures 3-70 and 3-71, the high residuals on May 6 are unlikely to be a GAM overprediction based solely on unaccounted influence from the Los Angeles Basin. When the GAM evidence is coupled with stratospheric intrusion evidence from Sections 3.1 through 3.5, we suggest by weight of evidence, that the enhancement in ozone is due to a stratospheric intrusion over the northwest U.S. which was transported to Clark County, Nevada.

3.6 Clear Causal Relationship Conclusions

The analyses conducted in this report support the impact of a stratospheric intrusion over the northwestern U.S. and the eastern Pacific (off the coast of California and Oregon), which was transported to Clark County, Nevada, and enhanced ozone concentrations on May 6, 2020. We find that:

1. Visible satellite imagery, model results, tropospheric measurements, and back/forward trajectories support the conclusion of ozone-rich air being transported from the source region off the coast and over California and Oregon to Clark County between May 4, 00:00 UTC and the EE date.
2. A large mixing layer, demonstrated with (a) skew-T sounding diagrams and boundary layer modeling and (b) meteorological analyses from the source region and Clark County, support the transport and mixing of ozone-rich air down to the surface in Clark County on the EE date.
3. Comparisons with non-event concentrations, regionally high ozone concentrations on the EE date, meteorologically similar day analysis, and GAM statistical modeling support the conclusion that the ozone concentrations seen in Clark County were well above typical seasonal concentrations and likely due to outside influences, such as an upwind SOI.

The analyses presented in this report fulfill the requirements for both a Tier 1 and 2 stratospheric intrusion EE demonstration, and all conclusions for each type of analysis are summarized in Table 3-20. The effect of the SOI event in Clark County caused ozone exceedances at the Paul Meyer, Walter Johnson, Joe Neal, Jerome Mack, Green Valley, Apex, and Jean monitoring stations. Even a small enhancement in ozone concentrations from an SOI on May 6—in addition to typical photochemical production and transport of anthropogenic ozone and ozone precursors—can push MDA8 ozone concentrations above the NAAQS threshold. Since stratospheric intrusions are classified as natural events, and we provide a clear causal relationship between the SOI event and the monitored exceedances, we conclude that the ozone exceedance event on May 6, 2020, in Clark County was not reasonably controllable or preventable.

Table 3-20. Results for each tier analysis of the May 6, 2020, EE.

Type of Analysis	Requirement	Finding
Historical comparison	• ≥ 5 years of peak daily ozone data with other high event days flagged. • Table with percentile ranks of days. • Historical diurnal profile comparison (Tier 2).	• The May 6 ozone exceedance occurred during a typical ozone season and event concentrations were significantly higher than non-event concentrations. • Percentile ranks for all affected sites were ≥ 98th percentile
Event overview	• Spatial and temporal depictions of ozone during the event. • Description of surface and upper air meteorological conditions during the event. • Begin to establish the complex relationship between the intrusion and eventual impact at surface (Tier 2).	• The SOI source region off the coast and over California and Oregon shows stratospheric-tropospheric exchange on May 4 from 00:00 to 23:00 UTC. • Ozone-rich air is transported across Oregon and northern California and descends into Clark County during the May 6 EE.
Establish stratospheric intrusion	Several of following are likely needed: • Water vapor imagery • Total column ozone • Meteorological evidence	• Visible water vapor, ozone satellite imagery, and meteorological data were consistent with an SOI event off the coast of and over the northwest U.S. on May 4. • Model results of IPV, ozone, and CO are also consistent with an SOI in the source region on May 4.
Establish stratospheric air reached surface	Several of following are likely needed: • LIDAR, rawinsonde data • Meteorological evidence • Online AQ model cross sections • Trajectory models	• Trajectory analysis to and from the source region and Clark County show transport of an ozone-rich air mass. • Meteorological and LIDAR (from Boulder, CO) analysis show the transport of ozone from the source region along with measurements of ozone from the source region. • Model cross-sections of ozone and CO data confirm a descending branch of high ozone and low CO from an SOI event.
Impacts at the surface	Several of following are likely needed: • Coincidence between high ozone and meteorological/AQ conditions characteristic of stratospheric intrusions • Statistical model evidence of impacts	• Surface measurement on May 6 in Clark County show abnormally low water vapor and abnormally, regionally high ozone, with normal NOx levels. This suggests SOI influence, but not unusually high photochemical influence on ozone concentrations. • Meteorologically similar day analysis shows that average MDA8 ozone across similar days was well below the ozone NAAQS and 10 ppb lower than the May 6 exceedance at all affected sites. • GAM statistical modeling of May 6 indicates an outside source of ozone enhancing ozone concentrations during the EE.

4. Natural Event

The Exceptional Events Rule (81 FR 68216) states that a "[n]atural event, which may recur, is one in which human activity plays little or no direct causal role." The preamble to the Exceptional Events rule notes that the EPA considers stratospheric ozone intrusions to be natural events, as humans have no direct impact on their occurrence. The Clark County Department of Environment and Sustainability has shown through the analyses provided in Section 3.6 of this demonstration that the hypothesized stratospheric intrusion, which existed simultaneously with local photochemical production of ozone, contributed to identified ozone exceedances at the Paul Meyer, Walter Johnson, Joe Neal, Jerome Mack, Green Valley, Apex, and Jean monitoring sites on May 6. Through these analyses and the fact that stratospheric intrusions are purely natural, the Clark County Department of Environment and Sustainability has satisfied the "human activity that is unlikely to recur at a particular location or a natural event" element of 40 CFR 50.14(c)(3).

5. Not Reasonably Controllable or Preventable

The documentation provided in Section 3.6 of this demonstration shows that the suspected stratospheric intrusion contributed to the identified ozone exceedances at Paul Meyer, Walter Johnson, Joe Neal, Jerome Mack, Green Valley, Apex, and Jean monitoring sites on May 6. Through these analyses and the fact that stratospheric intrusions are purely natural events that cannot be prevented or controlled, the Clark County Department of Environment and Sustainability has satisfied the "not reasonably controllable or preventable" criterion.

6. Public Comment

This exceptional event demonstration will undergo a 30-day public comment period concurrent with EPA's review beginning July 1, 2021. A copy of the public notice, along with any comments received and responses to those comments, will be submitted to EPA after the comment period has closed, consistent with the requirements of 40 CFR 50.14(c)(3)(v). **Appendix D** contains documentation of the public comment process.

7. Conclusions and Recommendations

The analyses conducted in this report support the conclusion that an SOI event occurred over the northwestern U.S. and off the coast in the eastern Pacific that injected ozone-rich air into the free troposphere and was then transported and mixed down into Clark County, Nevada, on May 6, 2020, affecting ozone concentrations. This EE demonstration has provided the following elements required by the EPA guidance for SOIs (U.S. Environmental Protection Agency, 2018):

1. A narrative conceptual model that describes the SOI event off the coast of and over California and Oregon, as well as how the transport of ozone-rich air led to ozone exceedances downwind in Clark County (Section 1.4).
2. A clear causal relationship between the SOI and the May 6 exceedance through ground and satellite-based measurements, trajectories, comparison with non-event concentrations, vertical profile analysis, and statistical modeling (Section 3).
3. Event ozone concentrations at or above the 98th percentile when compared with the last five years of observations (yearly and ozone season-only) at each site and among the four highest ozone days at each site (Section 3).
4. Stratospheric intrusions are considered to be natural events, as humans have no direct impact on their occurrence (Section 4).
5. Demonstrated that transport from an SOI event is neither reasonably controllable or preventable (Section 5).
6. This demonstration went through the public comment process via Clark County's Department of Environment and Sustainability (Section 6).

The major conclusions and supporting analyses found in this report are:

1. Visible satellite imagery, model results, tropospheric measurements, and back/forward trajectories support the conclusion of ozone-rich air being transported from the source region off the coast and over California and Oregon to Clark County between May 4, 00:00 UTC and the EE date.
2. A large mixing layer, supported by (a) skew-T sounding diagrams and boundary layer modeling and (b) meteorological analyses from the source region and Clark County, support the transport and mixing of ozone-rich air down to the surface in Clark County on the EE date.
3. Comparisons with non-event concentrations, regionally high ozone concentrations on the EE date, meteorologically similar day analysis, and GAM statistical modeling support the conclusion that the ozone concentrations seen in Clark County were well above typical summer concentrations and likely due to outside influences, such as an upwind SOI.

The analyses presented in this report fulfill the requirements for both a Tier 1 and 2 stratospheric intrusion EE demonstration, and all conclusions for each type of analysis are summarized in Table 3-20. The effect of the SOI event in Clark County caused ozone exceedances at the Paul Meyer, Walter Johnson, Joe Neal, Jerome Mack, Green Valley, Apex, and Jean monitoring stations. Since stratospheric intrusions are classified as natural events, and we provide a clear causal relationship between the SOI event and the monitored exceedances, we conclude that the ozone exceedance event on May 6, 2020, in Clark County was not reasonably controllable or preventable.

8. References

Alvarado M., Lonsdale C., Mountain M., and Hegarty J. (2015) Investigating the impact of meteorology on O_3 and $PM_{2.5}$ trends, background levels, and NAAQS exceedances. Final report prepared for the Texas Commission on Environmental Quality, Austin, TX, by Atmospheric and Environmental Research, Inc., Lexington, MA, August 31.

Arizona Department of Environmental Quality (2016) State of Arizona exceptional event documentation for wildfire-caused ozone exceedances on June 20, 2015 in the Maricopa nonattainment area. Final report, September. Available at https://static.azdeq.gov/pn/1609_ee_report.pdf.

Arizona Department of Environmental Quality (2018) State of Arizona exceptional event documentation for wildfire-caused ozone exceedances on July 7, 2017 in the Maricopa Nonattainment Area. Final report, May. Available at https://static.azdeq.gov/pn/Ozone_2017ExceptionalEvent.pdf.

Camalier L., Cox W., and Dolwick P. (2007) The effects of meteorology on ozone in urban areas and their use in assessing ozone trends. *Atmospheric Environment*, 41, 7127-7137, doi: 10.1016/j.atmosenv.2007.04.061.

Clark County Department of Air Quality (2019) Ozone Advance program progress report update. August.

Clark County Department of Environment and Sustainability (2020) Revision to the Nevada state implementation plan for the 2015 Ozone NAAQS: emissions inventory and emissions statement requirements. September. Available at https://files.clarkcountynv.gov/clarknv/Environmental%20Sustainability/SIP%20Related%20Documents/O3/20200901_2015_O3%20EI-ES_SIP_FINAL.pdf?t=1617690564073&t=1617690564073.

Code of Federal Regulations (1997) Title 40, Part 58, Appendix D. Network design for SLAMS, NAMS, and PAMS.

Gong X., Kaulfus A., Nair U., and Jaffe D.A. (2017) Quantifying O_3 impacts in urban areas due to wildfires using a generalized additive model. *Environ. Sci. Technol.*, 51(22), 13216-13223, doi: 10.1021/acs.est.7b03130.

Jaffe D.A., Bertschi I., Jaegle L., Novelli P., Reid J.S., Tanimoto H., Vingarzan R., and Westphal D.L. (2004) Long-range transport of Siberian biomass burning emissions and impact on surface ozone in western North America. *Geophys. Res. Let.*, 31(L16106).

Jaffe D.A., Wigder N., Downey N., Pfister G., Boynard A., and Reid S.B. (2013) Impact of wildfires on ozone exceptional events in the western U.S. *Environ. Sci. Technol.*, 47(19), 11065-11072, doi: 10.1021/es402164f, October 1. Available at http://pubs.acs.org/doi/abs/10.1021/es402164f.

Kroll J.H., Heald C.L., Cappa C.D., Farmer D.K., Fry J.L., Murphy J.G., and Steiner A.L. (2020) The complex chemical effects of COVID-19 shutdowns on air quality. *Nature Chemistry*, 12(9), 777-779, doi: 10.1038/s41557-020-0535-z. Available at https://doi.org/10.1038/s41557-020-0535-z.

Langford A.O. (2014) Las Vegas ozone study (LVOS). Final report prepared for the Clark County Department of Air Quality, Las Vegas, NV, by the National Oceanic and Atmospheric Administration Earth System Research Laboratory, Chemical Sciences Division, Boulder, CO, MOU #CBE 602948-13, July 25. Available at https://csl.noaa.gov/projects/lvos/LVOSfinalreportCBE602948-13.pdf.

Langford A.O., Senff C.J., Alvarez R.J., Brioude J., Cooper O.R., Holloway J.S., Lin M.Y., Marchbanks R.D., Pierce R.B., Sandberg S.P., Weickmann A.M., and Williams E.J. (2015) An overview of the 2013 Las Vegas Ozone Study (LVOS): impact of stratospheric intrusions and long-range transport on surface air quality. *Atmospheric Environment*, 109, 305-322, doi: 10.1016/j.atmosenv.2014.08.040, 2015/05/01/. Available at http://www.sciencedirect.com/science/article/pii/S1352231014006426.

Langford A.O. and Senff C.J. (2019) Fires, asian, and stratospheric transport-Las Vegas ozone study (FAST-LVOS). Report prepared for the Clark County Department of Air Quality, Las Vegas, NV, by the National Oceanic and Atmospheric Administration Earth System Research Laboratory, Chemical Sciences Division, Boulder, CO, and the Cooperative Institute for Research in Environmental Sciences, University of Colorado, Boulder, CO, CBE 604318-16, December. Available at https://csl.noaa.gov/projects/fastlvos/FAST-LVOSfinalreport604318-16.pdf.

Louisiana Department of Environmental Quality (2018) Louisiana exceptional event of September 14, 2017: analysis of atmospheric processes associated with the ozone exceedance and supporting data. Report submitted to the U.S. EPA Region 6, Dallas, TX, March. Available at https://www.epa.gov/sites/production/files/2018-08/documents/ldeq_ee_demonstration_final_w_appendices.pdf.

McClure C.D. and Jaffe D.A. (2018a) US particulate matter air quality improves except in wildfire-prone areas. *Proceedings of the National Academy of Sciences*, 115(31), 7901-7906, doi: 10.1073/pnas.1804353115. Available at https://www.pnas.org/content/pnas/115/31/7901.full.pdf.

McClure C.D. and Jaffe D.A. (2018b) Investigation of high ozone events due to wildfire smoke in an urban area. *Atmospheric Environment*, 194, 146-157, doi: 10.1016/j.atmosenv.2018.09.021, 2018/12/01/. Available at http://www.sciencedirect.com/science/article/pii/S1352231018306137.

McVey A., Pernak R., Hegarty J., and Alvarado M. (2018) El Paso ozone and $PM_{2.5}$ background and totals trend analysis. Final report prepared for the Texas Commission on Environmental Quality, Austin, Texas, by Atmospheric and Environmental Research, Inc., Lexington, MA, June. Available at https://www.tceq.texas.gov/assets/public/implementation/air/am/contracts/reports/da/582188176307-20180629-aer-ElPasoOzonePMBackgroundTotalsTrends.pdf.

National Weather Service Forecast Office (2020) Las Vegas, NV: general climatic summary. Available at https://www.wrh.noaa.gov/vef/lassum.php.

Parker H.A., Hasheminassab S., Crounse J.D., Roehl C.M., and Wennberg P.O. (2020) Impacts of traffic reductions associated with COVID-19 on Southern California air quality. *Geophysical Research Letters*, 47(23), e2020GL090164. Available at https://agupubs.onlinelibrary.wiley.com/doi/abs/10.1029/2020GL090164.

Pernak R., Alvarado M., Lonsdale C., Mountain M., Hegarty J., and Nehrkorn T. (2019) Forecasting surface O_3 in Texas urban areas using random forest and generalized additive models. *Aerosol and Air Quality Research*, 19, 2815-2826, doi: 10.4209/aaqr.2018.12.0464.

Sacramento Metropolitan Air Quality Management District (2011) Exceptional events demonstration for 1-hour ozone exceedances in the Sacramento regional nonattainment area due to 2008 wildfires. Report to the U.S. Environmental Protection Agency, March 30.

Simon H., Baker K.R., and Phillips S. (2012) Compilation and interpretation of photochemical model performance statistics published between 2006 and 2012. *Atmospheric Environment*, 61, 124-139, doi: 10.1016/j.atmosenv.2012.07.012.

Solberg S., Walker S.-E., Schneider P., Guerreiro C., and Colette A. (2018) Discounting the effect of meteorology on trends in surface ozone: development of statistical tools. Technical paper by the European Topic Centre on Air Pollution and Climate Change Mitigation, Bilthoven, the Netherlands, ETC/ACM Technical Paper 2017/15, August. Available at https://www.eionet.europa.eu/etcs/etc-atni/products/etc-atni-reports/etcacm_tp_2017_15_discount_meteo_on_o3_trends.

Solberg S., Walker S.-E., Guerreiro C., and Colette A. (2019) Statistical modelling for long-term trends of pollutants: use of a GAM model for the assessment of measurements of O_3, NO_2 and PM. Report by the European Topic Centre on Air pollution, transport, noise and industrial pollution, Kjeller, Norway, ETC/ATNI 2019/14, December. Available at https://www.eionet.europa.eu/etcs/etc-atni/products/etc-atni-reports/etc-atni-report-14-2019-statistical-modelling-for-long-term-trends-of-pollutants-use-of-a-gam-model-for-the-assessment-of-measurements-of-o3-no2-and-pm-1.

Texas Commission on Environmental Quality (2021) Dallas-Fort Worth area exceptional event demonstration for ozone on August 16, 17, and 21, 2020. April. Available at https://www.tceq.texas.gov/assets/public/airquality/airmod/docs/ozoneExceptionalEvent/2020-DFW-EE-Ozone.pdf.

U.S. Census Bureau (2010) State & County QuickFacts. Available at http://quickfacts.census.gov/qfd/states/.html.

U.S. Environmental Protection Agency (2015) 40 CFR Part 50, Appendix U: interpretation of the primary and secondary National Ambient Air Quality Standards for ozone. Available at https://www.ecfr.gov/cgi-bin/text-idx?SID=43eb095cc6751633290941788ab4f3bd&mc=true&node=ap40.2.50_119.u.

U.S. Environmental Protection Agency (2016) Guidance on the preparation of exceptional events demonstrations for wildfire events that may influence ozone concentrations. Final report, September. Available at www.epa.gov/sites/production/files/2016-09/documents/exceptional_events_guidance_9-16-16_final.pdf.

U.S. Environmental Protection Agency (2018) Guidance on the preparation of exceptional events demonstrations for stratospheric ozone intrusions. Report by the U.S. Environmental Protection Agency Office of Air Quality Planning and Standards, Air Quality Policy Division, Air Quality Assessment Division, Research Triangle Park, NC, EPA-457/B-18-001, November. Available at https://www.epa.gov/sites/production/files/2018-11/documents/exceptional_events_soi_guidance_11-8-2018.pdf.

U.S. Environmental Protection Agency (2020) Green Book: 8-hour ozone (2015) area information. Available at https://www.epa.gov/green-book/green-book-8-hour-ozone-2015-area-information.

Venter Z.S., Aunan K., Chowdhury S., and Lelieveld J. (2020) COVID-19 lockdowns cause global air pollution declines. *Proceedings of the National Academy of Sciences*, 117(32), 18984-18990, doi: 10.1073/pnas.2006853117. Available at https://www.pnas.org/content/pnas/117/32/18984.full.pdf.

Wood S. (2020) Mixed GAM computation vehicle with automatic smoothness estimation. Available at https://cran.r-project.org/web/packages/mgcv/mgcv.pdf.

Wood S.N. (2017a) *Generalized additive models: an introduction with R*, 2nd edition, CRC Press, Boca Raton, FL.

Wood S.N. (2017b) *Generalized additive models: an introduction with R, second edition*, 2nd Edition, Chapman and Hall/CRC.

Zhang L., Lin M., Langford A.O., Horowitz L.W., Senff C.J., Klovenski E., Wang Y., Alvarez R.J., II, Petropavlovskikh I., Cullis P., Sterling C.W., Peischl J., Ryerson T.B., Brown S.S., Decker Z.C.J., Kirgis G., and Conley S. (2020) Characterizing sources of high surface ozone events in the southwestern US with intensive field measurements and two global models. *Atmospheric Chemistry & Physics*, 20, 10379-10400, doi: 10.5194/acp-20-10379-2020. Available at https://acp.copernicus.org/articles/20/10379/2020/acp-20-10379-2020.pdf.